PhD-FSTM-2020-48
The Faculty of Sciences, Technology and Medicine

DISSERTATION

Defence held on 11/09/2020 in Luxembourg

to obtain the degree of

DOCTEUR DE L'UNIVERSITÉ DU LUXEMBOURG

EN SCIENCES DE L'INGÉNIEUR

by

Qingjie ZHANG
Born on 17 May 1990 in Henan, (China)

MOMENT AND LONGITUDINAL RESISTANCE FOR COMPOSITE BEAMS BASED ON STRAIN LIMITED DESIGN METHOD

-

ELASTIC-PLASTIC DESIGN FOR COMPOSITE BEAMS CONSIDERING DEEP NEUTRAL AXIS POSITION

Dissertation defence committee

Prof. Dr.-Ing. Markus Schäfer, dissertation supervisor
Professor, Université du Luxembourg

Prof. Dr.-Ing. Michél Bender
Professor, University of Trier

Prof. Dr.-Ing. Daniele Waldmann, Chairman
Professor, Université du Luxembourg

Prof. Dr. Stephen Hicks
Professor, University of Warwick

Prof. Dr. Olivier Francis, Vice Chairman
Professor, Université du Luxembourg

University of Luxembourg

Moment and longitudinal resistance for composite beams based on strain limited design

QINGJIE ZHANG

UNIVERSITÉ DU
LUXEMBOURG

Forewords

The content of this dissertation has been worked out from Sept 2016 to Sept 2020, during my study and work at University of Luxembourg as a Ph.D. candidate. It concluded parts of the research results developed during this period, mainly related to the design of composite beams related to the deep neutral axis position for bending and longitudinal shear design.

My special thanks go to Prof. Dr.-Ing. Markus Schäfer, who is not only an excellent supervisor in academic career but also one of the most respectable mentors and role models in personal life. The guidance from Prof. Schäfer and his contribution to this dissertation are significant. I would like also to thank the CET members: Prof. Dr. Michél Bender, Prof. Dr. Daniele Waldmann, and Prof. Dr. Olivier Francis for the valuable guidance and advice during the four years. As well as Prof. Dr. Stephen Hicks for the suggestion of improvements of the Dissertation. Furthermore, my thanks go to all my family, friends and colleges, who provided much supports.

From Sept 2016 to Oct 2018, I was mostly working on the European Project AVEC BNT, which focused on the comparison of Eurocodes and Chinese national standards for building design. Although the work results are published elsewhere in the book of AVEC BNT report [104] and not been presented in the dissertation, the experience and knowledge from the project have indirectly helped the outcome of this dissertation. Thus I would like also to send my gratitude to Dr. Helmut Nikolay, Prof. Dr. Michél Bender, Prof. Dr. Simon Wong and all other co-workers, students in the project.

After the successfully finalizing of the project AVEC BNT in 2018, the work of the following two years was shifted to researches on composite structures especially the composite beams. Although further researches related to such as composite columns and shear connectors have been also carried out, it was not possible to compress all of them into one dissertation without losing a clear structure. Thus only topics related to the influence of deep neutral axis positions for bending and longitudinal shear design of composite beams are presented. Never the less, the research topics are never isolated static "gear-wheels", they are inside a dynamic knowledge "gear-box" connected and influenced by each other. We are limited to the certain focused area but should bear the overall map in mind. We are limited to a certain time period but should appreciate the past and embrace the further. Thus I hope this work can still do a small contribution to the research committee and the further design for composite structures.

Abstract

The bending and longitudinal shear design of composite beams of steel and concrete follows often the plastic design method, which is a simplification based on rectangle stress blocks. The application of the plastic design method requires cross-section to have enough rotation capacity allowing most parts of the critical cross-section reach plastic at failure. There are different types of compact composite beams, such as the slim-floor beams. For them, the neutral axis position often gets deeper at failure, which reduces the rotation capacity and brings questions to the bending resistance and longitudinal shear design according to the plastic design resistance.

For a composite beam with deep neutral axis position, advanced numerical methods such as strain-limited design and FEM simulations can provide more accurate results than the plastic cross-section resistance. However, they are challenging to perform for general design engineers. In this work, simplified non-linear strain-limited design approaches, a strain-limited design software "SL.com" and an Abaqus add-in "CivilLab" have been developed to simplify the numerical calculations. They have also been applied in other chapters of this work to check the conventional plastic design results and to provide simplified design rules through parametric studies.

With full shear connection, a deep neutral axis position in composite beam under sagging bending may cause an important part of the steel section not to reach plastic at concrete failure. In this case, plastic bending resistance calculated based on rectangle stress blocks can result in an overestimation of the resistance and therefore leads to unsafe design. Thus, according to EN1994-1-1 [22], a reduction factor β on plastic bending resistance ($M_{pl,Rd}$) needs to be applied for cross-sections with steel grade S420 and S460 and the relative compression zone height (z_{pl}/h) is over 0.15. However, with the developments in industry as well as the second generation of Eurocode, this reduction factor still needs to be updated to consider new types of composite beams and wider ranges of steel grades.

While the conventional plastic design method has its limitations and only applicable when the beam cross-section has enough rotation capacity to allow full plastic development, the more advanced strain-limited numerical calculation and FEM can be used for a much wider range regardless of the position of the neutral axis. The investigations in this dissertation through comparing the plastic bending resistance with advanced numerical calculation results, have confirmed that besides the cross-sections with high steel grades (S420, S460), also certain cross-sections with lower steel grades can have an overestimated plastic bending moment resistance. At least this effect is more important for compact cross-section types such as slim-floor sections or composite beams with asymmetrical structural steel profiles or with a small concrete slab effective width. Therefore vast amount of parametric studies based on strain-limited method and FEM have been developed to check the topics, such as limitation of plastic design methods for different types of composite beams. Furthermore new reduction β functions on $M_{pl,Rd}$ for engineering practice considering much wider variates of composite beam cross-sections have been deviated.

For the design with partial shear connection, the partial shear diagram developed based on plastic analysis has been widely used. As discussed above, the plastic design may not be suitable when the position of neutral axis is too deep, similar problems can occur for the partial shear diagram. This problem is especially significant for slim-floor beams, for which due to the compact cross-section, the relative compression zone height (z_{pl}/h)

is usually much higher than conventional composite beams. Thus the limitation of using the partial shear diagram for slim-floor beams is provided, and additional simplified engineering design rules are proposed.

Plastic development inside the cross-section increases the longitudinal shear force in the plastic zones, furthermore with ductile shear connectors and respecting the minimum degree of shear connection, the non-linear redistribution of longitudinal shear force allows equal distance arrangement of shear connectors by the conventional design. For which, the full plastic development of the cross-section allowing plastic bending moment resistance and ductile shear connectors allowing non-linear longitudinal shear force distribution are the two fundamental conditions. The deep neutral axis position brings questions directly to the first assumption, as full plastic development of cross-section may not be able to reach. Thus the impact of a deep neutral axis position in the composite beams on longitudinal shear force distribution has been analysed. For which, the influence of plastic development inside beam cross-sections on longitudinal shear force with full shear interaction is theoretically explained. The different stages of non-linear distribution of longitudinal shear force due to shear connectors are investigated through FEM parametric studies. Based on the theoretical and numerical calculation, the design suggestions of composite beams with deep neutral axis position are given.

Contents

Notations

In general, the notation used in this work follows the EN1994-1-1:2004 [22] for composite beams. The concepts and symbols not provided in the codes are specially defined. Also to clearly distinguish between notations related to plastic design ("pl") and strain limited design ("sl"), some symbols in the EN1994-1-1 are modified. For example in the code, the concrete compression force of full shear connection is noted as $N_{c,f}$, here is changed to $N_{c,f,pl}$ and $N_{c,f,sl}$ to distinguish the results from plastic and strain limited design. Most notations are explained where they first appear, some of the most important ones are listed here.

Strain-limit refers to the maximum or minimum allowed strain for certain types of material in a cross-section analysis. If the strain limit values are exceeded, the structure member is considered as failed. The strain limit is related to the material model, however may be changed for certain purposes. For example, the concrete tensile strain limit is not considered in most of the analysis and the steel compression strain limit may be reduced due to local buckling.

Full shear connection according to Eurocode 4 states the situation that further increase of shear connectors will not lead to the increase of plastic bending resistance. It is a concept originally only for plastic design, however, we can borrow it for strain-limited design as well.

Degree of shear connection (η) according to Eurocode 4 is defined as the ratio between sum of shear connector resistance inside a critical section ($\sum P_{Rd}$) and required concrete compression force ($N_{c,f,pl}$) at full shear connection. The equation is as follow: $\eta = \sum P_{Rd}/N_{c,f,pl}$.

Full shear interaction is a term for strain-limited design, Johnson [43] defined it as the assumption that there no slip in the joint between steel and concrete, thus the two parts can deform as one. Full interaction indicates only one neutral axis existed in the cross-section. It is a stronger requirement compared to full shear connection, as a composite beam reaches full shear connection does not necessary at the same time reaches full interaction [68]. However, for many cases, the difference can be neglected. And EN1994-1-1 [22] also assumes full shear interaction for plastic resistance moment of a composite cross-section.

Degree of shear interaction (η_i) can be similarly defined as the ratio between sum of shear connector resistance inside a critical section ($\sum P_i$) and required concrete compression force ($N_{c,f,sl}$) at full shear interaction. The equation is as follow: $\eta_i = \sum P_i/N_{c,f,sl}$. For plastic design, it is assumed all shear connector reached their design resistance (P_{Rd}) and the increase of the degree of shear connection will always increase the bending moment resistance of the composite beam. For strain limited design, the shear connectors may have different resistance (P_i) at failure, and an increase of the degree of shear interaction is not necessary to increase the bending moment resistance.

Slip strain (ε_{slip}) is the strain difference between steel and concrete at the joint inside one cross-section. Due to slip, the original cross-section can be discontinued at the joint, however, they will still be regarded as the same cross-section.

Critical sections for longitudinal shear design are defined by the end of the beams and where bending moment reaches maximum or minimum. Furthermore the sections with loading or cross-section sudden changes such as openings or haunched beams zones in which the relationship of the moment resistance is greater than 1.5 are also considered

as critical sections. Between adjacent critical sections, longitudinal shear forces are to analyse.

Relative compression zone height refers to the ratio between compression zone height (z) and the beam total height (h), if the plastic design is used the relative compression zone height is calculated as z_{pl}/h, for strain-limited design it can also be z_{sl}/h.

Symbols used in the dissertation

Symbols related to geometrical definition

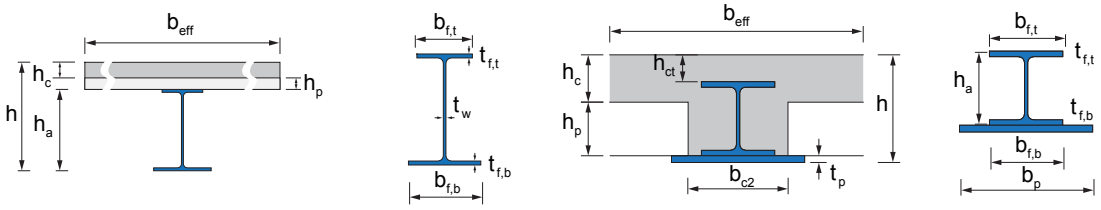

A_a	Cross-section area of the structural steel section
A_c	Cross-section area of the concrete part
A_p	Cross-section area of the welded additional steel plate
A_s	Cross-section area of the reinforcement
b_{eff}	Effective width of concrete slab
$b_{f,t}$	Width of steel profile top flange
$b_{f,b}$	Width of steel profile bottom flange
b_p	Width of the welded additional steel plate
b_{c2}	Width of the concrete chamber part
$t_{f,t}$	Thickness of structural steel section top flange
$t_{f,b}$	Thickness of structural steel section bottom flange
t_w	Thickness of structural steel section web
t_p	Thickness of the welded additional steel plate
h	Total height of the cross-section
h_a	Height of the structural steel section
h_c	Height of the concrete slab, if profiled sheeting is used, only refers to the part above profile sheeting main top flat surface
h_{ct}	Distance of structural steel section to the top of the whole cross-section
h_p	Height of the steel profiled sheeting
s	Spacing of shear connectors

Symbols related to strain-limited and plastic design

β	Reduction factor applied on plastic bending moment resistance
β_N	Reduction factor applied on concrete compression force calculated by plastic design method (newly defined)
δ	Deformation of shear connectors, deflection of the beam
$\varepsilon_{a,t}$	Strain at top of the steel cross-section part
$\varepsilon_{a,b}$	Strain at bottom of the steel cross-section part
ε_y	Yielding strain of structural steel
ε_{sh}	Strain hardening strain of structural steel
$\varepsilon_{a,u}$	Ultimate steel strain limit
$\varepsilon_{c,t}$	Strain at top of the concrete cross-section part
$\varepsilon_{c,u}$	Ultimate concrete strain limit
ε_{slip}	Slip strain at the composite joint
ε_{lim}	Strain limit of the cross-section
σ_a	Stress in structural steel section
σ_c	Stress in concrete section

σ_s	Stress in reinforcement section
κ	Curvature of beam cross-section
θ	Rotation angle of beam cross-section
η	Degree of shear connection
η_i	Degree of shear interaction
f_{cd}	Design compression strength of the concrete $f_{cd} = f_{ck}/\gamma_c$
f_{ck}	Characteristic compression strength of the concrete
f_y	Yielding strength of the structural steel
f_s	Yielding strength of the reinforcement
n_m	Parameter related to integral strain method for normal force calculation (newly defined)
m_m	Parameter related to integral strain method for bending moment calculation (newly defined)
z_{el}	Elastic design neutral axis location
z_{pl}	Plastic design neutral axis location
z_{sl}	Strain limited design neutral axis location
z_{psl}	Modified plastic neutral axis location based on parametric study compared to strain limited design (newly defined)
E_a	Modulus of elasticity of structural steel
E_{cm}	Secant modulus of elasticity of concrete
P_{Rd}	Design resistance per shear connector
M	Bending moment of the whole cross-section
$M_{el,Rd}$	Elastic design bending moment resistance
$M_{pl,Rd}$	Plastic design bending moment resistance
$M_{pl,a,Rd}$	Plastic design bending moment resistance of structural steel section only
$M_{sl,Rd}$	Strain limited design bending moment resistance
N	Normal force of the whole cross-section
N_a	Normal force of the steel section
N_c	Normal force of the concrete section
$N_{c,f}$	Normal force of the concrete section with full shear connection
V_L	Longitudinal shear force

Abbreviations

EC4	Eurocode 4 part 1-1
EC2	Eurocode 2 part 1-1
OOP	Object orient programming
FEM	Finite element method
SLS	Serviceability limit state
ULS	Ultimate limit state
PNA	Plastic design neutral axis
NA	Neutral axis
Fig.	Figure
Eq.	Equation

Chapter 1

Introduction

Composite beams of steel and concrete, which combine the advantages of both the steel and concrete constructions, provide economical solutions for bridge and building structures. Since their early developments in the 1950s, composite beams have gained more and more applications, especially after the invention of headed studs and the welding pistols, which provides fast and reliable shear connector installation. The conventional composite beam cross-section for building is shown in Fig.1.1 A). It consists of a concrete slab on the top of the steel beam and connected by headed studs. The slab can be a solid concrete slab or composite slabs with steel profiled sheeting. The metal sheeting provides permanent shuttering of concrete, thus improves construction speed. Chamber concrete inside or around the steel profile can also be provided to improve the beam mechanical behavior and fire protection. Nowadays conventional composite beams are still the most popular types, however, more and more new innovative composite beam systems or components lead to slimmer solutions. Examples such as the slim-floor beams (Fig.1.1 B) have increasing applications. They reduce the structural floor height and create a more appealling appearance. With new composite beam systems, innovative shear connectors have been developed to allow better mechanic performance or to fit the new requirements such as dismount-able constructions.

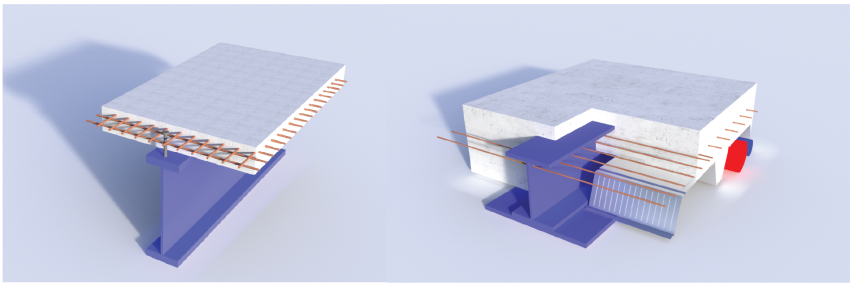

Figure 1.1 – Example of a conventional composite beam and a slim-floor beam

The European design codes Eurocode 4 [22] are used by many countries today. The engineering design methods (plastic and elastic design) in Eurocode 4 were mostly developed and benchmarked based on the conventional type of composite beams and headed studs shear connectors. However, after its publication in 2004, innovation was going on. It is known that the plastic bending resistance according to EN1994-1-1

does not always lead to reliable design results for specific cross-section types which has a deep neutral axis position at failure. The limitation of plastic bending resistance needs to be further analysed

To provide such evaluations and improvement, advanced non-linear numerical methods such as non-linear strain-limited design or Finite Element Method (FEM) can serve as important benchmark and parametric study tools. It is not difficult to run a few numerical analyses, the challenge is a vast amount of reliable parametric studies are needed to cover possible application ranges and the following tasks to analyze the generated data. Strain-limited design for composite beams, which considers material and geometrical non-linearity, is further developed in this work with simplified approaches. Strain limited design based software "SL.com " has been developed and applied together with FEM analyses to investigate the problems related to bending and longitudinal shear design regarding to deep neutral axis position. Compared to FEM, strain-limited design allows simply cross-section analysis, which is easier to be further transferred into simplified engineering approaches.

Among all the design aspects, the bending resistance of composite beams is focused. Eurocode 4 allows plastic bending resistance ($M_{pl,Rd}$) with cross-section class 1 or 2. And allows the equal distance arrangement of shear connectors when ductile shear connectors are used. The classification of cross-sections represents however only the buckling of steel plates and the influence of concrete is neglected. To prevent overestimation of plastic resistance a β factor is applied considering the difference between plastic and strain-limited bending resistance for steel grade S420 and S460 For conventional composite beams, the relative compression zone height is often small. Thus a high percentage of steel section can reach plastic when concrete fails due to compression under sagging bending moment. However, for e.g. slim cross-sections with a usually much deeper relative compression zone height, it is possible only a small percentage of steel section yields at concrete failure. The limitation of plastic bending resistance and the new β factor considering more varieties of composite beam types are necessary to be developed. As the partial shear diagram in Eurocode 4 is based on the plastic design resistance, the application for slim-floor beams needs to be checked as well.

When plastic bending resistance can not be reached, it is also questionable, what the longitudinal shear force redistribution is. The plastic development in steel section can change the longitudinal shear distribution. The current longitudinal shear design and equal distance arrangement of shear connectors with ductile shear connector should be checked for this case.

1.1 Objectives of the dissertation

With above-mentioned developments and challenges for the design of composite beams, it is aimed through this work, the limitation of the plastic bending resistance for composite beams due to deep neutral axis position can be pointed out and new β reduction factors considering both conventional and slim-floor beams can be provided. Furthermore, the influence of the neutral axis position on longitudinal shear distribution is also analyzed. In the information era, computers are essential for engineers. Developments of new nonlinear numerical or engineering calculation approaches to accelerate the design procedure are also included. The work focuses on sagging bending design only, application on the continuous beam is not included. Furthermore, local buckling

of steel sections, long-term effects on concrete, the influence of sequences of loading are also excluded. The main objectives are as follow:

- To improve non-linear numerical strain-limited design methods and develop FEM based automatic composite beam design and parametric study tools.
- To use non-linear strain-limited software and FEM application to figure out the limits of plastic bending resistance according to EN1994-1-1 for full shear connection, pointing out the application ranges of the plastic resistance for slim-floor beams related mainly to relative compression zone height. To use parametric studies to investigate the reduction factors (β factor in EC4) of plastic bending resistance considering more important variate of traditional composite and slim-floor cross-sections.
- Furthermore, to check if there are any further limitations of the partial shear diagram defined in EN1994-1-1 [22] to be applied on slim-floor cross-sections. And to develop simplified design methods based on the partial shear diagram beyond the limitation.
- To analyse the longitudinal shear force distribution in the composite joint, especially longitudinal shear distribution at full shear interaction with different relative compression zone heights. To check the impact of compression zone height on the longitudinal shear distribution with ductile shear connectors.

1.2 Structure of the dissertation

A deep neutral axis position influences both the bending moment resistance and longitudinal shear, where the plastic bending resistance may give unsafe results. Advanced numerical methods can be used as a benchmark of the plastic bending resistance and point out its limitation and to develop simplified approaches. Thus the main part of the dissertation can be divided into 3 sub-parts providing:

1) Why deep neutral axis position causes problems in plastic bending resistance?
2) How to use advanced calculation methods to analyze these problems?
3) What are the results? i.e. the limitation of plastic bending resistance and its reduction factor β as well as the impact of deep laying neutral axis to longitudinal shear design.

The first sub-part (chapter 2) is state of the art, where the developments related to subtopics includes the development of composite beams, rotation capacity limitations, engineering and advanced design methods for composite beam bending as well as the researches related to bending moment resistance and longitudinal shear design of composite beam. This part also explains why deep laying neutral axis causes overestimation of plastic bending resistance and influences the longitudinal shear distribution.

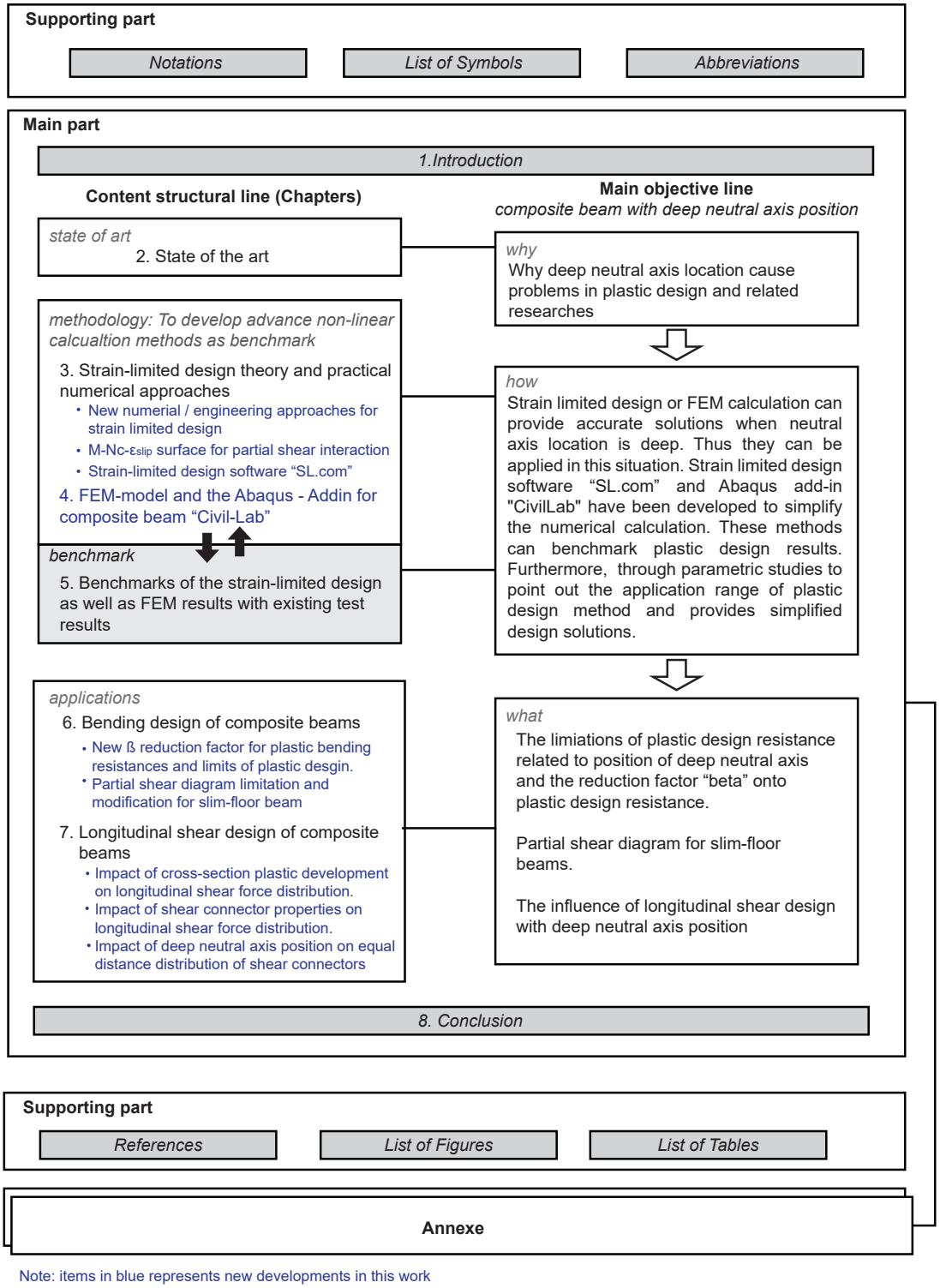

Figure 1.2 – Structure of the dissertation

In the second sub-part, chapter 3 and 4 present the methodology of the non-linear advanced methods which are applied later, whilst chapter 5 contains the benchmark of these approaches. The principles of non-linear strain limited design method and the newly developed practical numerical approaches such as "cell method" and "integral strain method" are given in chapter 3. The FEM model for composite beams and the

Abaqus add-in "Civil-Lab" is explained in chapter 4. The benchmarks of the numerical results with existing composite beam test results are given in chapter 5. The challenge is to develop reliable and simple non-linear numerical calculation methods able to perform vast parametric studies and also easy for results visualization and data statistic analysis. The newly developed strain limited approaches and Abaqus add-in "Civil-Lab" allow simplified numerical applications and overcome these challenges.

The third sub-part (chapter 6 and 7) shows the application of these methods and answers to the impact of deep neutral axis position onto bending moment resistance and longitudinal shear design. Chapter 6 focuses on bending design. For full shear connection, the limitation of plastic bending resistance and the new reduction factor "β" are provided. For partial shear connection, the application of a partial shear diagram on slim-floor beams is investigated and improved rules are proposed. Chapter 7 focuses on the longitudinal shear design. The impact of steel section plastic development and non-linear longitudinal shear redistribution with ductile shear connectors are discussed. A simplified solution for longitudinal shear distribution with full shear interaction considers steel reaches full plastic are proposed. Furthermore the impact of deep laying neutral axis onto longitudinal shear distribution has been analyzed.

To improve the reading experiences, a few supporting sections are added both before and after the main content. Before the main contents, the notations, list of symbols and the abbreviations used in the dissertation are listed. After the main contents, list of figures and tables as well as all the references are given. Non-essential details such as mathematical or theoretical proofs as well as additional parametric study results of related topics are moved into appendixes.

Chapter 2

State of the art

In this chapter, the state of the art related to different design methods of composite beams (section 2.3) and the influence of deep neutral axis on them are given. The conventional elastic and plastic bending resistance are limited to the rotation capacities and cross-section classes. For example, according to Eurocode 4 [22], only class 1 and 2 cross-sections, which have sufficient rotation capacity, are allowed for a plastic cross-section bending resistance. Thus the topics related to rotation capacity and cross-section classification and related design methods are summarized in section 2.2. Different composite beam types (section 2.1) show the tend towards to more compact cross-sections such as slim-floor beams. These sections usually have deeper neutral axes at failure, which can bring problems to the popular plastic bending resistance, due to limited cross-section area reach plastic strength at failure. Advanced numerical methods such as strain-limited design or FEM based non-linear calculations (section 2.3) are not limited by cross-section plastic development. Thus they can be used to find the limitation of plastic bending moment resistance regarding deep neutral axis position. Furthermore, to develop simplified design approaches. The current researches related to the bending design are explained in section 2.4 and in section 2.5 topics related to longitudinal shear design are discussed. Fig. 2.1 provides an overview of the topics in this chapter.

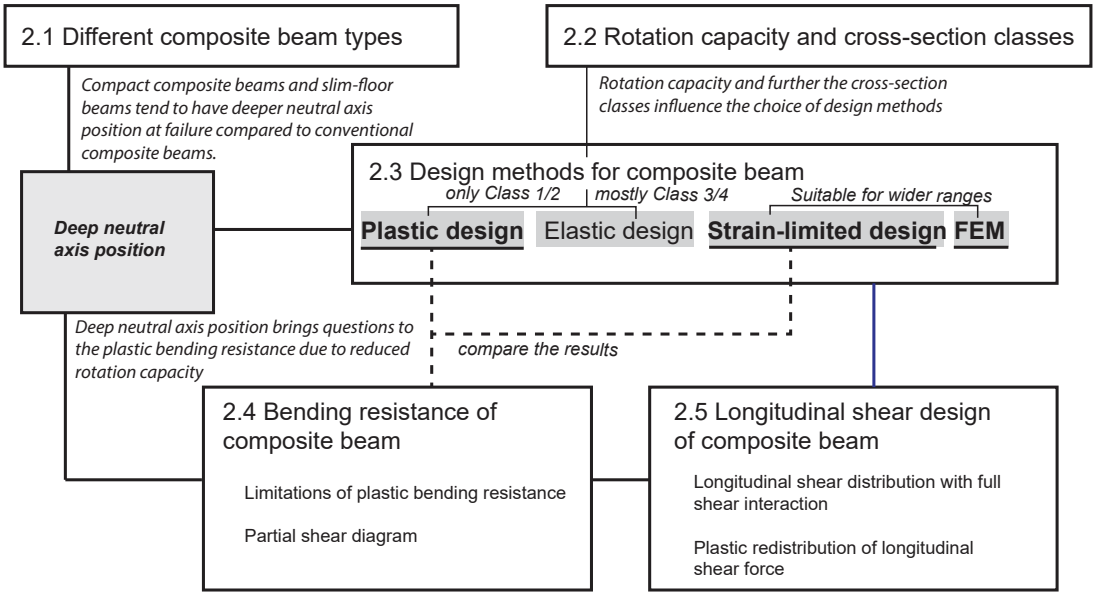

Figure 2.1 – Sections of the chapter 2

2.1 Different composite beam systems

The application of the steel-concrete composite beam can be traced back to the 19th century when engineers embedded steel sections into the concrete to increase its strength. The very first types of composite beams usually have very stiff shear connectors such as the welded L or channel sections on the beam. Introduction of headed studs and the welding guns greatly accelerate the application of composite beams, and standardized the conventional composite beam (Fig. 2.2) for buildings. It consists of a concrete slab laying on the top of the steel beam and connected by headed studs. The solid concrete slab was among the first developments, some of the early researches can be found in [14, 78, 93, 31]. Nowadays with solid slabs, researches move to new types of concrete such as fiber-reinforced concrete or high-strength [36, 40, 50, 16] and lightweight concrete [100] as well as new types of shear connectors. Profiled sheeting or partially prefabricated composite slab systems were successfully adopted. With the sheeting used as the permanent concrete form-work, the construction speed can be increased. However, the profile sheeting shapes can greatly change the shear connector behaviour, thus researches with different types of profile sheeting continues until today, some recent publication examples are [74, 58, 17, 52, 39]. The conventional composite beams usually have a large height ratio between the steel profile and concrete slabs, compact composite beams which have a smaller steel section height were researched in [76, 77, 37]. The composite beams with steel T-section (without the steel top flange) [102, 29, 37, 12] increases the moment of inertia with the same amount of material under sagging bending. Due to lack of top flange, the shear connectors are welded on the web or concrete dowel connectors can be used.

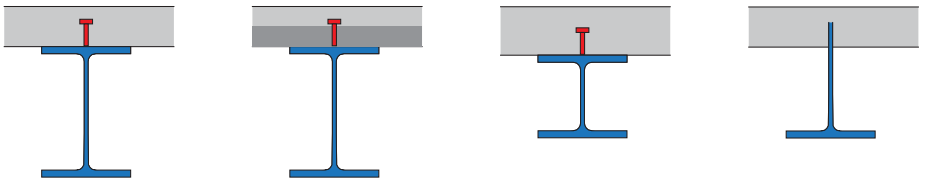

Figure 2.2 – Variations of conventional composite beams

Slim-floor composite beams (or shallow floor beams) refer to the composite beam system with the steel section partially or fully embedded into the concrete slabs. Compared to regular composite beams, slim-floor systems have a lower structure height. The flat appearance allows the easy arrangement of building services [15]. By using prefabricated members in slim-floor beams, it enables fast construction. Furthermore, fire-resistance is improved due to the concrete cover, for example, the "Thor Beam" can reach fires resistance grade R120 without applying any fire protection [65]. Usually, steel profiled sheeting or prefabricated slab members are used, which are supported by the steel bottom flange. Thus, the steel bottom flange is extended creating an asymmetric profile. There are many varieties of cross-section shape, especially of the steel beam profiles. In general, the steel beam section can be categorized into closed (boxed) forms and open forms. A summary of the commonly used steel beam section in Europe is given in Fig. 2.3. There are also different shear connector types designed for slim-floor beams. Because the space to install headed studs is limited, concrete-dowels connector created by cutting holes on the web or top flange are often used.

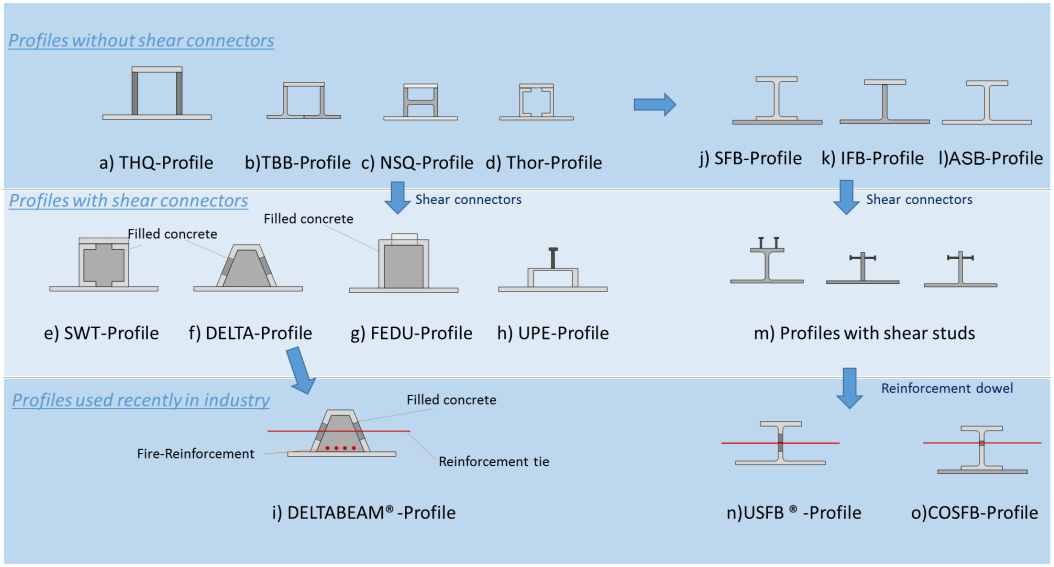

Figure 2.3 – Development of Composite Slim-floor steel profiles (also see [81])
references: a-g) [81], e) [80] j-l) [91, 57, 5], i) [81, 70], n) [98, 97], o) [10]

2.2 Composite beam rotation capacity and cross-section classification

The available rotation capacities (ϕ_{cap}) are represented by the maximum rotation angle of the beam at failure. In the design, it should be no less than the required rotation capacity (ϕ_{req}) which is related to different design methods. Another popular expression of rotation capacity is represented by the "R" value [53, 89, 33] (Fig. 2.5) which indicates the plateau length of the M-ϕ curve.

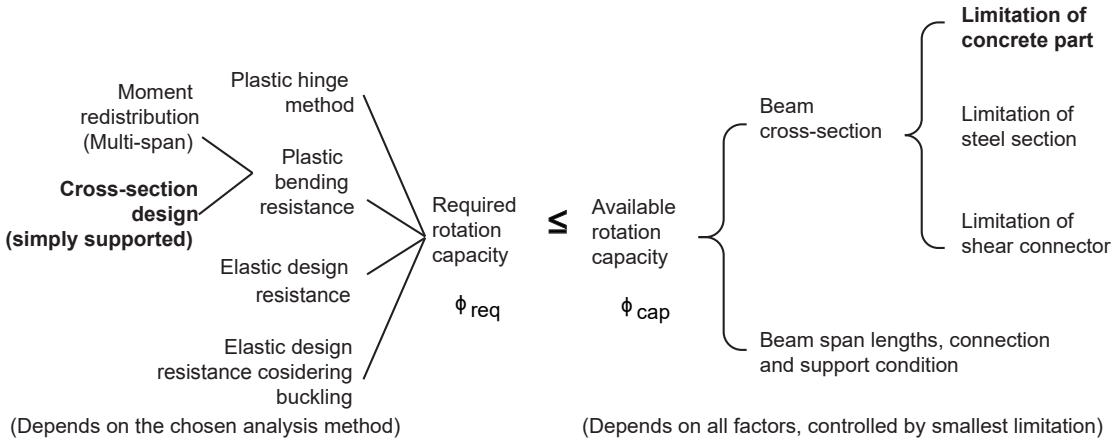

Figure 2.4 – Available and required rotation capacity (items in bold are main focus points for this work)

The required rotation capacity depends on analysis methods: For the plastic hinge method, rotation capacity is required to allow full redistribution of the bending moments in the structure until plastic hinges turn it into a mechanism. For plastic bending resistance, the required rotation capacity is linked to the strain distribution at the critical section for a simply supported beam, allowing to reach the plastic bending resistance (ϕ_{pl}); as well as plastic redistribution ability in continuous beam or frames ($\phi_{req} = \phi_{pl} + \Delta\phi$). The latter

requires higher rotation capacity, as the plastic resistances need to be further retained to allow bending moment redistributed to other sections. However, it is still less required than that for plastic hinge analysis. Eurocode 3 [20] classifies the steel sections into 4 classes related to their rotation capacity as shown in Fig. 2.5: Class 1 allows plastic hinge analysis; class 2 can be used for elastic analysis with consideration of plastic redistribution; class 3 and 4 sections only allow elastic analysis to calculate the action effects.

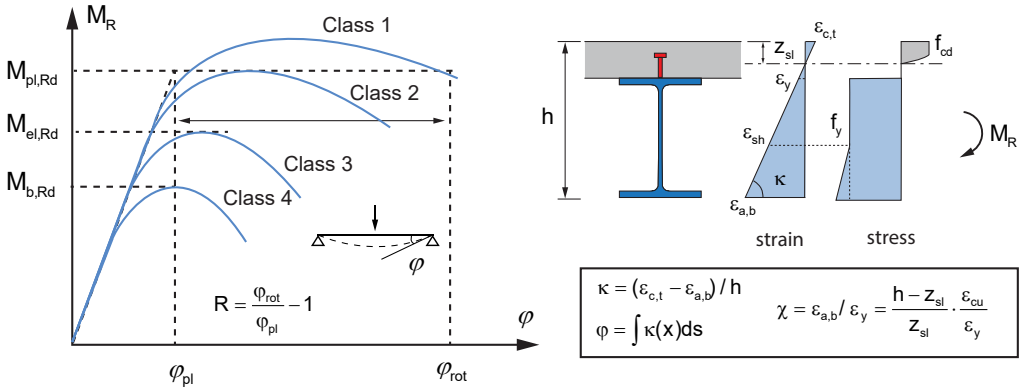

Figure 2.5 – Rotation Capacity and cross-section classification (also see [32])

The available rotation capacity for a steel beam is usually controlled by the local buckling of compression plates in the cross-section level. Thus local buckling checking based on maximum c/t ratios became the cross-section classification in current Eurocode 3. Haaijer[30] proposed that for steel construction, the plastic bending resistance should be performed only when the strain hardening can be reached before buckling. However due to strain-hardening after local buckling the beam can still further carry loads greater then plastic bending moment resistance, thus Kuhlmann [53] suggested adjustment of c/t ratio to represent the real rotation capacity based on the parameter "R" (Fig. 2.5) from test results. In [53] R=2 is suggested to be sufficient for a continuous beam, and R=5 can be reached under very severe conditions. The value also suggested to be 5 in [46] and 3 in [101].

The concept of cross-section classification and its determination based on the c/t ratio for steel plates were further adapted into Eurocode 4 [22] for composite structures. With cross-section classes, different global analysis methods and design resistances can be used (Fig. 2.6). For class 1 and 2 cross-sections, plastic bending resistance is allowed, class 3 only allows elastic analysis, and reduction of elastic bending resistance due to local buckling needs to be considered in class 4 cross-section.

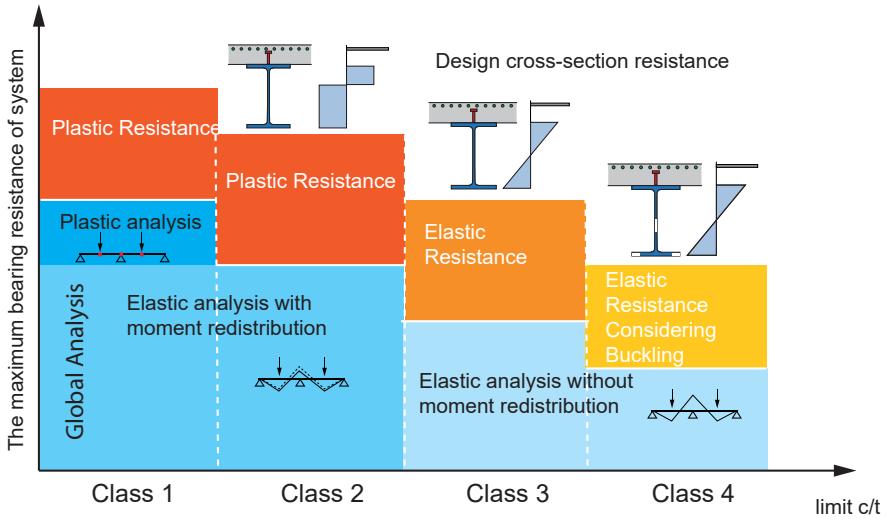

Figure 2.6 – Classification and design methods according to Eurocode 4 (also see [33])

However, the behavior of steel beams and composite beams are not exactly the same, as composite beams are also impacted by the concrete slab. For concrete beams, concrete compression failure before reinforcement yield is the main limitation of the rotation capacity. Thus the relative compression zone height is limited in Eurocode 2 [19]. Sedlacek [89] analyzed the plastic hinge theory of composite beams. He mentioned that for a composite beam under sagging bending, the concrete strain is the main limiting factor for rotation capacity while under hogging bending it is mostly controlled by the local buckling of steel plates. Further, he pointed out that due to the non-linear properties of concrete, the composite beam behaves non-linearly and does not have a clear boundary between elastic and plastic, which are different from the steel structure. Furthermore, sagging bending moment resistance can be much higher than hogging for a typical composite beam, thus it is questionable if the design rules for steel beam can be directly used for composite beams as well.

The required rotation capacity for composite beams was also investigated by other researchers. In [61, 64], the relationship between the amount of moment redistribution and required rotation capacity was provided. Nethercot [64] concluded, that in order to reach 30% moment redistribution in a semi-rigid composite frame rotation capacities should be greater than 20mRad. Rotter and Ansourian [79, 3] used a parameter $\chi = \varepsilon_u/\varepsilon_{sh}$ to represent steel bottom flange strain hardening level at concrete compression failure under sagging bending. $\chi = 1.0$ suggests strain hardening just reached at bottom of steel profile(ε_u), which indicates 10 times of yielding strain ($\varepsilon_{sh} = 10 f_y/E_a$). He suggested $\chi \geq 1.4$ should provide enough rotation capacity for plastic design collapse load in the worst combination of spans of loading. The required rotation capacity for different systems can however have a big variation, theoretical equations for continuous composite beams with semi-rigid connection were suggested in [49] with partial material and load safety factors considered, it is partly based on the work of [48, 64].

The available rotation capacity in a composite beam is related to many factors. Ban [7] researched composite beams with high strength steel, he concluded that the available rotation capacity of composite beams is mostly affected by span to depth ratio, as well as the depth ratio of the plastic neutral axis and steel yield strength, empirical equations are provided based on parametric studies. Sedlacek [89] also concluded different influence parameters and provides simplified equations for hogging bending.

In this work, only the required rotation capacity for the cross-section plastic bending moment design is focused. It should be noticed to apply moment redistribution and plastic hinge methods for continuous composite beams bigger rotation capacities are needed. Also as sagging bending is focused, the limitation of concrete strain rather than the buckling of steel section is usually the limiting factor for available rotation capacity if the cross-section is in class 1 and 2. (Fig. 2.4 item in bold)

2.3 Conventional engineering and advanced non-linear designs for composite beams in building

Both the elastic and plastic bending resistance are well established for composite beams. In Eurocode 4, choices of design methods are related to the cross-section classes (see section.2.2). The plastic bending resistance uses rectangle stress blocks, implying that plastic strains can be reached in nearly whole cross-section, thus class 1 or 2 cross-sections are necessary. Due to the redistribution of stresses by plastic behavior, the sequence of loading, effects of shrinkage and creep can be neglected at ULS. If, in addition, ductile shear connectors are used and slip is limited to the shear connector deformation capacity, also equal distance arrangement of studs is allowed. The elastic design method is used for SLS verification and the design resistance of class 3 or 4 cross-section. By the elastic design method, the sequence of loading, time-effects, cracking of concrete and influences of temperature can not be neglected. On the other hand, the shear connectors should be arranged based on the longitudinal shear force (V_L) distribution. Both methods consider the shear lag effects in the composite slab by using an effective width method. For composite beams with solid slabs, the effective width was well established. For slim-floor beams and compact composite beam further researches [25, 11, 77, 81, 32] were carried out.

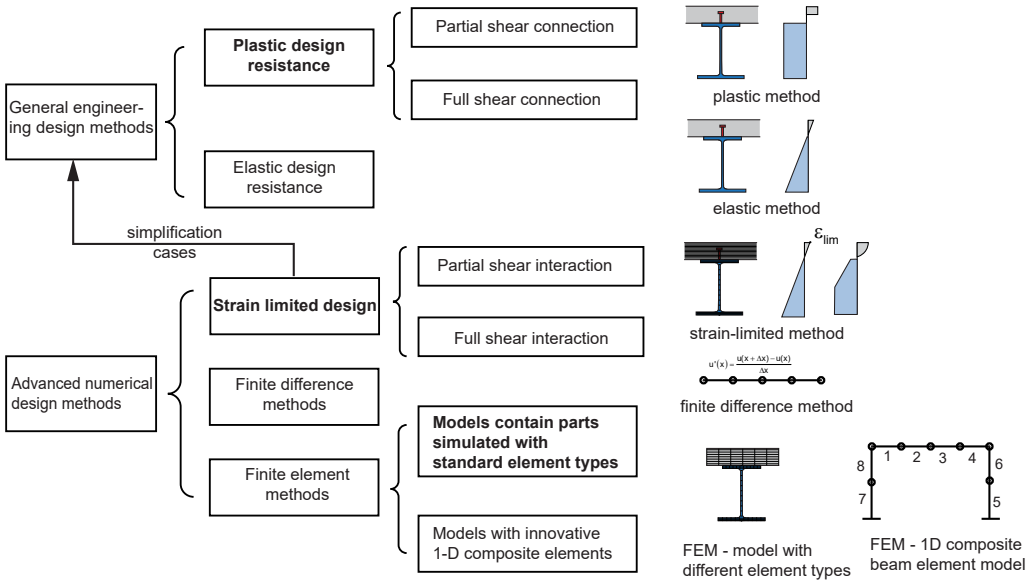

Figure 2.7 – Conventional elastic, plastic bending resistance and advanced numerical design methods

The conventional elastic or plastic bending resistance allow easy hand calculation. The design rules are usually developed for common composite beams and allow easy application in practice. To achieve more exact design results or to do designs out of

the code scopes, advanced design methods are important. Conventional approval for bending resistance based on plastic design with rectangle stress blocks, strain limits and uses assumption such as linear strain distribution inside the cross-section, and allows considering non-linear material properties. Strain-limited design is still required by Eurocode 2 [19], and suggested by Eurocode 4 for advanced analysis. Many former researches [34, 44, 92, 8, 16, 81, 103] were based on strain-limited design program for numerical analyses. With the development of computational tools and computers, Finite Element Methods (FEM) became more popular. With the fast development of multi-physics commercial FEM software such as ABAQUS or ANSYS, FEM grows more powerful and easier to use. Compared to strain-limited design, FEM has border application ranges, shear lag effects, buckling, fatigue etc. can be well simulated with the various element types to choose. Meanwhile, the strain-limited design still keeps its advantage in certain areas. It is based on the simplified mechanical model, thus it is usually faster and easier to perform and to transfer into simplified engineering solutions.

2.3.1 Strain-limited design for composite beams

Strain limited design for composite beam was well developed. Similar to concrete T-beam design in Eurocode 2 [19], linear strain distribution (Bernoulli-hypothesis) is assumed and the effective width is used. The partial shear interaction design assumes linear strain distribution only in individual concrete and steel part and the two strain curves are parallel to each other. The "Newmark model" [66], which is used in finite difference method analysis, also uses this assumption. For numerical approaches, the finite fiber method (see chapter 3.4.1) is often used. To use it, the cross-section is divided in to finite amount of tiny fibers, the stress is integrated over cross-section in each fiber to obtain the resultants such as normal force and bending moment. It is suitable for flexible dominated members where the influences from torsion and shear can be neglected. Local buckling can be neglected if the cross-section is class 1 or class 2 [22], otherwise, it can be checked based on the buckling strain limitations suggested by Kemp [47]. Although material constitutive relations are defined as uni-axial type, influences multi-axial stress states can be included through modifying the material properties. Such as the reduction of steel web strength due to bending-shear interaction [22] and the reduction of slim-floor bottom flange strength due to longitudinal and transversal bending interaction [33].

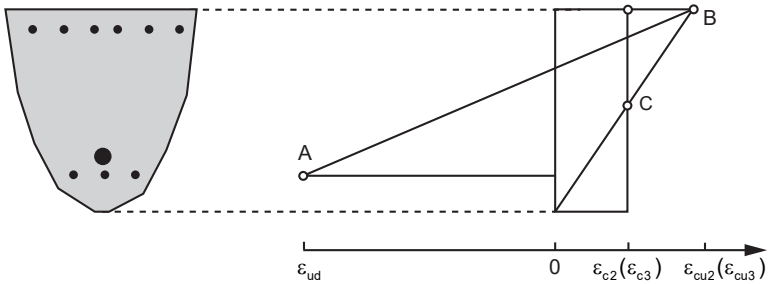

Figure 2.8 – Strain-limit points according to EN1992-1-1 [19]

The strain-limits can be taken as the ultimate material strain with certain modifications. For sagging bending, the concrete compression strain limit is usually the controlling strain limit. Its value can be taken as the ε_{cu} in Eurocode 2 [19]. For concrete classes no bigger than C50/60, $\varepsilon_{cu} =$ -3.5 ‰ is used. in addition, In the current Eurocode 2, the concrete compression strain needs to be reduced if the whole cross-section is in compression

(Fig. 2.8), similarly for the case if the slab in the concrete T-beam is mostly in compression. However, this rule has still been modified in the draft version of the second generation code prEN1992-1-1:2019 [72]. The modification considers fixed strain limited point at the top, section 3.2.1 gives more details of the comparison of strain -limited points. [103] provides a summary of strain-limited design for slim-floor beams as well.

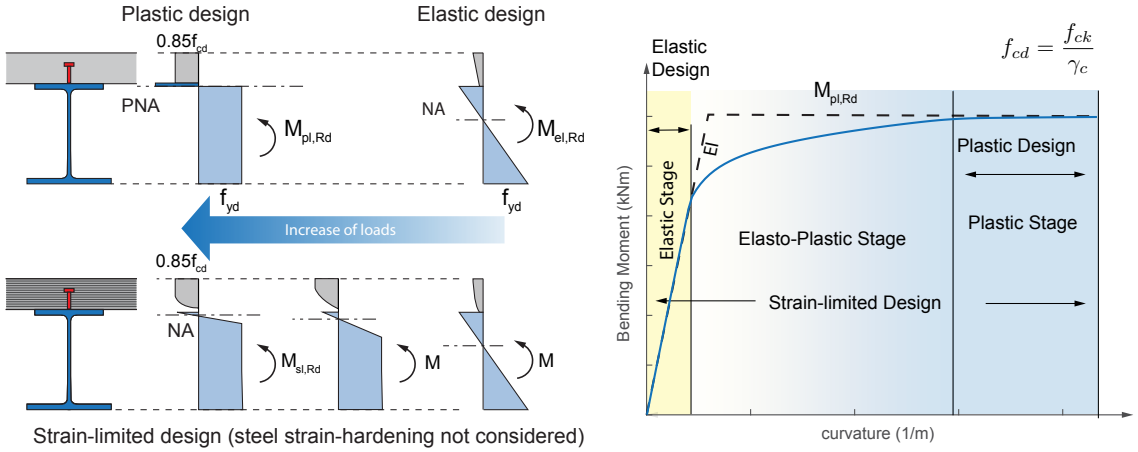

Figure 2.9 – Comparison of strain-limited design to elastic and plastic bending resistance according to EN1994-1-1:2004

Non-linear numerical strain limited design was applied in many research topics. It reflects the non-linear material properties. Elastic and plastic bending resistances are the simplifications of strain limited design for special cases (see Fig. 2.9). In [34] non-linear strain limited design is used to analyse plastic bending resistance limitation and reduction of composite beam with steel grade S420 and S460. In [44], the program "EPPIB" was used to analyse the minimum degree of shear connection. In [8], a program developed by the University of Kaiserslautern was used to analyse longitudinal shear force distribution and the influence of shear connector stiffness. Through the Moment-curvature relationship calculated by strain-limited design, the non-linear stiffness changes with load can be obtained. The rotation capacity of a composite beam and the moment redistribution due to plastic development can be calculated (Fig. 2.9). Recently in [37] use strain limited method to analyse the composite beams with concrete dowel shear connector and ultra-high strength concrete.

2.3.2 Plastic bending resistance for composite beams

The plastic bending resistance of composite beams is well established in many design standards, such as Eurocode 4 [22], Chinese JGJ138 [42]. When applying plastic cross-section resistance it is assumed that plastic strains are reached in most parts of the cross-section; thus rectangle stress blocks are used as simplification. The method is based on the equilibrium of the inner forces. With this assumption, the design is much simplified. For composite beams with small compression zone height, which big rotation capacity is expected, the plastic bending resistance has been proven to be reliable and safe [78]. For longitudinal shear design, with ductile shear connector used in addition, plastic redistribution of longitudinal shear force allows shear connectors to be installed with equal distance.

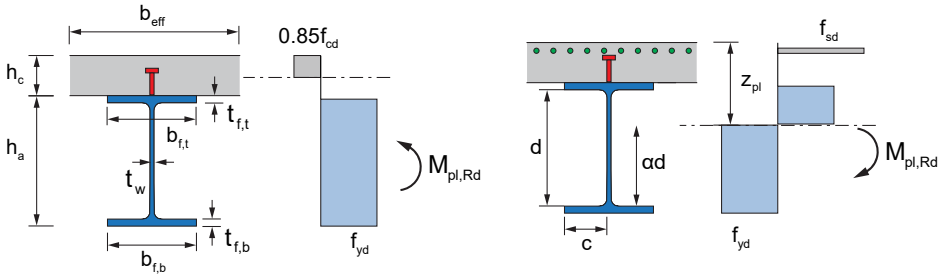

Figure 2.10 – Plastic bending resistance of composite beams according to EN1994-1-1:2004

2.3.3 Elastic design for composite beams

The elastic design method is widely used to calculate the stiffness and deflection of a composite beam in Serviceability Limit State (SLS). It represents the strain-limited design with low strain value and neglects the non-linear behavior of concrete. For class 3 and 4 cross-sections, only elastic design bending resistance is allowed according to the Eurocode 4. And for class 4, in addition reduction of bending resistance due to buckling should be considered. The changing of concrete properties with time influences the beam stiffness and resistance. For the convenience of calculation, the concrete slab can be ideally transferred into equivalent steel section with a reduction factor $n = E_a/E_{cm}$ applied on the cross-section area A_c and moment of inertia I_c (total cross-section method [33]). For long-term loads, except the elastic deformation, shrinkage and creep will cause additional deformation. It results primary effects in the simply supported beam and secondary effects in the continuous beam, thus further impacting the inner forces and stress distribution. For the hogging bending, the stiffness are influenced by concrete cracking.

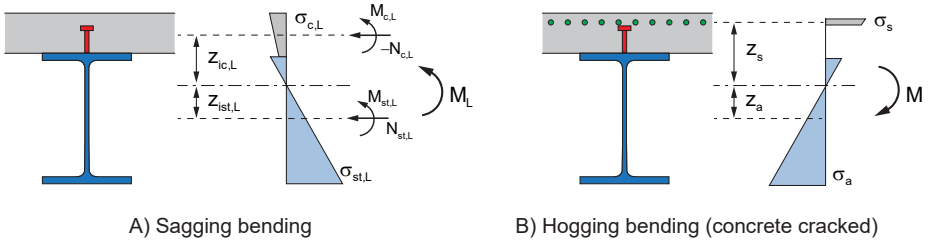

Figure 2.11 – Inner forces and stress of elastic design

Shrinkage of concrete will cause additional sectional forces due to the constrain of the steel part, which prevents the concrete from reducing its size. The additional inner force from shrinkage will form an internal equilibrium if the beam is statically determinate. First, the concrete section can be assumed to be isolated, the deformation caused by the free shrinkage strain $\varepsilon_{cs}(t,t_s)$ is reversed by the shrinkage force N_{sh}. Then the shrinkage force N_{sh} acts on the composite section as a compression force in the centroidal axis of the concrete slab. The forces acting of the whole cross-section can be calculated in the end [33].

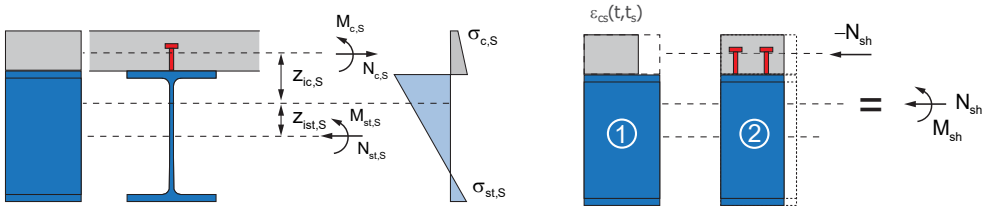

Figure 2.12 – Consider additional stresses from shrinkage of concrete

Additionally, the influence of the sequence of loading should also be considered for elastic design. If the beam is propped, the composite section will resist the loads together. For un-propped construction, the steel beam will take all the loads from self-weight, the weight of wet concrete, form-work and additional loads in the construction phase. Only after the concrete hardening, the extra loads applied afterward are shared by composite beams. In other cases, the concrete slab can be pre-stressed or additional deformation can be introduced at props, further increasing the steel section stress. The different sequence of loading greatly influences the stiffness of the composite beam.

2.3.4 Additional design rules for slim-floor beams

Current Eurocode 4 [22] does not provide specific design rules for slim-floor beams. The design methods are mostly derived from the plastic bending resistance for traditional composite beams with additional consideration of their special features. Additional design rules to Eurocode 4 are given for hot-rolled and box-sections in many research works [9, 57, 81, 56, 35, 84, 60]. The general design principles are summarized as follow: In the case of the full shear connection (Fig. 2.13) and sagging bending moment, the compression force consists of the integral of concrete stress bock ($0.85 f_{cd}$) and the compression blocks in the steel part (f_{yd}), while concrete in tension is neglected. For the concrete inside a box-section f_{cd} can be used, due to the better hardening conditions and confinement effects. Due to the interaction of vertical shear and normal stress from bending moment, according to EN1994-1-1 section 6.7.3.2, the steel strength of the steel web is reduced if half of the shear resistance is surpassed. In the case of important web openings, secondary bending moments due to Vierendeel-effects are to be considered for moment resistance and vertical shear design [82]. Furthermore, the effects of torsional moments can lead to an additional reduction of the moment and shear capacity. When the extended bottom flanges are used as supports for the concrete slab, a significant amount of transverse local bending moment can be generated. The interaction of the compression stress and tensile stress in the longitudinal direction reduces the design resistance. Thus, the bottom flange's design strength needs be reduced to $f_{yd,eff}$ (Fig.2.13) [81]. For the open sections, some researchers [9] have suggested using a reduced steel plate thickness to reflect this impact.

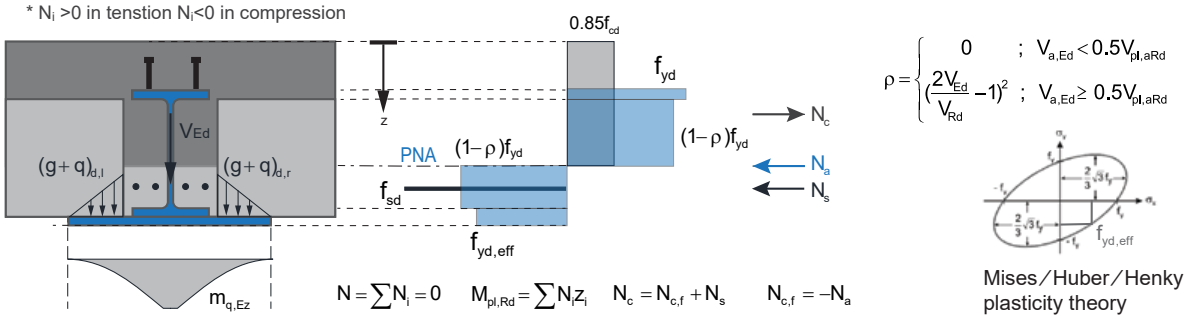

Figure 2.13 – Design of slim-floor beams by plastic method

2.3.5 Finite difference and finite element methods for composite beams

In elastic stage and with full shear interaction, the composite beam can be ideally simplified as a common beam member for global analysis. However with partial shear interaction, the influence of shear connector on beam stiffness is important. Based on the simplified models, differential equations related to inner forces and deformation can be built and solved by finite difference methods. One of the early applications is the "Newmark model" [66]. He provided the governing equations for one span composite beams in the elastic stage, considers the influence of shear connector stiffness. Impact of uplift at the joint were further introduced in [2, 62]. Application in continuous beams was expended later in [71, 41]. The consideration of non-linear material properties was also considered in a few works based on finite difference methods [23, 99, 75].

Recent years, the finite element analysis for composite beam becomes more popular. They can be divided into two categories: For the first category, each part of the composite beams (i.e., slabs, steel beam shear connectors) are modelled individually using the combination of standard 3D, 2D or beam/link finite elements. Different material models can be applied to each part. Usually, this type of model is used for member analysis instead of a global analysis. Often the shear connectors are simplified as non-linear spring connection elements instead of 3D explicit models.

The second category introduces innovative 1-D beam elements for composite beams. Slip and influence of shear connectors are simulated by introducing additional degrees of freedom at the nodes and redefined stiffness metrics. Currently, many new beam elements have been developed. They can be divided into two sub-groups considering the ability to simulate only full shear interaction or partial shear interaction. Alternatively, based on the approaches, they can be divided into displacement-method, force-method or mixed-method. The extensive developments of new finite element models cover the behaviour of material non-linearity, concrete cracking, slip, creep and shrinkage, fatigue and other features. However, due to the difficulty of integration into the common commercial FEM software, their application is limited. Detailed summaries of the related FEM models can be found in [6, 75, 95].

2.4 Bending design resistance of composite beams

The bending resistance for strain-limited design is calculated on the conditions that the equilibrium of internal force is reached, meanwhile strain limits are not exceeded. For elastic design linear stress blocks are assumed, and for plastic bending resistance

rectangle stress blocks are assumed. Elastic and plastic bending resistances are in-fact simplifications of the strain-limited resistances for special cases (section 2.3.1). If the beam has enough rotation capacity allowing most fibers to yield, rectangle stress blocks provide close enough result to non-linear stress distribution if strain-hardening is not considered [78]. Elastic bending resistance is calculated based on linear stress distribution for the situation, in which the critical fibers of cross-section first reach plastic strain. If at failure, only a limited part of cross-section fibers can yield due to limitation of either concrete compression strain or buckling of steel plates, plastic bending is not suitable. Thus elastic resistance should be used unless more advanced non-linear calculation is provided. The design resistance is calculated using the design material strength for ULS with consideration of material safety factors.

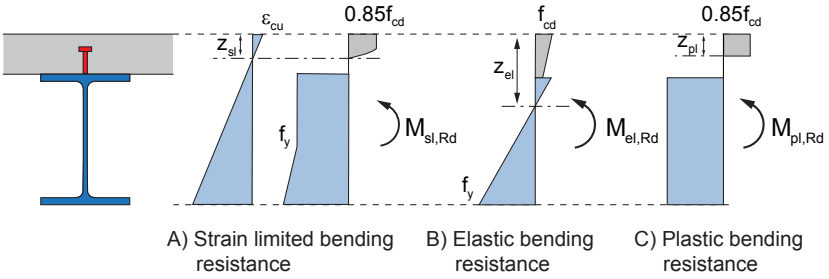

Figure 2.14 – Bending resistance of strain-limited, plastic and elastic design of composite beam with full shear interaction

For the design of reinforced concrete beams according to Eurocode 2, the plastic bending resistance based on rectangle stress blocks is not preferred. Instead, the parabolic rectangle stress block is assumed for concrete and the concrete design strength is $f_{cd} = \alpha_{cc} f_{ck}/\gamma_c$ which for the EN1994-1-1 $f_{cd} = f_{ck}/\gamma_c$ is used. The parabolic shape of stress distribution and its rectangle simplification results in different neutral axis position. For the design of composite beams according to Eurocode 4, concrete strength is taken as $0.85 f_{cd}$. However, the reduction factor of "0.85" is related to the long-term effects of concrete and calibration from tests rather than the different neutral axis position [87]. As the plastic bending resistance is based on the equilibrium of forces in steel and concrete, when relative compression zone height "z_{pl}/h" is small, the difference of bending moment resistance caused by stress block shapes are very small [87].

The full shear connection is reached when an increase of the number of shear connectors within the critical length does not lead to a further rise in the moment resistance. The section is assumed to remain plain, and only one neutral axis exists (Fig. 2.14). This assumption is in-fact an approximation of full interaction, which means no slip happens at the joint [43]. Usually at full shear connection, the slip is small enough to be neglected. However, if the shear connector stiffness is too small, this approximation may be inaccurate due to significant slip still exists at full shear connection [68].

When shear connector arrangement is controlled by detailing, such as the geometry of profile sheeting allows only one or two connectors installed per rib or the proof in SLS become decisive, often partial shear connection is realized in the sagging bending area. For hogging bending, partial shear connection is not allowed by Eurocode 4, due to the risk of failure at the support area. On the other hand, in the hogging bending regions, the longitudinal shear force from reinforcements is small; thus, full shear connection can be easily reached. With partial shear connection, the bending moment resistance is limited by the longitudinal shear resistance transferred by shear connectors inside the

shear span. The neutral axes in (reinforced) concrete part and in the steel beam are separated. By plastic bending resistance and ductile shear connectors, the equilibrium between total longitudinal shear force transferred by shear connectors inside a shear span ($\sum_{P_{Rd}}$) and the compression force in concrete and tensile force in steel (N_c and N_a) results in two separated neutral axis position. By strain-limited design, a pair of parallel strain curves in the two parts are assumed (Fig. 2.15). The strain-limited bending resistance can be calculated by using an iterative numerical procedure; details can be found in [103].

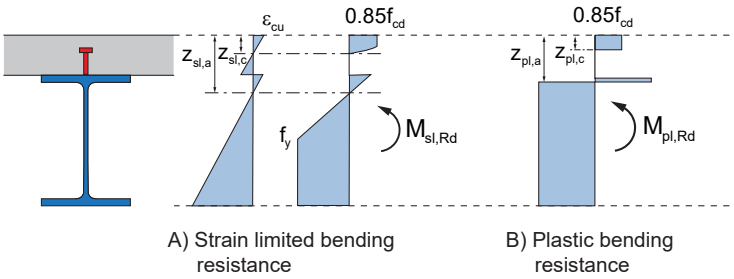

Figure 2.15 – Bending resistance of strain-limited, plastic and elastic design of composite beam with partial shear interaction

2.4.1 Limitation of plastic bending design resistance and the β reduction factor

The plastic bending resistance does not always give precise results. For full shear connection, if the compression zone height is petite, due to strain-hardening of the steel section, an increase up to30% of sagging design bending resistance by strain limited method compared by plastic bending resistance may be expected [53, 26].

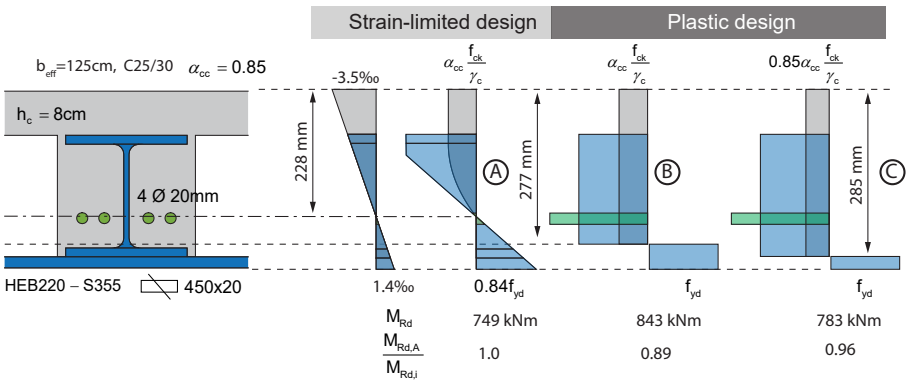

Figure 2.16 – Comparison of plastic bending resistance and strain-limited resistance of slim-floor beam

On the other hand, according to Eurocode 4, if the value of relative compression zone height "z_{pl}/h" is bigger than 0.15 for steel grades S420 and S460, a reduction factor β (Fig. 2.17B) on plastic bending moment resistance should be applied to prevent overestimation of plastic bending resistance. The reason for it is shown in Fig. 2.16. When the neutral axis is deep, due to the limitation of the small concrete compression strain limit, a high percentage of steel section can not yield (Fig. 2.16 A). Thus the assumption of rectangle stress blocks by plastic bending resistance Fig. 2.16 B) is not suitable and may lead to an overestimation of design resistance. Even with the concrete strength further reduced by 0.85 Fig. 2.16 C), the plastic design result is still higher. This overestimation is

more serious with high strength steel, which has higher yield strain. For a conventional composite beam to reach economical designs, the relative compression zone height z_{pl}/h is usually small. Thus plastic bending resistance gives good results. For slim-floor beam or compact composite beams, z_{pl}/h is much bigger; thus, limitations of plastic bending resistance should be rechecked. The background for this rule can be found in the work of Hanswille and Sedlacek [34], in the work a reduction start from $z_{pl}/h = 0.15$ was applied until $z_{pl}/h = 0.3$ a reduction of $\beta = M_{sl,Rd}/Mpl,Rd = 0.9$ was applied. This proposal was later modified and included in the current Eurocode 4. However, [34] was only based on the conventional composite beam cross-section, and strain hardening is not considered. Further analysis [16, 83, 81, 37, 87, 85, 86] were provided to include also slim-floor beam and other types of composite beam cross-section. For example, in the dissertation of Schäfer [81], the reduction factor for slim-floor beams are provided for the first time. Schäfer and Banfi [83] later extended the cross-section types to asymmetric composite beams and slim-floor beams. Helnmeyer [37] and Döinghaus [16] also investigate the β factor considering the high strength concrete and conventional composite beams. The [86] also adopted the new concrete and steel models for draft versions of new Eurocode 2 PrEN1992-1-1:2019 and prEN1993-1-14 a newly added code for non-linear numerical design.

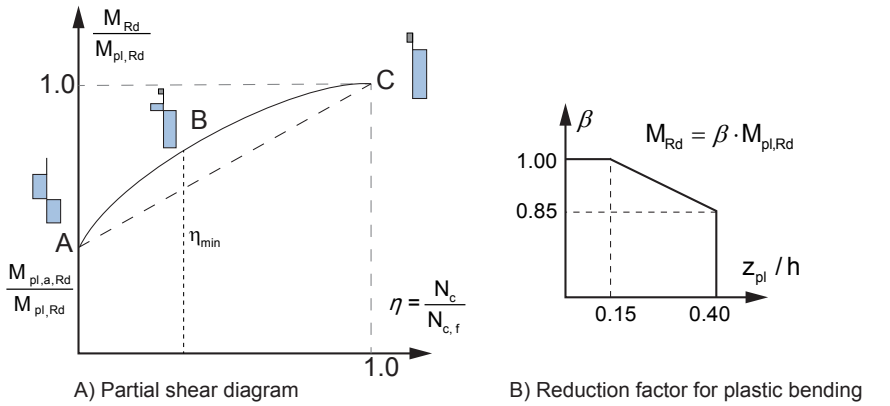

Figure 2.17 – Partial shear diagram and reduction factor for bending moment according to Eurocode 4

2.4.2 Partial shear diagram of composite beam

The bending moment resistance of partial shear connection can be calculated by solving the equilibrium equation according to plastic theory. A more practical way is to use the partial shear diagram provided in Eurocode 4 [22] (Fig. 2.17 A). This diagram is developed using the plastic bending resistance. A non-linear ABC curve or a simplified linear line AC can be adopted (A: no shear connection, B: zone of partial shear connection, C: full shear connection). Here the degree of shear connection is defined as $\eta = N_c/N_{c,f}$ where N_c is the total normal force in concrete slab, and $N_{c,f}$ is the value with full shear connection. Design moment resistance in the case of partial shear connection can be then easily obtained from the previously calculated plastic bending moment of composite section $M_{pl,Rd}$ and the pure steel section $M_{pl,a,Rd}$. If a solid slab with a large amount of reinforcement is used, the slab's contribution should also be considered at least in SLS [35]. The partial shear diagram is widely used for composite beams. Eurocode 4 does not limit its usage for beams with limited rotation capacity where the plastic bending resistance may overestimate the bending resistance. It is usually not

a problem for conventional composite beams as the deep neutral axis is rare to see, for slim-floor and compact composite beams, it is still questioned if the partial shear diagram can still be used.

2.5 Longitudinal shear design of composite beam

The shear connectors' principal task is to join the steel effectively and concrete parts both vertically (uplifting) and longitudinally (longitudinal shear). For most conventional composite beams with headed studs, the impact of uplifting is usually small [45]. Thus the reliable transfer of the longitudinal shear force is the most important design aspect. Longitudinal shear can be transferred through mechanical shear connectors, friction and surface bond. Surface bound can significantly increase the initial stiffness in the elastic stage, as shown in beam tests. However, it is prone to concrete shrinkage and creep [14] and extensive slip. In the plastic stage, the bond is mostly lost in the connection [60]. Thus it is usually not considered in the design. Friction can contribute to longitudinal shear, however this is influenced by many factors such as surface treatments, concrete cracking, and loading types. A few pure friction-based shear connectors have been developed for demountable composite beams and slim-floor beams. The most popular method is through mechanical shear connectors, Normally ductile shear connectors such as headed studs are used to allow longitudinal shear redistribution. Shear connectors are usually installed with small distance to transfer the longitudinal shear smoothly.

For longitudinal shear design with mechanical shear connectors, two principal criteria should be fulfilled:

- The resulted longitudinal shear force from the loads in any part of the composite beam joint should be no bigger than the design longitudinal shear resistance provided by shear connectors. And the concrete parts should also be designed to prevent shear off around the connector or at critical sections. ($V_{L,Ed} \leq V_{L,Rd}$)
- The slip developed at the joint ($\delta_{E,i}$) should be no bigger then the deformation capacity of shear connectors ($\delta_{u,i}$) to prevent "un-zip" type of shear connector failure. ($\delta_{E,i} \leq \delta_{u,i}$)

The shear connector properties and arrangements influence the longitudinal shear force and slip distribution. Thus it is difficult to directly verify the two design criteria. Numerical iterative procedures are required for most of the situations. However, based on simplified shear connector mechanical models, a few special cases can be solved easily:

- Composite beam with zero shear interaction, where longitudinal shear force equal to zero.
- Composite beam with full shear interaction, where slip equal to zero.
- Composite beam with rigid-ideal plastic shear connector model for ductile shear connectors, allowing plastic redistribution of longitudinal shear force (Eurocode 4 [22]).

The first two situations mark the theoretical boundaries of a composite beam. With zero shear interaction, the longitudinal shear force equal zero for the whole joint. Thus the theoretical maximum slip value and lowest beam stiffness and resistance can be obtained.

On the other hand, with full shear interaction, the slip equals zero, the highest beam stiffness can be achieved (however not necessarily the maximum bending resistance). The rigid-ideal plastic shear connector model for ductile shear connectors allows plastic redistribution of longitudinal shear force. Thus shear connector with equal distance inside one shear span is allowed, and linear longitudinal shear force distribution is expected.

The current plastic bending resistance in Eurocode 4 [22] considers plastic development in cross-section as well as plastic redistribution of longitudinal shear force to allow equal distance arrangement of ductile shear connectors. The impact of the two types of plastic are explained below:

2.5.1 Longitudinal shear distribution with full shear interaction considering plastic development

Full shear interaction refers to the situation where the concrete and steel parts are perfectly connected with zero slip happen at the joint [43, 68]. The assumption results in only one neutral axis in the cross-section and linear strain distribution, which allows effective stiffness of cross-section easily obtained. In this case, the infinite stiffness and resistance of shear connectors are assumed. Thus longitudinal shear force distribution is separated from the shear connector influences, and the maximum possible stiffness of a composite beam can be obtained.

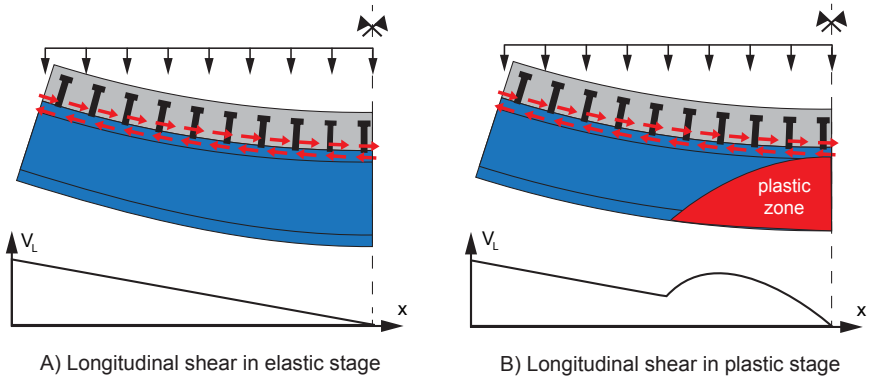

Figure 2.18 – Longitudinal shear distribution of full shear interaction in elastic and plastic stage (also see: [33])

In the elastic stage, it is well known that the longitudinal shear force is proportional to the vertical shear force. For a simply supported composite beam with uniform distributed load, inside the shear span longitudinal shear force linear increases from mid-span to beam end. This relationship is used for the elastic design method [33]. In the post-elastic stage, non-linear distribution of longitudinal shear force influenced by the plastic development of steel section and concrete [78]. In [8], the longitudinal shear force distribution at full shear interaction was compared with different shear connector stiffness. In [81] based on FEM calculation of a slim-floor beam, the shear forces with high stiffness shear connectors were plotted, which shows a similar distribution pattern. However, the calculation of the non-linear longitudinal shear force distribution without plastic redistribution requires usually numerical calculation methods. If the exact longitudinal shear distribution at the plastic stage is known, shear connectors can be arranged based on it to allow plastic bending resistance [33].

2.5.2 Plastic redistribution of longitudinal shear force with ductile shear connectors

Rigid-plastic shear connector model (where the shear connectors have infinite initial stiffness and followed by a perfect plastic behavior, Fig. 2.19) for ductile shear connector allows considering plastic redistribution of longitudinal shear force at ULS in a simple way. For partial shear connection, if the longitudinal shear force is limited by the shear connector resistance (P_{Rd}), its value is proportional to the shear connector numbers per unit length. With the uniform distance of shear connectors and low degree of shear connection, theoretically a constant longitudinal shear force distribution inside the critical shear span is expected. However, with partial shear connection, considerable slip can develop at the joint. Thus ductile shear connectors should be provided to prevent the shear connector failure. Furthermore, the rigid-plastic shear connector model does not consider the influence of shear connector initial stiffness. Low stiffness shear connectors can still reduce the effective degree of shear connection [68] as part of the connectors does not reaches design resistance at failure, thus the required shear connector numbers calculated by N_c/P_{Pd} should be increased, in order to provide enough compression force (N_c) in concrete slab.

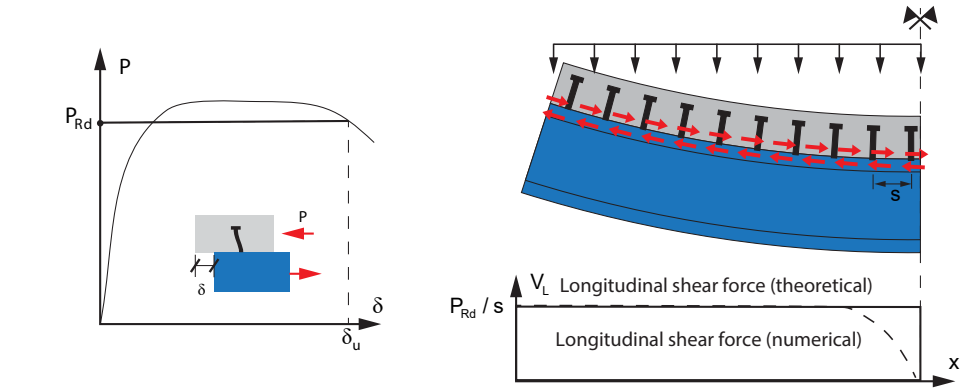

Figure 2.19 – Longitudinal shear design of composite beam by plastic method

Chapter 3

Strain limited design for composite beams

General strain-limited design can refer to all design methods based on strain limits checking, no matter if it is based on FEM, other numerical methods, or analytical approaches. Design resistance and other design values are limited by ultimate strain Thus, it is named "Strain limited design". Eurocode 2 provides the principles of strain limited design for concrete structure members, which are further extended to Eurocode 4 by integrating structural steel. In this work, strain limited design is more focused on this approach from the Eurocode.

The strain-limited design resistance is calculated by setting the strain-limits at critical fibers and find the strain distribution through an iterative process until reaching the equilibrium between inner forces and external forces in the cross-section. To link the deformation to loads, the Moment-curvature relationship ($M-\kappa$ curve) can be used instead of the constant stiffness "EI" in the elastic analysis. The $M-\kappa$ curve represents the continuous change of stiffness with loading representing the non-linear material behaviour. Thus, it can be used to calculate beam deformation at different loads. For partial shear connection, another ingredient "the slip strain ε_{slip}" can be added into the $M-\kappa$ curve, the three parameters can create a 3D solution surface. With the $M-\kappa(\varepsilon_{slip})-N_c$ surface, which is newly introduced in this work and shear connector information. It is possible to calculate the load-deformation relationship as well as the slip development of a composite beam.

In this chapter, the theoretical background of strain limited design is provided in the section 3.1, mechanical assumptions, and basics of the mechanical relationship such as the material constitutive laws, equilibrium conditions, kinematic compatibility are discussed. Afterwards in section 3.2 and section 3.3, the special solutions such as the design bending resistance and load-deflection curves calculated with "$M-\kappa(\varepsilon_{slip})-N_c$" surface as well as longitudinal shear distribution are given. In section 3.4, the different numerical approaches to effectively solving the mechanical models presented in the sections mentioned before are presented. The conventional finite slice method and innovative methods developed in this work, i.e. finite cell method, material strain integral method and simplified direct analytical method are compared. In section 3.5, a new developed simplified engineering approach allowing strain-limited design by hand calculation is explained. Fig. 3.1 provides an overview of the content of this chapter.

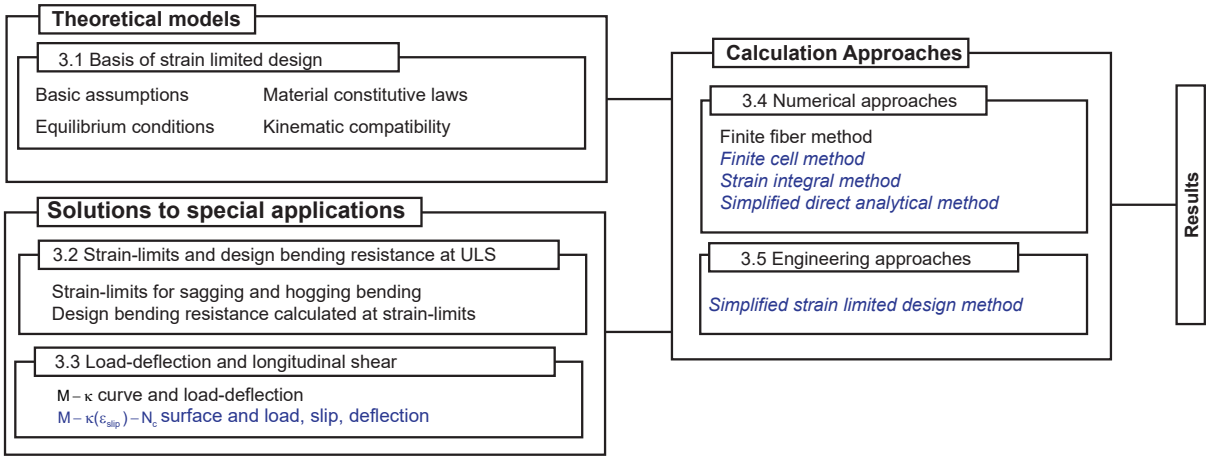

Note: font in italic and blue represents topics with new developments

Figure 3.1 – List of content for chapter 3

3.1 Basis of strain limited design

3.1.1 Basic assumptions and limitations

The strain-limited design of the composite beam used in this work bases on the Eurocode 2 [19], where linear strain distribution (Bernoulli hypotheses) is assumed. For composite beam with full shear interaction, no slip exists at the joint, the cross-section always keeps plain. For partial shear interaction slip exists, linear strain distribution is validated only inside each of the steel and concrete parts. Furthermore, the two separated strain curves are assumed parallel to each other i.e. the curvatures keep the same. The stress distribution is the outcome of strain distribution and material constitutional law. In this work, only uni-axial strain-stress relationships are used; multi-axial stress interaction can be considered through the equivalent simplified approaches for example to apply a reduction factor on the design strength. Such methods can also be extended for strain limited design. The following assumptions are made to simplify the calculation procedure with strain limitation design and remain acceptable accuracy:

- Linear strain distribution is assumed in the whole cross-section with full shear interaction or two parallel strain lines in steel and concrete, each with partial shear interaction. The considered beam should be flexural behavior controlled.
- Shear-lag effects of the concrete flange are simplified by the effective width. The strain value at the same height of cross-section is assumed to be equal. The cross-section can be vertically divided into different fibers.
- Strain-limited design resistance achieved when any of the cross-section fibers reaches its strain limits defined by the material model or other limitations while design strength values are used. If not specified, concrete in tension should be neglected.
- Different uni-axial material models can be adopted, multi-axial stress interaction is considered by the simplified method according to Eurocode 4 [22] or other simplified methods.
- For partial shear connection, slip exists along the longitudinal direction, but no separation is considered at the joint.
- Stress concentration at support regions or pointed load applied areas is not considered, shear deformation is also neglected.
- Stability problem such as local bucking of steel section or global buckling is not considered. The steel plates under compression either have big enough c/t ratio or proper detailing to prevent the buckling. Thus only class 1 or class 2 cross-sections according to Eurocode 4 are assumed in this work.

3.1.2 General mechanical relationships

Based on the assumptions, the mechanical relationship among the action effects, strain, stress, deformation and shear connectors for strain-limited design is shown in Fig. 3.2. It can be divided into cross-section and longitudinal shear analyses. For cross-section analysis, the relationship between action effects (inner force) and strain distribution can be formulated. The design resistance of the cross-section can also be directly calculated

at the defined strain-limits. For longitudinal analysis, the beam can be divided into finite slices along the beam length, with each slice is represented by an individual cross-section. The strain information in each can be obtained by cross-section analysis. Based on kinematic compatibility and boundary conditions and deformation compatibility, beam deformation can be numerically calculated from strain distribution. Furthermore, the longitudinal shear force distribution and slip development can also be obtained.

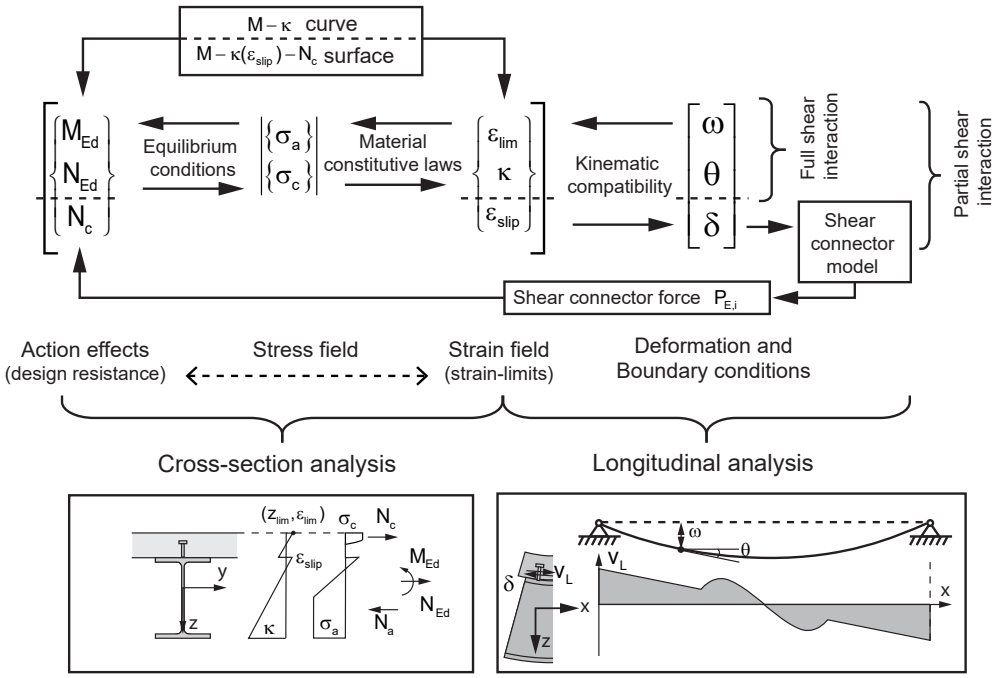

Figure 3.2 – Mechanical relationship for strain-limited design

The mechanical relationship of the full shear interaction situation is much simpler than the partial shear interaction situation, for which only the part above the dashed line in Fig. 3.2 is needed. The strain field can be determined by the strain limit point ($z_{lim}, \varepsilon_{lim}$) and curvature ($\kappa$). For action effects, at least the bending moment (M_{Ed}) and normal force (N_{Ed}) are necessary to find the related strain field. With partial shear connection, a new variable slip strain (ε_{lim}) is added in the strain field. To determine the strain field with three unknown, it requires also compression force in the concrete part (N_c) as additional action effects parameter. The value of N_c, however, can not be determined only within cross-section analysis. Furthermore, the information of shear connector $P-\delta$ relationship and arrangement are also needed as $N_c = \sum P_{Ei}$. The details of equilibrium conditions, material constitutive laws, and kinematic compatibility are given in the following subsections.

$$\{M_{Ed}, N_{Ed}, N_c\} = F\{\varepsilon_{lim}, \varepsilon_{slip}, \kappa\} \tag{3.1}$$

$$\{\varepsilon_{lim}, \varepsilon_{slip}, \kappa\} = F^{-1}\{M_{Ed}, N_{Ed}, N_c\} \tag{3.2}$$

With the known strain distribution, it is easy to obtain the inner forces inside a cross-section, which can be formulated as Eq. 3.1. However, it is more difficult to find the reverse function of F^{-1}, i.e. to find the strain distribution, which is represented by the curvature values (κ), strain at limiting point (ε_{lim}) and slip strain (ε_{slip}), from the action effects. One practical way for full shear interaction is to use the $M-\kappa$ curve to backward-calculate the curvature from the moment. For partial shear connection as the slip strain

is unknown, the newly developed $M-\kappa-N_c$ surface can be used instead. The details are given in section 3.3. It has to be mentioned that because the Function "F" is a continuous but not necessary monotonically increasing function, the F^{-1} may have multi solutions. However, the correct solution can be selected out through other mechanical limitations and numerical calculation techniques.

3.1.3 Material constitutive laws

3.1.3.1 Concrete

The concrete models used in the analysis are based on Eurocode 2. The parabolic-rectangle stress-strain relationship in EN1992-1-1 3.1.7, and the non-linear stress-strain relationship defined in EN1992-1-1 3.1.6 are adopted in this work (Fig. 3.3). The compression strain limits are related to concrete classes, up to C50/60, the value of 3.5 ‰ is used in the current code. While with high strength concrete, the ductility is reduced, thus a smaller strain limit is expected. However, test results show for many cases, the concrete strain limit can go much beyond the given value in the code. Thus the draft version of the next generation of prEN1992-1-1:2019 [72] suggests to use 3.5‰for all concrete classes; on the other hand, the design resistance is reduced to consider the brittle properties.

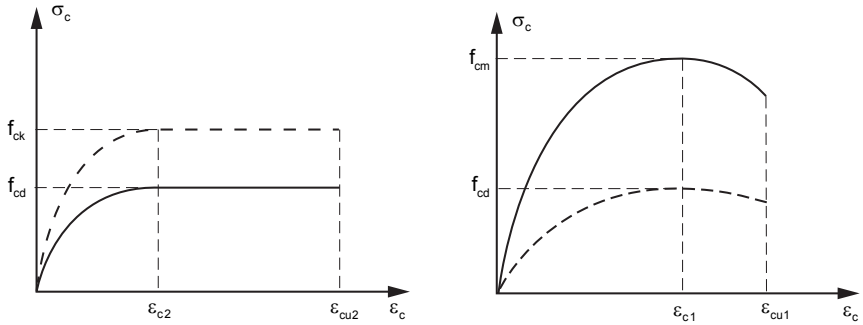

Figure 3.3 – Parabolic-rectangle and nonlinear concrete model according to Eurocode 2 [19]

The non-linear concrete model uses mean concrete strength (f_{cm}), which represents the strength values by tests according to EN12390-13 [18]. However if the model is used for design purpose, according to EN1992-1-1 5.8.6, the f_{cm} should be substituted by f_{cd}, and the E_{cm} should be replaced by E_{cd}, with $E_{cd}=E_{cm}/\gamma_{cE}$. In the new draft version of code prEN1992-1-1:2019 [72] this model still have been partly modified due to new concrete stiffness values. Other non-linear materiel models collected from literature are listed in Appendix A. It is also important to notice the definition of f_{cd} in Eurocode 2 is $f_{cd}=\alpha_{cc}f_{ck}/\gamma_c$, however in Eurocode 4 and also in this dissertation $f_{cd}=f_{ck}/\gamma_c$. The term α_{cc} is removed, and usually a reduction factor 0.85 is used, as $0.85f_{cd}$ represents the concrete strength in design situation of a composite beam.

3.1.3.2 Reinforcement

The bilinear stain-stress relationships by Eurocode 2 with or without strain-hardening are used in the analysis. The strain-stress relationships are shown in Fig. 3.4. The strain-hardening is considered by a factor k of the ratio between ultimate tensile strength to characteristic yielding strength. The yielding strain values can be calculated based on

the strength, and the elastic modulus E_s is $2 \times 10^5 N/mm^2$, however, it is allowed to use also $2.1 \times 10^5 N/mm^2$ in EN1994-1-1 for composite structures. The k values and the characteristic ultimate strain values "ε_{uk}" are given in EN1992-1-1.

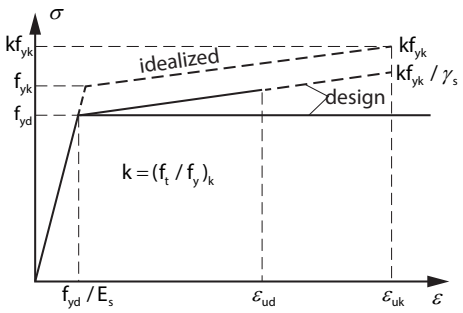

class	A	B	C
f_{yk}	400-600 N/mm²		
k	≥1.05	≥1.08	1.15 to 1.35
ε_{uk}	≥2.5	≥5.0	≥7.5

Figure 3.4 – Reinforcement stress-strain relationship by Eurocode 2

3.1.3.3 Structural steel

EN1993-1-5 provides four different strain-stress relationships: The model a) is the bi-linear relationship without strain hardening. Model b) considers a nominal plateau slop with a very small value, which can be similar to the model a). The model c) is a bi-linear curve with strain hardening. The model d) is the stress-strain curve modified from tests. The stress-strain relationship models are illustrated in the figure below:

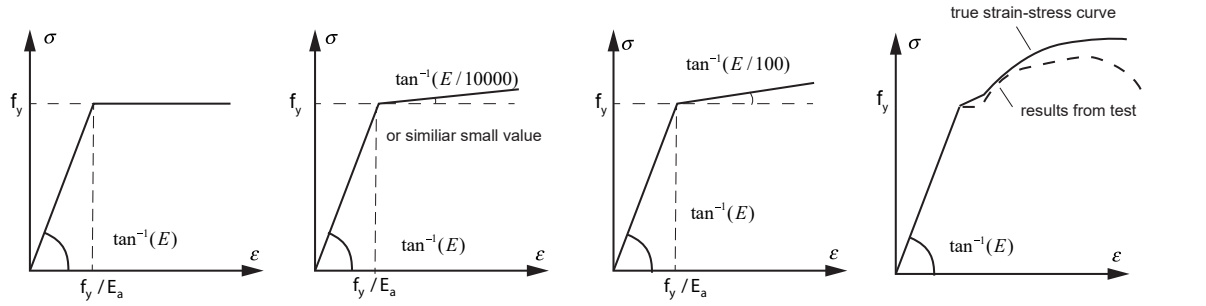

a) elastic-plastic without strain hardening

b) elastic-plastic with a nominal plateau slope;

c) elastic-plastic with linear strain hardening;

d) true stress-strain curve modified from the test results

Figure 3.5 – Steel stress-strain relationship according to EN1993-1-5 [21]

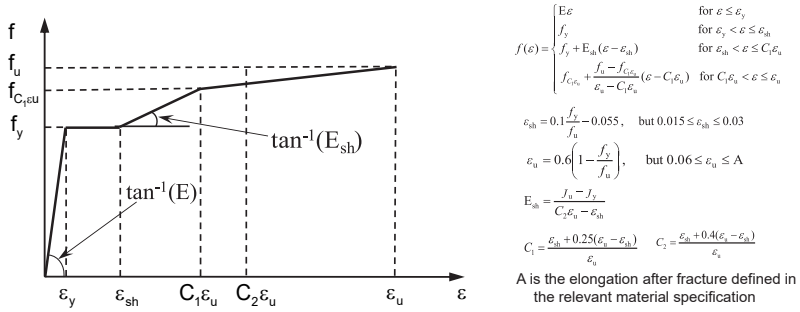

Figure 3.6 – Steel stress-strain relationship by multi-linear model according to document AHGFE2017-019 [73]

In the case of the more advanced analysis, a non-linear curve from experimental tests or a quart-linear approximation according to the draft version of new background

document AHGFE2017-019 which to be prEN1993-1-14 [73] can be used. For the quart-linear curve, the following parameters provided in Fig. 3.6 can be applied. These values are only suitable for hot-rolled steel sections. In the case of cold-formed steel and stainless steel sections, other models should be applied. In the compression zone, the reduced ultimate strain value considering local buckling should be considered, for which the c/t limitations should be checked depending on the steel strength.

3.1.4 Equilibrium conditions

3.1.4.1 Equilibrium inside normal cross-section

For strain limited design with full shear interaction, the stain and stress diagrams are shown in Fig. 3.7 A). There is only one neutral axis in the whole cross-section and linear strain distribution is assumed. The resultant stress can be calculated by the stress-strain relationship defined by the material models. Furthermore, the resultant inner forces should be in equilibrium with the applied external actions.

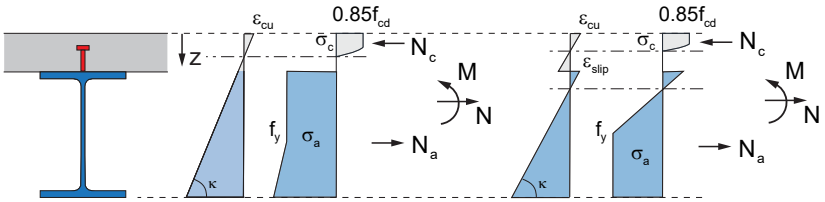

Figure 3.7 – Cross-section analysis based on strain-limited design

The equilibrium conditions for full shear interaction are as follow:

$$N_c = \int_{A_c} \sigma_c \, dA; \qquad N_a = \int_{A_a} \sigma_a \, dA; \qquad N = N_c + N_a;$$
$$M = \int_{A_c} \sigma_c z \, dA + \int_{A_a} \sigma_a z \, dA$$

For partial shear connection, there are two separate strain curves and neutral axes in the cross-section (Fig. 3.7 B). The curvature (κ) of the strain curves are same. A difference of strain $\varepsilon_{slip} = \Delta\varepsilon$ exists at composite joint defined as slip strain. The resultant stress curve and inner forces can be obtained the same way as the full shear connection situation. However, the normal force in steel and concrete is limited by the longitudinal shear force transferred by a limited amount of shear connectors inside a critical shear span.

$$N_v = N_c = -N_a \qquad N_v = \sum P_{Ei}$$

3.1.4.2 Equilibrium inside longitudinal cross-section

Fig. 3.8 shows a finite small slice of a composite beam in the longitudinal direction. The longitudinal shear force transferred by shear connectors equals the change of normal force in concrete or steel sections. Which can be expressed as:

$$\sum P_{E,i} = \Delta N_c + N_c - N_c = \Delta N_c$$
$$\sum P_{E,i} = \Delta N_a + N_a - N_a = \Delta N_a$$

The total longitudinal shear force N_v is the sum of all shear connector forces and equal to the normal force in the concrete (N_c) and steel (N_a). With a smear shear connector model and equal distance of shear connectors, continuous longitudinal shear force (V_L) can be assumed, which is calculated as the average shear connector forces within the distance "s".

$$V_L = \frac{P_{E,i}}{s} \qquad N_v = \sum P_{E,i} = \int V_L dx$$

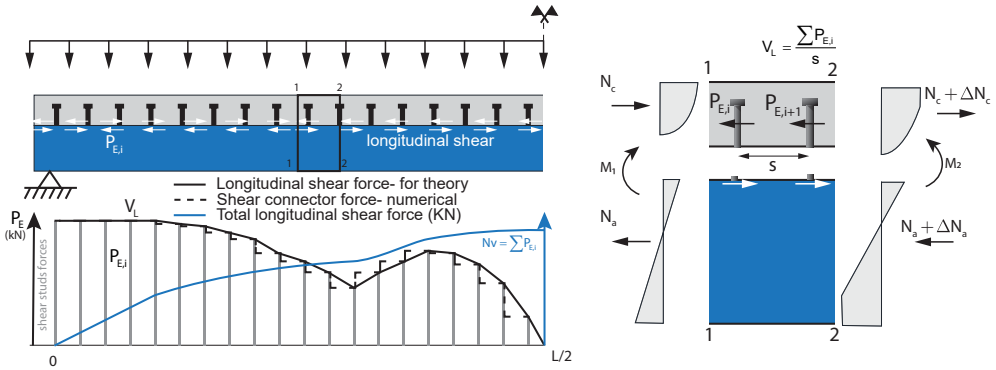

Figure 3.8 – Equilibrium in longitudinal direction and longitudinal shear distribution

3.1.5 Kinematic compatibility

For composite beams under pure bending, the deformation in the longitudinal direction can be neglected. The flexural deformation can be calculated from the curvature (κ). Due to plain cross-section assumption, the curvature keeps the same in whole cross-section. Thus the beam can be simplified as a line member, the relationship between curvature, rotation angle (θ) and deformation (ω) are well known as shown below. Similarly, the slip developed at the joint is the integral of slip strain from the zero slip point to the calculation location. These equations are validated for both elastic and post-elastic stage.

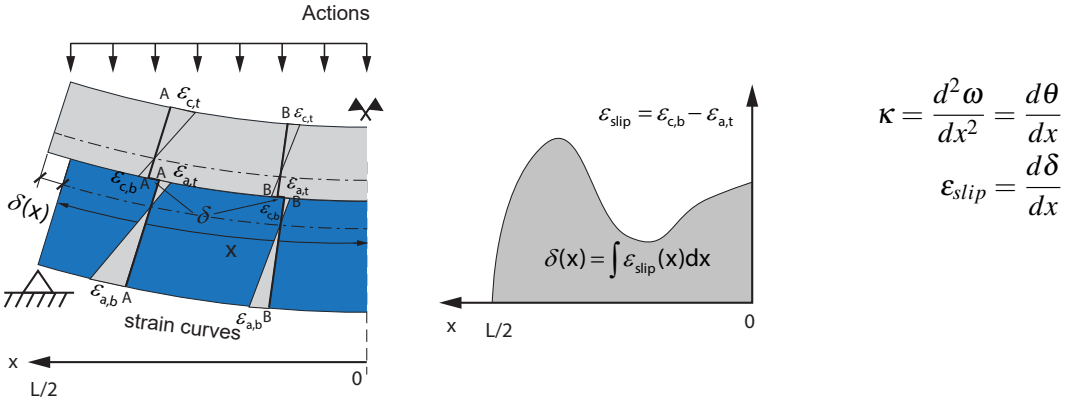

$$\kappa = \frac{d^2\omega}{dx^2} = \frac{d\theta}{dx}$$
$$\varepsilon_{slip} = \frac{d\delta}{dx}$$

Figure 3.9 – Relationship of slip and slip strain

3.2 Strain-limits and design bending resistance at ULS

Unlike the plastic bending resistance, the strain-limited bending resistance at ULS is calculated from strain failure indicated by the ultimate strain limits (ε_u). They are depended on the material models with necessary modifications. For example, the concrete tensile strain-limit is suppressed unless for a cracking analysis. For steel compression strain limits, special care should be taken to consider the buckling of compression plates. For composite beam under the pure sagging moment, the concrete slab is under compression, and the steel section is mostly in tension. The concrete compression strain is usually the controlling strain limit due to steel being a much more ductile material. For composite beam under hogging bending, the strain limits can be taken as reinforcement or steel strain limits if buckling of steel plates can be prevented.

3.2.1 Stain-limits under sagging moment

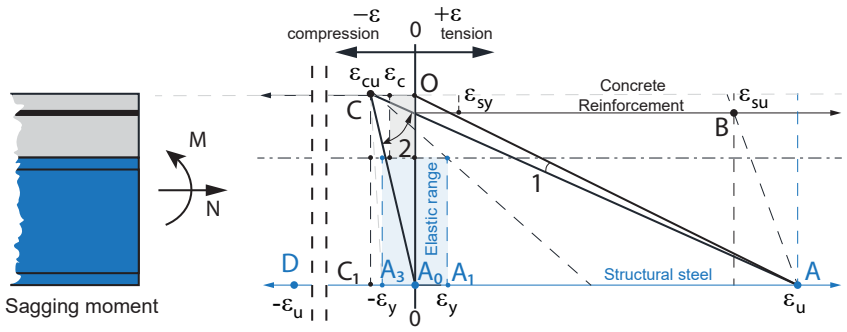

Figure 3.10 – Strain limit of composite beam with full shear interaction under sagging moment according to prEN1992-1-1:2019 [72] with fixed strain limit point for concrete

Fig. 3.10 shows the the possible strain distributions with full shear interaction under sagging bending. The strain line is limited from OA to CA_0 for pure bending situation, while expended to (AB) to (CC_0) together with normal forces. Below is the meaning of the different strain curve areas:

- $AB \rightarrow AO$: All cross-section in tension, N>0.
- $AO \rightarrow AC \rightarrow A_0C$: Part of the cross-section in compression, part in tension.
- $A_0C \rightarrow A_3C$: Cross-section in compression, part of steel section in elastic stage, N<0 .
- $A_3C \rightarrow CD$: Cross-section in compression and all in in plastic stage. If strain hardening is not considered, the stress and inner force keeps constant.

According to current Eurocode 2 [19], clause 6.1(5), if the parts of the concrete beam cross-section such as the concrete flange of box girder are subjected to approximately concentric loading with $e_d/h \leq 0.1$ then the strain should be limited to ε_{c2}. This rule is also seen in Zilch [105] for concrete T-beams design, where the strain rotation point is changed from ε_{cu2} at top fiber to ε_{c2} at near middle area. For the design of composite beams, a similar method is applied in some of the works for example, by Hanswille [34], the strain limits are reduced when the neutral axis gets deeper. For simplification, the limit of $e_d/h \leq 0.1$ can be represented by the stage where the concrete slab starts to

fully under compression. If the above-mentioned rule is applied, the strain-limit area is shown in Fig. 3.11. Zilch [105] mentioned that the reduction of concrete slab strain is due to lacking the capacity of stress redistribution inside the concrete slab, and the parabolic-rectangle strain-stress curve does not represent the decreasing branch after ε_{c2}. Thus an overestimation of beam resistance is possible if the strain limit is set as ε_{cu2} at the top. However, this rule can lead to a significant reduction of composite beam with deep relative compression zones. And the new draft of prEN1992-1-1 [72] also removed this rule. For a non-linear concrete model with a compression softening part, the reduction is not necessary to be applied. A comparison is seen in [86].

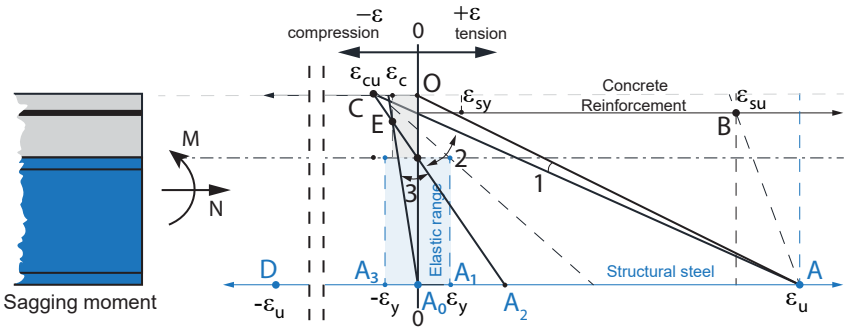

Figure 3.11 – Strain limit of composite beam with full shear interaction under sagging moment according to EN1992-1-1:2004 [19] with changing strain limit point for concrete. Concrete parabolic-rectangle model is used

The strain-limit area considering the change of strain limit point illustrated in Fig. 3.11 can now be divided into three different regions for sagging bending design.

- $AO \rightarrow AC$: The steel strain-limit reaches first, steel tensile failure is the governing failure mode. The beam has very shallow compression zone.
- $CA \rightarrow CA_2$: Concrete ultimate strain ε_{cu2} at top fiber controls, the strain curve rotate from point A to A_2 with point C fixed. Strain curve CA_2 is the begin of concrete slab in full compression. Point E is the point on CA_2 where strain equal to ε_{c2}.
- $CA_2 \rightarrow EA_0$: The strain curve is fixed at point E and rotates from point A_2 to point A_0 the maximum allowed strain at top fiber is between ε_{c2} and ε_{cu2}.

3.2.2 Stain-limits under hogging moment

For composite beam under hogging moment, if no local buckling of steel plate, the strain limits ε_u can be taken from the material model, otherwise a reduced strain limit should be used. The same conditions for a beam under sagging moment condition can be considered; the strain boundaries should be changed as follow:

- $BA_0 \rightarrow BD$: Start from full cross-section in tension to structural steel in ultimate compression (reinforcement ultimate strain controlled).
- $BD \rightarrow B_3D$: Reinforcement tensile strain reduce until to zero which full cross-section in compression (structural steel ultimate strain controlled).

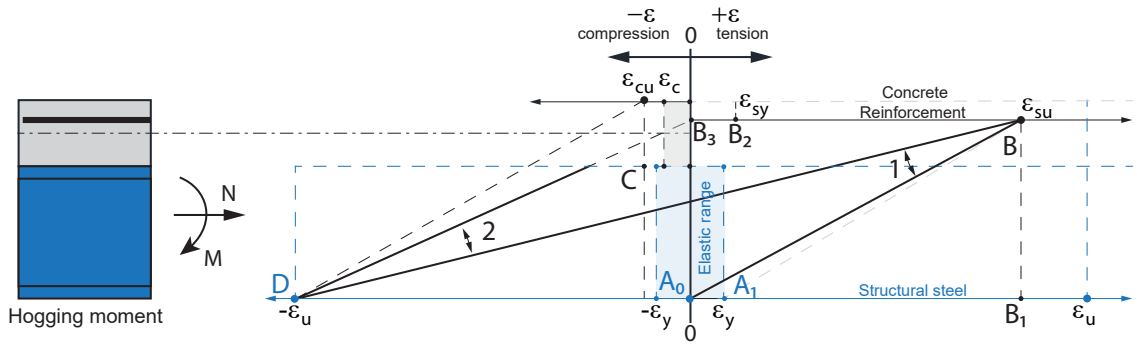

Figure 3.12 – Strain limit of composite beam with full shear interaction under hogging bending moment

3.2.3 Strain limited design bending moment resistance

The design strain limited bending resistance $M_{sl,Rd}$ is calculated at full shear interaction with following conditions fulfilled:

1. The equilibrium $N = N_a - N_c = 0$ for pure bending should be fulfilled for the whole cross-section, and
2. Either concrete compression strain limit (ε_{cu}), reinforcement strain limits (ε_{su}) or the steel strain limit (ε_u) should be reached in the critical fibers and the other fibers are within the strain limits. The critical fibers are top or bottom of each part.
3. The design material strength with partial safety factors should be used in the material models.

The sagging bending moment resistance can be calculated as follow: First, the strain-limit point can be set at the top of the cross-section with the concrete compression strain limit. With the fixed point, strain distribution is determined by the curvature. Through an iterative procedure, the corresponding strain curve to reach equilibrium $N = N_a - N_c = 0$ can be found. If the strain of steel section is within the steel strain limits, the resulted bending moment is the design bending resistance. Otherwise, the strain limits should be changed to the steel strain limit and calculate the strain distribution following a similar procedure.

3.3 Load-deflection and longitudinal shear of composite beams by strain limited method

Strain limited design is able to calculate the composite beam deformation at any given loads, which further enables verification of rotation capacity and ductility and the more precise deflection in SLS. For full shear interaction, the $M-\kappa$ curve obtained from cross-section analysis is the bridge linking loads and deformation. For partial shear interaction, as slip strain is unknown, the $M-\kappa$ curve can be extended to a $M-\kappa(\varepsilon_{slip})-N_c$ surface. With the information of shear connector arrangement and shear connector models, the longitudinal shear force, slip and deformation at given loads can be numerically calculated.

3.3.1 $M-\kappa$ curve and load-deflection with full shear interaction

For full shear interaction, linear strain distribution inside a cross-section is assumed. The strain curve can be determined by a fixed critical strain point and the curvature. As the critical strain point height and its strain value can be pre-defined, by rotating the strain curve, the total normal force of whole cross-section changes. A strain stage that allows total normal force equal to zero while other critical points are still inside their strain-limited is a solution for pure bending at the pre-defined limiting strain value. Additional information such as stress distribution, inner forces, and bending moment can also be obtained. Thus by varying the strain value at critical strain point from zero to its strain-limit and recording each responding bending moment resistance and curvature, the $M-\kappa$ curve of the given cross-section can be obtained. Fig. 3.13 shows one example of the $M-\kappa$ curve of a composite beam section and the changes of strain stress distribution of each step. The fixed critical strain point is chosen at the top surface (z=-150mm); its strain values changed step-wisely from 0 to -3.5 ‰.

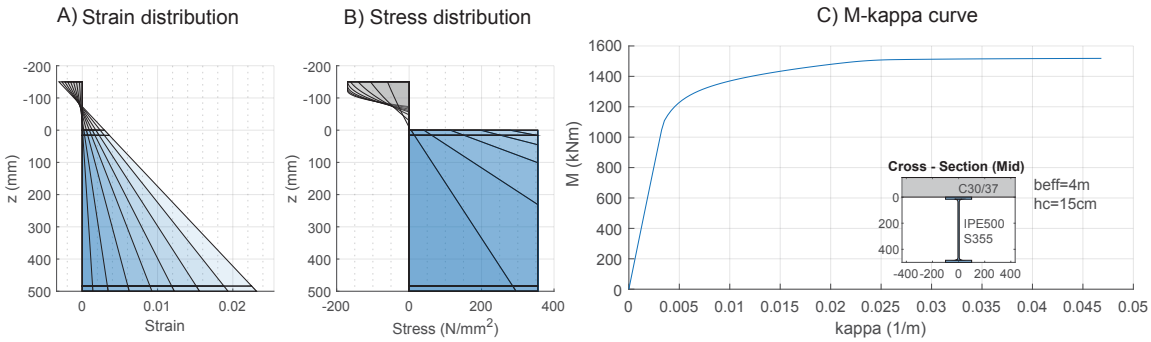

Figure 3.13 – $M-\kappa$ curve of a simply supported composite beam

With the $M-\kappa$ curve, the load-deflection relationship can be easily calculated. First, we can investigate a simple support composite beam under uniformly distributed loads (Fig. 3.14). The bending moment along the beam is already known. The curvature (κ) at each location can be obtained by simply interpolation with the given $M-\kappa$ curve. The deflection (ω) can be calculated with the numerical integral of curvature along the beam length and using the given boundary conditions to determine the unknown parameters during the integral.

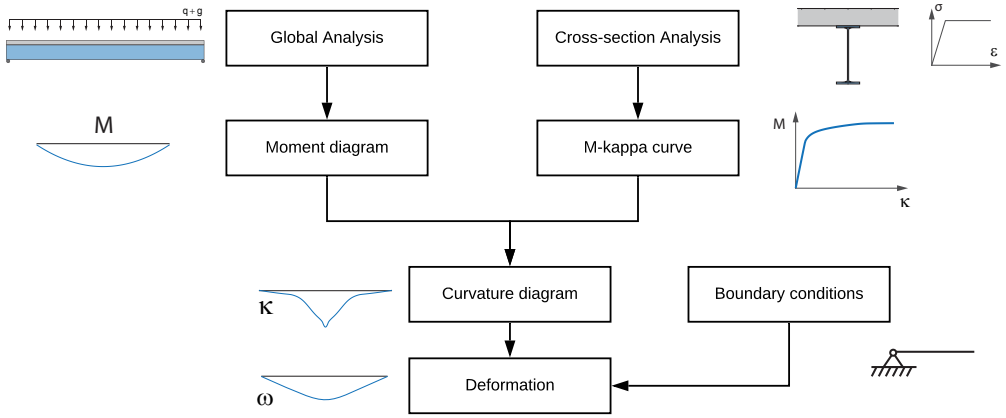

Figure 3.14 – Non-elastic deflection of simply supported beam with $M-\kappa$ curve

Regarding the statics-undetermined structures, for example, a two-span continuous beam, the classical "Force Method" can be used together with the $M-\kappa$ curve (Fig. 3.15). First, we can assume the middle support as an additional unknown force applied on the simply supported beam and set an approximate value by the elastic method. The total bending moment is the superposition of the bending moment from the external load and the assumed support reaction. The curvature and deflection of the beam can be acquired similar to the simply supported situation. However, the deflection at mid-span may not fit its position. By an iterative procedure, we can find the real additional force fits all the boundary conditions. One requirement of this method is that the $M-\kappa$ curve of both the bending and hogging part should be obtained, where the effective width should be calculated differently. Also, the steps in the iterative procedure should be controlled well to always stay inside the solution range.

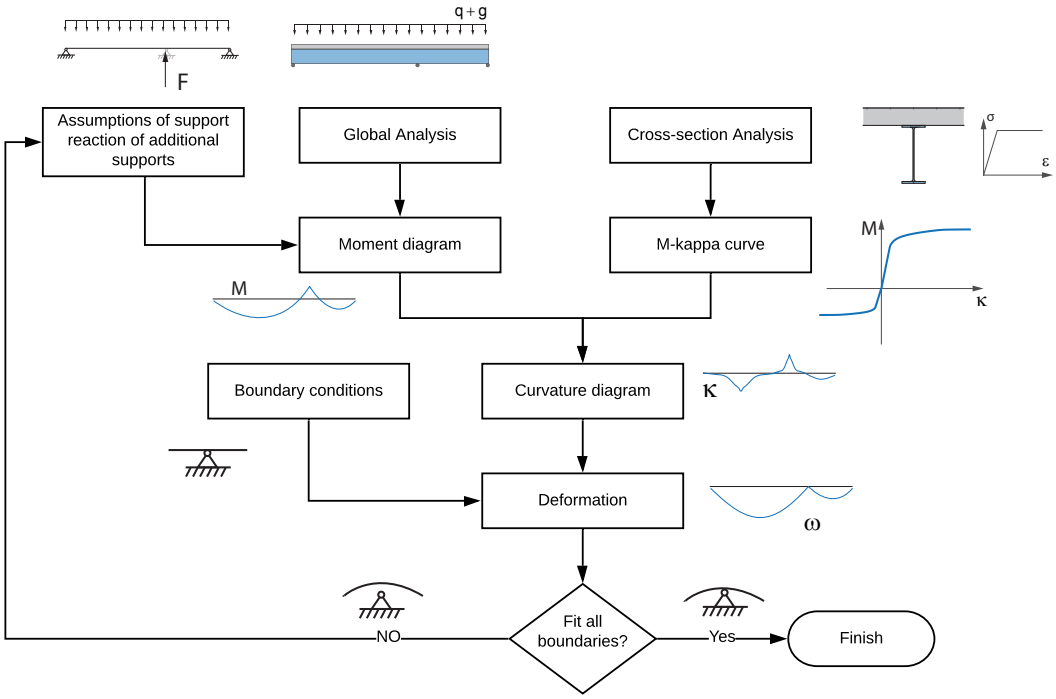

Figure 3.15 – Non-elastic deflection of continuous beam with $M-\kappa$ curve

3.3.2 $M-\kappa(\varepsilon_{slip})-N_c$ surface and load-deflection with partial shear interaction

For partial shear interaction, the stiffness of a composite beam is influenced not only by the plastic development and non-linear material behavior but also by the shear connectors, thus is beyond the application range of $M-\kappa$ curve. At least, the slip strain (ε_{slip}) is also necessary to be considered. Similar as the $M-\kappa$ curve, The relationship between the bending moment (M), total longitudinal shear force(N_c) and slip strain ε_{slip}, as well as the curvature κ, can be expressed in a 3D solution surface as shown in Fig. 3.16. In the figure, the κ value is plotted in z-axis, and the color represents the ε_{slip}. Such a solution surface can be obtained by step-wisely varying the ε_{slip}, κ, and the limiting strain value ε_{lim} at a critical point in the cross-section strain curve and calculate the other related parameters. Using the solution surface, if N_c and M are known, a fixed point on the surface is obtained, and the responding strain information is known.

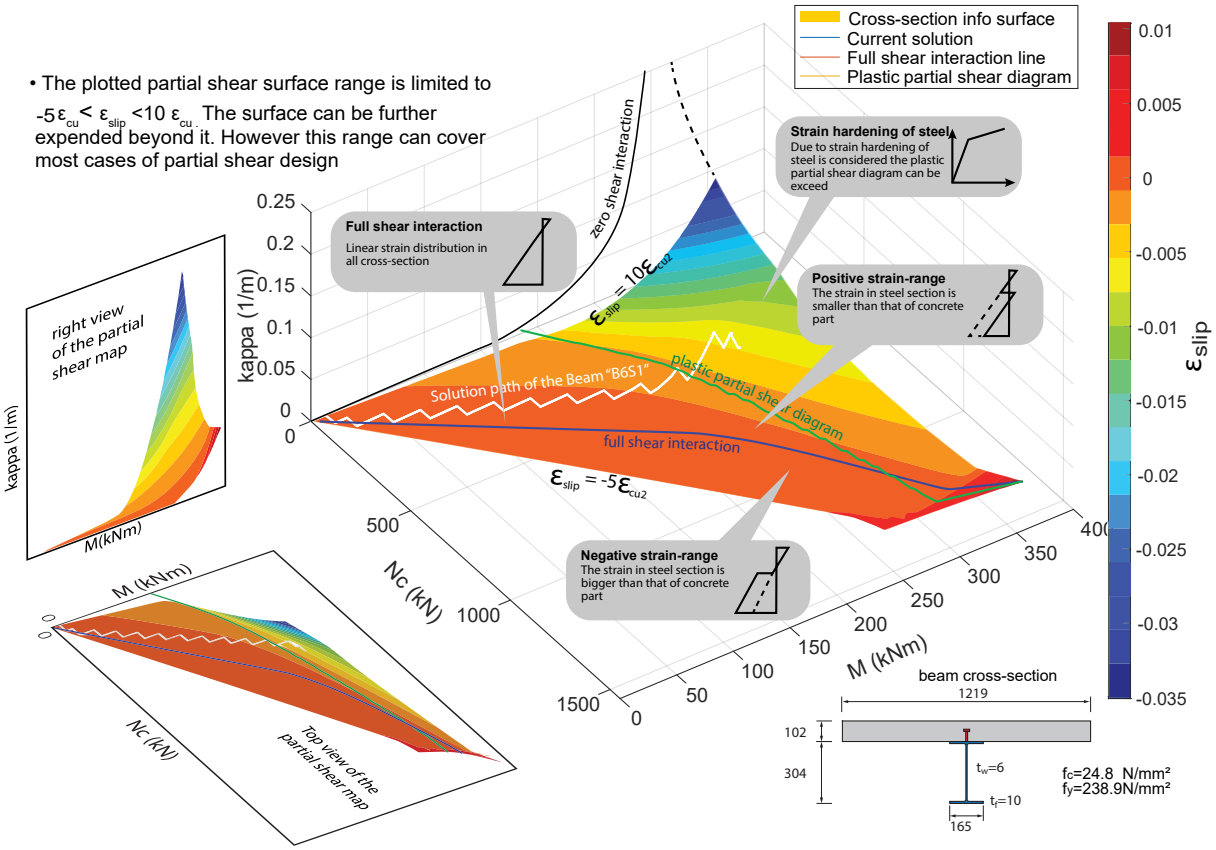

Figure 3.16 – Solution path on a composite beam on $M-\kappa(\varepsilon_{slip})-N_c$ surface and mechanical meanings, (details of the beam see section 5.1.1)

One example of the $M-\kappa(\varepsilon_{slip})-N_c$ surface is given in Fig. 3.16, the related cross-section is the composite beam "B6S1" from test program [14]. Details of the specimen and benchmark results can be found in section 5.1.1. The surface represents the cross-section proprieties, with more details overlay on it: The full shear interaction line represents where the slip strain equal to zero. Above this line is the positive slip strain area, inside which the steel strain is smaller than the concrete strain at the joint. Below it is the negative slip strain area where the strain of the steel part is bigger. The plastic partial shear diagram is the partial shear diagram calculated by the plastic method. Due to the strain-hardening of the steel section is used. Thus the solution range is beyond this line. If strain-hardening

is not considered, it will overlap with the upper boundary line of the surface. The zero interaction is the surface interaction line with the $N_c = 0$ plane. As the solution range is limited only to $-5\varepsilon_{cu2} \leq \varepsilon_{slip} \leq 20\varepsilon_{cu2}$, thus zero interaction is not shown in the diagram. From the surface, the plastic development is expressed by the bending part near the plastic shear connection line, where the slip strain and κ values greatly increased. The solution line represents the values of $M, \kappa, \varepsilon_{slip}, N_c$ of each cross-section along the beam longitudinal direction projected on the solution surface. As the N_c value is the sum of each shear connector's forces, it increases step-wisely, which results in the zip-zap shape of the solution path. The angle between the full shear connection line and the solution path line roughly indicates the degree of shear connection. It has to be noticed that the shear degree is not a constant value with different loads arrangement and at different location of the beam.

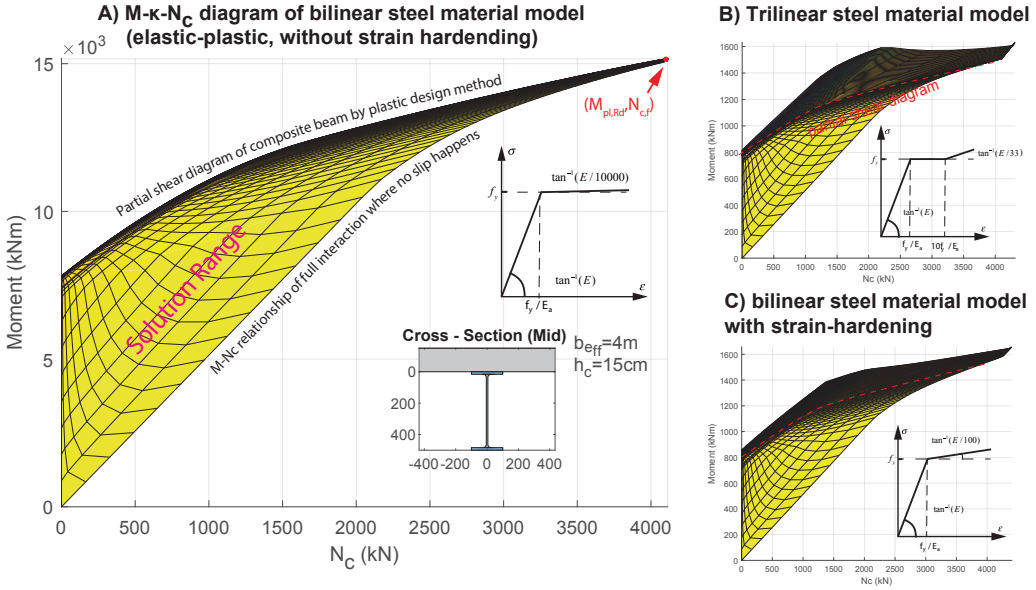

Figure 3.17 – $M - \kappa(\varepsilon_{slip}) - N_c$ map of a composite beam with different steel stress-strain models

The choice of steel material model can significantly change the surface shape in the plastic range. With a bi-linear steel stress-strain model without strain-hardening and parabolic-rectangle model for concrete, a solution surface of composite beam cross-section is plotted in Fig. 3.17 A) viewing normal to κ axis. The area represents the solution range of considered cross-section for pure sagging bending. The upper boundary line is approximately the partial shear diagram of the cross-section calculated by the plastic method according to current Eurocode 4, and the lower boundary line is the $M - N_c$ relationship if the beam has full shear interaction. If strain-hardening of steel is considered, the solution range can be extended over the partial shear diagram line, which represents the strain-hardening stage, as shown in Fig. 3.17 B, C). In practice, even without strain-hardening, the post-elastic branch of steel stress-strain curve should use a slop of E/10000, according to EN1993-1-5 3.17 A).

3.3.2.1 Analysis of a simple support beam with partial shear connection

With the $M - \kappa(\varepsilon_{slip}) - N_c$ solution surface is obtained, the load-deformation behavior, as well as the slip development can be calculated. In Fig. 3.18 a procedure for a simply supported beam solution is provided. First, the distribution of the total longitudinal shear

force (N_{c0}) can be assumed. An optimal way is to start with the full shear connection. Then the slip strain ε_{slip} along the whole beam can be obtained, as well as the slip and reaction forces in each shear connectors. The responding total longitudinal shear forces (N_{c1}) can then be calculated and compared with the old value. If the difference is within the limitation, then the iterative procedure is finished. Otherwise, a new N_{c0} value can be assumed based on the difference. After the solution is obtained, the curvature and deflection of the beam are also known.

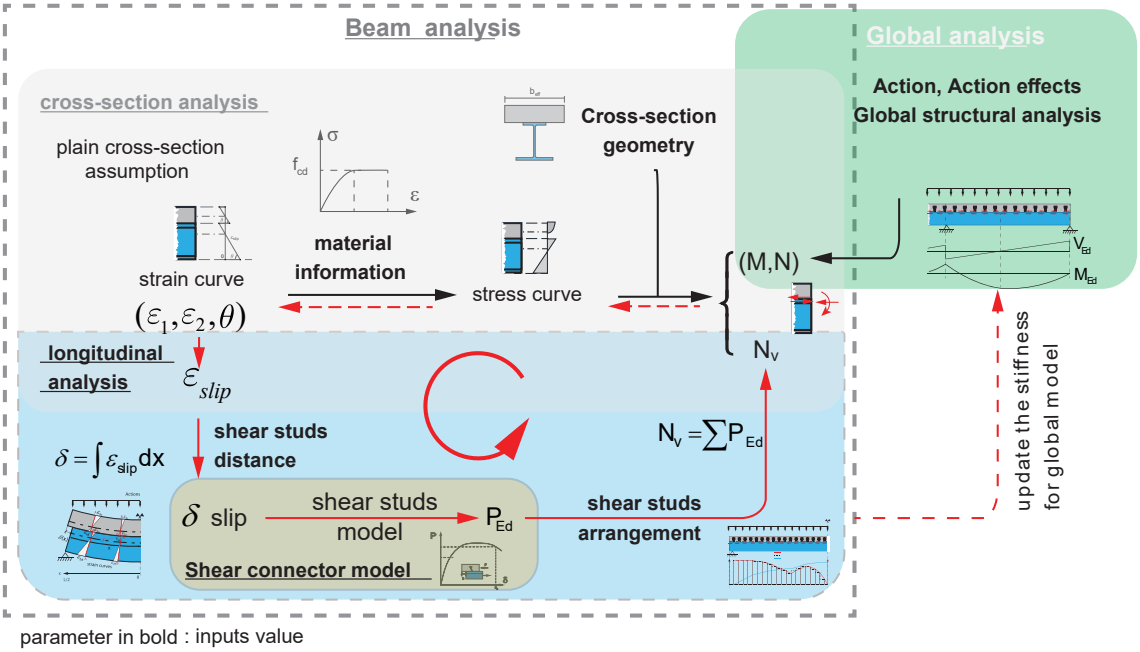

Figure 3.18 – Methodology of analysis of longitudinal shear

After strain distribution of each cross-section along the beam direction is obtained, further information such as curvature (κ), rotation angle (θ), deflection slip, and shear connector forces can also be calculated out. Fig. 3.19 plotted solutions of a load stage of the composite beam "B6S1" from test program [14]. This approach can directly obtain the results at any loading degree, the load-deflection curve of the beam can be obtained by calculating the deflection at mid-span of each load step from zero to ultimate load state.

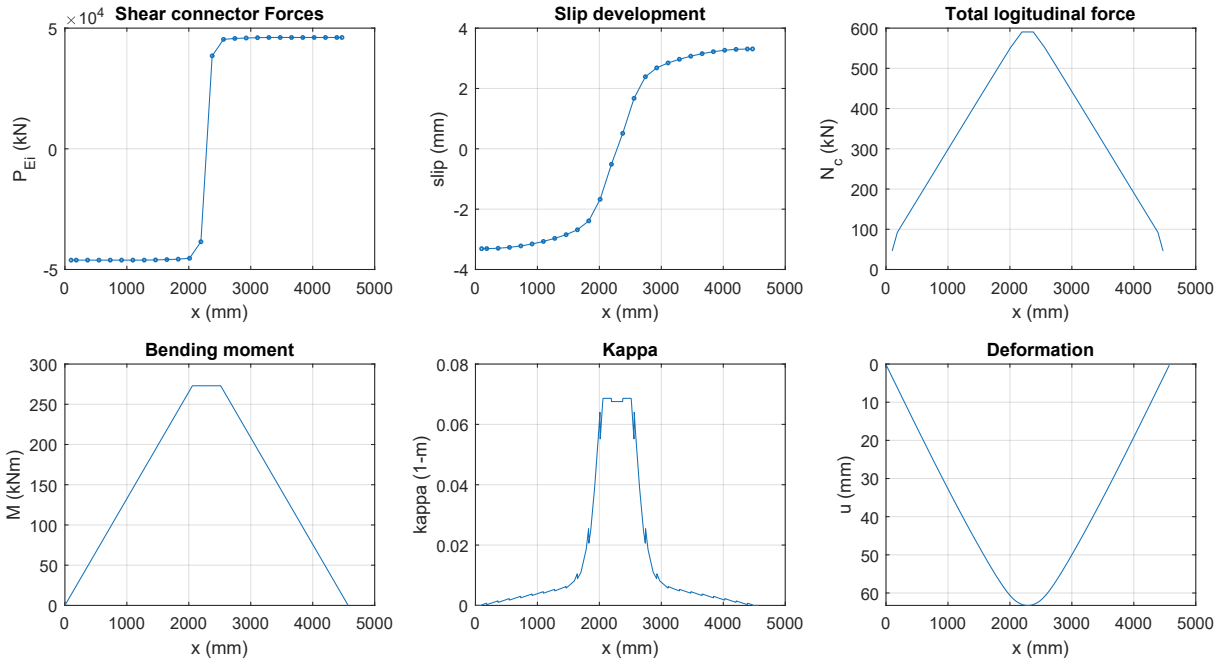

Figure 3.19 – Example of solution of a composite beam with partial shear connection

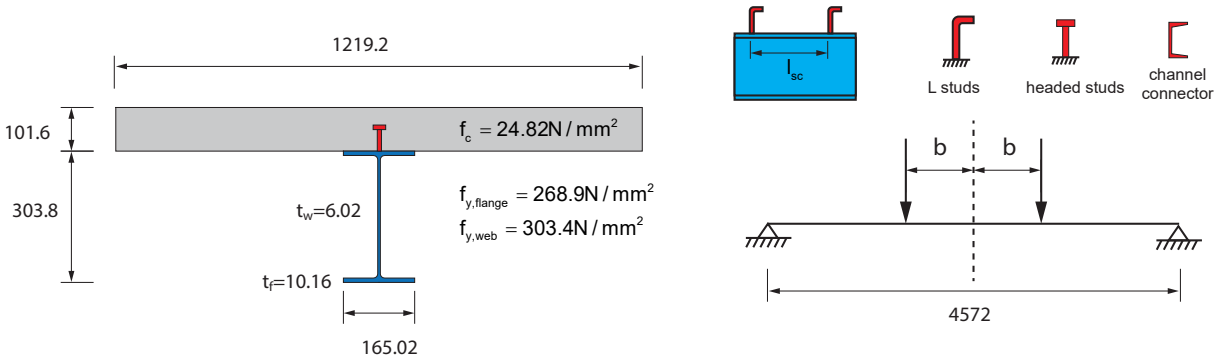

Figure 3.20 – Cross-section of the calculated beam "B6S1" (details see section 5.1.1)

3.4 Practical numerical approaches for strain-limited design

Due to the non-linearity in geometry and material models, it is almost impossible to develop an exact analytical solution for strain-limited design. Thus iterative numerical approaches are often used. The most commonly used and well-known one is the finite fiber methods (section 3.4.1). It divides the cross-section into fibers in the horizontal direction. Inside each fiber, average strain and stress are assumed. This method is straight-forward; however, it is not very efficient. A few alternative methods such as the "Finite-cell method" (section 3.4.2) and "Integral strain method" (section 3.4.3) or "directly analytical method" (section 3.4.4) have been developed in this work to simplify the strain limited design for composite beams and to improve the efficiency.

Table 3.1 – Different strain-limited design methods

Methods	Geometrical nonlinear	Material models	Element number*	Calcualtion speed	Results Accuracy
Finite fiber method	any type	nonlinear	high (≈1000)	slow	depending on elements
Finite cell method	rectangle simplification	multi-linear simplification	medium (≈10-40)	medium	medium-high
Integral strain method	rectangle simplification	nonlinear	low (4)	fast	high
Directly analytical method	rectangle/line simplification	bilinear & rectangle-parabolic	low (4)	very fast	medium

* the numbers are based on a conventional composite beam cross-section

The new methods all take advantage, that the composite beam cross-sections usually can be further simplified as group of rectangle or line members. It is possible to solving each rectangle individually and assembly afterwards to whole cross-section. Thus the material and geometric non-linearity are solved separately. By solving the mechanical relationship locally, the required elements can be reduced. Fig. 3.21 compares the basic elements of each method.

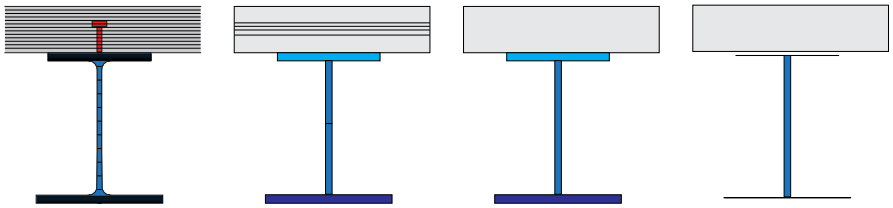

Figure 3.21 – Elements of different methods of strain-limited design

The finite cell method divides the cross-sections into a few cells. Inside each cell linear stress distribution instead of uniform stress value is assumed. The assumption results in a bending moment and normal force components pair inside each cells. To use the "integral strain" method, the cross-sections need to be able to disassemble into a few rectangles. It calculates first two newly defined non-geometrical parameters "n" and "m" by integral the material strain-stress diagram. Then the normal force and bending moment of each rectangle can be directly calculated through "n" and "m" with the rectangle size and position (see section 3.4.3). The "directly analytical method" is a further simplification. It provides the simplified equations to directly calculate bending moment and normal force inside each rectangle from assumed neutral axis position. However, it

is limited to the bi-linear and parabolic-rectangle strain-stress relationship only. Table. 3.1 provides comparisons of all methods.

3.4.1 Finite-fibers method

For the strain-limited design of composite beams, shear-lag effects in transversal direction (y-axis) can be simplified by effective width. Thus for pure bending, the strain values are identical at the same height. The cross-section can be meshed horizontally into a finite number of fibers, assuming the strain value inside each fiber is the same. With small enough fiber sizes, the numerical results can be very accurate. Fig. 3.22 illustrated such fiber meshes and related strain, stress, and normal force in each fiber. Due to different strengths, the steel part's fiber size is suggested to be finer than that of concrete. In practice, each part of cross-section such as concrete slab, steel beam top flange, steel beam web, etc. can be meshed independently, or a global mesh of all parts can be used. Moreover, consider partial shear connection, the concrete and steel parts should be set into different groups. The application can be seen in [37, 23] and many other publications.

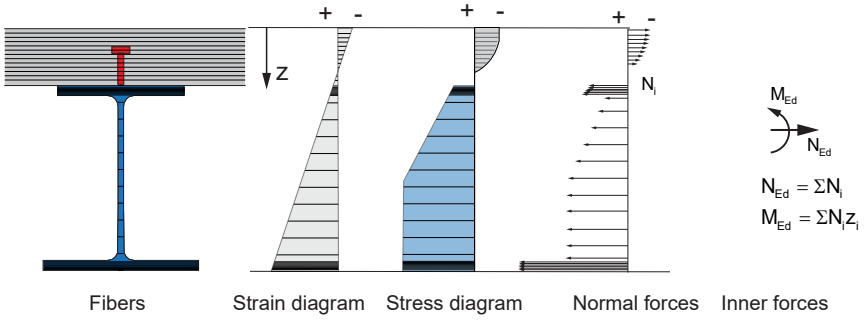

Figure 3.22 – Finite fiber method of strain-limited design

3.4.2 Finite-cells method

For the finite fiber method, the cross-section must be divided into many small fibers to reach enough accuracy. For simplification, the material models can be simplified as bi-linear or multi-linear curves. As shown in Fig. 3.23. when a bi-linear material model is used, the stress into cells 1 and 2 are linear changes with height. For the finite fiber method, the cross-section needs to be divided into many small fibers, and each fiber is resulting in a normal force partial N_i. However, we can also divide the cross-section only into two cells, with inside each cell the stress only linear changes. The normal force of the first cell is $N_1 = bh_1(\sigma_1 + \sigma_2)/2$ and the bending moment is $M_1 = bh_1^2(\sigma_2 - \sigma_1)/12$. The normal force and bending moment of the second part can be calculated by using the same relationship. The cross-section can now be calculated with only two cells instead of hundreds of fibers.

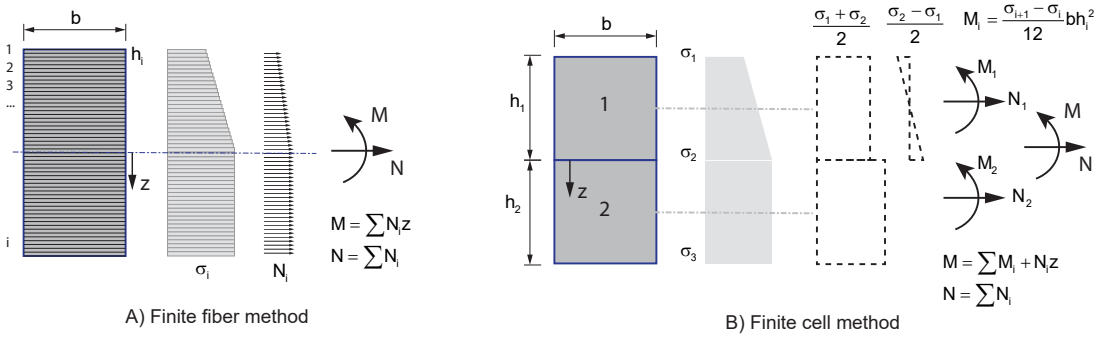

Figure 3.23 – Compare of finite fiber method and cell method of strain-limited design

Thus, to use the finite cell method, the material model should first be simplified as multi-linear curves, and the cross-section should be divided into different rectangles. Based on the material model and strain curve, the rectangles is further divided into separate cells. And afterward, the normal forces and bending moments of each cell can be obtained, and the inner forces of the whole cross-section can be calculated.

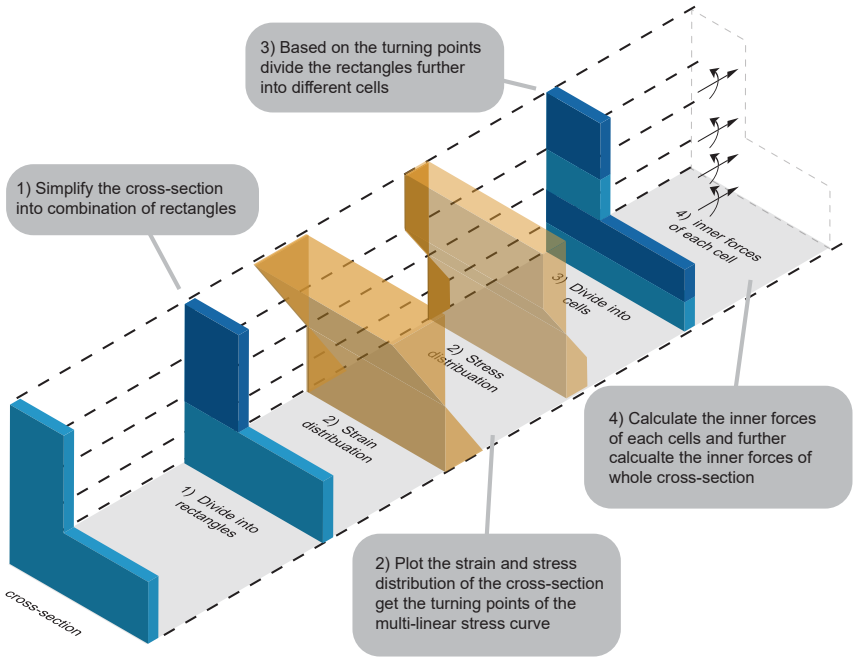

Figure 3.24 – Finite cell method for strain-limited design

The finite cell method can significantly reduce the element number. However, there are still a few limitations. First, the cross-section should be able to be simplified into rectangles easily. For composite beam sections, it is feasible, however for concrete-filled circle tubes type composite columns, the method is not suitable. Second, the material stress-strain curves should also be easily simplified as a multi-linear curve. A four-point or five-point curves can represent the concrete parabolic-rectangle curve without losing too much accuracy. The mesh needs to be continuously updated based on the strain stage, thus slowing down the calculation for some cases.

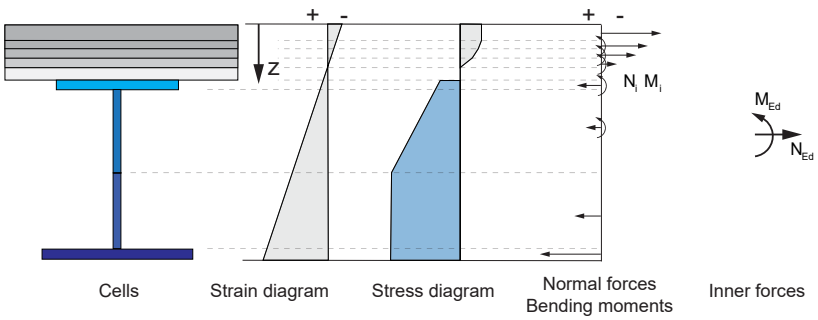

Figure 3.25 – Using cell method to solve a composite beam

An Example of using the cell method for the composite beam is given in Fig. 3.25. The parabolic-rectangle model for concrete is simplified as four points multi-linear curve. The cross-section is first divided into rectangles and based on the stress further divided into small cells, allowing linear stress distribution inside each cell. The responding normal force and bending moment can be calculated and summarized into final inner forces.

3.4.3 Integral strain method

The cross-section of a conventional composite beam or a typical slim-floor beam can be simplified into groups of rectangles without losing too much accuracy. For a rectangle part, with a given material model, the strain and stress values are only related to the strain-limited point and the location of neutral axis z_i. Thus for normal forces and bending moment, it is possible first to calculate the dimensionless material related parameters and then multiply them with the dimensional values. These dimensionless parameters can be obtained by the integral of strain and stress values. Thus, it can be named as "strain integral parameters".

3.4.3.1 General concept of strain integral parameters

To calculate the strain integral parameters, we can begin with a simple rectangle cross-section with breadth of b and height h. Linear strain distribution (Eq. 3.5) is assumed as shown in Fig. 3.26 A) with the strain at bottom equals to zero and at top equals to ε_i. The stress-strain relationship is expressed by the constitutive relationship function $\sigma(\varepsilon)$. With the stress value $\sigma_z = \sigma(\varepsilon)$ at location z, the normal force and bending moment can be calculated by Eq. (3.3) and Eq. (3.4). With linear strain relationship in Eq. (3.5), the differential equation can be transferred into Eq. (3.6) and Eq. (3.7) bases on strain values instead of height. The dimensionless components $n_m(\varepsilon)$ and $m_m(\varepsilon)$ from Eq. (3.8) and Eq. (3.9) are the strain integral parameters for internal normal force and bending moment. As they are only related to the material stress-strain model $\sigma(\varepsilon)$, they can be calculated separately and plotted in design diagrams afterwards be used for rectangles of any size and position.

$$N = \int_0^h b \cdot \sigma(\varepsilon) dz \tag{3.3}$$

$$M = \int_0^h b \cdot \sigma(\varepsilon) z dz \tag{3.4}$$

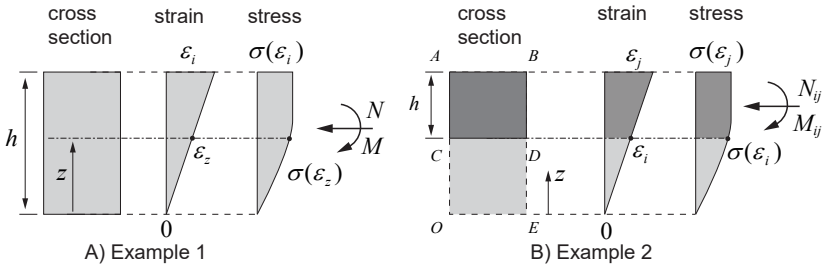

Figure 3.26 – Internal-force of rectangle cross-section

$$\varepsilon = \varepsilon_i \cdot \frac{z}{h} \Rightarrow z = \varepsilon \cdot \frac{h}{\varepsilon_i} \tag{3.5}$$

$$N = \int_0^{\varepsilon_i} b \cdot \sigma(\varepsilon) d(\varepsilon \cdot \frac{h}{\varepsilon_i}) = \frac{bh}{\varepsilon_i} \int_0^{\varepsilon_i} \sigma(\varepsilon) d\varepsilon \tag{3.6}$$

$$M = b(\frac{h}{\varepsilon_i})^2 \int_0^{\varepsilon_i} \sigma(\varepsilon) \varepsilon d\varepsilon \tag{3.7}$$

$$set:$$

$$n_m(\varepsilon_i) = \int_0^{\varepsilon_i} \sigma(\varepsilon) d\varepsilon \tag{3.8}$$

$$m_m(\varepsilon_i) = \int_0^{\varepsilon_i} \sigma(\varepsilon) \varepsilon d\varepsilon \tag{3.9}$$

$$k = \frac{h}{\varepsilon_i} \tag{3.10}$$

$$N_{0,i}(\varepsilon_i) = bk \cdot n_m(\varepsilon_i) \tag{3.11}$$

$$M_{0,i}(\varepsilon_i) = bk^2 \cdot m_m(\varepsilon_i) \tag{3.12}$$

However, for most cases, the strain does not start from zero, as shown in Fig. 3.26 B). If the strain at top and bottom has same sign (the whole cross-section either in compression or tension), the normal forces and the bending moment of rectangle ABCD can simply be calculated as the difference between the rectangle ABOE and CDOE ($N = N(z_i) - N(z_j)$; $M = M(z_i) - M(z_j)$). For a rectangle with strain value $\varepsilon_i, \varepsilon_j$ at top and bottom, the normal force and bending moment can be calculated by Eq. (3.14) and Eq. (3.15). In Eq. (3.13) the parameter "h" is different from the one in Eq. (3.10), however both "k" and "k_{ij}" represent curvature of the cross-section.

$$k_{ij} = \frac{h}{\varepsilon_i - \varepsilon_j} \tag{3.13}$$

$$N_{ij}(\varepsilon_i) = bk_{ij}(n_m(\varepsilon_i) - n_m(\varepsilon_j)) \tag{3.14}$$

$$M_{ij}(\varepsilon_i) = bk_{ij}^2(m_m(\varepsilon_i) - m_m(\varepsilon_j)) \tag{3.15}$$

When the neutral axis is inside the cross-section, it results in different signs of the strain at the top and bottom. If a point symmetric material model is used which can be expressed as $\sigma(-\varepsilon) = -\sigma(\varepsilon)$, for example the steel models, only $n_m(\varepsilon)$ and $m_m(\varepsilon)$ of the positive strain part is needed. Meanwhile, the resistance can be calculated by Eq. (3.16) and Eq. (3.17). These equations are also suitable for the whole cross-section either in compression or tension. If the material strain-stress relationship is different for compression and tension, the cross-section needs to be further divided into compression parts or tensile parts and

be calculated separately. Alternatively, integral from the ultimate compression strain to tensile strain instead of starting from strain equal to zero can be applied.

$$\boxed{N_{ij} = bk_{ij}(n_m(|\varepsilon_i|) - n_m(|\varepsilon_j|))} \tag{3.16}$$

$$\boxed{M_{ij} = bk_{ij}^2(m_m(|\varepsilon_i|) - \frac{|\varepsilon_j|}{\varepsilon_j} \cdot m_m(|\varepsilon_j|))} \tag{3.17}$$

3.4.3.2 $n_c(\varepsilon)$ and $m_c(\varepsilon)$ for concrete parabolic-rectangle model

In this example, the parabolic-rectangle concrete model according to Eurocode 2 is used (Eq. 3.18). for concrete class up to C50/60 the ε_{c2} and ε_{cu2} are constants. Thus it can also be expressed as $\sigma_i = f_{cd} \cdot s_f(\varepsilon_i)$, where f_{cd} is the design resistance and $s_f(\varepsilon_i)$ is the basic shape function of strain-stress curve. As $s_f(\varepsilon_i)$ is same for all concrete classes up to C50/60, we can separate the f_{cd} out and only integral the rest part n_c/f_{cd} and m_c/f_{cd} as shown in (Eq. 3.19 and Eq. 3.20) The two parameters are the n_m and m_m in Eq. 3.8 and Eq. 3.9 for concrete thus the subscript changed from "m" to "c". A dimensionless diagram is provided in Fig. 3.27 for these two equations.

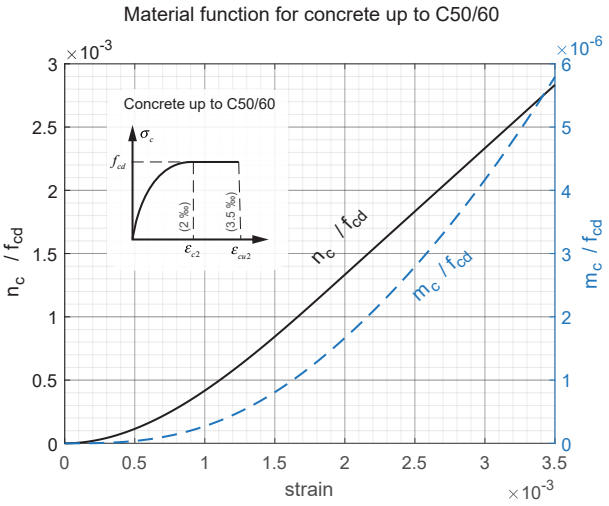

Figure 3.27 – Material functions for concrete up to C50/60 and parabolic-rectangle model

$$\sigma_c(\varepsilon) = f_{cd} \begin{cases} (1 - (1 - \frac{\varepsilon}{\varepsilon_{c2}})^2) & 0 \le \varepsilon_c \le \varepsilon_{c2} \\ 1 & \varepsilon_{c2} \le \varepsilon_c \le \varepsilon_{cu2} \end{cases} \tag{3.18}$$

$$\begin{aligned} n_c(\varepsilon_i) &= \int_0^{\varepsilon_i} \sigma_c(\varepsilon) d\varepsilon \\ &= f_{cd} \begin{cases} \frac{\varepsilon^2}{\varepsilon_{c2}} - \frac{\varepsilon^3}{3\varepsilon_{c2}^2} & 0 \le \varepsilon \le \varepsilon_{c2} \\ \varepsilon - \frac{1}{3}\varepsilon_{c2} & \varepsilon_{c2} < \varepsilon \le \varepsilon_{cu2} \end{cases} \end{aligned} \tag{3.19}$$

$$\begin{aligned} m_c(\varepsilon_i) &= \int_0^{\varepsilon_i} \sigma_c(\varepsilon) \varepsilon d\varepsilon \\ &= f_{cd} \begin{cases} \frac{2\varepsilon^3}{3\varepsilon_{c2}} - \frac{\varepsilon^4}{4\varepsilon_{c2}^2} & 0 \le \varepsilon \le \varepsilon_{c2} \\ \frac{5}{12}\varepsilon_{c2}^2 + \frac{1}{2}(\varepsilon^2 - \varepsilon_{c2}^2) & \varepsilon_{c2} < \varepsilon \le \varepsilon_{cu2} \end{cases} \end{aligned} \tag{3.20}$$

3.4.3.3 $n_s(\varepsilon)$ and $m_s(\varepsilon)$ for bilinear material model with / without strain-hardening

In this example, the bilinear strain-stress relationship (Eq. 3.21) for structural steel according to EN1993-1-5 is applied. Strain hardening of E/100 after reaching steel yielding strain ε_y is assumed. The resulting strain integral functions are given in Eq. (3.22) and Eq. (3.23). the results are also plotted in Fig. 3.28 for different steel grades. If strain-hardening is not considered, the last term of the functions can be neglected as shown in Eq. (3.24) and Eq. (3.25) . For other steel models such as a tri-linear model or non-linear model, similar approach can be followed. As the considered steel material models are symmetric for tension and compression, thus the function Eq. (3.16) and Eq. (3.17) can be used to calculate the bending moment and normal force. The two parameters n_s and m_s are the n_m and m_m in Eq. 3.8 and Eq. 3.9 for steel thus the subscript changed from "m" to "s".

$$\begin{aligned} \varepsilon_y &= \frac{f_y}{E_a} \qquad\qquad E_a = 210000N/mm^2 \\ \sigma_a(\varepsilon) &= \begin{cases} E_a\varepsilon & |\varepsilon| \le \varepsilon_y \\ f_y + E_a(\varepsilon - \varepsilon_y)/100 & \varepsilon_y < |\varepsilon| \le \varepsilon_u \end{cases} \end{aligned} \tag{3.21}$$

$$\begin{aligned} n_{s,sh}(\varepsilon_i) &= \int_0^{\varepsilon_i} \sigma_a(\varepsilon)d\varepsilon \\ &= f_y \cdot \begin{cases} \frac{\varepsilon^2}{2\varepsilon_y} & |\varepsilon| \le \varepsilon_y \\ (\varepsilon - \frac{\varepsilon_y}{2}) + \frac{(\varepsilon-\varepsilon_y)^2}{200\varepsilon_y} & \varepsilon_y < |\varepsilon| \le \varepsilon_u \end{cases} \end{aligned} \tag{3.22}$$

$$\begin{aligned} m_{s,sh}(\varepsilon_i) &= \int_0^{\varepsilon_i} \sigma_c(\varepsilon)\varepsilon d\varepsilon \\ &= f_y \cdot \begin{cases} \frac{\varepsilon^3}{3\varepsilon_y} & |\varepsilon| \le \varepsilon_y \\ \frac{\varepsilon_y^2}{3} + \frac{\varepsilon^2-\varepsilon_y^2}{2} + \frac{(\varepsilon-\varepsilon_y)^2(\varepsilon_y+2\varepsilon)}{300\varepsilon_y} & \varepsilon_y < |\varepsilon| \le \varepsilon_u \end{cases} \end{aligned} \tag{3.23}$$

$$n_{s,bl}(\varepsilon_i) = f_y \cdot \begin{cases} \frac{\varepsilon^2}{2\varepsilon_y} & |\varepsilon| \le \varepsilon_y \\ \varepsilon - \frac{\varepsilon_y}{2} & \varepsilon_y < |\varepsilon| \le \varepsilon_u \end{cases} \tag{3.24}$$

$$m_{s,bl}(\varepsilon_i) = f_y \cdot \begin{cases} \frac{\varepsilon^3}{3\varepsilon_y} & |\varepsilon| \le \varepsilon_y \\ \frac{\varepsilon_y^2}{3} + \frac{\varepsilon^2-\varepsilon_y^2}{2} & \varepsilon_y < |\varepsilon| \le \varepsilon_u \end{cases} \tag{3.25}$$

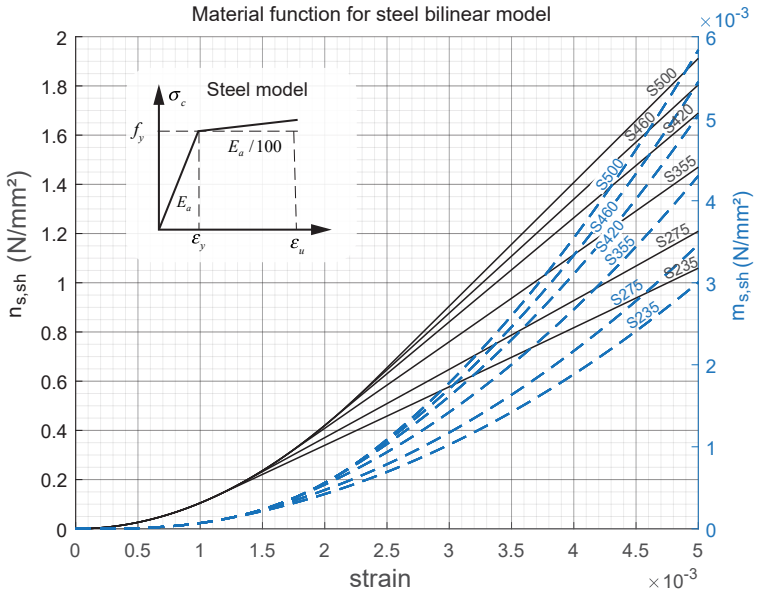

Figure 3.28 – Strain-integral parameters for steel strain-hardening model

3.4.3.4 Solution for composite beams

An example of using the integral strain method for the composite beam is given in Fig. 3.29. The cross-section is divided into rectangles, and strain at the top and bottom of each rectangle is calculated based on a given strain curve. the responding normal force and bending moment can be calculated through the strain integral parameters and summarized into final inner forces. It has to be noticed the bending moment component of each rectangle is calculated related to position of neutral axis. A small calculation example of using this method is also partially shown in Appendix. B-step 3.a.

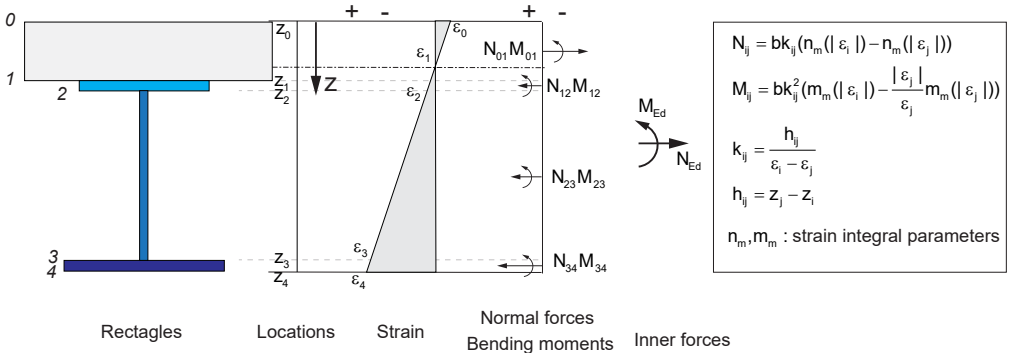

Figure 3.29 – Using integral strain method for composite beam

3.4.4 Simplified directly analytical method

By the direct analytical method, the cross-section should be disassembled into different rectangles (or lines). Then the normal forces and bending moments of each part can be calculated separately and summed up afterward. However, due to complex mathematical expressions with multi-linear or non-linear material strain-stress relationships, simply material strain-stress models are more suitable for this method. Thus only the steel bi-linear model and concrete parabolic-rectangle model are discussed in this work.

3.4.4.1 Solutions of a steel line member

A line member is a rectangle with its height considerably smaller than the total cross-section height. For example, the flanges of an IPE steel profile. The moment of inertia based on its own geometrical center is small enough to be neglected. Considering the strain limited point is at the top $(0, \varepsilon_{cu})$ and separates from the center of the line member with z_i. With a bi-linear material model without strain hardening, the two boundary values (z_{ti} and z_{ci}) for the position of neutral axis (z_i) indicate yielding due to tension or compression as shown in Fig. 3.30. Their values are given in Eq. (3.26). When $z_i < z_{ti}$ the considered line member yields due to compression, similarly $z_i > z_{ci}$ for tension. In between, the line member is in the elastic stage. The resulting stress f_i can be obtained by Eq. (3.27) and the normal forces N_i and bending moment M_i (calculated based on the neutral axis) are given in Eq. (3.28) and Eq. (3.29).

$$z_{ti} = z_i \cdot \frac{\varepsilon_{cu}}{\varepsilon_{cu} + \varepsilon_y}; \qquad z_{ci} = z_i \cdot \frac{\varepsilon_{cu}}{\varepsilon_{cu} - \varepsilon_y} \tag{3.26}$$

$$f_i = f_y \cdot \begin{cases} 1 & z_i \le z_{ti} \\ (\frac{z}{z_i} - 1)\frac{\varepsilon_{cu}}{\varepsilon_y} & z_{ti} < z_i \le z_{ci} \\ -1 & x_{ci} < z_i \end{cases} \tag{3.27}$$

$$N_i = f_i A_i \tag{3.28}$$

$$M_i = N_i \cdot (z - z_i) \tag{3.29}$$

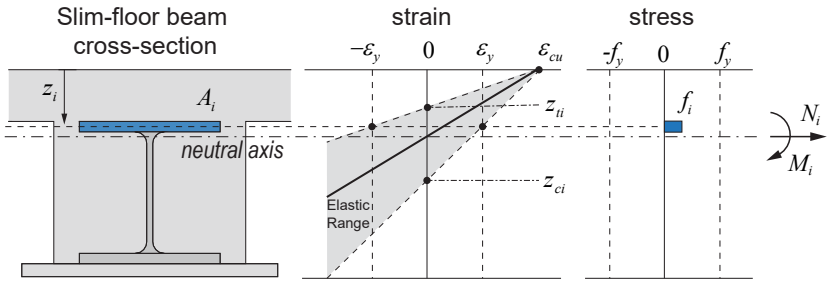

Figure 3.30 – Strain and stress distribution by strain-limited design

3.4.4.2 Solutions of a steel rectangle member

When the height of the rectangle can not be neglected, with a bi-linear material model, there will be four boundary points of stresses related to the position of neutral axis z_i. Two of them ($z_{t,t}$ and $z_{c,t}$) is calculated based on location of the rectangle top surface z_t, the other two ($z_{t,b}$ and $z_{c,b}$) related to the location of bottom z_b. Similar as the line member explained in section 3.4.4.1, when $z_i < z_{t,t}$ the considered rectangle member yields due to compression, when $z_i > z_{c,b}$ the whole rectangle yields due to tension. In between, part of the rectangle is in elastic stage (Fig. 3.31). The resulting normal forces N_i and bending moment M_i of location of neutral axis z_i are given in Eq. (3.34) and Eq. (3.35). In order to calculated them, two parameters h_t and h_c related to the plastic zone height, as well as the stress at top and bottom fiber f_t and f_b should be calculated first by Eq. (3.32) and Eq. (3.33).

$$z_{t,t} = z_t \cdot \frac{\varepsilon_{cu}}{\varepsilon_{cu} + \varepsilon_y}; \qquad z_{c,t} = z_t \cdot \frac{\varepsilon_{cu}}{\varepsilon_{cu} - \varepsilon_y} \tag{3.30}$$

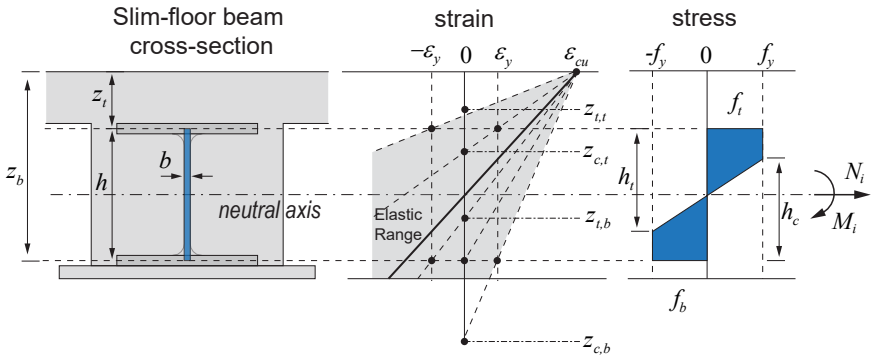

Figure 3.31 – Strain and stress distribution by strain-limited design

$$z_{t,b} = z_b \cdot \frac{\varepsilon_{cu}}{\varepsilon_{cu} + \varepsilon_y}; \quad z_{c,b} = z_b \cdot \frac{\varepsilon_{cu}}{\varepsilon_{cu} - \varepsilon_y} \tag{3.31}$$

$$h_t = (1 + \frac{\varepsilon_y}{\varepsilon_{cu}}) \cdot z_i - z_t; \quad h_c = z_d - (1 - \frac{\varepsilon_y}{\varepsilon_{cu}}) \cdot z_i \tag{3.32}$$

$$f_t = f_y \cdot \begin{cases} 1 & z_i \le z_{t,t} \\ (\frac{z_t}{z_i} - 1)\frac{\varepsilon_{cu}}{\varepsilon_y} & z_{t,t} < z_i \le z_{c,t} \\ -1 & z_{c,t} < z_i \end{cases}$$

$$f_b = f_y \cdot \begin{cases} 1 & z_i \le z_{t,b} \\ (\frac{z_b}{z_i} - 1)\frac{\varepsilon_{cu}}{\varepsilon_y} & z_{t,b} < z_i \le z_{c,b} \\ -1 & z_{c,b} < z_i \end{cases} \tag{3.33}$$

$$N_i = b \cdot \begin{cases} f_y h - \frac{1}{2}(f_b - f_t)h_t & z_i \le z_{c,t} \\ f_y(h_c - h_t) & z_{c,t} < z_i < z_{t,b} \\ \frac{1}{2}(f_b - f_t)h & z_{t,b} < z_i < z_{c,t} \\ \frac{1}{2}(f_b - f_t)h_c - f_y h & z_{t,b} \ge z_i \end{cases} \tag{3.34}$$

$$M_i = N_i \cdot (h_c - h_t) + \frac{b(f_d - f_t)}{12} \cdot a_m$$

$$a_m = \begin{cases} 3hh_t - 2h_t^2 & z_i \le z_{c,t} \\ 3h_t(h - h_t) + 3h_c(h - h_c) + (h_c + h_t - h)^2 & z_{c,t} < z_i < z_{t,b} \\ h^2 & z_{t,b} < z_i < z_{c,t} \\ 3hh_c - 2h_c^2 & z_{t,b} \ge z_i \end{cases} \tag{3.35}$$

3.4.4.3 Solutions of a concrete T-section member

For a slim-floor beam with profiled steel sheeting placed transversal to the beam longitudinal direction, The concrete part can be divided into two sections: the one above the profiled sheeting and the one in the chambers. For simplification, the area occupied by steel profile and reinforcement embedded into the concrete is not deducted. The parabolic-rectangle strain-stress relationship by Eurocode 2 is used here as shown in Eq. (3.36). For concrete class up to C50/60, the parameters ε_{cu2} and ε_{c2} are fixed to 3.5‰ and 2.0‰ respectively following a parabolic-rectangle strain-stress relationship. For the part above profiled sheeting, the reduction factor for normal forces α_{N1} and for bending moment α_{M1} can be calculated by Eq. (3.37) and Eq. (3.39). Similarly the values α_{N2} and α_{M2} for part in the chamber can be obtained by Eq. (3.38) and Eq. (3.40). To avoid

the complex calculation, a dimensionless chart in Fig. (3.32) allows the values to be directly checked out. The normal forces and bending moments of each parts can be calculated by Eq. (3.41) to Eq. (3.44).

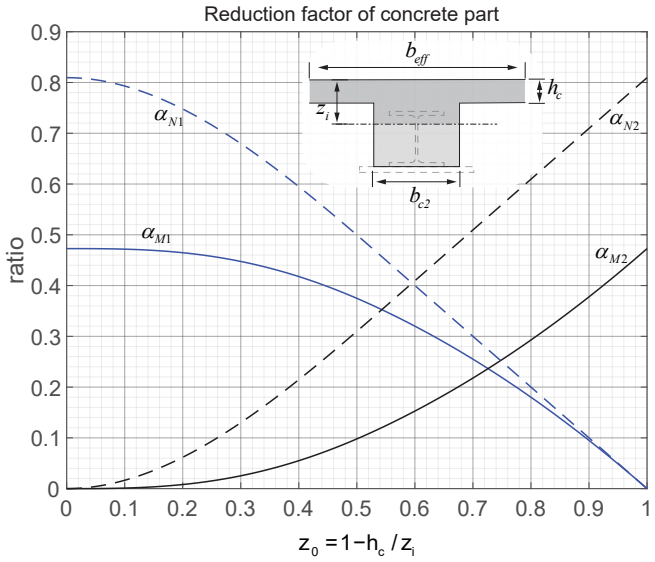

Figure 3.32 – Reduction factors related to concrete part

$$\sigma_c = f_{cd} \begin{cases} (1-(1-\frac{\varepsilon}{\varepsilon_{c2}})^2) & 0 \le \varepsilon_c \le \varepsilon_{c2} \\ 1 & \varepsilon_{c2} \le \varepsilon_c \le \varepsilon_{cu2} \end{cases} \tag{3.36}$$

$$z_0 = 1 - \frac{h_c}{z_i}$$

$$\alpha_{N1} = \begin{cases} \frac{17}{21} & z_0 \le 0 \\ \frac{17}{21} - \frac{7}{4}z_0^2 + \frac{49}{48}z_0^3 & 0 < z_0 \le \frac{4}{7} \\ 1 - z_0 & \frac{4}{7} < z_0 < 1 \end{cases} \tag{3.37}$$

$$\alpha_{N2} = \begin{cases} 0 & z_0 \le 0 \\ \frac{7}{4}z_0^2 - \frac{49}{48}z_0^3 & 0 < z_0 \le \frac{4}{7} \\ \frac{2}{3} + (x - \frac{4}{7}) & \frac{4}{7} < z_0 < 1 \end{cases} \tag{3.38}$$

$$\alpha_{M1} = \begin{cases} \frac{139}{294} & z_0 \le 0 \\ \frac{139}{294} - \frac{7}{6}z_0^3 + \frac{49}{64}z_0^4 & 0 < z_0 \le \frac{4}{7} \\ \frac{1}{2}(1 - z_0^2) & \frac{4}{7} < z_0 < 1 \end{cases} \tag{3.39}$$

$$\alpha_{M2} = \begin{cases} 0 & z_0 \le 0 \\ \frac{7}{6}z_0^3 - \frac{49}{64}z_0^4 & 0 < z_0 \le \frac{4}{7} \\ \frac{20}{147} + \frac{1}{2}(z_0^2 - \frac{16}{49}) & \frac{4}{7} < z_0 < 1 \end{cases} \tag{3.40}$$

$$N_{c1} = \alpha_{N1} \cdot f_{cd} b_{eff} z_i \tag{3.41}$$

$$N_{c2} = \alpha_{N2} \cdot f_{cd} b_{c2} z_i \tag{3.42}$$

$$M_{c1} = \alpha_{M1} \cdot f_{cd} b_{eff} z_i^2 \tag{3.43}$$

$$M_{c2} = \alpha_{M2} \cdot f_{cd} b_{c2} z_i^2 \tag{3.44}$$

3.4.4.4 Solution for composite beams

For a traditional composite beams, the concrete part can be calculated as rectangles by Eq. (3.41) and Eq. (3.43). For composite beams with chamber filled concrete or slim-floor beams, it can be divided into two parts, the lower part can be calculated according to Eq. (3.42) and Eq. (3.44). For the steel section, the flanges and additional steel plates can be treated as line members, and the web can be calculated according to section 3.4.4.2. With hot rolled steel sections, the round corners between the web and flanges are neglected, to remedy the loss of this cross-section area, the web rectangle can be further extended to the center-line of flanges. In this way, parameters for flanges and webs can be shared, thus simplifies the calculation. Furthermore, this method is also suitable for composite slabs and reinforced concrete beams or slabs by simplifying the reinforcement layers as line members. A small calculation example of using this method is also partially shown in Appendix. B-step 3.b.

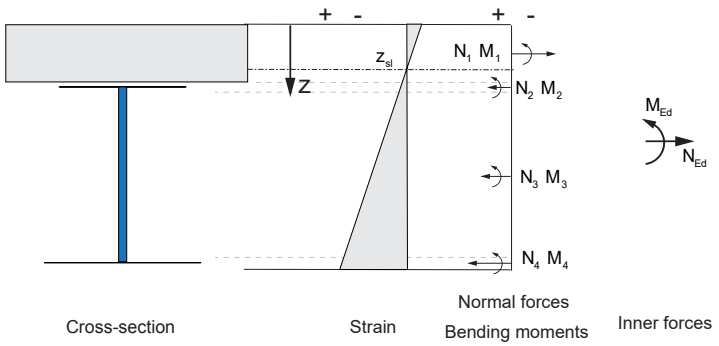

Figure 3.33 – Using direct analytical method for composite beam

3.5 Simplified strain limited design approach allowing hand-calculation

Strain-limited bending resistance is important for composite beams with a deep neutral axis. For many of the slim-floor beams are necessary to do a nonlinear calculation. However, programming skill is not available to everyone. Thus a simplified hand calculation method is needed, this section provides such a method for slim-floor beams; it is also suitable for conventional composite beams.

3.5.1 Procedures to calculate neutral axis location z_{sl}

To calculate the location of the neutral axis, normally, an iterative procedure can be followed. Alternatively, an indirect procedure can also be applied: Instead of the error-trial procedure, the resulting normal forces in steel section ($N_{a,i}$) and concrete section ($N_{c,i}$) of each z_i from top to bottom of the cross-section can be first calculated out and plotted together. The x_{sl} for pure bending can be found when $N = N_c - N_a = 0$, which is the intersection of the $N_{a,i} - z_i$ and $N_{c,i} - z_i$ lines as shown in Fig. 3.34. This procedure needs to calculate values for each z_i; however, it does not need an interactive solver; thus, it is easier for programming.

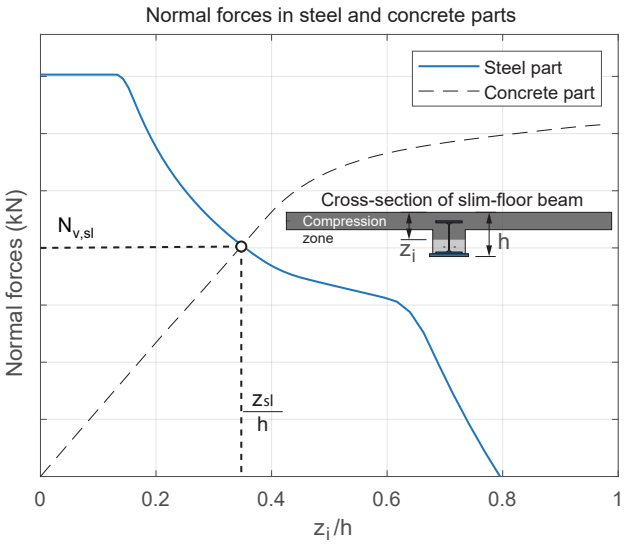

Figure 3.34 – Normal forces in steel and concrete parts

Using the numerical method, the normal forces in steel and concrete at each z_i from top to bottom of the cross-section are plotted in Fig. 3.34. Parameter studies found the $N_i - z_i$ curves follow a certain shape. For simplification, the nonlinear curves can be represented by polylines, which consist of a few key points. As shown in Fig. 3.35, the curve of steel part can be simplified by five points polyline $\overline{ABCDE}$, the key points are related to the location of the top flange and bottom flange. The concrete curve can be similarly represented by four-point polyline $\overline{abcd}$, which are associated with the concrete slab thickness h_c. By this method, the approximate location of the neutral axis x_{sl} for sagging bending can be obtained much more straightforward. In practice, if the position of the neutral axis can be roughly predicted, not all the points are needed. For example, if the compression zone is roughly predicted inside the concrete slab above the profiled sheeting, point E and b, c, d are not necessary for the first trail.

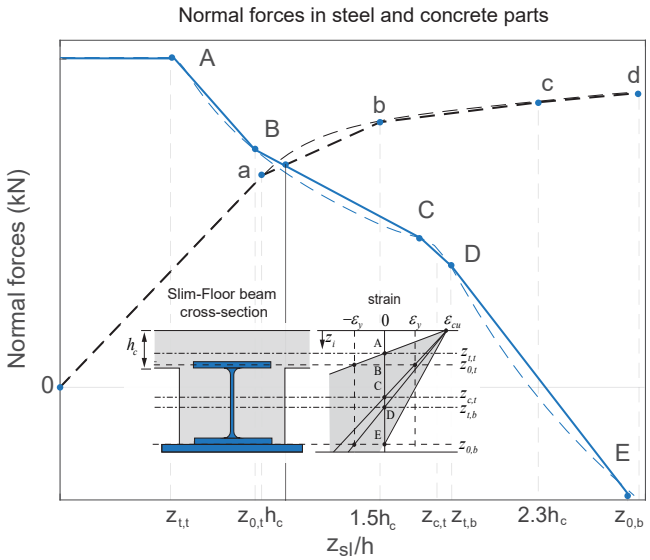

Figure 3.35 – Material functions for steel strain-hardening model

3.5.1.1 Key points A, B, C, D, E for steel part

Table 3.2 – Points for the steel section

Points	z_i	f_t	f_b	N_w		$N_{f,t}+N_{f,b}+N_p$
A	$z_{t,t}$	$-f_y$	f_y	$A_w f_y$		$(A_{f,t}+A_{f,b+p})\cdot f_y$
B	h_1	0	$f_y \cdot min(\frac{d\cdot\varepsilon_{cu}}{h_{ct}\cdot\varepsilon_y},1)$	$A_w f_y - \frac{1}{2}t_w h_{ct}\frac{\varepsilon_y}{\varepsilon_{cu}}f_y$ $A_w f_y \frac{d\cdot\varepsilon_{cu}}{h_{ct}\cdot\varepsilon_y}$	$:\frac{h_{ct}\cdot\varepsilon_y}{d\cdot\varepsilon_{cu}}\le 1$ $:\frac{h_{ct}\cdot\varepsilon_y}{d\cdot\varepsilon_{cu}}>1$	$A_{f,b+p}\cdot f_b$
C	$z_{c,t}$	$-f_y$	$f_y \cdot min(\frac{z_{t,b}-h_{ct}}{h-z_{t,b}},1)$	$(h+h_{ct}-2z_{c,t})t_w f_y$		$A_{f,t}f_t+A_{f,b+p}\cdot f_b$
D	$z_{t,b}$	$-f_y \cdot min(\frac{z_{t,b}-h_{ct}}{h-z_{t,b}},1)$	f_y	$(h+h_{ct}-2z_{t,b})t_w f_y$		$A_{f,t}f_t+A_{f,b+p}\cdot f_b$
E	$h-t_p$	$-f_y \cdot min(\frac{d\varepsilon_{cu}}{h\varepsilon_y},1)$	0	$A_w f_y/2$		$A_{f,t}\cdot f_t$

t_{ft}, ,t_p, t_w : thickness of steel top flange, additional steel plates and steel web. Other nominations see Fig . 3.36 and Eq. (3.30), Eq. (3.31). $A_{f,b+p}=A_{f,b}+A_p$

The points A, B, C, D, E are related to the stress states of steel section: when neutral axis location z_i is above Point A, whole steel sections reach yielding. When the neutral axis is between A and C, the top flange is in elastic, while at point B, the neutral axis is located at the center of top flange thus, the average stress in it equals zero. Above point D, the bottom flange (and additional steel plates) is fully plastic. At point E, the neutral axis is at the center of the lower flange (or center of the bottom flange and additional plate together). The points should be ordered by their z_i values, for example, with shallow sections, the z_i of point D can be smaller than that of point C. The compression zone height z_i and total cross-section internal normal forces N_i of each point are provided in Tabel. 3.2. For simplification, the additional plates and lower flange of steel sections are considered as one part together. Furthermore, the rounded corners between flanges and web are omitted in the calculation. To accommodate the reduced cross-section area, the web height is extended to the distance of the center of flanges (d). The values related to neutral axis locations ($z_{t,t}$, $z_{c,t}$ and $z_{t,b}$) are given in Eq. (3.30) and Eq. (3.31) in section 3.4.4.2.

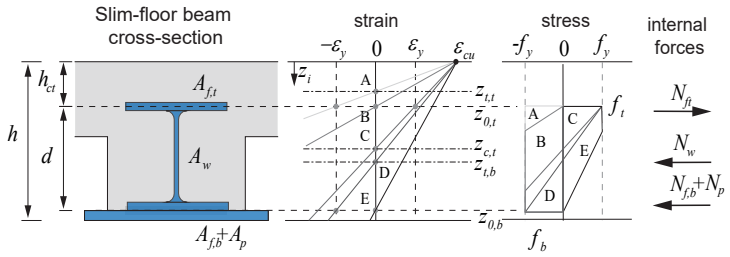

Figure 3.36 – Key points for steel part

3.5.1.2 Key points a, b, c, d for concrete part

The location of the 4 points a, b, c, d are based on the concrete slab thickness above profiled steel sheeting h_c. Point a is the boundary of the neutral axis above the profile sheeting, A solidification ratio of 0.81 is used for the parabolic-rectangle strain-stress model. Point c represents the limit of strain in the concrete slab above profile sheeting are all bigger than ε_{c2}, which indicates a rectangle stress distribution in this part. The Point d represents the neutral axis lying at the bottom of profiled sheeting. To more accurately accommodate the nonlinear changes between point a and c, an intermediate point b is added. Point d is only needed when the location of point c is much smaller than the slab thickness. The values of the four points can be calculated with the help of Table. 3.3 for sagging bending.

Table 3.3 – Points for the steel section

Points	z_i	N_c
a	h_c	$f_{cd} \cdot z_i \cdot 0.81 b_{eff}$
b	$1.5h_c$	$f_{cd} \cdot z_i \cdot (0.65 b_{eff} + 0.16 b_{c2})$
c	$2.3h_c$	$f_{cd} \cdot z_i \cdot (0.43 b_{eff} + 0.37 b_{c2})$
d^*	$h_c + h_p$	according to section 3.4.4.3 or section 3.4.3.2

$*$: point d is needed if $x_c = 2.3h_c < h_c + h_p$, and neutral axis is beyond x_c

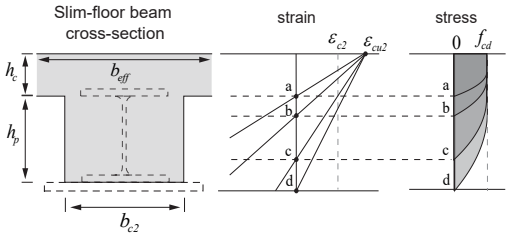

Figure 3.37 – Key points for concrete part

3.5.2 Calculation of strain-limited design resistance

The procedure in the flowchart of Fig. 3.38 can be followed. First, all the points for steel and concrete parts can be calculated according to section 3.5.1.1 and section 3.5.1.2 and $N - z_i$ curves can be plotted. If the neutral axis location can be roughly predicted by experience, the points far away from the predicted neutral axis can be neglected. After the $N - z_i$ curves shown in Fig. 3.35 is obtained, the theoretical location of x_{sl} for pure bending is the intersection of the two curves, the corresponding internal normal

force value N_v is the total longitudinal shear force. Afterwards, the normal forces N_a and N_c in steel and concrete at x_{sl} can be obtained by the exact methods explained in section 3.4.4 or section 3.4.3. For more precise results, if N_a and N_c is less than 5% different, the bending moment of each part M_i can be calculated out by the exact methods, and the bending moment resistance is the sum of all parts ($M_{sl,Rd} = \sum M_i$). If the differences is more than 5%, the new calculated results P_{ai} (x_{sl}, N_a) and P_{ci} (x_{sl}, N_c) should be added into the polylines and new x_{sl} and N_v should be calculated until the criteria is fulfilled. When the additional points P_{ai} or P_{ci} has a similar z_i value to one of the original points, the nearby original point should be replaced by the new point. Normally $\Delta z_i/h = 5\%$ can be used as the limitation of replacing old points or only adding new ones. If great precision is not required the checking of 5% limitation can also be neglected for certain cases. However more parametric studies to check the design model safety factor are still needed.

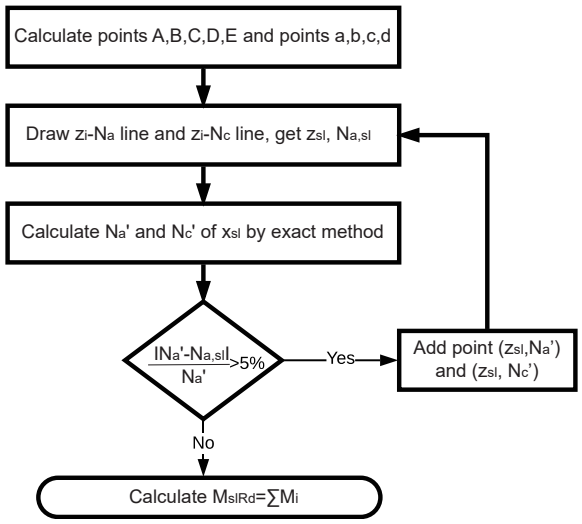

Figure 3.38 – Simplified method procedure

For traditional composite beams, a similar procedure can be used, if chamber concrete is not included, the value of b_{c2} can be set as zero. Furthermore, without the additional steel plate, the z_i of Point E should be changed to the center of the bottom flange. An example for the simplified method and benchmarks is provided in the Appendix E.

3.6 Strain-limited design based software "SL.com"

Following the above mentioned strain-limited design concepts and numerical approaches, a strain-limited design based software "SL.com" for composite structural members has been developed. The software allows cross-section analysis for composite beams, slabs to calculate the resistance, moment-curvature relationship, partial shear diagram as well as to calculate the M-N interaction diagram for composite columns. Furthermore it supports full beam analysis of different types of cross-sections to plot the load-deflection curve as well as the deformation and strain, stress information of whole beam.

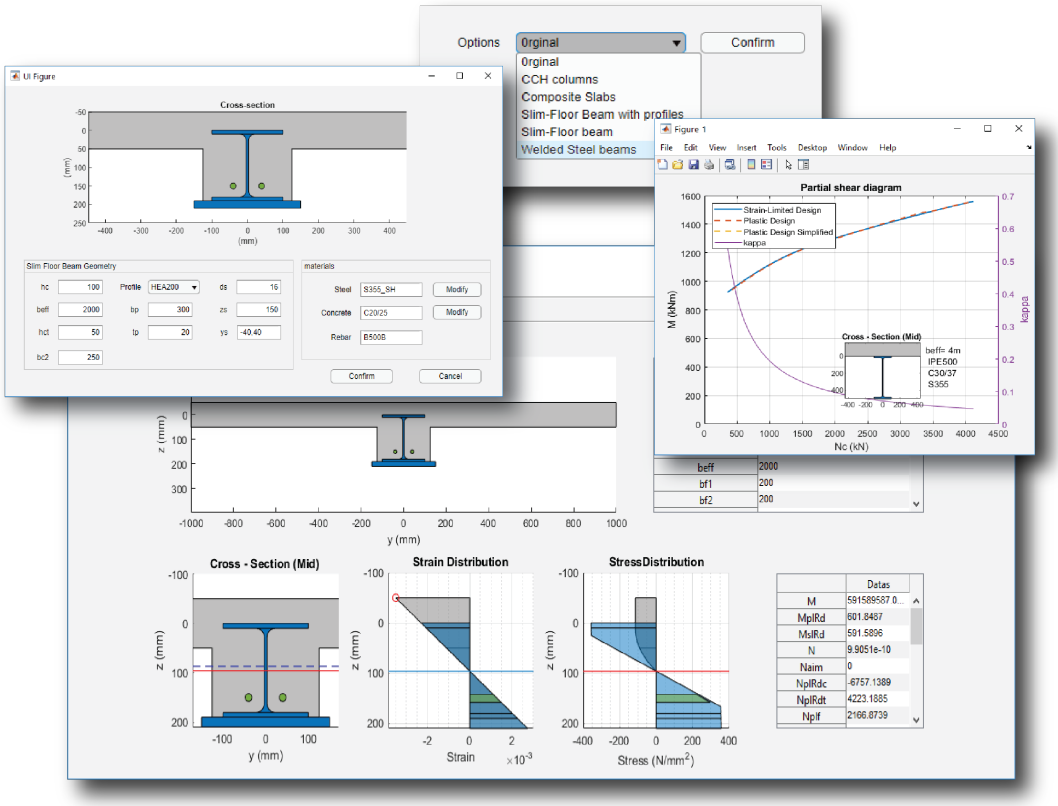

Figure 3.39 – Interfaces of strain-limited design based software "SL.com"

The software has user-friendly graphical design interfaces and built in databases for structural steel, profiled sheeting profiles and different predefined non-linear material strain-stress models according to Eurocodes and other literatures. It supports the typical composite beams, slab, columns, and furthermore supports user-defined cross-section types and materials. Some of the results from the software are provided in the subsections below. The software is also used for parametric studies in the following chapters.

3.6.1 Moment redistribution of composite beams

Due to plastic development is considered, the bending moment calculated by this method allows moment redistribution. Fig. 3.40 shows one example of a two-span composite beam moment with the full shear connection calculated by self-developed software "SL.com". The deformed shape, strain distribution, and moment redistribution at ULS are shown in Fig. 3.41. Moment-redistribution from the mid-span to other parts allows more loads carried by the beam. By step-wisely changing the loads, the load-deflection curve can also be obtained. However, the change of effective width along beam longitudinal direction can only be considered according to the simplified method provided in Eurocode 4. For more advanced applications considering the changing of effective width, FEM simulation can be used.

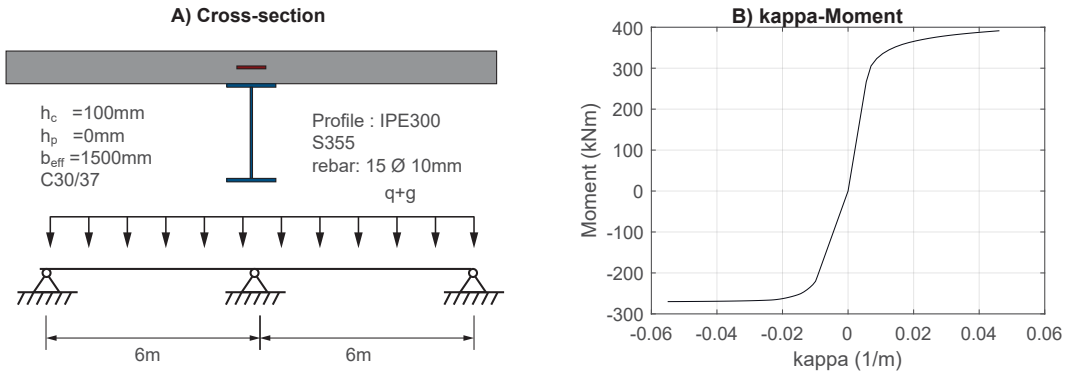

Figure 3.40 – Cross-section and $M - \kappa$ curve of composite beam example

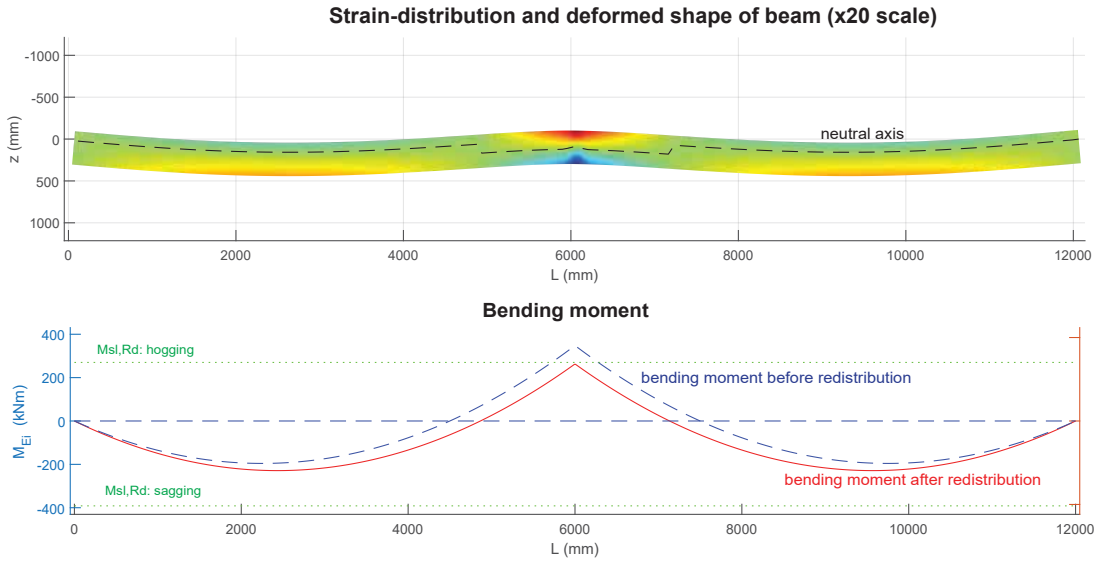

Figure 3.41 – Deformation shape strain distribution and moment redistribution of composite beam calculated by self-developed software using strain limited design method

3.6.2 Application for composite columns

The strain-limited design method can also be expanded for the application of columns with including $\sum N = N_{Ed}$. In this case, the M-N interaction diagram can be obtained by solving different values of N_{Ed}. Fig. 3.42 below shows an example of the interaction diagram of a composite column calculated by the strain-limited method.

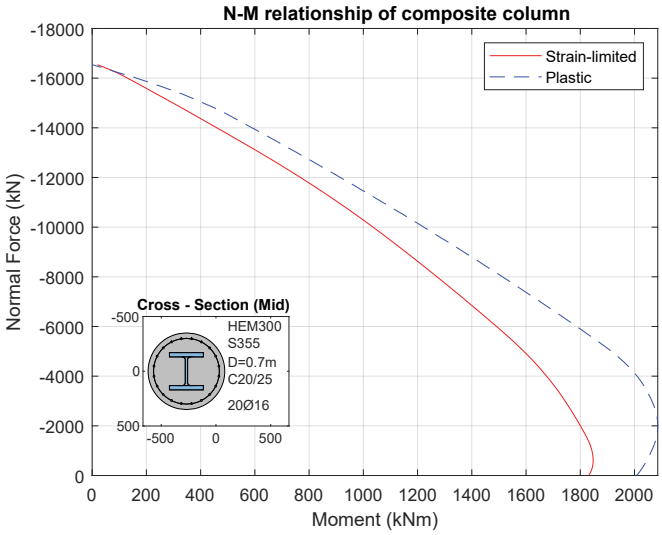

Figure 3.42 – Example of N-M interaction curve of composite columns

The N-M interaction curve noted the ultimate resistance at strain-limits reached. If we also calculate the strain values smaller than the strain-limit stage, record the curvature (κ) and the average compression strain of each case. The $N-M-\kappa$ diagram can be obtained, as shown in Fig. 3.43 below. This diagram can be used to numerically calculate composite beam buckling deformation under a combination of bending moment and normal forces considering the stiffness changes at each height of the composite column. With moment and normal forces at each height is known, the curvature can be obtained as well as the column deformation shape. Then the second-order effects can be considered with an updated moment value. For this procedure, more accurate results can be obtained.

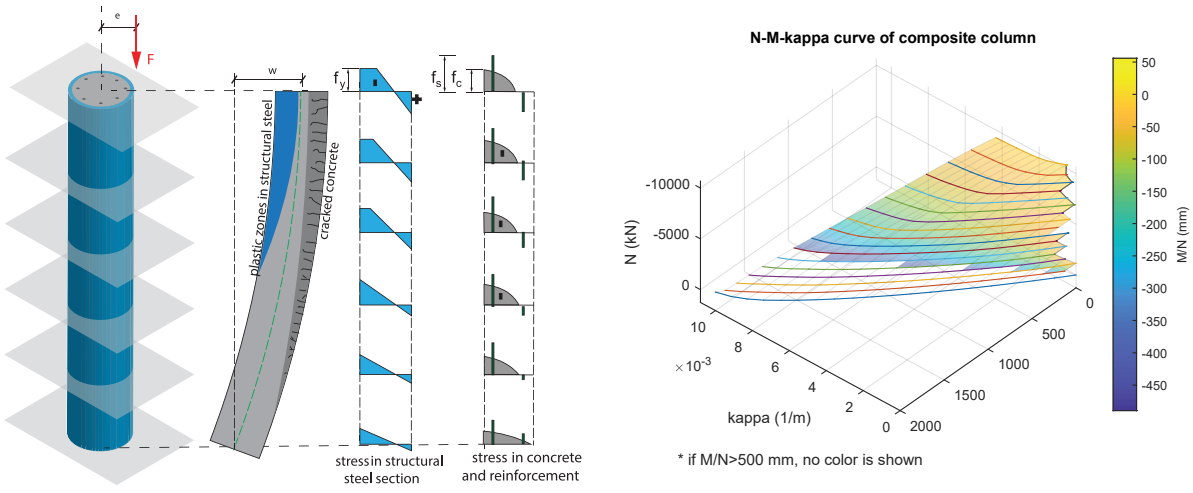

A) illustration of stiffness changes in composite column B) N-M-κ curve of a composite column section

Figure 3.43 – N-M-kappa relationship of composite column considering change of stiffness

3.7 Chapter summary

In this chapter, the theoretical background of strain limited design for composite beams is provided in the section 3.1. It mostly follows the strain-limited design according to EN1992-1-1 for concrete beams with a few necessary modifications to consider the structural steel and slip. The basics of mechanical relationships such as the material constitutive laws, equilibrium conditions, kinematic compatibility are discussed.

In section 3.2, strain-limited bending moment resistance is discussed, The bending moment resistance is calculated with full shear interaction (i.e. no slip exists in the joint) and at the load reaches strain limits. In section 3.3, calculation of load-deflection curves calculated with "$M-\kappa$" curve is reviewed first. To consider partial shear interaction, "$M-\kappa(\varepsilon_{slip})-N_c$" surface is developed and can be used similarly as the "$M-\kappa$" curve to obtain the load-deflection curves and longitudinal shear force distribution.

The conventional numerical approach - finite slice method is simple and straight-forward, however is not most efficient and difficult to programming with. Thus more simplified innovative numerical approaches such as finite cell method, material strain integral method and simplified direct analytical method are provided in section 3.4. These new methods take advantages of that composite beams can be simplified as groups rectangles, thus can solve each rectangle first to avoid dealing with non-linear material and non-linear geometry at the same time.

In section 3.5, a new developed simplified engineering approach allowing strain-limited design by hand calculation is explained. This method can provide a simple strain-limited design with acceptable accuracy.

Chapter 4

FEM models and abaqus Add-in "CivilLab" for composite beams

FEM software is no doubt a potent tool for civil engineers. However, an excellent car does not automatically make a good driver. General multi-physics FEM software Abaqus usually faces a similar situation in civil engineering application; poor results may be expected with a bad model or wrong settings. And many repeated works are done in the simulations which decreases efficiency. One solution is to create a reliable "auto-pilot" or "pilot-aids" system, which can simplify the FEM modelling procedure and reduce the mistakes and efforts during modelling and post-processing. Thus the Abaqus add-in "CivilLab" is created.

With this add-in the bending resistance and longitudinal shear distribution of composite beam considering non-linear material properties and different shear connectors can be easily obtained. Furthermore, parametric studies can be easily carried out to investigate the topics related to the deep neutral axis.

In this chapter, an introduction of the add-in is first given with help with a simple example in section 4.1. Afterward, a short introduction of the general program module structure and capability of the CivilLab system is given in section 4.2. More focus lays on the FEM model's technical details for conventional composite beams and slim-floor beams. They are presented in section 4.3, with more details are also presented in the Appendix A for material models and Appendix C for model calibration.

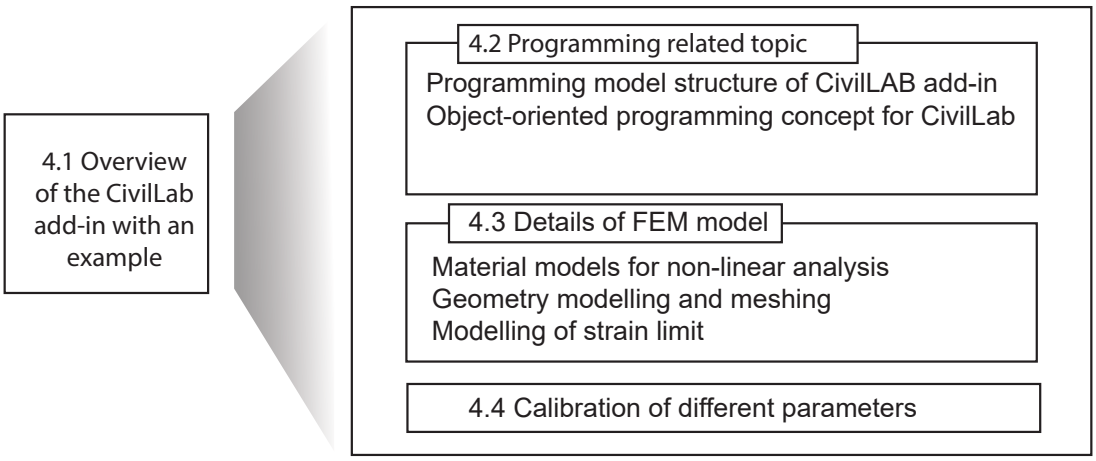

Figure 4.1 – Overview of contents in chapter 4

4.1 A bit of taste with a simple example for CivilLab

Abaqus fully integers Python, it is possible to gain full control of the modelling and post-process with programming. Thus the general modelling procedures can be packed into standard objects within the CivilLab add-in using the object-oriented programming concept. In this way, users can easily create composite beam models with only a few lines of codes or in combination with using the CAE interface. The calculation results of Abaqus are stored in a ".odb" database; however, it is cumbersome for inexperienced users to extract the critical information. Thus CivilLab add-in also added the post-process enhanced functions and a MATLAB based visualization and post-processing software.

In this section, a small calculation example in the "CivilLab" environment is shown. A traditional composite beam with full shear connection is calculated. Material and geometrical properties of the beam are summarized in Fig. 4.2.

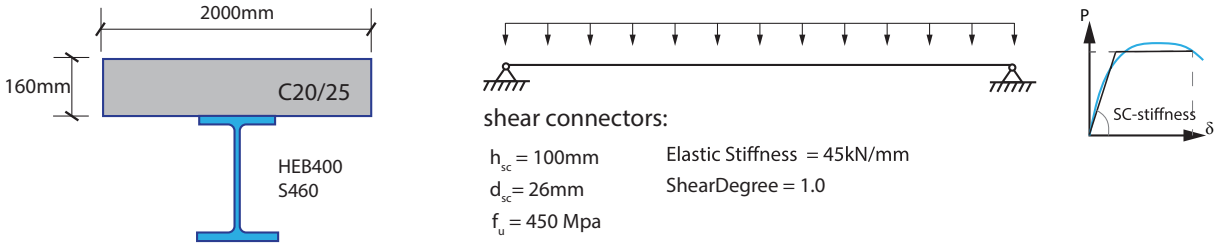

Figure 4.2 – Inputs of a normal composite example

Modelling of the beam with Abaqus CAE usually takes much time as one must create the geometry, choose appropriate material model, add boundary conditions and deal with other special features, which may also cause some mistakes during the process. With the help of the CivilLab add-in, it is possible to type in a few lines of code as shown below in the ABAQUS Python command widow (the "»» " button) to thoroughly perform the modelling process and retrieve desired results.

```
from AB_NCB import *
# to calcualte a beam
NCBRun(ID_= 1, GroupID = 'eta1', modeltype = 'half_model',hc=160, bc= 2000, Length
   = 10000, SteelProfile='HEB400', steel_grade = "S460", concrete_grade = "C20/25"
   , ns = 19,hsc = 100, dsc= 26, fu = 450, stiff = 45000, Load_ratio= 1.1,
  ShearDegree = 1.0)


```

The function used here "NCBRun" is the main function which builds and solves the model exporting the results into the "CivilLab" framework. More parameters can be added to get detailed controls related to meshing, material model types, results and others. Instead of creating a full composite beam with all predefined features, it is also possible to make use of only a specific part of the function as mentioned above. For example only to create the steel beam or add reinforcement meshes in a concrete slab. This significantly adds to the flexibility of the modelling process.

Fig. 4.3 shows the model generated by the code. With the simple, compact function, the parametric study can be easily performed neatly.

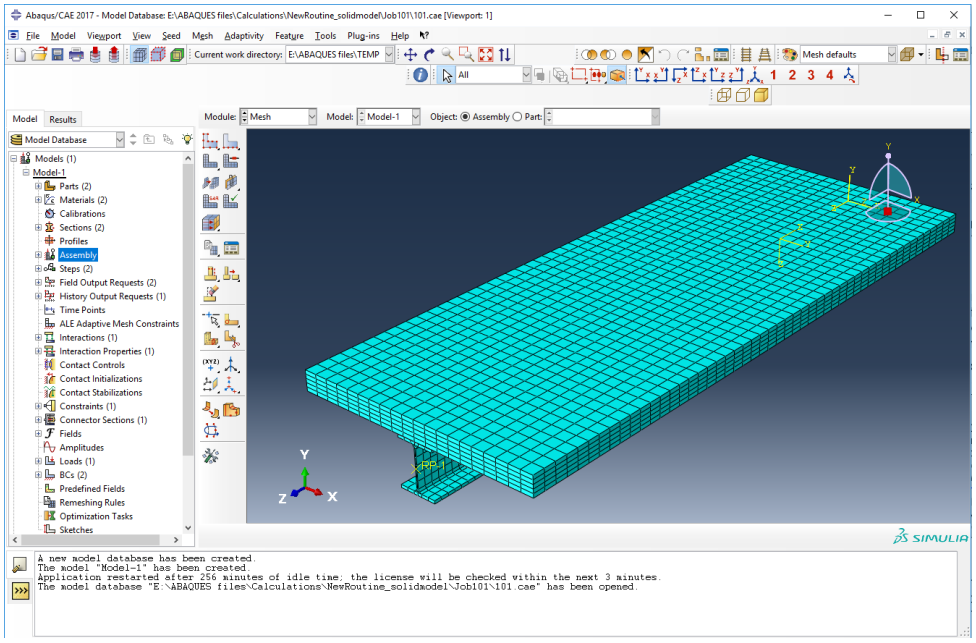

Figure 4.3 – Model of a normal composite example generated by the code

In the case of the parametric studies with a large quantity of data, it is necessary to create a tool which can be used in order to access the critical information and present them in a well-organized way, making it easier for the researchers to understand the results better. These results can be automatically extracted and stored in a database file. Some of the potentially valuable information is listed below:

- Bending moment
- Total longitudinal shear force at mid-span
- Deformation of each shear connector and slip distribution
- Longitudinal load of each shear connector
- Vertical load of each shear connector
- Load-deflection, load-slip, slip-deflection relationship
- Strain distribution at mid-span symmetric axis
- Stress distribution at mid-span symmetric axis

A MATLAB based program can further open the database file for the purpose of further analyses and visualizations. Some of results from the developed software are shown in Fig. 4.4.

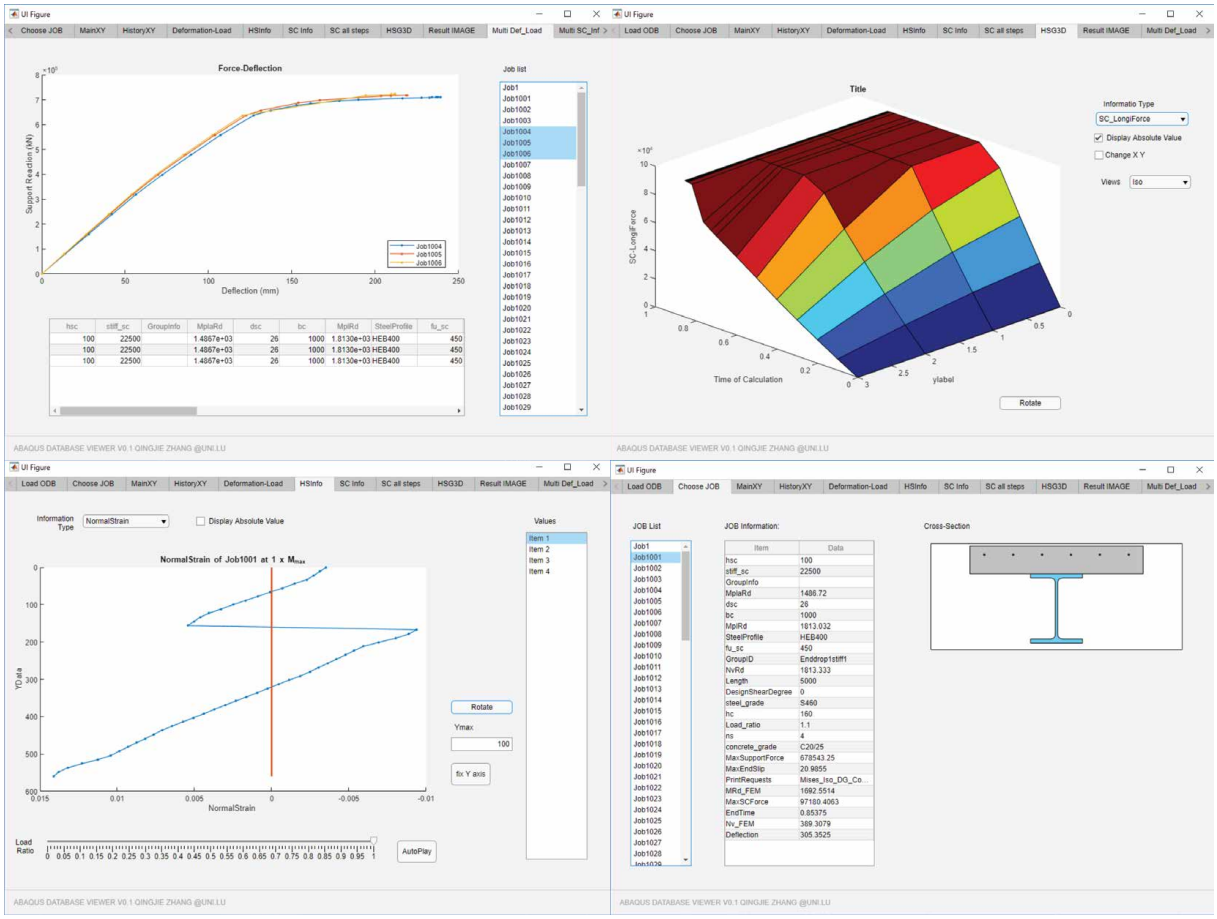

Figure 4.4 – Calculation results in self-developed Matlab-based Abaqus viewer (top-left: Comparison of load-deflection of the beam; top-right: 3D surface of shear connector force-shear connector location - load ratio; bottom-left: strain distribution at mid-span symmetric axis; bottom-right: cross-section information list)

4.2 CivilLab programming modules and flexibility

The CivilLab add-in is developed as a useful toolbox for building-engineering practice specific for composite structures in abaqus. It compiles the most common material models such as the CDP concrete model with Eurocode non-linear concrete strain-stress relationship and many others; standard produces such as IPE, HEA steel beams as well as post-processing visualization tools. It is developed based on the object-oriented programming concept, thus is flexible to use, the user can create a full composite beam or just a part of it. Otherwise, it is possible to use only the post-process tools to abstract critical information from the calculation. The Add-in is still in developing to have more functionalities.

4.2.1 Programming model structure of CivilLAB add-in

The function "NCBRun" presented in the example in section 4.1 is a function for creating conventional composite beam model. This function is developed based on different function classes as shown in the Fig. 4.5 below.

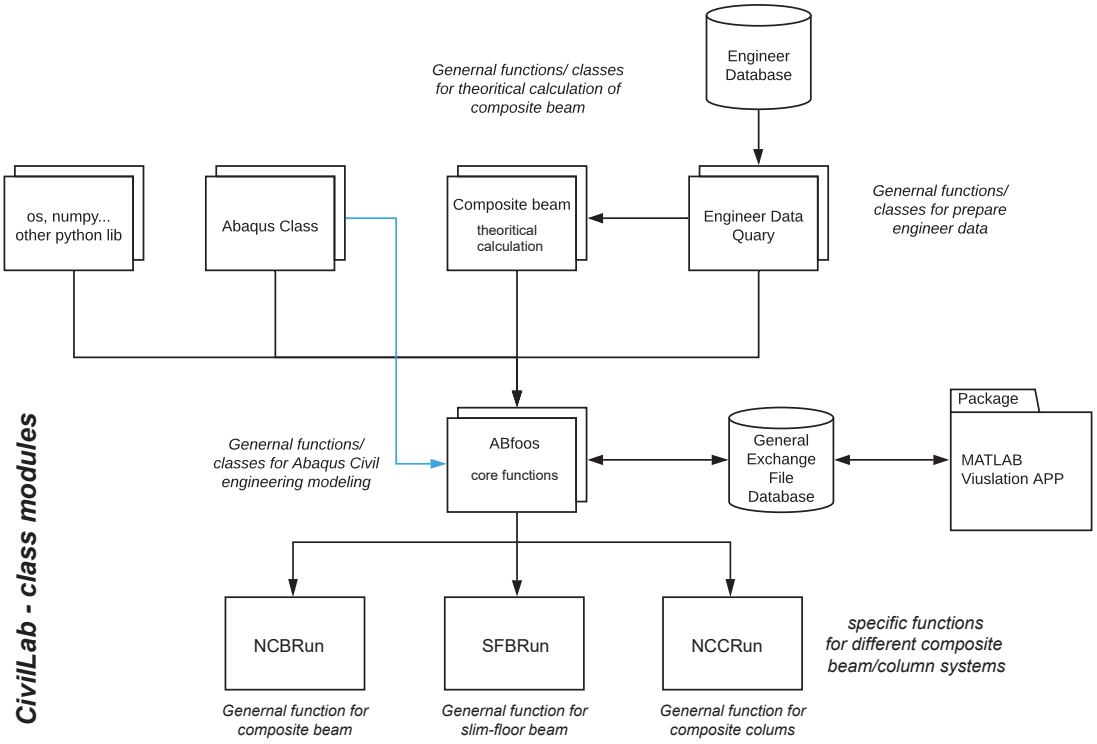

Figure 4.5 – The programming model structure of CivilLAB add-in

The "Engineer Database" contains all of the standard information required for structural analysis such as detailed geometry of a steel profile, material properties according to the relevant codes and others. The information can be queried with the help of the class "Engineer Data Query" to use for further calculation. The class "Composite beam" performed the design of a composite beam according to Eurocodes 4 for example to calculate the plastic bending resistance and required total shear connector numbers. The calculation results can be conveniently used as an input for FEA and for validation purposes. The classes "Abaqus Class" are the classes originally from Abaqus CAE, and is a core of the communication with Abaqus software. Also, other standard python libraries such as "numpy" are necessary. The core class of "CivilLab" is "ABfoos". It contains all the basic functions needed to create geometry material, and more. Furthermore, it controls the output data from Abaqus which are stored in a General Exchange File in SQLite database. Based on the "ABfoos" specific child functions for different types of composite structures are developed. For example, function NCBRun is for creating a Conventional composite beam, and function SFBRun are for creating a slim-floor beam. The details of the add-in are given in the program documentation.

4.2.2 Object oriented programming concept for CivilLab

The CivilLab add-in is developed using the object-oriented-programming concept. For which each part of the composite beam member is programmed as an individual object and different objects can be combined easily. In this way, high flexibility and reuse ability of the program can be achieved. For example, a steel beam is defined as an individual class with public properties of own name, geometry database, meshing, material model and critical surfaces, edged, nodes to apply interaction. Users can generate only a steel beam member as well by using the following code. The result of the code is shown

below in Fig. 4.6.

```
from ABFoos import *
# to add a steel prifile IPE400 of length 400 mm
mysteelbeam = AddSteelProfiles(Name='Beam1',Profile='IPE400',Length=400,Steel='S355',MaterialModel='Bilinear', Location=(0,0,0))
# mysteelbeam will recive parameters related to geometry and material,
# the Profile can also be welded section with providing addtional infomation such as: Profile='Welded', h=400mm, bft=200, bfb=300, tft=20, tfb=20, tw=15
# there are hidden parameters such as meshing quality
# the surface will be generated as Name+surface name such as "Beam1_TFu" for steel top flange upper suface.

```

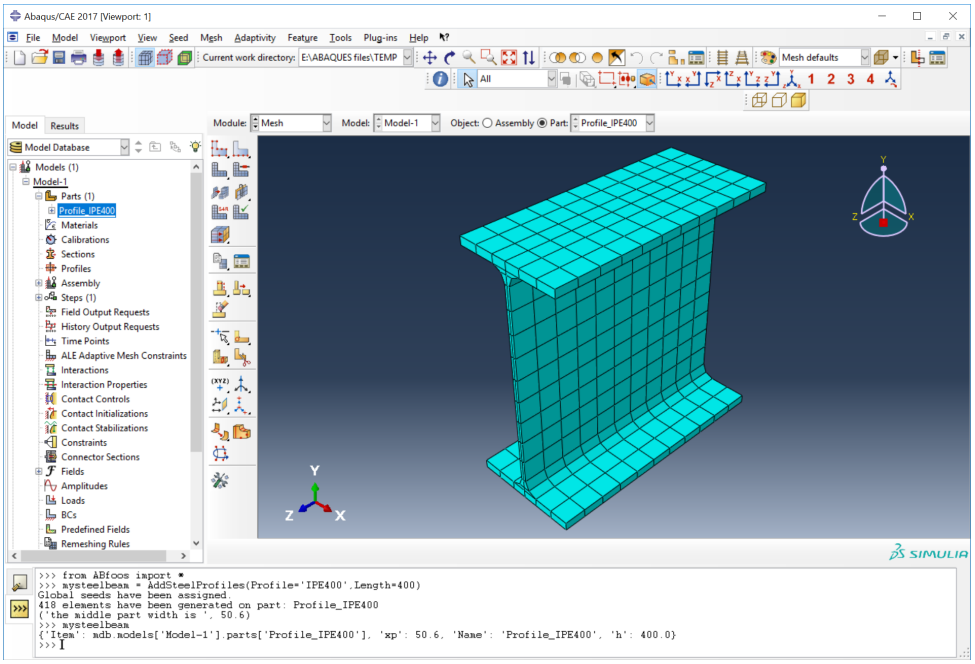

Figure 4.6 – Adding an IPE beam by codes

Another example shown below is to extract force-deflection data from ABAQUS. Required force and observed deflection can be obtained from two different reference nodes in the model - one is usually a point where applied/reaction force is acting, and the other is a point where deflection is being monitored.

```
from ABFoos import *
# to get the load – deflection curve of the model, two nodes are defined before
FDdata=GetForceDeflection(Odbname,SPName,DPName)
# Odbname is the databasename leave blank if is the current opened database
# SPName is the reference point name to calcualte the loads
# DPName is the reference point name to moniter the deflection

```

4.3 Details of FEM model for conventional composite beam and slim-floor beam

The purpose of the conventional and slim-floor beam FE-model is to analysis the global Load-deflection behaviour, the bending moment resistance and longitudinal shear distribution at the joint. Thus local failure such as concrete failure near shear connectors and loading apply area should be avoided in the model. Furthermore, buckling of steel plates is not considered as well. The models are used for vast parametric investigation, thus are much simplified to accelerate the calculation and improve stability. Slot fasteners simulate the shear connectors instead of the explicit model with real shear connector geometry and interactions. The slab reinforcement is simulated with embed surfaces. For slim-floor beams, the overlapping of concrete and steel sections is neglected; however, the surface interaction of steel upper-flange and concrete is simulated. Due to the solution is within static loading and small deformation criteria, the standard solution type is used. In this section, only some key features are introduced. More details are available in the Appendix C.

4.3.1 Material models for non-linear analysis

Concrete exhibits a special sort of quasi-brittle behaviour, showing a decline in strength after reaching its peak. Also, the compression strength differs greatly from the tensile strength. For the modelling of concrete on a macro scale, the Material model "Concrete Damaged Plasticity" (CDP) [1] is used. CDP model is a modification of the Drucker-Prager model. A few parameters should be defined for it. The failure surface roundness in the deviatoric plane is controlled by the input parameter K_c, which is usually chosen as $K_c = 2/3$ by default. (if $K_c = 1$, the failure surface will be a circle which is same as Drucker-Prager model). The meridian surface of the concrete is usually a curve instead of a straight line - CDP model reflects this through a hyperbolic plastic potential surface, adjusted by parameter "plastic potential eccentricity". It can be calculated as a ratio of tensile strength to compressive strength, usually taken as 0.1. (if plastic potential eccentricity is taken as 0, the meridional plane becomes a straight line as in DP-model). Another parameter needed in the CDP model is the strength ratio in the bi-axial stage to uni-axial one, which is suggested to be taken as 1.16. The last input parameter is the dilatation angle which reflects an amount of the plastic volumetric strain developed during plastic shearing and is often assumed to be 36° and in the range of 25° to 40° is suggested [69]. The General inputs are summarized in the table 4.1 below. Concrete uni-axial properties can be tested in a standard compression test, splitting test or in a three-point bending test. Different theoretical concrete tensile/ compressional stress-strain relationship are suggested in the design codes [19, 27] or research articles. Civil-Lab add-in included a few different models to choose, they are provided in the Appendix A, in it more details of the concrete model is provided as well.

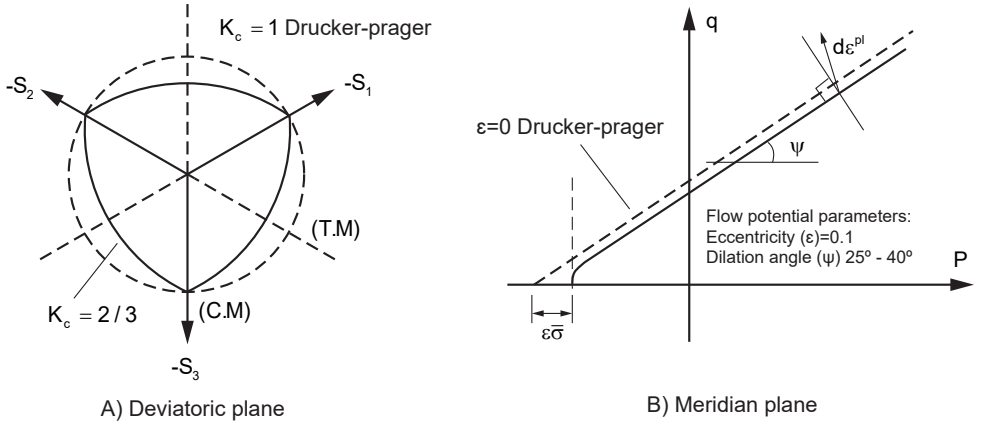

Figure 4.7 – Yield surface and flow rule of CDP model (also see [1, 69])

Parameter name	Dilatation angle	Eccentricity	fbo/fco	κ	Viscosity parameter
Values	36	0.1	1.16	0.667	0

Table 4.1 – The general inputs for CDP model in Abaqus

The structural steel and reinforcement are modelled with the elastic-plastic model, with uni-axis strain-stress relationship as input. The same relationship for strain-limited design explained in section 3.1.3 can be used for FEM calculation as well.

4.3.2 Geometry modelling and meshing

In order to reduce the element number and calculation time, the traditional composite beam uses a half-model, and slim-floor beam uses a quarter model (CivilLab support full-beam model as well). The concrete slab is modelled with the solid element (C3D8), and steel beam can be either a solid element or shell element by choice. Surface element with enabling rebar sub-option model the reinforcement mesh. As the global bending behaviour is the main focus in this work, thus the model is simplified by neglecting the local details such as stirrups or local reinforced reinforcement around shear connectors. However, concrete tension softening is not considered. Instead, a small concrete tension strength value is set without cracking strain.

Shear connectors between the steel beam and concrete slab are modelled as the fastener with slot connector formulation, where the vertical deformation is suppressed. The influence area of the fastener takes a bigger value than the physical size in order to avoid local failure of concrete near the connectors due to local reinforcement are omitted. The support is modelled as pin connection. The end surface was constrained by coupling to a reference point located at the centre of steel beam cross-section. Then the vertical and transverse displacement of the point is set to zero. The mid-span surface is constrained by the symmetric region method. Depending on the research purpose, the loads can be applied to different locations - as the concentrated load applied through the loading pads, or uniformly distributed load on steel beams or concrete slabs. The calibration of model mesh density is provided in Appendix C.

4.3.2.1 Simplified model of traditional composite beam

The simply supported traditional composite beam is modelled as follow: The slab uses solid element (C3D8), and at least five layers of elements in the vertical direction are provided. The mesh reinforcements are modelled with embedded surface enabling rebar sub-option. The steel beam is modelled with also the solid element (C3D8) of two layers of elements in the thickness direction. Fasteners simulate the shear connector connected to the steel upper flange surface and concrete slab lower surface. To avoid local failure of shear connectors, the influence radius of each fastener should be at least 200mm. Calibration parametric study (Appendix C.8) shows little influence if the value is bigger; however, if too small, the stress concentration in concrete near the shear studs will cause convergence problems and reduced shear connector stiffness. The end surface of the steel section is coupled with reference points at ends of the beam to simulate the support.

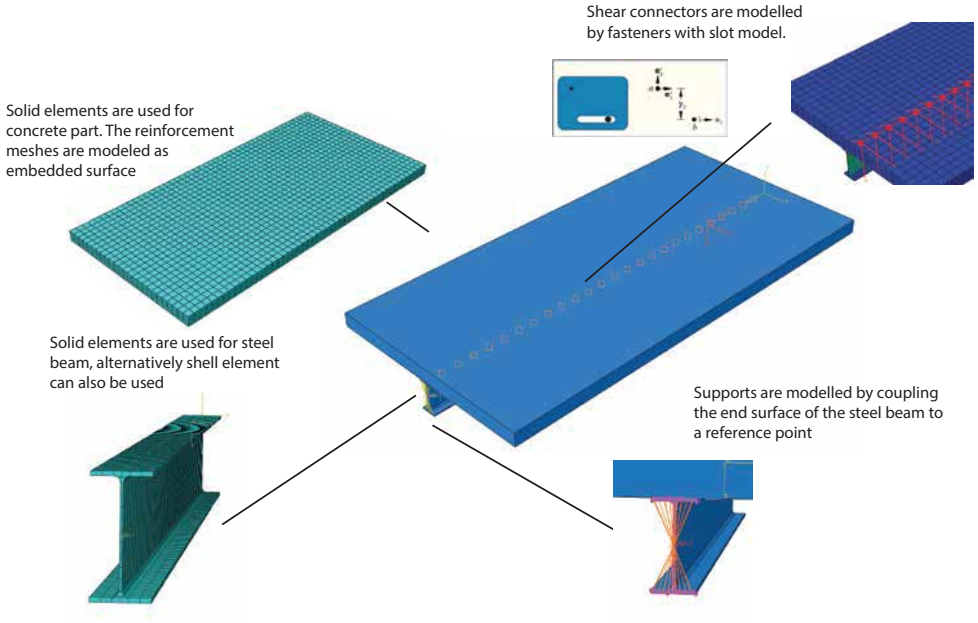

Figure 4.8 – The geometry model of FEM calculation of a normal composite beam

If profile sheeting is used in the concrete slab and is in traversal direction of the composite beam, only the concrete above the profile sheeting can be modelled, with creating an initial spacing between the concrete and steel beam in the model. Benchmark with experiments and more explicit FEM full models (with profiled sheeting and concrete slab including the concrete in the ribs) found little differences of the global load-deflection curve.

4.3.2.2 Simplified model of slim-floor beam

For slim-floor beams, the steel profile is embedded into the concrete slab. First, an explicit full model was calculated; however, the complex geometry and contact between steel and concrete caused often difficulty to converge. Thus a much simplified and more stable model has been developed later: The concrete part is modelled as a "T-beam" without caving out the volume taken by the embedded steel sections. Thus the meshing is more uniform in size and is also less prone to distortion failure. The steel

beam is modelled as the shell element. It is overlapped with the concrete part, and contacts with the concrete part are set at lower and upper flanges. The difficulty is to directly set the contact at upper flanges as there is no interacting surface to the simplified concrete slab part at that location due to cut-outs of overlapping part is neglected. A work-around way is to embed an artificial surface, which has very low stiffness and strength in the longitudinal direction, into the concrete slab at the location of steel top flange to set the contact easily on the surface. As a quarter beam is modelled, thus the contact between the web of steel profile and concrete is not necessary to be added. The shear connectors can be installed at either web or flanges of the slim-floor beams based on the shear connector types and installation requirement. Although this model is much simplified, benchmarks with the tests and explicit full model found small differences in global behaviour.

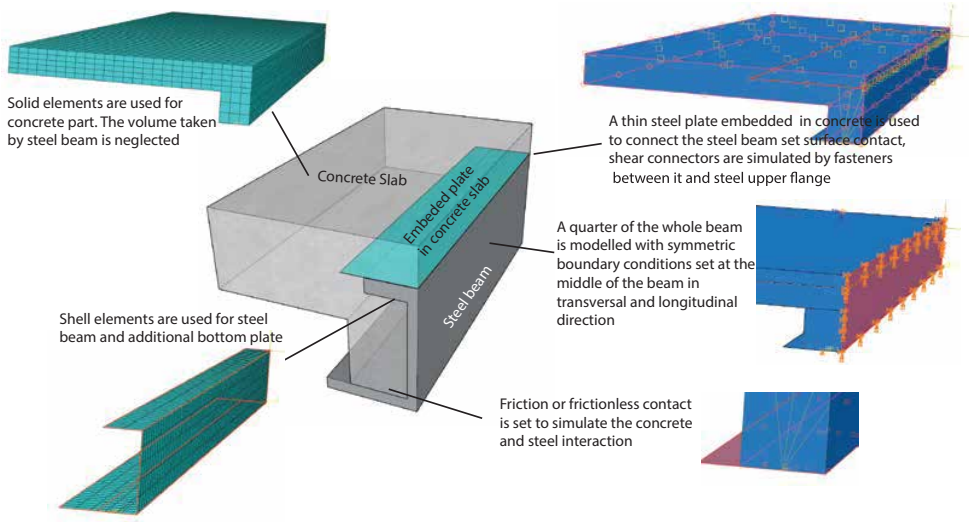

Figure 4.9 – The simplified geometry model of a slim-floor composite beam in Abaqus

4.3.2.3 General meshing control

The overall mesh size was decided by a parametric study in order to reach a good balance between accuracy and calculation demand. As the first order element C3D8 model is used, the aspect ratio (maximum edge length over minimum edge length of one element) should be less than 10 and sudden change of mesh sizes should be avoided according to the Abaqus documentation [1]. In height direction the slab is divided into at least 5 layers to capture more detailed non-linear stress changes. In order to capture the bending behavior of the steel flanges, they should be meshed at least in two layers. However for pure bending of composite beam one-layer of elements still gives very similar results. The auto-meshing of CivilLab is able to consider these factors and provide an optimized mesh based on user defined mesh density level. One example of mesh with default setting is shown below.

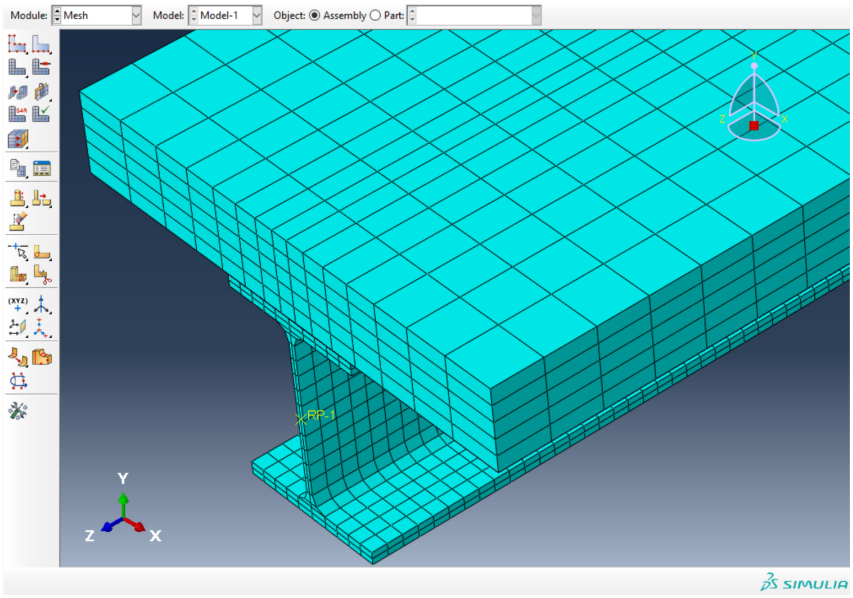

Figure 4.10 – Meshing of a conventional composite beam

4.3.2.4 Modelling of shear connector

Shear connectors are modelled by fasteners element using non-linear slot connector option. The Force-deformation inputs of shear connectors are assigned as the push-out results. This type of connector acts in fact like a non-linear spring between the surfaces, and the surfaces cannot separate from each other. Another possibility is to assign an axial connector section which allows separation of the slab. The big deflection option should be checked in the analysis to allow updating the local axis of the shear connector with the deformation of the surface.

The surface connected by the shear connectors is chosen as the surfaces where shear connectors are installed. By setting an influence radius, Abaqus will select the nodes within the radius to the connector assigned point. The forces will be distributed to these nodes by a user assigned formulation (uniform, linear or others). Due to the bending moment, usually concrete lower surface is in tension in longitudinal direction - the additional shear connector forces can cause local failure and big local deformation if the influence radius is small. Thus it is suggested to choose relatively bigger values of influence area to avoid this problem.

4.3.3 Modelling of strain limit

In order to perform a strain-limit design, it is necessary to set a strain-limit for the materials, especially the concrete compression strain-limit. In these cases, it is desirable to terminate the calculation process when the strain-limit is exceeded. A small trick is to add a sudden drop of stress values when strain exceeds its limit in the material definition, as shown in Fig. 4.11. Then the simulation will not be able to converge after a big amount of elements have strain exceeded the limit; however, stress concentration may terminal earlier the calculation then expected. Otherwise, the strain at certain areas can be monitored and find the responding "failure load" at the strain value. For example, the strain at the top of the mid-span of a concrete slab can be monitored. With the large deformation option is

on, Abaqus provides only inelastic strain values (ε_c^{in}). Thus it should be later converted to real strain value for checking of the strain limit.

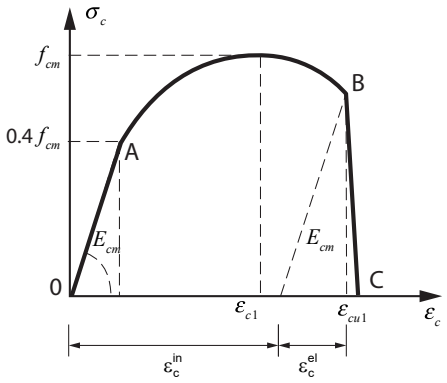

0A: Elastic part of the curve

AB: Non-linear part of the curve
B : Strain limit
BC: Artificial stress sudden-drop to stop the simulation after reaching strain limit

Figure 4.11 – Concrete nonlinear stress-strain relationship according to Eurocode 4 with added strain limits

4.4 Calibration of different FEM model parameters

FEM model in Abaqus requires many different parameters related to geometry, material, meshing and solving process. Choice of suitable values are important, for global analysis (Load-deflection, longitudinal shear distribution) the parameters have different influences on the results. Thus it should be carefully chosen. It is also interesting to see their impact to help later to improve the simulation results. Thus different parametric study on them was carried out. Some of the results are summarized in table 4.2 below, the details are provided in the Appendix C.

4.5 Chapter summary

In this chapter, the self-developed Abaqus Add-in "CivilLab" is introduced. It is designed to simplify the FEM modelling for building engineering in Abaqus. With object-oriented programming, the add-in can be used more flexibly. The conventional composite beam and slim-floor beam models are much simplified, concentrate on simulating the beam overall bending behaviour rather than the details. During the development of the add-in and FEM model, calibrations and parametric studies have been performed to improve the reliability of the FEM results.

Table 4.2 – The calibration and sensitivity results of FEM-model

Parameter	**Remarks**
Mesh size	The mesh in the concrete slab in the vertical direction is suggested to be no less than five layers to capture the non-linear stress changes. For structural steel, the mesh along each plate length direction should have small enough divisions, generally, at least ten elements in flanges or web are set. In thickness direction, due to pure bending, one layer and two layers give similar results. The longest edge to shortest edge of any hex element is controlled to be smaller than 10.
Loading pad size	Bigger loading pad size helps to avoid the stress concentration; however, parametric study shows a similar load-deflection response from 100mm to 200mm size.
Friction at the joint	Friction at the joint increases the degree of shear connection and thus stiffness of the composite beam. It is usually taken as a value of around 0.5 for a concrete-steel interface.
Steel uni-axial strain-stress relationship	The strain hardening model can increase the bending moment resistance up to around 30% compared to the bi-linear model. Usually, the steel strain-limit will not be the controlling factor.
Concrete uni-axial strain-stress relationship	the non-linear and parabolic-rectangle concrete strain-stress relationship give similar results in Load-deflection curve. The concrete strain-limit values impact the endpoint of the simulation greatly. If strain-limits are not considered, the plastic bending resistance can usually be reached; however, the much smaller value is obtained with strain limit for certain cases
Shear connector influence areas	In Abaqus the shear connector is simulated as a non-linear "spring" or "slot" attached on two different surfaces. The force will be distributed to the attached point and nodes inside the influence areas to avoid stress concentration. The parametric study shows that a large influence area does not change much of the Load-deflection relationship. However, a tiny influence area intends to soften the shear connector and cause the local failure in concrete. That is due to stress concentration causes unexpected deformation in the concrete section.

Chapter 5

Benchmark of the FEM and strain-limited design results

In this chapter, the results from FEM simulation and the self-developed strain-limited calculation application are benchmarked with the experimental results from existing literature. In order to test the reliability of the numerical calculations, different types of composite beams with variable sources are taken. Three groups of experimental data are used for the benchmark. The first group is the traditional composite beams with a solid concrete slab from the Lehigh University tests from the 1960s [14] which was the one of the pioneering work of composite beam research. The second group is traditional composite beams with profile sheeting tests from the project DISCCO [58], which aimed at research on the shear connector and composite beams with various modern profile sheeting. The last groups are a collection of different slim-floor beam tests, the CoSFB beam [11], ASB beam [59] and others open-form slim-floor beams have been benchmarked. The benchmarks are to check if the FEM and strain-limited design software are able to correctly predict the composite beam behaviour with different cross-section types and material strength thus the geometrical and material properties are taken from the test reports.

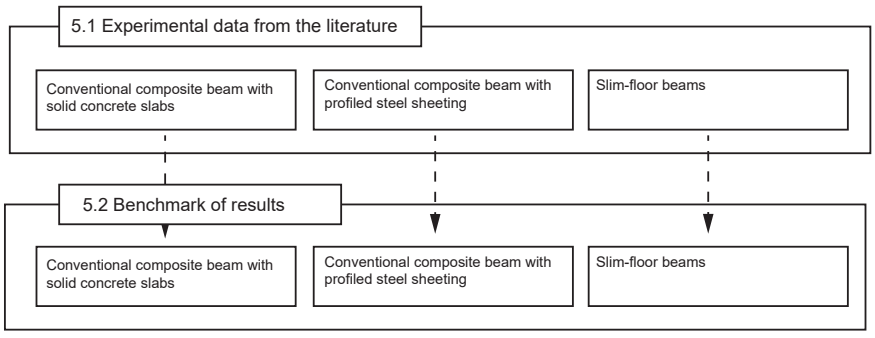

Figure 5.1 – Sections of the Chapter 5

In section 5.1, the experimental data collected from literature are first summarized. Afterwards, the benchmark of Load-deflection curves between FEM, Strain-limited design software and test results are shown in section 5.2.

5.1 Experimental data from literature

5.1.1 Traditional composite beams (solid slab)

A series of composite beam with solid slab tests in Lehigh University [14] in the 1960s is used as a benchmark. They were conducted as part of the research program to establish a specification of AISC codes for composite beams for buildings. The tests were aimed to analyse the impact of friction at the interface, influence of different types of shear connectors and shear degree. In total, 12 beam tests in 5 groups together with six push-out tests were conducted. The beam tests had two different loading setups - one was loaded on the upper surface of concrete slab, the other was loaded on a steel-web trough drilled holes in order to reduce the friction between the composite elements. Two types of shear connectors were used in the beam test - one was with L-shaped shear studs which are similar to headed shear studs, and the other was with welded channel sections. The specimens have the same geometry shapes and material for steel beam and concrete slab. The differences are shear connectors type and layouts as well as the loading methods. The test-related data are given in Fig. 5.2 and Table. 5.1. The beams were mostly designed with full shear connection, with the only group B6 for partial shear connection.

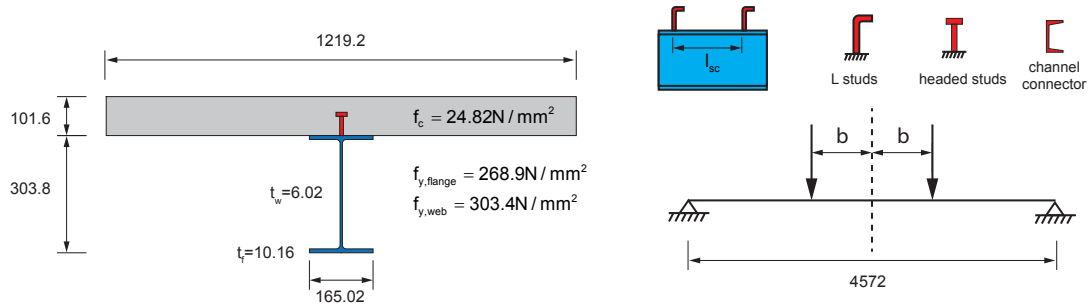

Figure 5.2 – The cross-section and loads position of test in [14] (units are transferred to mm)

Table 5.1 – Detail information of the experiments in [14]

ID	SC type	SC location	f_u	l_{sc} (mm)	b mm	Loading
B3-S1	L-studs	2@190,2*13	496.4	190.5	228.6	Top
B3-S2	L-studs	2@190,2*13	496.4	190.5	457.2	Top
B3-S3	L-studs	2@190,2*13	496.4	190.5	711.2	Top
B4-S1	L-studs	2@190,2*13	496.4	190.5	228.6	Hanging
B4-S2	L-studs	2@190,2*13	496.4	190.5	457.2	Hanging
B4-S4	L-studs	2@190,2*13	496.4	190.5	762	Hanging
B5-S1	channel	L 4 " @510 4.5	N.A.	508.0	228.6	Top
B5-S2	channel	L 4 " @510 4.6	Non	508.0	457.2	Top
B5-S5	channel	L 4 " @510 4.7	Non	508.0	965.2	Top
B6	L-studs	1@190,1*13	496.4	190.5	228.6	Top

5.1.2 Traditional composite beams (with profile sheeting)

The beam tests in the research project DISCCO [58] was used as a benchmark for composite beams with profiled sheeting. In the test project, composite beams with Cofraplus60 profiles or ComFlor80 decking have been tested. The details are shown in Fig. 5.3 and Table. 5.2. The beams were designed with a low degree of shear connection

from 0.15 to 0.42. Push out tests related to each beam were also provided. Analysis of the data is also available in the Dissertation of Nellinger [63] and Eggert [17].

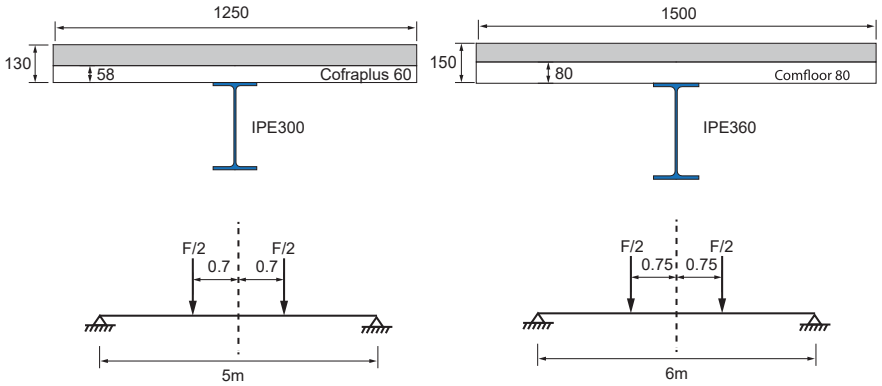

A) Beam test 2-01 to 2-08 B) Beam test 2-09, 2-10

Figure 5.3 – The cross-section and loads position of test in DISCCO project [58]

Table 5.2 – Beam tests configurations from DISCCO test project [58]

ID	Cross-section	d_{sc} (mm)	method	shear connector per rib	Concrete Classes	Rebar layers	Degree of shear connection
B2-01	IPE300 beam, 5m span with 130mm slab thickness comprising CP60 decking	19	through-weld	1	C30/37	1	21%
B2-02		19	punched hole	1	C30/37	2	17%
B2-03		19	through-weld	2	C30/38	1	42%
B2-04		19	punched hole	2	C30/37	1	37%
B2-05		19	punched hole	1	C30/37	1	29%
B2-06		22	punched hole	1	C30/37	2	28%
B2-07		22	punched hole	1	C40/50	2	34%
B2-08		19	punched hole	1	C40/50	2	28%
B2-09	IPE360 beam, 6m span with 150mm slab thickness comprising CP80 decking	19	through-weld	1	C30/37	1	15%
B2-10		19	through-weld	2	C30/37	1	17%

5.1.3 Slim-floor beams

The slim-floor beam tests from different literature have been collected as benchmark references. In [59], three slim-floor beams with the ASB beams were tested. The third beam is with web-opening, which is not taken into consideration in the comparison. No shear connectors were used in these beams; however, the embossed upper surface still enables full shear connection as only small end-slip was observed. In [90] and [96] similar customized asymmetric slim-floor beams were tested to research the slim-floor bending moment resistance. All the beams also behaved similarly as full shear connection with a tiny amount of slip at the interface. In [11], two CoFSB beams "B1" and "B2" with innovative shear connectors are tested for flexure bending.The test details are shown in table. 5.3. The newly conducted tests in SlimAPP projects [55] still found using the shear connectors can increase the bending resistance.

Table 5.3 – Slim-floor beam tests information and configurations

ID	h_c	b_{eff}	b_{c2}	h_{ct}	Profile	b_{f1}	t_{f1}	b_{f2}	t_{f2}	h	t_w	t_p	b_p	f_c	f_y	Length	Load position
CoSFB_B1	134	2500	300	50	HEM220							20	450	30.1	392	8000	
SYJ-1	90	830	120	50	others	140	12	230	12	150	8	0	0	30.5	397	4000	1500 2500
Wang-FSB1	98	750	170	40	others	150	12	250	12	250	8	0	0	27.8	313	6000	3000
Wang-FSB2	98	750	170	40	others	150	12	250	12	250	8	0	0	26.6	313	6000	3000
Lawson-ASB280	82	1000	200	31.6	280ASB	183	16.7	280	18.3	278	19.5	0	0	27.5	405	7500	750 2750 4750 6750
Lawson-ASB300	90	1000	200	30	300ASB	198	21.7	306	20.6	306	17.2	0	0	28.3	389	7500	750 2750 4750 6750

References: CoSFB-B1 [11], SYJ-1 [90], Wang [96], Lawson [59]

5.2 Benchmark of results

For the modelling of the composite beam in Abaqus, the non-linear concrete strain-stress relationship from Eurocode 2 is used. The structural steel and reinforcement are both modelled with the bilinear model, according to EN1993-1-5 [21]. The shear connector is mostly modelled with regards to the push-out test results provided in the reports; theoretical values are used if the beam is designed as full shear connection and push-out data is not available. Friction coefficient at the interface is not given, here it was taken into account through a value of 0.3, however with full shear connection friction does not change much beam behaviour. For the simulation with the own developed strain-limited design software, the same data for FEM analysis are used as the inputs. The software is capable of calculating the full shear connection for both simply supported and continuous beam as well as partial shear connection situation for a simply supported beam. However, the friction at the joint is neglected. Because simulations found that the reinforcement in the top of the concrete slab has little influence of beam bending behaviour for simply supported beam as they are in compression zone and has limited cross-section area, thus they can be neglected in the calculation if high accuracy is not required. For the first group with solid concrete slab and full shear connection, the strain-limited software uses the option full shear interaction which set slip to zero in the joint.

5.2.1 Benchmark results of traditional composite beams with solid slab

The composite beam with solid slab test listed in section 5.1.1 is compared. B1 and B2 are beams without shear connectors, which is not "real" composite beams, thus is not shown in the benchmark. For the test group B3, three beams had been tested varying the location of the applied loads - 228 mm, 457 mm, 711 mm, measured from the centre of the beam. The beams were loaded at the top of the concrete slab. L-shape shear connectors of 0.5-inch diameter were placed in two rows and were spaced at a distance of 190mm. All the beams were loaded until the failure. The comparison of experimental, FEM and strain-limited design results are shown in Fig. 5.4. For strain-limited design, full shear interaction is assumed expected for beam B6S1.

In the case of the test B3-S1 and B3-S2, the beams were unloaded and reloaded during the test. The FEM model and strain-limited software; however, does not consider the impact of the loading history. Regarding the B3-S3 test results, the plot shows the failure of the shear connectors, whereas in the FEM and strain limited simulation shear connector is modelled with infinite deformation capacity, thus not able to capture the descending branch of the experimental curve. For the test group B4, three beams were tested with different location of applied loads (228 mm, 457 mm, 762 mm) measured from the centre

of the beam. The beams were loaded on the bottom flange until failure. The beam specimens are similar to the test Group B3. For the test B4-S1 the specimen was unloaded and reloaded during the test as well. The part before unloading fits very well, however in the FEM and strain limited model unloading/reloading phase was not considered. B4-S2 shows the failure of shear connectors in the test results; thus, an earlier failure is seen in the benchmark. Compared to the group B3, due to simple concrete stress state in B4 (no vertical compression under the load-pad), the simulation gives better results.

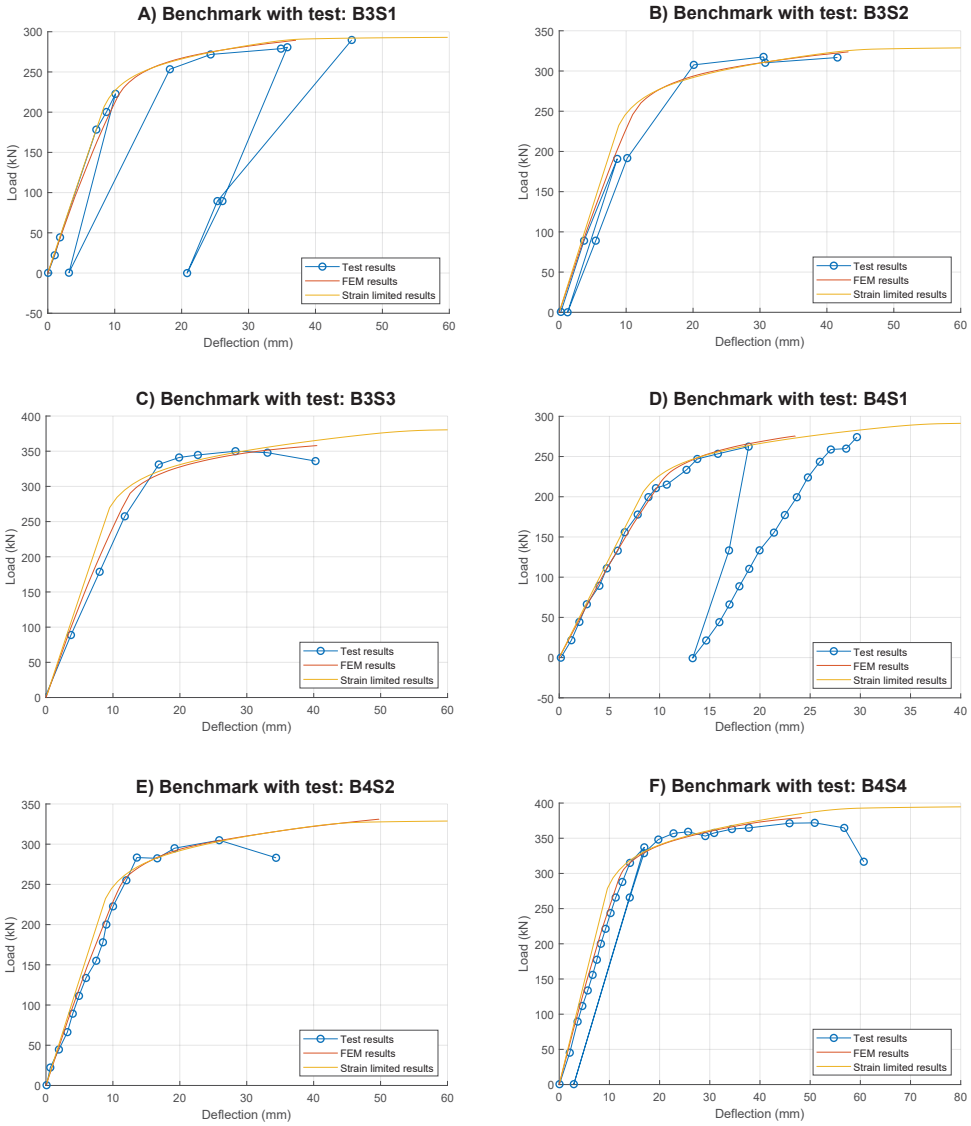

Figure 5.4 – Benchmark of the test results of traditional composite beams and numerical simulations (part A)

For the test group B5, three beams were tested with different location of applied loads (228 mm, 457 mm, 965 mm) measured from the centre of the beam. The beams were loaded at the top of the concrete slab. Channel shear connectors, with a height of 3 inches, were welded with a distance of 510mm. All the beams were loaded until they reached failure. The comparison of experimental strain limited and FEM results is shown in Fig. 5.5. Test B5-S1 shows the failure of concrete. When looking at the B3-S2 and S5 results, although a very similar initial stiffness and maximum resistance are observed, different stiffness is predicted in the plastic region. The test results show a bigger elastic zone

and a quick transition into the full plastic behaviour. The uncertain of shear connector load-deformation proprieties may cause the difference as only one push-out test for channel connector was conducted, which generally may exhibit different behaviour in the beam tests. Also, only a few numbers of shear connector was installed in the full beam, with the precise location being unknown - in the FEM simulation, they were assumed to be equally distanced, which may cause the difference in the results.

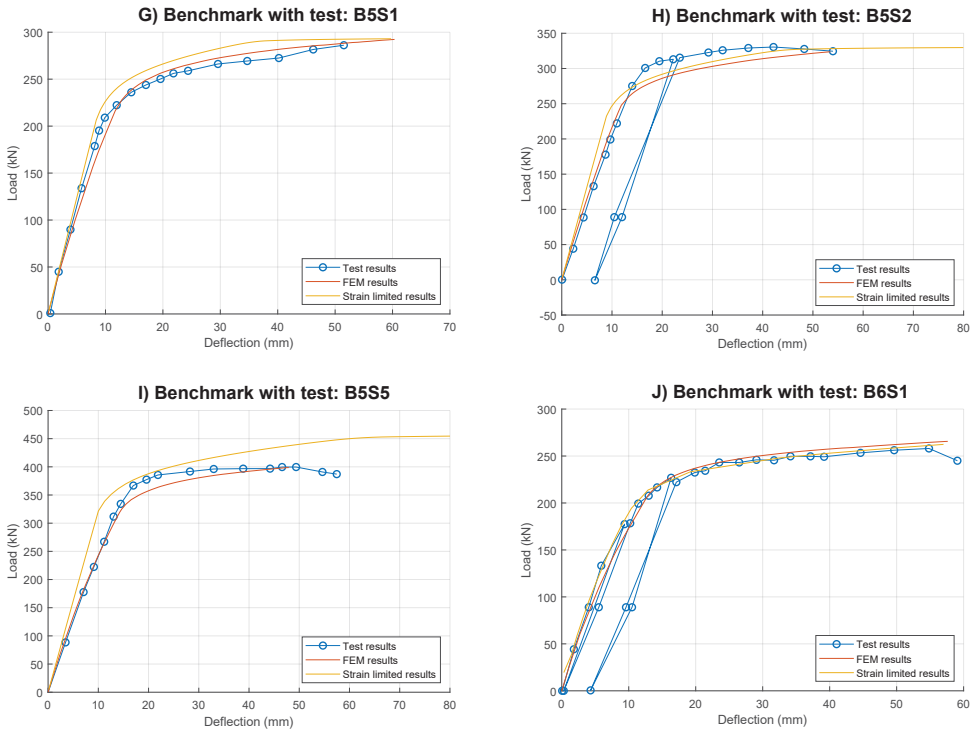

Figure 5.5 – Benchmark of the test results of traditional composite beams and numerical simulations (part B)

For the test group B6-S1, the beam specimen is similar to B3-S1 but with partial shear connection employed, as only one row of shear connectors were installed with a distance of 190mm between each (two rows in test group B3). The comparison of experimental and FEM results is shown in Fig. 5.5 below. Except for the unloading-reloading part, FEM and strain limited design predict almost identical results with the experimental tests, before the failure is reached. The test report shows the failure type of shear connectors, which is depicted by the drop of the last point in the load-deflection curve. The maximum resistance by FEM is a bit overestimated (around 3%), and strain-limited software gives closer results.

Overall both FEM model and strain-limited design software give similar results compared to the tests; the strain-limited design software gives slightly higher initial stiffness due to assumption of full shear interaction (zero slip); however, the calculated resistance is very close. Test B5S5 shows a bigger difference between strain limited design and tests. It is possible due to for the test as a few block shear connectors were installed with great distance, slip exists between shear connectors, which reduces the composite beam stiffness.

5.2.2 Benchmark results of traditional composite beam with profiled sheeting

For composite beams with steel profiled sheeting, the experimental results from test program DISCCO [58] (Development of Improved Shear Connection rules in Composite beams) are used. The program consists of seven work packages, while work package one (WP1) contains various push out tests and work package two (WP2) provides ten beam tests. The beam-tests are designed with very low degrees of shear connection with less than 40% in all but one case. (Details see section 5.1.2)

The responding push-out test results from WP1 was directly used as shear connector input first. The Load-deflection of composite beam tests shows softening ranges after reaching the maximum bending resistance, which later turns into a typical plastic plateau. In the initial benchmarks, the first part of the load-deflection curve follows well the test results; however, the softening part is not seen, and much higher resistance has resulted. Further analysis (see Appendix C.10) suggested that the difference may be caused by shear connector behaves differently in push-out tests and real composite beams. A softening behaviour of shear connector in the test is often noticed in combination with profile sheeting as explained in work of [28] from the test in Lehigh University in the 1980s. The similar softening effects in beam tests are also noticed in the longitudinal shear force - slip relationship backwards-calculated from the beam tests stain values in the steel beam, in the work of Nellinger [63] of the same specimen B2-10, for which the push-out tests did not capture the response. He also suggested a trilinear shear connector model with a softening part after 6mm deformation.

Thus in the benchmark, the shear connector model is modified from the push-out results by adopting a multi-linear curve considering softening part. The initial stiffness and maximum resistance are taken from the test data, after reaching maximum resistance a softening branch is added afterwards following with a constant plateau. The stiffness of the softening range is acquired by benchmarks with the beam behaviour and choosing the best fit values, which is not from the push-out test result. For the strain-limited design solution, the same shear connector Load-deformation curve is used. However, due to the limitation of solver, it is only possible to calculate until the maximum bending moment resistance point. The results are given in Fig. 5.6 and Fig. 5.7.

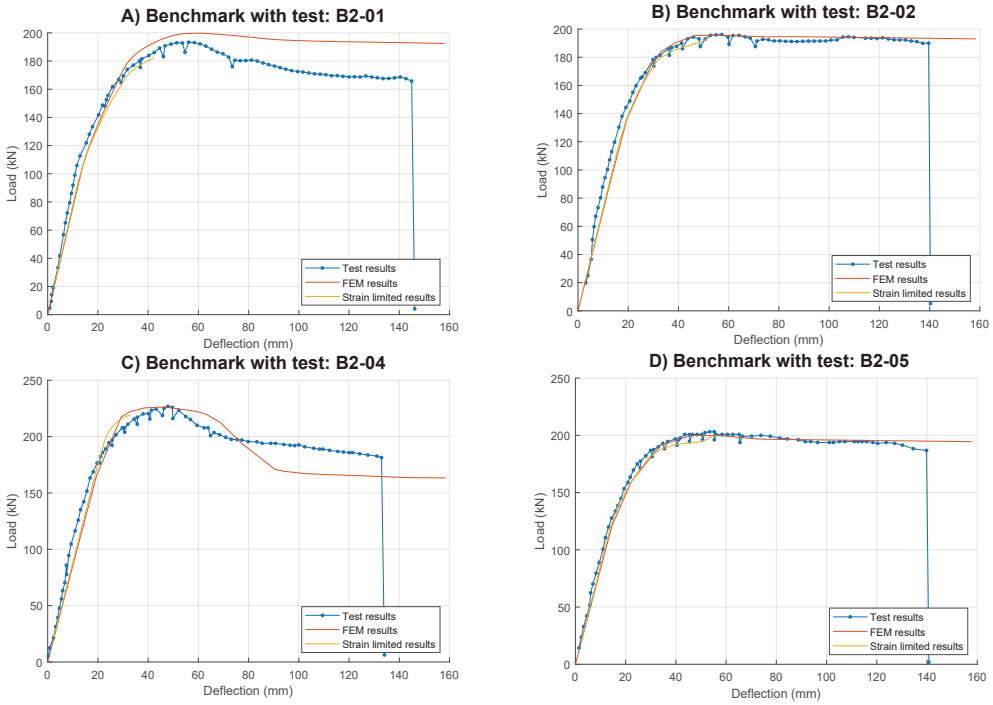

Figure 5.6 – Benchmark of the test results of composite beams from DISCCO and numerical simulations (Part A)

The load-deformation curves from the tests B2-01 to B2-09 all display a decrease of the resistance after reach the peak. For the benchmark, if the original push-out curve without softening is used, the first part until the peak resistance fit well, but the softening behaviour is not able to be captured with an overestimated bending moment resistance. With including the softening part, the curves fit better. For beam test B2-03, errors in the weld beards in the headed studs are reported, which caused significant losses of the bearing capacity. Thus it is not taken into consideration of the comparison. For beam test B2-09, asymmetric beam failure of the shear interface was observed during the test procedure, which is later confirmed by the evaluation of the measured strains. Thus it is also not used for the benchmark.

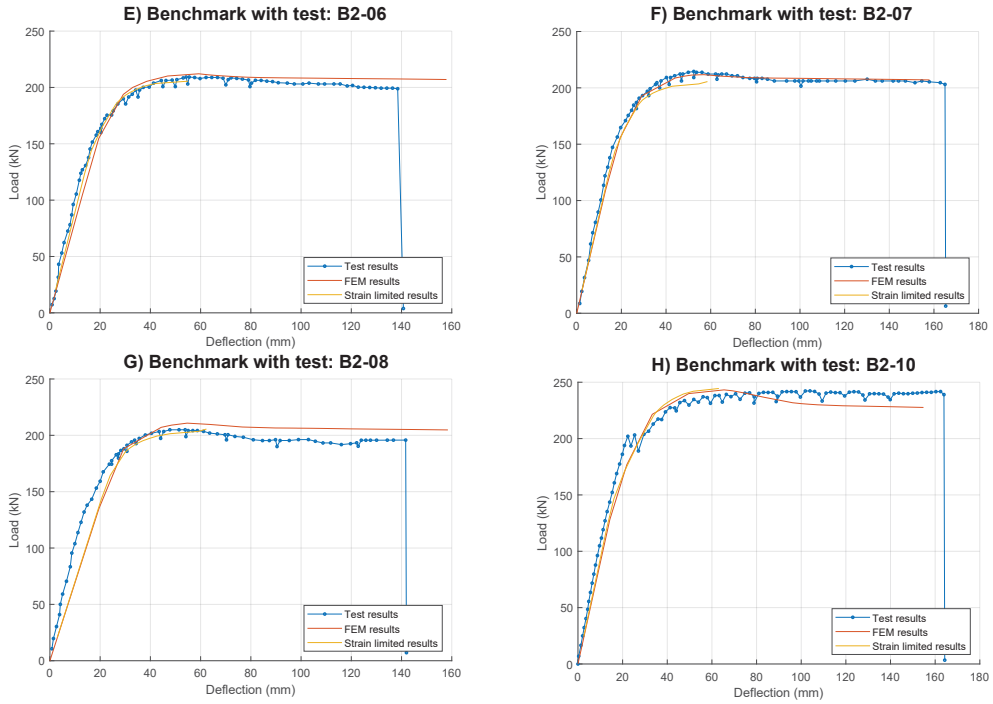

Figure 5.7 – Benchmark of the test results of composite beams from DISCCO and numerical simulations (Part B)

For all the benchmarks, the first part of the load-deflection curve can be predicted very well by both FEM and strain-limited design software for the composite beams with profile sheeting. However, with the push-out results as spring model, even with the reduced maximum resistance of 10% considering the static loading, the FEM and strain limited design shows higher resistance and no softening part of Load-deflection curve. Also, literature [28, 63] suggested the push-out tests may lacking a softening behaviour which is shown in a beam test. With artificial softening added, the load-deflection curve of FEM can be captured well.

5.2.3 Results of slim-floor beams

The benchmark results of various slim-floor beams are shown in Fig. 5.8. As test reports show little end-slip (smaller than 1mm), the beams are treated as full shear interaction in the simulation of FEM and the strain-limited design method. Despite the fact that the model has been much simplified with neglecting the mesh reinforcement and local reinforcements, good agreements in the load-deflection curve are still obtained. Both slim-floor beams with Asymmetric Slimflor Beam (ASB) and with welded additional steel plates are compared.

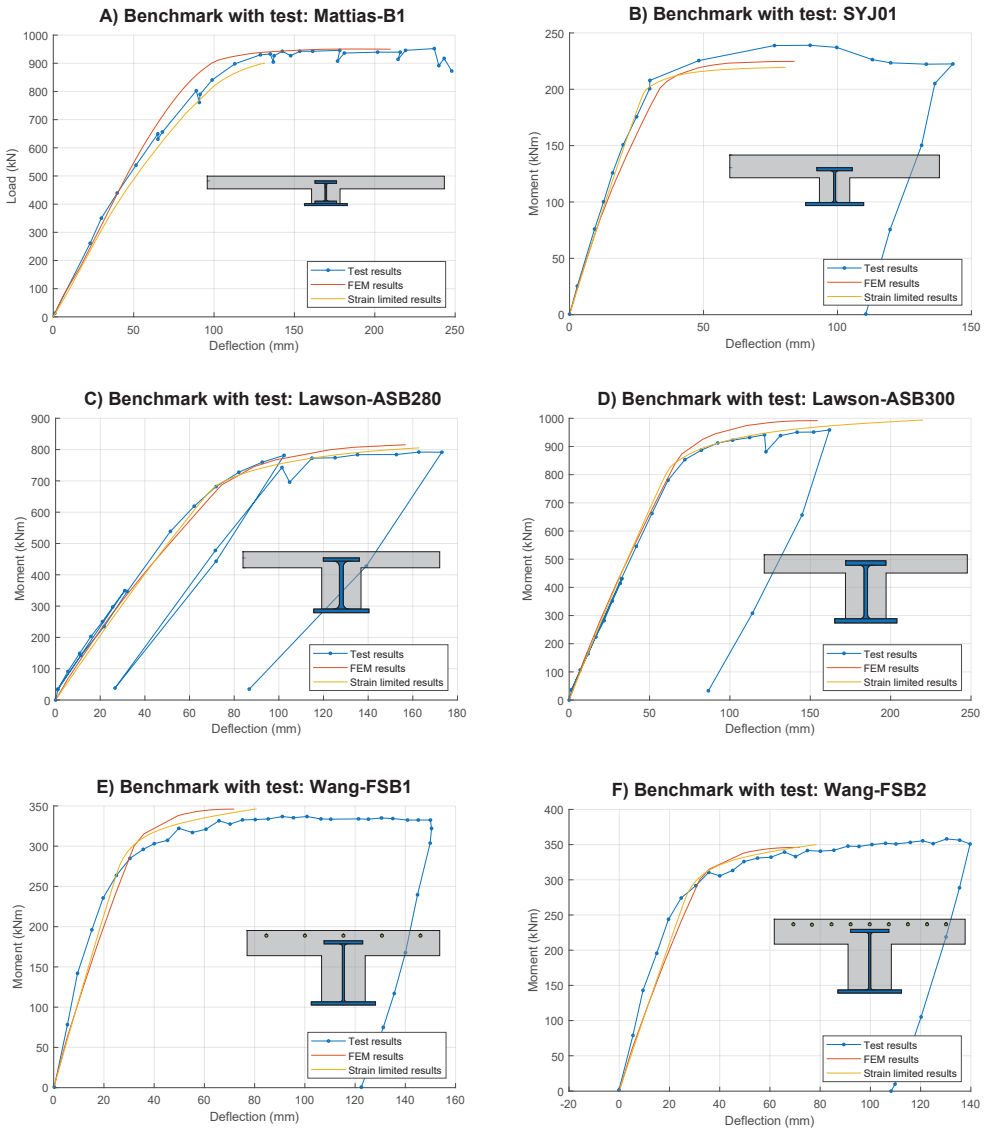

Figure 5.8 – Benchmark of the test results of slim-floor beams and numerical simulations

Overall the slim-floor beams reaches plastic range at deflection around 1/100 of the span length. However a smooth transfer from elastic to plastic region is seen without a clear boundary.

5.3 Chapter summary

The benchmark results show the correct prediction by both FEM model and self-developed strain limited design software in the case of traditional composite beams with solid concrete slab and slim-floor beams. The load-deflection curves fit well for the test with traditional composite beams with solid concrete slabs, for which mostly the full shear interaction is realized. For slim-floor beams, the open form slim-floor beams such as the CoSFB beams and ASB beams have been benchmarked and shows good agreement between test results FEM and strain-limited design calculation. For composite beams with profile sheeting, with push-out results as shear connector spring model, the program can only capture the initial parts correctly. A modification of the softening part in the

push-out result is suggested. Compared to the FEM results, the strain-limited design software shows slightly higher beam initial stiffness in the load-deformation curve partly due to the full shear interaction assumption overestimate the shear connector stiffness.

Chapter 6

Bending moment resistance of composite beams

The bending moment resistance of composite beams can be calculated by plastic design method according to Eurocode 4 [22]. To get more precise design results, advanced non-linear strain limited design or FEM calculation explained in former chapters can be used. However, for sagging bending with full shear interaction, if the neutral axis is deep, plastic bending resistance can be overestimated. Thus limitations on neutral axis position should be set to use plastic design. Beyond the limitation, advanced design methods can be used. Otherwise, a reduction factor of plastic bending moment resistance needs to be applied. For partial shear connection, the partial shear diagram developed based on plastic analysis is commonly used. However, the impact of deep laying neutral axis position is not mentioned. As slim-floor beams usually have bigger relative compression zone height at failure due to its shallow cross-section, the application of partial shear diagram on slim-floor needs further researches.

This chapter discusses the sagging bending design for both full and partial shear connection. For a full shear connection in section 6.1, the β reduction factor applied on plastic bending moment resistance according to Eurocode 4 [22] is further developed from a vast amount of parametric studies considering new types of composite beam cross-sections. The influence of deep neutral axis position on plastic bending moment resistance is first explained in subsection 6.1.1. Then based on the analysis on millions of parametric calculation results comparing plastic bending resistance and strain-limited bending resistance, the key parameters are able to be selected out in subsection 6.1.4. Later based on statistic results, the improved β reduction factor functions are proposed in subsection 6.1.5 and subsection 6.1.6.

For the partial shear connection in section 6.2, considering the deep neutral axis position of slim-floor beams, limitations on the partial shear diagram and the simplified design methods are proposed. In subsection 6.2.1 partial shear diagrams obtained by plastic and strain limited methods are compared. The influence of neutral axis position on partial shear diagrams are discussed in subsection 6.2.2, based on a vast amount of parametric study results, the limitation of plastic partial shear diagram can be drawn in subsection 6.2.4 and beyond the limitation, a simplified engineering approach is proposed in subsection 6.2.5

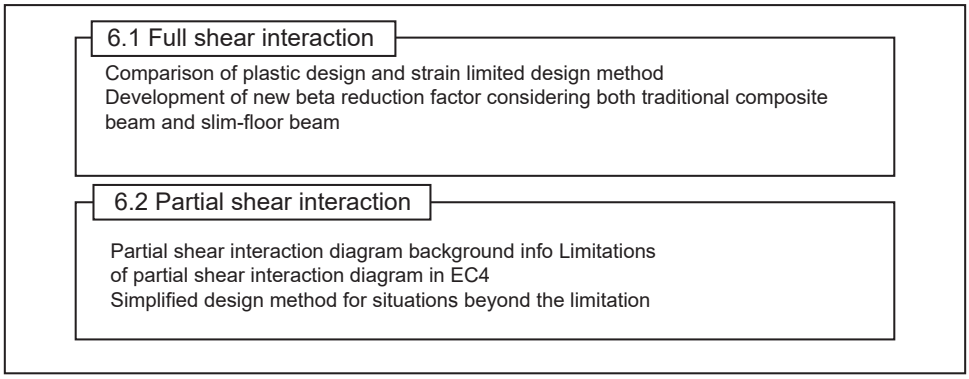

Figure 6.1 – Structure of chapter 6

6.1 Bending moment resistance with full shear connection

In the case of composite beams with cross-section classes 1 and 2 usually, plastic bending resistance can be taken into account. While composite cross-sections according to Eurocode are often characterized by a double-symmetrical steel profile with an upper concrete flange; today even slimmer, more compact and more individual beam systems become important (section 2.1). The trend in the last years often shows sections which are integrated into the concrete slab (shallow floor or slim-floor beams), partially encased composite cross-sections as well as sections with a low construction height and asymmetrical cross-sections. For such sections, the plastic bending resistance can lead to an overestimation. Therefore, further verifications are necessary.

6.1.1 Influence of deep neutral axis position on plastic and strain-limited design resistance

In case of standard composite beams according to Eurocode 4[22], a classification into four cross-section classes based on the c/t-ratio of the flanges and web of the steel section reflects the rotation capacity indirectly and prevents local buckling effects. If a classification into the cross-section classes 1 or 2 is possible, the plastic moment resistance can be taken into account. Otherwise, an elastic design for class 3 or an elastic design considering the buckling effects (class 4) is necessary. For partially or fully encased sections, cross-section classification only considers the steel plate local-buckling. However, the influence of the concrete part is not included.

Strain-limited design, on the other hand, calculates the bending resistance $M_{sl,Rd}$ based on the stress-strain relationship of the materials for concrete and reinforcement according to EN 1992-1-1:2004 [19], as well as Eurocode 3 for the structural steel. The solution is found by variation of cross-section strain until the equilibrium of internal force is reached. For the assumption of full shear interaction, the strain at the concrete, extreme outer fibre at the top is first fixed to the ultimate concrete strain $\varepsilon_{c,u}$ and the curvature, which indicates the slope of strain curve, is varied until an equilibrium condition is reached. If no solution is found, other strain limit points in the steel section should be used. The details are provided in section 3.2.

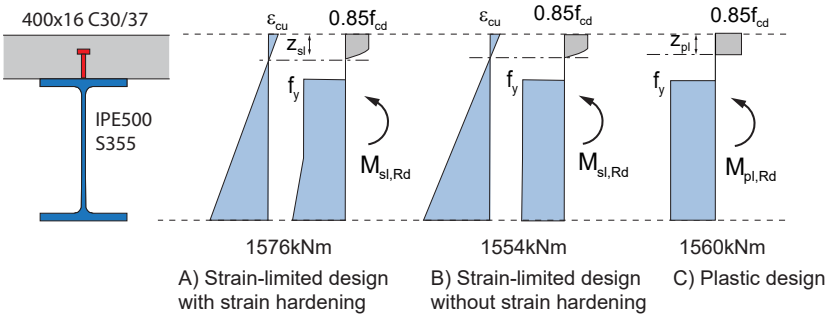

Figure 6.2 – Plastic and strain limited design for a conventional composite beam

For the plastic bending resistance, it is still assumed that each cross-sectional fibre can plastify without any limitation of the strains. For standard composite beams in the case of sagging moments and a high position of the plastic neutral axis, the plastic bending resistance and strain-limited bending resistance shows similar moment resistance (Fig. 6.2,

case B and C), if strain- limited design is based on a bilinear elastic, ideal-plastic stress-strain curve for steel section. When considering strain hardening for the stress-strain relation of structural steel, the strain-limited moment resistance, which is similar to test results is considerably greater than the plastic bending resistance. This is based on the large strains at the steel bottom flange so that that strain hardening can be taken into account (Fig. 6.2, compare case A and B).

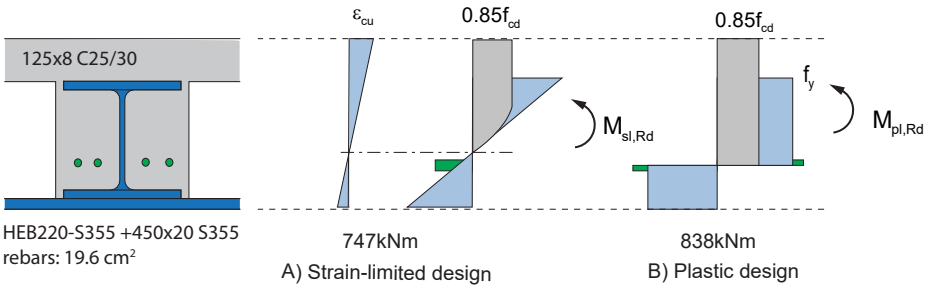

Figure 6.3 – Plastic and strain limited design for a slim-floor beam

In case of sections with a large relative compression zone height z_{pl}/h, a concrete failure in the compression zone can happen before reaching the plastic moment resistance $M_{pl,Rd}$ (Fig. 6.3). Therefore, the plastic moment resistance has to be reduced for the safety of the design. According to EN1994-1-1 clause 6.2.1.2 a reduction of the plastic moment resistance becomes important when the relation z_{pl}/h exceeds 0,15, alternatively, the strain limited design becomes decisive. The reduction factor β in current Eurocode 4 is only based on convectional composite beam cross-sections and steel grade S420 and S460. Also, other conditions [85] lead to a limitation of plastic moment resistance , especially for composite beams with:

- limited effective width (due to openings in the concrete flange or because of precast elements),
- increasing concrete contribution,
- partially encased sections,
- encased sections with a high degree of reinforcement,
- asymmetric steel sections with a larger bottom flange or additional bottom plate,
- individual section forms as e.g. for slim-floor sections,
- when using high strength steel.

The strain-limited design may become decisive because of the reduced rotation capacity. Therefore, additional rules have to be defined for the reduction factor of plastic design. To answer it, extensive parametric studies based on different material strengths and cross-section types have been carried out. Proposals of new reduction factors based on the statistical analysis of the results are also provided.

6.1.2 Benchmarks with existing beam test results and FEM results

Benchmark of the bending moment resistance at full shear connection has been provided by comparing the results of the developed software tool (details see chapter 3) to the experimental derived bending resistance documented in several research papers and FEM simulation.

The calculation results have also been compared to the former investigation provided in the background document [34] for application of steel grades S460 and S420 in composite structures in Eurocode 4. Based on this research, the β reduction factor of current EN 1994-1-1 was obtained. In order to achieve the same results, his assumptions were considered for the benchmark: no consideration of strain-hardening of steel and the shifting of strain-limited points explained in section 3.2.1. However, later it was found these assumptions in [34] give very conservative results. Furthermore, a few existing test results of slim-floor beams with full shear connection have been collected and benchmarked with different methods, as shown in Table 6.1. For these analyses, the material properties from tests are used instead of the design values. However, the currently collected tests are limited to a shallow compression zone, where plastic and strain limited design results are similar, additional tests with more important z_{pl}/h and higher steel grades are still not found. Thus, three artificial beams with deep compression zone height are calculated and benchmarked with FEM calculation. The results are provided in Table.6.1.

Table 6.1 – Benchmarks with experimental results

Beams	M_e KNm	$M_{pl,R}$ KNm	$M_{sl,R}$ KNm	$M_{sl,R0}$ KNm	$M^*_{sl,Rd,1}$ KNm	M^*_{FEM} KNm	z_{pl}/h	Reference
(1) B2	1608	1599	1596	1580	1580	1602	0.24	[54]
(2) Test	239	227	226	222	222	224	0.29	[90]
(3) FSB1	334	327	342	325	325	342	0.17	[96]
(4) 280ASB	789	825	818	810	797	815	0.24	[59]
(5) 300ASB	956	972	977	963	962	991	0.22	[59]
(6) KU	1026	1105	1043	1066	1066	1069	0.21	[37]
(7) Artifical1	—	2938	2480	2178	2503	2496	0.4	[37]
(8) Artifical2	—	2537	1969	1555	2052	2011	0.47	[37]
(9) Artifical3	—	886	669	650	714	754	0.47	[37]

M_e: moment resistance resulting from experimental investigation
$M_{pl,R}$: plastic moment resistance based on mean values
$M_{sl,R0}$: strain limited design without strain hardening for structural steel and parabola- rectangular stress-strain relation, considering strain-limit point change according to EN 1992-1-1, 6.1(5)
$M_{sl,R}$: strain limited design with steel strain hardening, non-linear concrete stain-stress relationship according to prEN 1992-1-1, 2019(D4) based on tested values
$M_{sl,R1}$: strain limited design with steel pr1993-1-14 model, parabolic rectangle concrete stain-stress relationship according to prEN 1992-1-1, 2019(D4) based on tested values, fixed strain limited point at top
M_{FEM}: results by Abaqus, bilinear steel stain-stress relationship without strain hardening and parabola-rectangular concrete stain-stress relationship.

6.1.3 Parametric study on the reduction factor β

In order to explore the possible differences between plastic and strain limited design resistance for composite beams, parametric studies have been carried out. Thereby, different parameters related to geometry and material have been considered. table 6.2 represents the parameters for conventional composite beam cross-sections and table 6.3 for shallow-floor sections. For conventional composite beams, double symmetrical

steel profiles such as IPE, HEA and HEB profiles are included. Also, asymmetrical sections with bottom flanges area increased from 1.25 to 4 times as well as profiles without top flanges are added.

For slim-floor section in total, 289 different steel profiles from various product catalogues on European market including both open forms and close-forms (box sections) are considered. Partially additional reinforcement in the chambers of the steel sections is considered with two Φ 20 reinforcements laying 50mm above the steel bottom flange. As the economical span to height ratio (L/h) for slim-floor beams is around 25. The effective width b_{eff} of the simply supported beam is around 1/4 of the beam length L. Thus, the effective width to height b_{eff}/h ratio is around 6 for slim-floor beams, in the parametric study the b_{eff}/h is set from 4 to 10. The steel grades are generally from S235 to S550, though some calculations are with S500 and S690.

Also, different concrete and structural steel strain-stress relationships have been used in the parametric studies. They are used for a different purpose, for the derivation of the β factor for plastic bending moment resistance, the non-linear concrete stain-stress relationship and quart-linear steel stain-stress relationship are used. For analysis for the partial shear diagram, the parabolic-rectangle concrete stain-stress relationship and bilinear steel stain-stress relationship without strain hardening is used. Additional limitations to exclude an uncommon combination of cross-sections are also shown in the figure and applied during the parametric study.

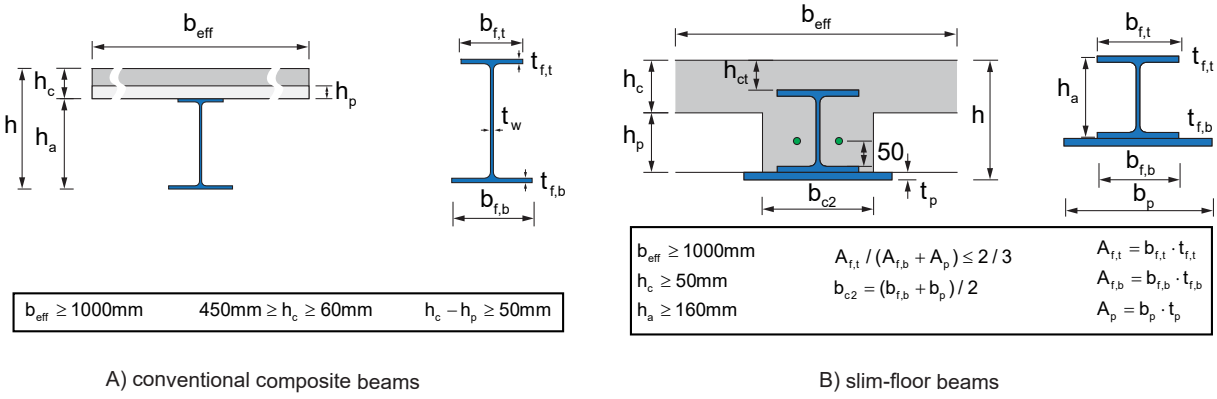

Figure 6.4 – Nomination and additional limitations for parametric study of traditional composite beam and slim-floor beams

Table 6.2 – Parameters for conventional composite beams

h_c/h_a	A_{ft}/A_{fb}	Profile*	b_{eff}/h	Concrete	Steel
0.2	1.0	IPE200 - IPE600	3-10	C20/25	S235
0.3	4/5	HEA200-HEA1000	(increase	C30/37	S275
0.4	2/3	HEB200-HEB1000	each 1)	C40/50	S355
0.5	1/2	UB profiles		C50/60	S420
0.6	1/4				S460
0.7					S550

Note: Geometrical nominations shown in Fig. 6.4 A)
*: UB profiles are: 203x102x23, 406x178x60, 610x229x101,610x305x238 , 838x292x176, 838x292x226, 1016x305x222, 1016x305x487

Table 6.3 – Parameters for slim-floor beams

h_{ct}	Profile	b_{eff}/h	h_p	d_s	Concrete	Steel
50	IFB [5]	3	75	0	C20/25	S235
100	SFB [5]	6	100	2*20	C30/37	S275
150	Delta [70]	8	150		C40/50	S355
	ASB [13, 24]	10	200		C50/60	S420
	SWT [80]		250			S460
						S550
						(S550,S690)

Note: Geometrical nominations shown in Fig. 6.4 B)

All the possible combinations of different parameters have been calculated which results in around 400,000 slim-floor cross-sections and around 500,000 conventional composite beam cross-sections after filtering out the extreme cross-sections for each set of data with a certain material strain-stress relationship. In total, more than 5 million pairs of results are generated and compared. For each, the plastic bending moment resistance $M_{pl,Rd}$, the strain limited resistance $M_{sl,Rd}$ and the ratio between them $\beta = M_{sl,Rd}/M_{pl,Rd}$ as well as other parameters such as z_{pl}/h, $N_{c,sl}$ and $N_{c,pl}$ have been calculated.

6.1.4 Influences of key parameters

The parametric study results of the reduction factor β and the relative compression zone height by plastic design z_{pl}/h are scatter plotted in Fig. 6.5 A). The data are calculated with a quart-linear steel stress-strain relationship and a non-linear concrete stain-stress relationship (details see section. 3.1.3). With high z_{pl}/h the results are more scattered, it is still possible that a reduction of plastic bending moment resistance is not necessary with $z_{pl}/h = 0.6$, while some profiles show a reduction of 30% of resistance is possible. The histogram of β in probabilistic density and cumulative distribution is plotted in Fig. 6.5 B), around 30% of all data shows that plastic bending resistance gives safe results ($\beta > 1$). Also Fig. 6.5 C) presents a 3D histogram of both β and z_{pl}/h, with the bar height representing the probability of data falling into the grids divided by the two variables. Most data still concentrated with z_{pl}/h smaller than 0.4 and near $\beta = 1$. It has to mention the results with different parametric ranges can be different.

6.1.4.1 Influence of concrete material strain-stress relationship types

The results of the parameter study based on the non-linear stress-strain curve according to prEN 1992-1-1: 2019(D4) [72], clause 5.1.6 and parabolic-rectangle concrete stain-stress relationship according to prEN 1992-1-1: D2019(D4), clause 8.1.2 as well as the assumption

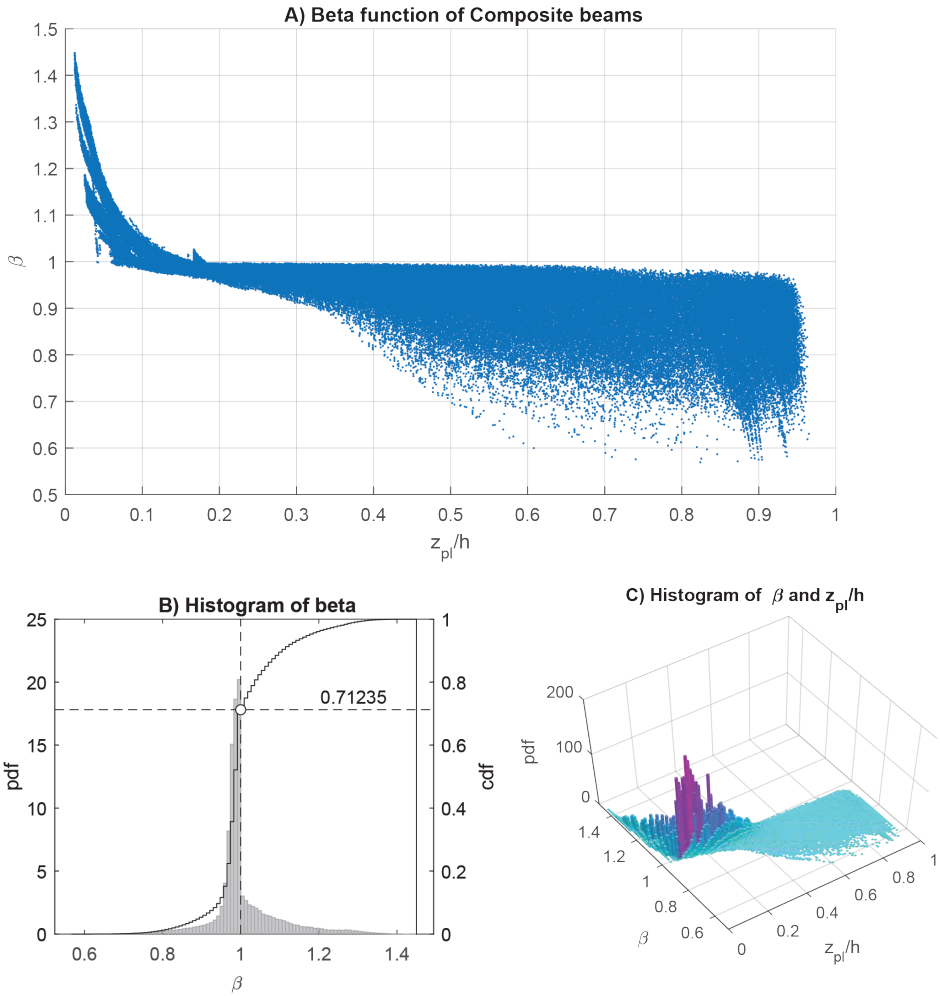

Figure 6.5 – Statistics on the β values and z_{pl}/h based on a non-linear concrete and quart-linear steel stain-stress relationship

with strain limitation according to EN 1992-1-1: 2004 [19], clause 6.1(5) considering the limitation of strains changed to ε_{c2} when flange near full compression are compared below for conventional composite beam sections (see also section 3.1.3 for details of the material strain-stress relationship). The results are grouped into different concrete classes, and the outer boundary of each group are plotted. The Fig. 6.6 B) gives in general lower values of $M_{sl,Rd}$ with maximum 4% and in average 0.85% smaller compared to Fig. 6.6 C). Whereas Fig. 6.6 A) shows significant differences to both other design assumption. However, clause 6.1(5) with the changing strain limit point (see section 3.2.1) is not introduced any more in prEN 1992-1-1. Therefore it will not be further discussed. With regard to the slight deviations of Fig. 6.6 B) and C), Fig. 6.6 B) is used for the development of the β-reduction, since the results are slightly more conservative. Since no test data for sections with a deep position of the plastic neutral axis are available, the evaluation of reduction functions for β is based on the comparison of plastic bending resistance according to EN 1994-1-1 and assumptions according to prEN 1992-1-1(D4).

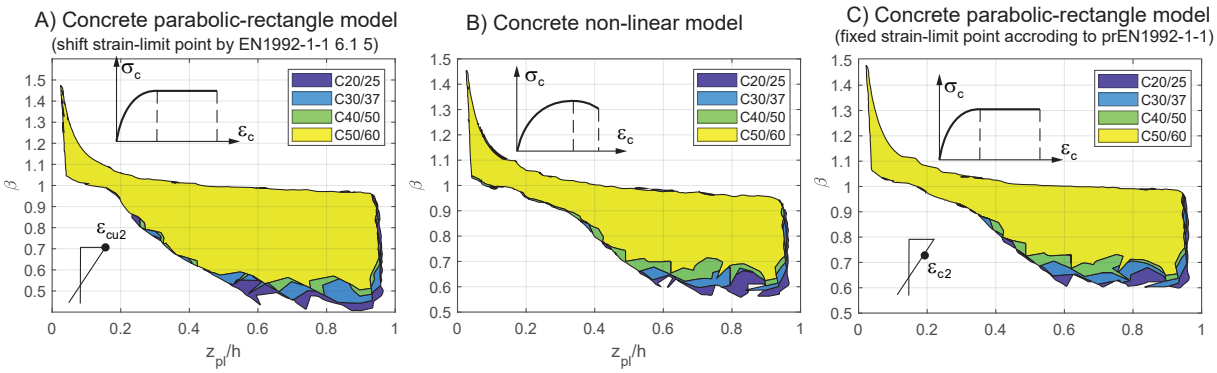

Figure 6.6 – Comparison of plastic and strain limited design for composite cross-section applying different stress-strain curves for concrete (*steel bilinear strain-hardening model*)

6.1.4.2 Influence of steel material model types

In the former literatures [34, 37] strain hardening of steel was not considered, in newer developments in [83, 88] it is. As shown in Fig. 6.7 for slim-floor beams strain hardening mostly influences the part with $z_{pl}/h < 0.4$. If strain hardening is not considered, reduction of plastic bending moment resistance becomes necessary at a smaller value of z_{pl}/h. For example, with steel grade S420, $\beta \leq 1.0$ when $z_{pl}/h \geq 0.4$ if strain-hardening is not considered, meanwhile $z_{pl}/h \geq 0.22$, if strain-hardening based on bi-linear model is used. Differences becomes visible when comparing e.g. Fig. 6.7 A) and Fig. 6.7 D). However, the differences are still less than 0.03 in resulting β values with the same z_{pl}/h.

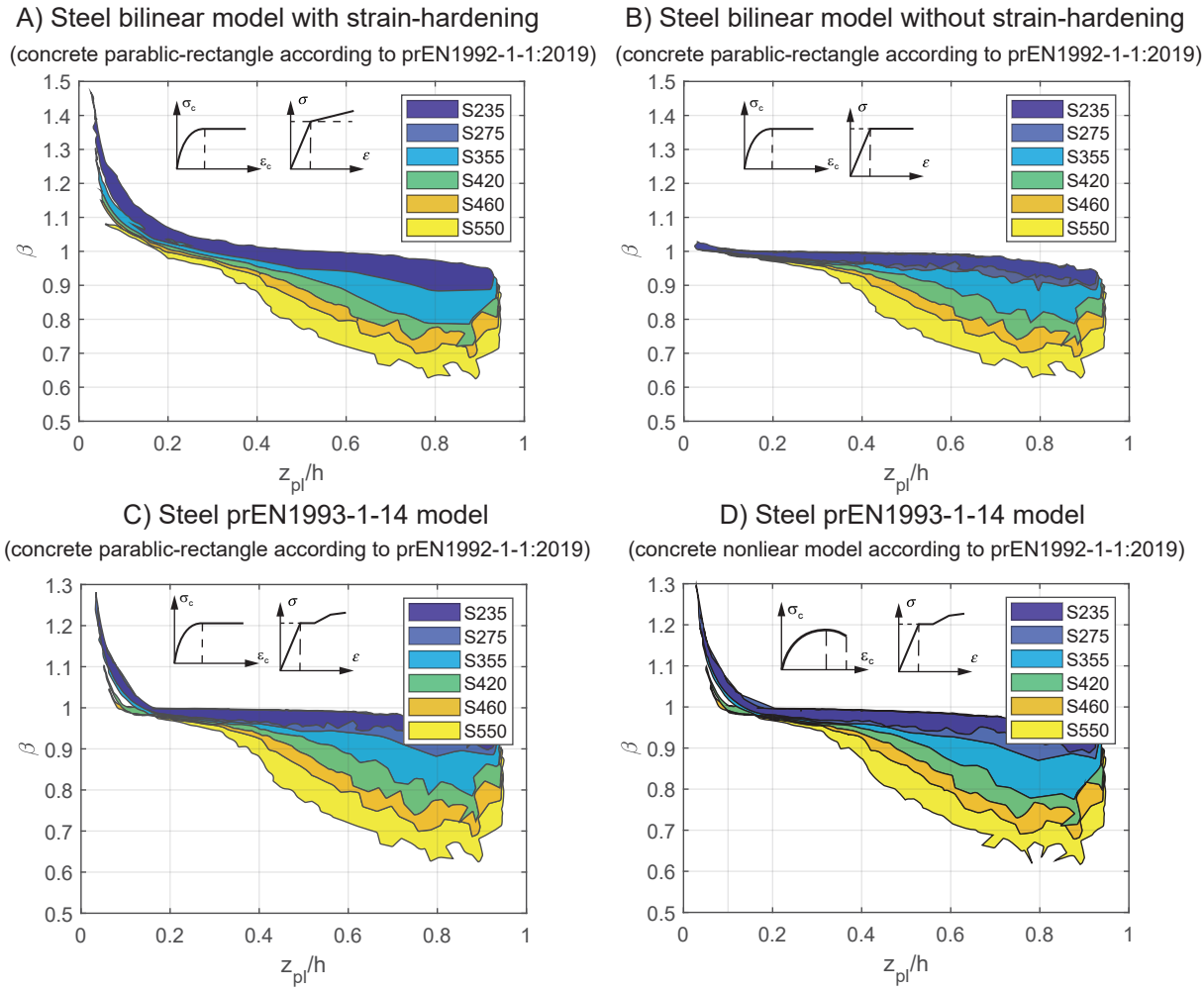

Figure 6.7 – Comparison of plastic and strain limited design by different steel grades and different steel material models (*see section 3.1.3*) (*for concrete parable-rectangular relation is used*)

6.1.4.3 Influences of different composite beam types

The calculation results are grouped by different types of composite beams. The probability densities of β values from different groups are plotted in Fig. 6.8 A). In the figure, "Slim-floor" represents slim-floor beams from Table.6.3. "Standard" represents the conventional composite beam with standard IPE, HEA or HEB steel profiles in Table.6.2. In the Fig. 6.8, "ASB1.25 to ASB4.0"represent the groups modified form the "Standard" beams with bottom steel flange area extended to 1.25 to 4.0 times which is linked to the "A_{ft}/A_{fb}" ratio in Table.6.3. The "T-section" means the cross-section with top steel flange removed. In Fig. 6.8 B) calculation results are first grouped and scatter-plotted in relationship of z_{pl}/h and β to create cloud-maps of results points similar as Fig. 6.8 A). Because it was found to be difficult to distinguish the groups as extensive data is presented, only the outside boundary line of each group is plotted to provide a clearer visualization. A similar method is used for the analyses of other parameters in the article. Statistics in Fig. 6.8 A) shows the slim-floor beams shows more possibilities with smaller β. From Fig. 6.8 B) compared the boundary lines of group Standard, ASB 1.25 to ASB 4.0 and T-section, it shows with smaller ratio top flange area to total steel area, the data represents smaller β value at same relative compression zone height z_{pl}/h.

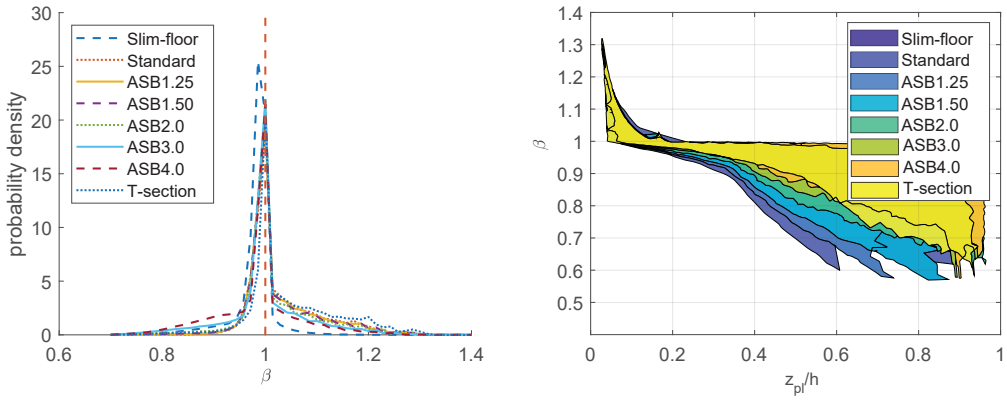

Figure 6.8 – Comparison of reduction factor related to different composite beam types

6.1.4.4 Influences of effective width to height

The impact of b_{eff}/h is shown in Fig. 6.9. With bigger concrete effective width, the location of the neutral axis is relatively higher, thus results in smaller z_{pl} and bigger β is also expected. However, with the same z_{pl}, the distribution of β is similar. Due to the parametric study limited the effective width to minimum 1m. Thus the influences of effective width are limited. Additional parametric studies still show that higher reduction is needed with a minimal effective width. Thus it is suggested the effective with be at least 1m to reach more economical design.

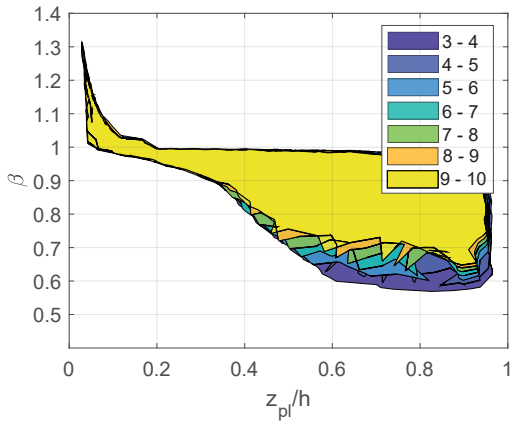

Figure 6.9 – Comparison of reduction factor related to different b_{eff}/h values

6.1.5 Proposal of new β reduction functions based on relative compression zone height z_{pl}/h

From the parametric study results, reduction factors β of plastic bending moment resistance for composite cross-sections and slim-floor beams have been developed. A simplified reduction function based on the value of z_{pl}/h can be generated by taking the lower boundary lines of the statistic results. The design reduction functions are calibrated by 1,0‰ criterion when comparing the point cloud for β. The statistics results are based on data calculated based on non-linear concrete stain-stress relationship according to the prEN1992-1-1, and prEN1993-1-14 quart-linear steel stain-stress relationship.

1) Limitations of application of the β reduction factor

In order to reach an acceptable application range when applying the β reduction factor, some limitations should be fulfilled to avoid the extreme or special cases dropping down the curve. Also, steel grade S690 is not taken as they are not common in beam design:

- Concrete classes should be no greater than C50/60. As a smaller strain limit is expected for high strength concrete.
- Concrete slab effective width should be no less than 1000 mm.
- The area of steel top flange should be no more than the area of steel bottom flange.

Furthermore, for slim-floor sections, the following requirements also need to be fulfilled:

- Steel profile height should be no less than 160mm.
- Concrete thickness above the profiled sheeting should be between 50mm to 150mm.
- If chamber reinforcement is used, the total reinforcement area should be no more than the area of steel bottom flange.
- The area of steel top flange should be no more than 2/3 of the area of steel bottom flange (plus the area of welded additional steel plates if any).

In addition, all general rules for the plastic bending resistance according to EN 1994-1-1 must be fulfilled.

6.1.5.1 The maximum relative compression zone heights z_{pl}/h

In order to reach an economical design in ULS, the resistance of steel sections should be effectively utilized, which requires at least the bottom flange yields. To do so, the maximum relative compression zone height $z_{sl}/(h-t_{fb})$ needs to be limited. The limitations can be approximately calculated, as shown in Equ.6.1. By approximately assuming the plastic neutral axis position z_{pl} same as the neutral axis for strain-limited design z_{sl}. The corresponding z_{pl}/h limits of different steel grades are given in Table 6.4.

$$\varepsilon_{cu} = 0.0035 \qquad \varepsilon_y = \frac{f_y}{E_a} \qquad \frac{z_{sl}}{h-t_{fb}} \leq \frac{\varepsilon_{cu}}{\varepsilon_{cu}+\varepsilon_y} \tag{6.1}$$

Table 6.4 – Limits of z_{pl}/h - plastic strains at bottom fibre (approximation)

f_y (Mpa)	550	460	420	355	275	235
limits	0.572	0.615	0.636	0.674	0.728	0.758

It is to be mentioned that the design of the composite beam of cross-section classes 1 and 2 benefits from several simplifications. Due to the redistribution of the stresses by yielding, the impact of the subsequence of loading, creep and shrinkage can be neglected

for the design in the ultimate limit state. Furthermore, an equidistant arrangement of ductile shear connectors becomes possible. When reaching the ultimate strains of concrete, rotation capacity is limited, and parts of the section may not yield. Therefore, the simplified reduction of the plastic moment resistance by a β factor should be applied carefully, and the application should be considered up to the limits as given in table 6.4. Otherwise, the assumption of the before mentioned benefits may disappear.

6.1.5.2 Proposal for reduction factor β for composite cross-section in general

The statistic results grouped by different steel grades are given in Fig. 6.10. Un the figure, the blue points represents at failure the strain at steel bottom surface is over the yielding strain, while the orange points represents the steel section is fully in elastic. To reach a more economic design, the neutral axis position should be limited to avoid area with many orange points. A multi-linear reduction model is used for different steel grades to accommodate the non-linear changes. The first point is fixed near to the z_{pl}/h value where reduction is necessary, and the last point is decided at the approximate limit of the bottom flange in plastic (blue points in the figure). The middle points are set at $z_{pl}/h = 0.2$ or 0.15 and $z_{pl}/h = 0.4$ as slop changes near this value. The responding β values are calculated considering 1.0‰ fractile-value for all the points.

The results underline that for higher steel grades, more important reduction is required. Also, in relation to the value of z_{pl}/h, the reduction starts earlier. The current rule of Eurocode 4 does not include strain hardening of structural steel while considering the strain limitation acc. to EN 1994-1-1, clause 6.1(5) for compresses flanges with an eccentricity of resulting compression force $N_{c,f} \leq 0.1$. Therefore the current rule is more conservative compared to the results from the presented parameter study, based on prEN 1992-1-1:2019 (D4). For engineering practices, a further simplification is suggested by linear and bi-linear curves in section 6.1.5.4.

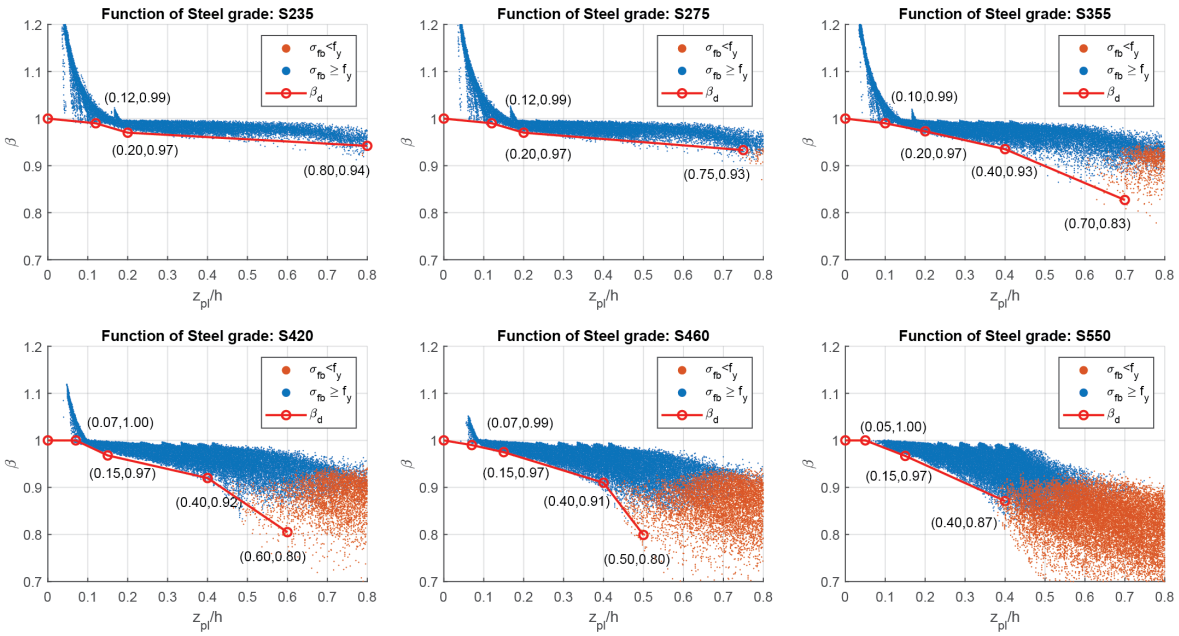

Figure 6.10 – Statistical evaluation for reduction of composite cross-sections in general

6.1.5.3 Proposal for reduction factor β for composite slim-floor sections

As slim-floor systems have much compact cross-section shape compared to conventional composite beams, those special composite cross-sections are analysed separately. The reduction functions are provided as shown in Fig. 6.11. Overall less conservative results can be achieved by applying more strict boundary conditions.

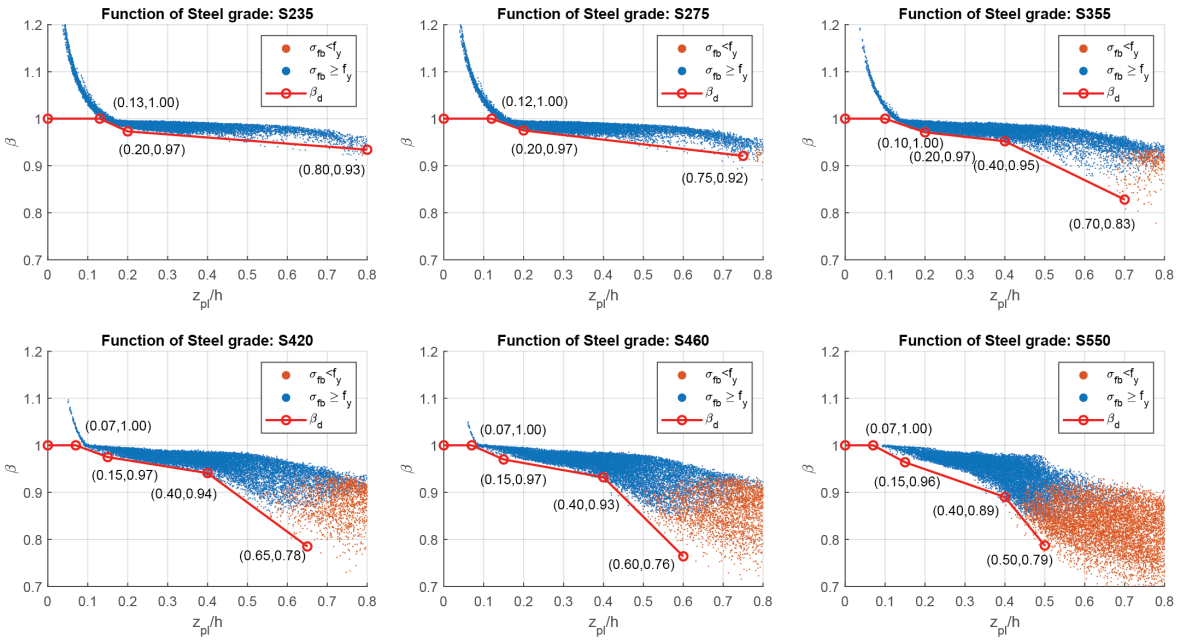

Figure 6.11 – Statistical evaluation for reduction of slim-floor sections

6.1.5.4 Proposal for determination of simplified moment resistance in engineering practice

For many practise relevant cases, plastic bending resistance leads to reliable results. However, this research investigation, as well as the further research papers [3, 83, 87] highlighting that the plastic moment resistance may lead to an overestimation of plastic moment resistance. An economical design will always ask for a strain-limited calculation. But for practical application, a validation by relation z_{pl}/h and simply reduction of the plastic moment resistance by the β function allows fast design.

Therefore, the outcomes of the statistical analysis have been further simplified to be integrated into prEN 1994-1-1. With regard to practical relevance, it was determined that reductions of less than approx. 3% in the area of small compression zone heights may be neglected in order to define significant start points for the required reduction, e.g. $z_{pl}/h > 0.15$. This start point for the reduction is also strongly depending of the material functions for concrete and steel. Furthermore, the approaches should be limited to steel grades up to S460. prEN 1994-1-1 does not include complete rules for the plastic bending resistance using high strength steel grade. The application of high strength steel grades as β function may lead to misinterpretation of prEN 1994-1-1.CEN/TC250/SC4.T6 proposes for such steel grades in general design based on strain-limitation. This proposal will be presented in the background report in [86].

6.1.6 Proposal of new β reduction functions based on the bottom flange stress state for slim-floor beams

The reduction functions in section 6.1.5 are easy to apply because z_{pl} is already known when plastic bending resistance has been calculated. However, this method has a few disadvantages: For each steel grades, different reduction function should be developed. Moreover, the reduction function is based on the lower boundary of the statistic, which indicates the worst case of reduction. With deep neutral axis location, it can cause over-reduction for many cases. For example, Fig. 6.12 shows histogram of reduction factors for slim-floor cross-sections with S460 steel when $0.55 < z_{pl}/h < 0.6$. The required reduction factor is around 0.78. However, static shows 57% of the cross-sections need only a reduction factor of less than 0.9. Thus a more economical reduction function is preferred. Also based on z_{pl}, it is difficult to distinguish if bottom flange in plastic stage at ULS. To better understand the cause and related factors of β, the relationship between the position of plastic neutral axis (z_{pl}) and strain-limited neutral axis (z_{sl}) is explained first. Then with the modified position of plastic neutral axis (z_{psl}) and the neutral axis location limitations directly related to the stress stage of the steel flanges. Finally, an improved function is suggested in this subsection. Here the calculations are based on steel bi-linear with strain-hardening and concrete parabolic-rectangle stress-strain relationships. A slight different parametric set is used to include also higher strength steel.

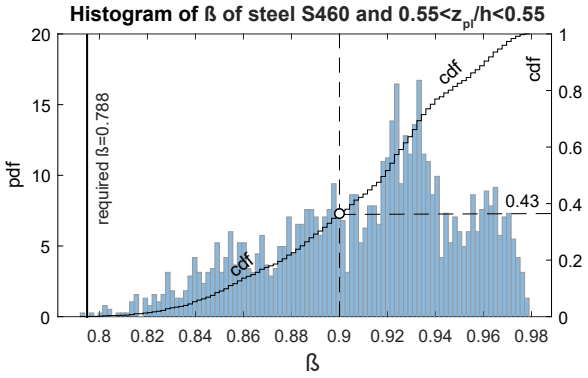

Figure 6.12 – Histogram of β values of steel S460 and 0.5<z_{pl}/h<0.55

6.1.6.1 Relationship of neutral axis location of plastic and strain-limited design

The positions of the plastic neutral axis and strain-limited neutral axis are compared in Fig. 6.13. The difference of z_{sl}/h and z_{pl}/h are calculated and plotted in relation with z_{pl}/h. When the $z_{pl}/h > 0.6$, nearly linear relationship of the two parameters can be observed. The relationship indicates the strain-limited design neutral axis is above the plastic neutral axis, i.e. smaller compression zone height calculated by strain limited design method. When $z_{pl}/h < 0.6$ the difference between z_{sl} and z_{pl} can reach a maximum $0.2h$, however no clear relationship between these two parameters can be found in this area.

For plastic bending resistance because the rectangle stress block is assumed, the change of plastic neutral axis (PNA) position only affects the stress of the sections near to the PNA ($f_y \leftrightarrow -f_y$ for structural steel and $f_{cd} \leftrightarrow 0$ for concrete). Thus the difference is more important when (PNA) is inside the top flange of the steel profile. In this case, with the same amount of change of position of z_{pl}, the change of internal normal forces in the

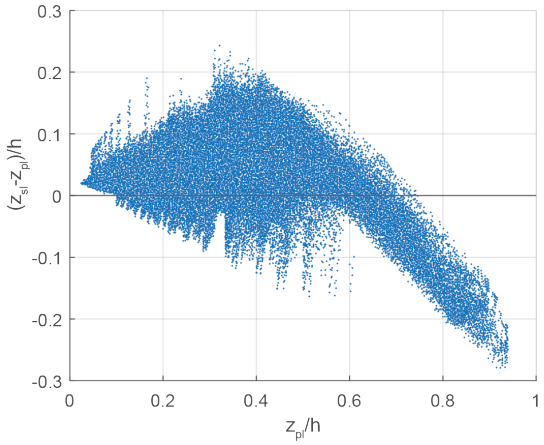

Figure 6.13 – Comparison of z_{sl} and z_{pl} based on z_{pl}/h

steel section is much bigger than the situation when PNA is inside the steel web. However, that is not the case for strain-limited design, as the neutral axis position is shifted, the strain distribution of the whole section also changes which resulting in stress altered in whole cross-section where plastic strain is not reached. Thus the changing rate of total normal forces is not affected by if the position of neutral axis is inside the flange or web. Because of the different behaviour of plastic and strain-limited neutral axis position changes. It should be distinguished if PNA is inside the steel top flange or not. Thus in Fig. 6.14, the z_{pl}/z_{sl} is plotted related to the relative position of z_{pl} to steel top flange. The figure is divided into three parts depending on if the neutral axis is above, inside or below the top flange. For each part, the relative position z is calculated differently. The linear regression of the z_{pl}/z_{sl} to z in each part is obtained and plotted in the figure as the solid line. Based on the relationship, the location of z_{sl} can be roughly calculated. The boundary lines (Eq. 6.2) are also plotted in dashed lines as a conservative evaluation of strain limited compression zone height (z_{psl}).

$$z_{psl} = z_{pl} \begin{cases} 1.7 - 0.5\frac{z_{pl}}{h_{ct}} & z_{pl} \leq h_{ct} \\ 1.2 + 0.3\frac{z_{pl}-h_{ct}}{t_{f1}} & h_{ct} < z_{pl} \leq h_{ct} + t_{f1} \\ 1.5 - 0.8\frac{z_{pl}-h_{ct}-t_{f1}}{h-h_{ct}-t_{f1}} & h_{ct} + t_{f1} < z_{pl} < h \end{cases} \tag{6.2}$$

6.1.6.2 Stress stages of steel flanges

As the steel flanges, especially the bottom flange have an important contribution to the beam bending resistance. The stress stages of them (if yield or not) also have a big influence on the $beta$ factor. For sagging bending moment and full shear connection, if a bilinear steel stain-stress relationship is used, the critical positions of neutral axis to determine the stress stages of top and bottom flange can be calculated by the Eq. 6.3 to Eq.6.5 (Fig. 6.15). The whole cross-section can be divided into four regions based on the top and bottom flange stress stages. The regions are marked with two labels, "P_t" means top flange reaches plastic at ULS, "E_t" means top flange stay elastic. Similarly "P_b" and "E_b" for bottom flange. Depends on the cross-section shape and material there are

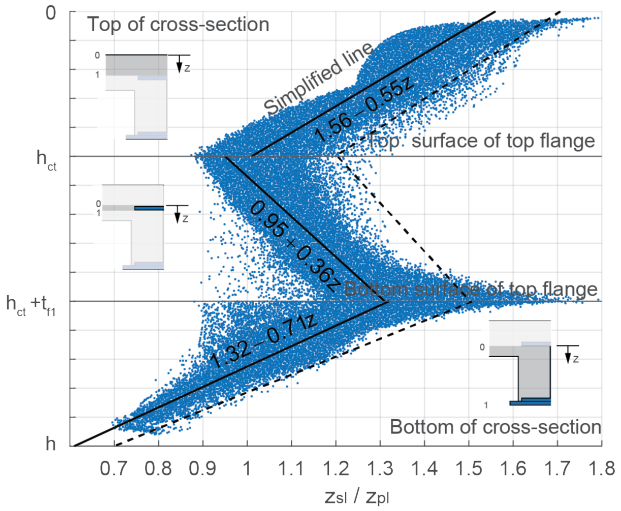

Figure 6.14 – Comparison of z_{sl} and z_{pl} based on position related to steel top flange

different types of division zones.

$$z_{t,t} = h_{ct} \cdot \frac{\varepsilon_{cu}}{\varepsilon_{cu} + \varepsilon_y} \tag{6.3}$$

$$z_{c,t} = h_{ct} \cdot \frac{\varepsilon_{cu}}{\varepsilon_{cu} - \varepsilon_y} \tag{6.4}$$

$$z_{t,b} = (h_{ct} + d) \cdot \frac{\varepsilon_{cu}}{\varepsilon_{cu} + \varepsilon_y} \approx (h - t_p) \cdot \frac{\varepsilon_{cu}}{\varepsilon_{cu} + \varepsilon_y} \tag{6.5}$$

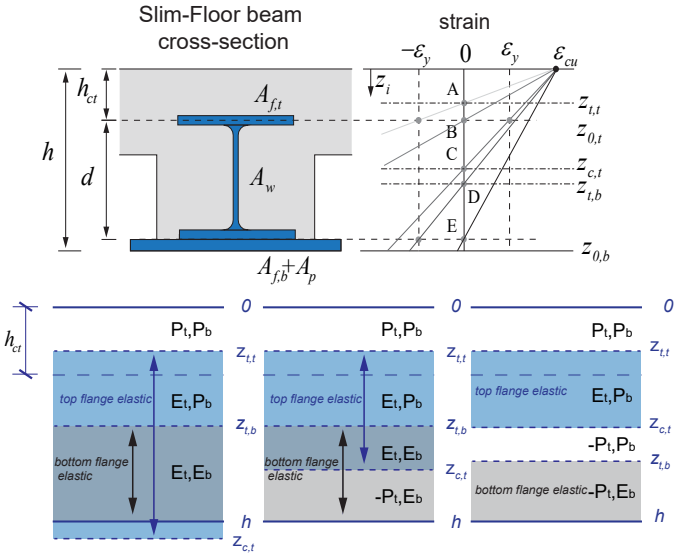

Figure 6.15 – Different zones related to the plastic of steel flanges

In Fig. 6.16 the data are grouped by the stress stages of top and bottom flanges calculated by the strain-limited method. Generally, if both flanges do not reach plastic, the reduction is most significant, which represents the region E_t, E_b in the figure (purple area), the minimum reduction can be around 0.7. If both flanges reach plastic, the reduction is usually the smallest which is shown in the region P_t, P_b (blue area). If only the top flange is

in the elastic stage, the reduction is shown in region E_t, P_b (orange area). There is also a situation where the bottom flange in elastic but top flange in plastic as shown in the region P_t, E_b (yellow area) but this situation needs very deep neutral axis location thus is not very often in general engineer practice. When the bottom flange stays elastic at failure, usually the utilization of steel strength capacity is very limited, thus should be avoided in the design.

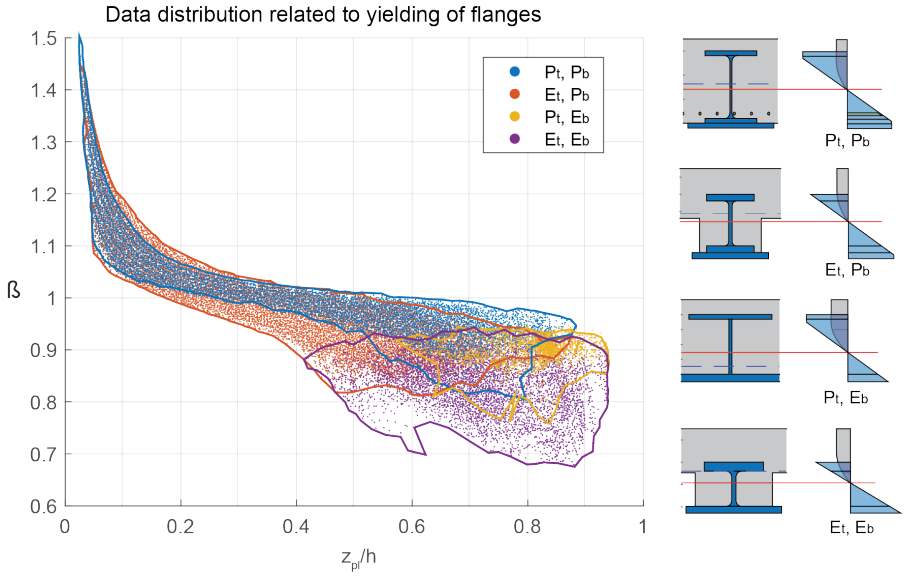

Figure 6.16 – Different zones related to the stress stage of steel flanges, three different possible situations for different cross-sections are shown in the figure

6.1.6.3 Reduction functions based on the flange stress stages

The relative compression zone height z_{pl}/h does not represent the demanding of strain to allow bottom flange reaching yielding; a better presentation is to calculate the reduction factor based on a new parameter z_{sl}/z_{tb}. Where "z_{tb}" is the position of the neutral axis where lower steel flange (including the additional plate) just reach plastic, which can be calculated by Eq. 6.5 and z_{sl} is compression zone height by strain-limited design. When $z_{sl}/z_{tb} \geq 1$, the bottom flange is in elastic stage, which can cause great reduction thus should be avoided. However, the value of z_{sl} is unknown unless a strain-limited design is conducted, but it can be approximately replaced by the value of z_{psl} calculated by Eq. 6.2.

Based on the adjusted location of plastic neutral axis z_{psl}, the distribution of β is shown in Fig. 6.17. In the analysis, both conventional composite beams and slim-floor beams are included, and cross-section of different steel grades do not need to be separated. The design function with 99.9% guarantee of the results above the design line is given in the figure. A simplified equation is also provided in Eq.6.6 with more than 99.99% guarantee. In the figure, the stress stage of steel bottom flanges are also illustrated, with orange dots means steel bottom flange in elastic at failure. It is suggested to only use the range of $z_{sl}/z_{tb} \leq 1.0$ (which covers more than 90% of all data) to avoid the situation where the bottom flange in the elastic stage. When the $z_{psl}/z_{tb} > 1.0$, the reduction function can be still applied however may expected very conservative results. Thus a simplified strain-limited design method or an exact strain-limited design by numerical approaches

can be used for validation.

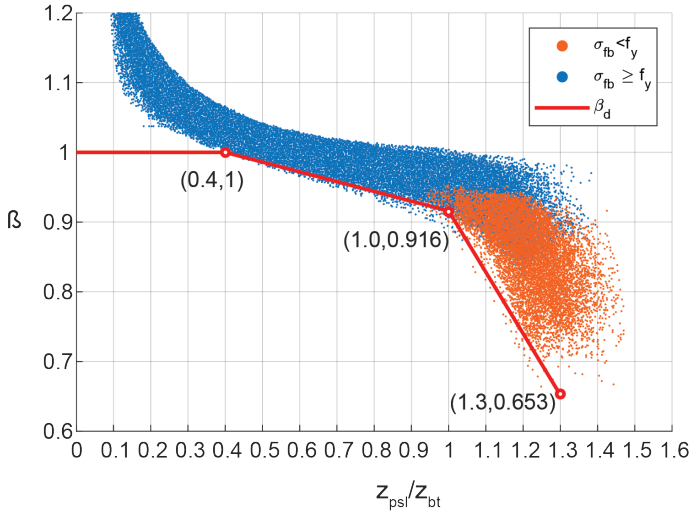

Figure 6.17 – Proposed reduction function based on the flange stress stages

$$\beta_1 = \begin{cases} 1.0 & \frac{z_{psl}}{z_{bt}} \leq 0.4 \\ 1.0 - \frac{1}{6}\left(\frac{z_{psl}}{z_{bt}} - 0.4\right) & 0.4 \leq \frac{z_{psl}}{z_{bt}} \leq 1.0 \\ 0.9 - \frac{2}{3}\left(\frac{z_{psl}}{z_{bt}} - 1\right) & 1.0 \leq \frac{z_{psl}}{z_{bt}} \leq 1.3 \end{cases} \tag{6.6}$$

Further validations have proven that Eq.6.6 also validated for situations where slim floor beams have top flange area bigger than 2/3 of bottom flange areas and additional plates area. Also, it allows a smaller effective width. Thus this function has much wider application ranges than the method proposed in section 6.1.5. Besides that, the new reduction function can more efficient separated the situation where lower steel flange in the elastic stage and provides a much more economical design with a maximum reduction of 10% for more than 90% of data.

The two methods can also be used in combination. If the plastic compression zone height is less than 0.4 times the total cross-section height ($z_{pl}/h \leq 0.4$), the method in section 6.1.5 can be applied, if the limitation is exceeded, the method based on stress stages in this section can be used, on condition of $z_{psl}/z_{tb} \leq 1.0$. Otherwise, a non-linear method such as strain-limited design or FEM method should be applied.

6.2 Slim-floor beam bending moment resistance with partial shear connection

Where the shear connector arrangement is controlled by detailing, such as the rib distance of profile sheeting, or the proof in SLS become decisive, often the partial shear connection is realized. The bending moment resistance of partial shear connection can be calculated by solving the equilibrium equation according to plastic theory. A more practical way is to use the partial shear diagram provided in Eurocode 4 (EC4) [22]. This diagram is developed using the plastic design method, where the maximum bending moment resistance at point C of Fig. 6.18 is the plastic bending moment resistance ($M_{pl,Rd}$). The partial shear diagram allows the quick design of the partial shear situation. However, for the situation where deep neutral axis exists with the usage of high strength steel, signification part of steel section cannot reach plastic at failure as shown in section 6.1.1. Thus, the bending resistance is no longer suitable. Regarding this situation, a reduction factor β on $M_{pl,Rd}$ can be used as a simplified method to expand the application range of the plastic bending resistance, as explained in section 6.1. However, the influence of β on the partial shear diagram is not mentioned. For conventional composite beams, due to relative compression zone height (z_{pl}/h) is usually small, the plastic bending resistance gives similar results as strain-limited design, however for slim-floor beams, due to the encased steel section into concrete slabs, a big z_{pl}/h value can be often met. Thus, a question arises if the current partial shear diagram can be directly applied if the reduction on $M_{pl,Rd}$ becomes necessary. If not, a simplified design rule covers this situation is necessary. Details of the development of slim-floor beams and the detailed theories related to plastic bending resistance and strain-limited resistance are also seen in [103].

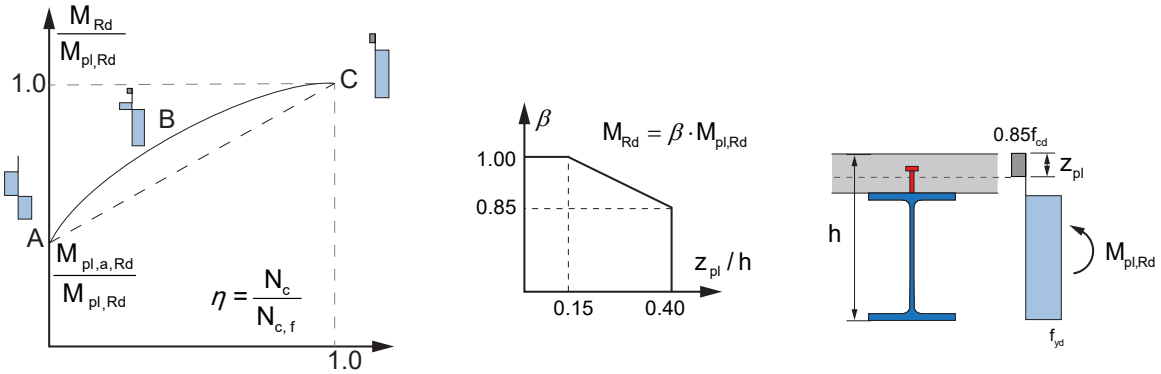

A) Partial shear design diagram (according to EN1994-1-1)

B) Reduction factor for plastic bending moment (according to EN1994-1-1)

Figure 6.18 – Partial shear diagram and reduction factor of plastic bending resistance

6.2.1 Partial shear diagram by plastic design and strain-limited design

Plastic bending resistance is allowed by EC4 if the composite beam has cross-section class 1 or 2. By plastic design method, rectangle stress blocks are used, which assumes enough rotation capacity to allow cross-section to reach fully plastic at failure. The partial shear design bending resistance is calculated by reducing the compression zone height in concrete to reach the total longitudinal shear resistance ($N_v = \sum P_{Rd}$) provided by all shear connectors between the critical sections and again find a separate plastic neutral axis (PNA) in steel section to reach an equilibrium of normal forces in the whole

cross-section. The shear diagram can be generated by obtaining the plastic bending moment resistance at each shear degree and plot them in one diagram.

Strain-limited resistance is calculated from the strain distribution. The stress inside critical cross-section is calculated from the assumed strain curve and material stress-strain relationships. For this section, a bi-linear steel stress-strain relationship without considering strain-hardening according to EN1993-1-5 [21] and a parabolic-rectangle stress-strain model according to Eurocode 2 [19] are used. In partial shear situation, parallel strain curves in steel and concrete part are assumed. The two strain curves separate with a distance indicated as "slip-strain" (ε_{slip}). With a fixpoint at strain-limited point, by changing the curvature and slip-strain value, equilibrium among normal force in concrete section (N_c), in steel section (N_a) and total longitudinal shear force ($N_v = \sum P_{Rd}$) provided by shear connectors between critical sections can be reached.

A comparison of the partial shear diagrams obtained by the two methods is shown in Fig. 6.19 A). In order to better show the differences, the axis is shown with bending moment resistance and required total longitudinal shear force values instead of the degree of shear connections and moment ratio in a typical partial shear diagram according to EN1994-1-1 [22]. The calculated beam cross-section and material is given in Fig. 6.19 B). While the strain and stress distribution at shear degree $\eta = 0.81$ is shown in Fig. 6.19 C). As it is not full shear connection, separated neutral axes exist for steel and concrete parts.

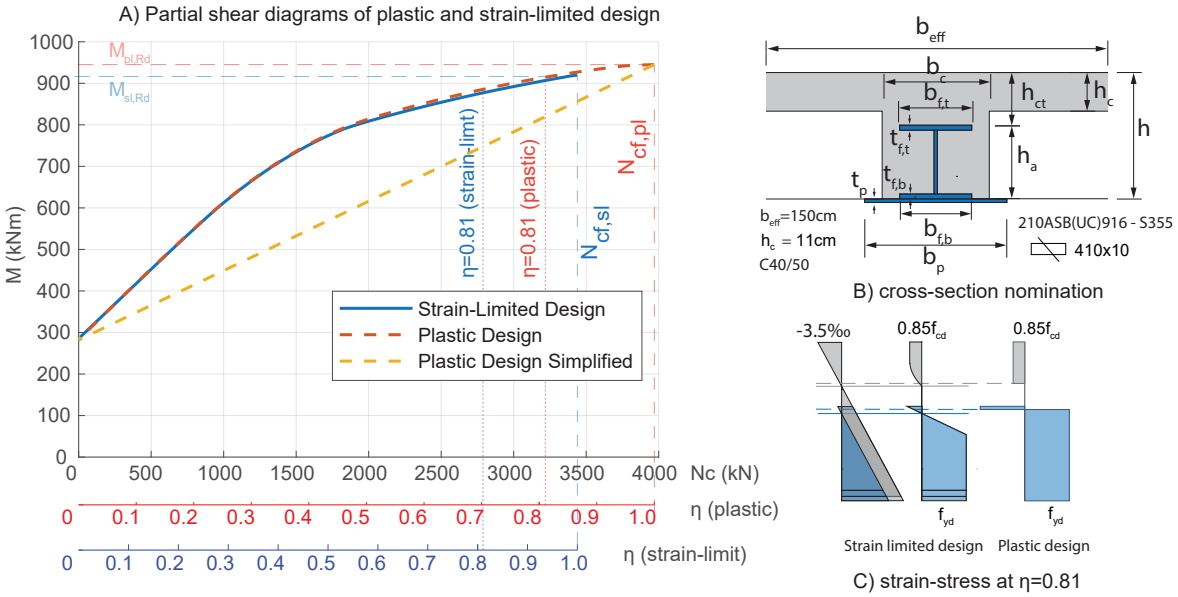

Figure 6.19 – Partial shear diagram by plastic and strain-limited design

The partial shear diagram by plastic bending resistance is based on **degree of shear connection**, which is calculated by the required total normal force in (reinforced) concrete (N_c) compared with N_{cf} at the end point representing full shear connection (same as full shear interaction for plastic design). For strain-limited method is based on **degree of interaction**, Where the N_c is compared with the value at **full shear interaction**. Full shear connection in Eurocode 4 determines to state the situation where a further increase of shear connectors will not lead further increase of plastic bending resistance. The "full interaction" is a term for strain-limited design, Johnson [43] refers to the assumption that there no slip in the joint between steel and concrete, thus the two parts can deform as one. Regarding to strain-limited design, full interaction indicates only one neutral axis in

the cross-section. It is a usually stronger requirement compared to full shear connection, as a composite beam reaches full shear connection does not necessary at the same time reaches full interaction [68]. However, for normal composite beams, if the slip is small at full shear connection, it can be roughly treated as full shear interaction, and degree of shear connection can be considered same as the degree of shear interaction.

6.2.2 Influence of deep neutral axis on partial shear diagrams

The partial shear diagrams calculated by plastic resistance method can be different from that calculated by strain-limited design methods. As steel strain-hardening is not considered, the bending resistance by strain limited design ($M_{sl,Rd}$) should be similar or smaller than that by plastic resistance ($M_{pl,Rd}$). On the other hand, the required total longitudinal shear force ($N_{cf,sl}$) by strain limited design at full interaction is not always smaller than that obtained by plastic cross-section resistance at the full shear connection ($N_{cf,pl}$) for slim-floor beams. Based on a few thousand parametric study results on the comparison of partial shear diagrams, their relationships can be generally categorized into three different situations:

- **Situation 1**: If relative compression zone height is small and reduction of plastic bending resistance is not necessary ($\beta = 1$), partial shear diagrams by these two methods are also similar for which the Eurocode 4 partial shear diagram can be directly applied.
- **Situation 2**: If the plastic bending resistance cannot be reached, ($\beta < 1$), a different situation can happen. First the required total longitudinal shear force can be smaller by strain-limited design.
- **Situation3**: The required total longitudinal shear force at full shear interaction by strain-limited design can also be bigger than that at full shear connection plastic design. In this case, the full shear interaction may not be the same time full shear connection for strain-limited design.

Parametric studies found with a lower degree of shear connection, the two curves are very similar, while they may separate at a higher degree of shear connection. That is due to a lower degree of shear connection, the beam rotation capacity increases, thus more cross-section parts able to reach plastic, resulting in similar results by plastic design and strain-limited design. As reinforcement is not considered in this study, both curves start with pure steel plastic bending moment resistance at zero degrees of shear connection.

6.2.2.1 Plastic and strain-limited design gives similar results (Situation 1)

When the relative compression zone height z_{pl}/h is small, and besides the concrete compression zone does not exceed half of the slab thickness above steel section ($z_{pl} < 0.5h_{ct}$), most parts of the steel can reach plastic at failure. Thus the strain-limited design and plastic design have a tiny difference in results of bending resistance and compression force in the concrete part. Fig. 6.20 shows one example. In this situation, the partial shear diagram calculated by plastic design method according to Eurocode 4 can be used.

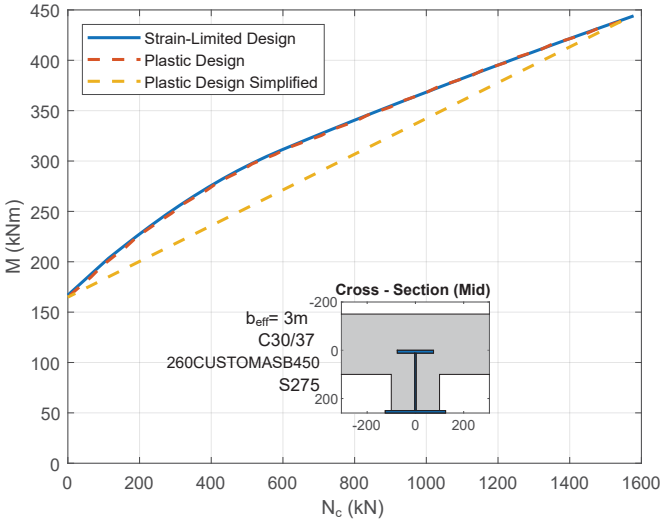

Figure 6.20 – Partial shear diagram example of situation 1

6.2.2.2 N_{cf} is smaller by strain-limited design method (Situation 2)

When the neutral axis is deeper, whereby strain-limited design the top flange is partly or fully in elastic stage, it may result in a big difference in the position of the neutral axis by these two methods as well as the value of total longitudinal shear force N_{cf}. Due to concrete strain limited, the rotation capacity of the cross-section is reduced. Thus rectangle stress block of steel top flange according to plastic bending resistance does not represent well the real stress distribution. However, the impact on bending moment resistances is usually smaller than that on concrete compression force, as the neutral axis is near to the steel top flange, a smaller lever arm makes the contribution of the top flange to whole cross-section bending moment resistances to be limited. In contrast, the impact on longitudinal shear resistance is bigger. The plastic design can overestimate the required N_{cf}, if steel top flange is in tension, the total longitudinal shear force by strain-limited design can be smaller than that by plastic design ($N_{cf,sl} < N_{cf,pl}$) . Fig. 6.21 shows example of this situation.

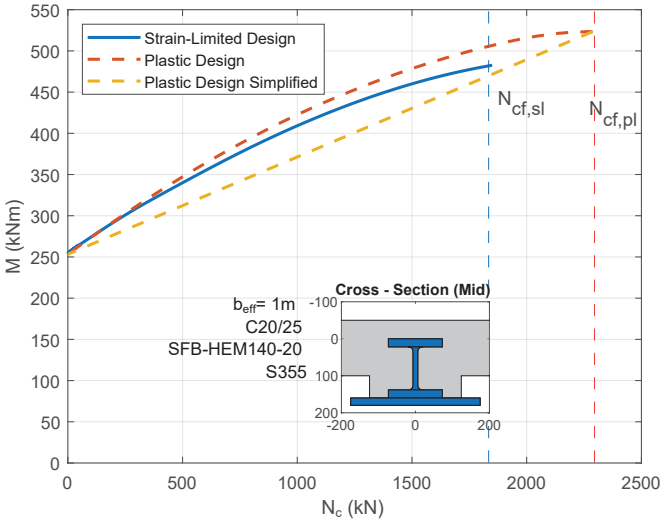

Figure 6.21 – Partial shear diagram example of situation 2

6.2.2.3 N_{cf} is bigger by strain-limited design method (Situation 3)

When the neutral axis locates further deeper resulting the steel top flange is in compression, similar effects as situation two can cause in opposite a bigger total longitudinal shear force by strain-limited design compared to plastic design ($N_{cf,sl} > N_{cf,pl}$). Fig. 6.22 shows an example of this situation. That is due to the normal force in the concrete part equals to that in the steel part. As a smaller compression force $N_{a,c}$ in top flange by strain limited design results in total normal force in steel part increases, the compression force in concrete also increases $N_{cf} = N_{a,t} - N_{a,c}$. This situation, however, requires the steel top flange is above the profile sheeting, or the ratio of effective width of slab to chamber concrete width (b_{eff}/b_c) is small to allow concrete section not fully in compression.

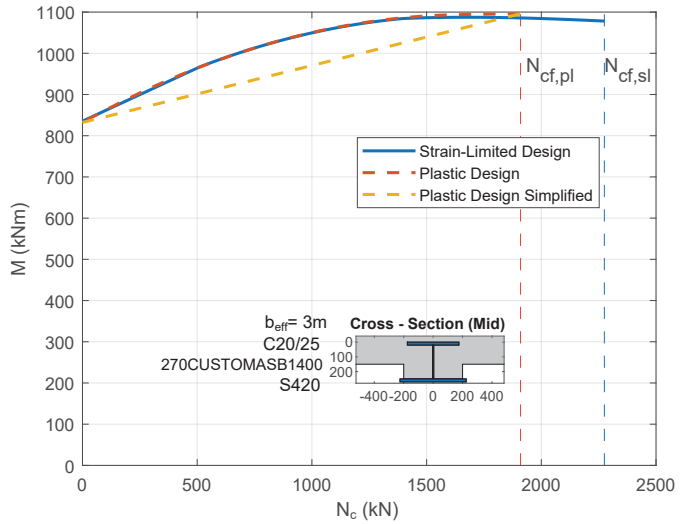

Figure 6.22 – Partial shear diagram example of situation 3

6.2.2.4 Bending moment resistance decreases with full shear interaction (end-drop effects)

For situation 2 and 3, It is sometimes found the maximum bending moment resistance by strain-limited design (full shear connection) is reached before full interaction as shown in Fig. 6.23. After a full shear connection, further increase of total longitudinal shear force decreases the bending moment resistance. These "end-drop" effects show an increase of total longitudinal shear force does not necessarily always increase the bending moment resistance.

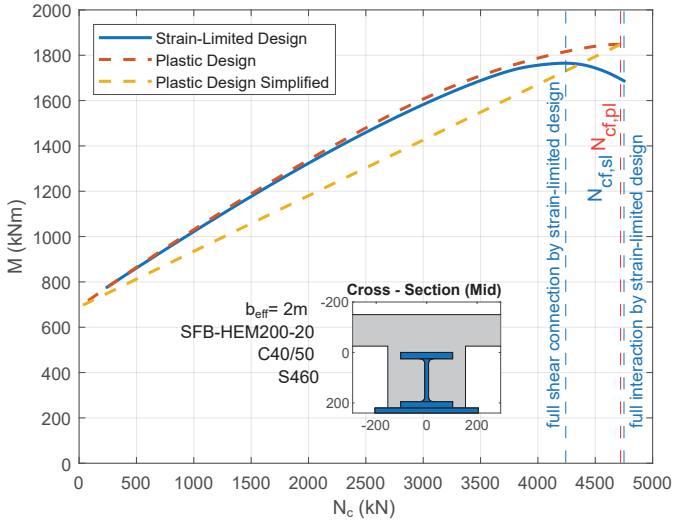

Figure 6.23 – Partial shear diagram "End-drop" by strain limited design

The unique "end-drop" effect does not only happen for slim-floor beams, for a conventional composite beam with an over-sized steel section, it may happen as well. Fig. 6.24 shows the example which is benchmarked with FEM calculation. To calculate the partial shear diagram by FE-Method, degree of shear connection is step-wisely changed, and the partial shear diagram is created by connecting all the results points. Here the parameters are modified to be similar as strain-limited design and the same strain limits of concrete and steel profiles are set in the FEM simulation. The results from FEM and strain-limited design are similar, with around 5% difference in maximum longitudinal shear force and around 1% of maximum bending resistance. The FEM results of strain in the longitudinal direction (LE33 of Abaqus) of step "P1" is shown in the figure, the strain values in mid-span and strain stress following path A-A are also plotted for the end-step, which shows the failure of concrete strain reaching its limit.

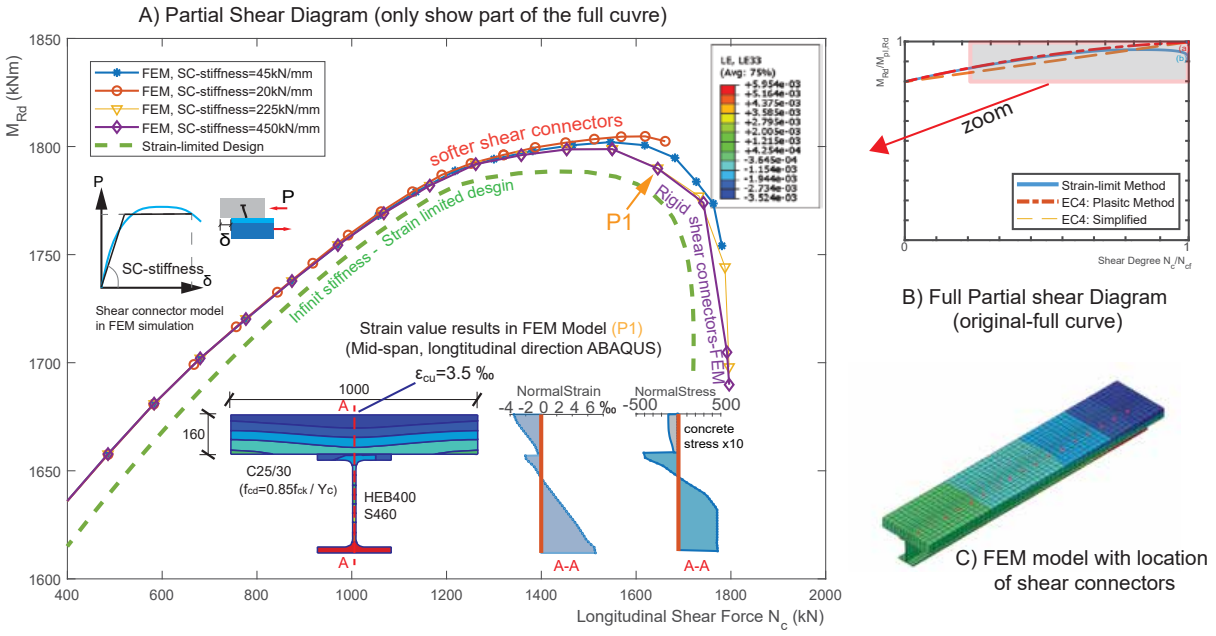

Figure 6.24 – Partial shear diagram and reduction factor of plastic bending resistance

Further analysis found that the decrease part at the end is due to with full interaction assumption, steel section is mostly in the elastic stage at concrete failure, which the resistance potential is not fully used. With the appearance of small amount slip strain, although the benefit from the composite action reduces, the increase of resistance from the steel section is much bigger, which increases overall bending moment resistance. However, theoretical full interaction is usually not reachable as most of the shear connectors have only limited stiffness. Thus the "end-drop" will have less impact. As shown in Fig. 6.24, the FEM results with shear connector initial stiffness equal 20 kN/mm almost have no "end-drop" effect. For a normal composite beam with profiled sheeting shear connector are usually have limited stiffness, thus will mostly free from it. In strain-limited design, the concrete strain is limited to 3.5‰ in tests the value can be much higher, especially for lower concrete classes. Still, people should notice the possibility of underestimate the strain-limit bending resistance with full interaction.

6.2.3 The parametric study results related to β_N=$N_{cf,sl}$/$N_{cf,pl}$

6.2.3.1 Parameter design

In order to explore the possible differences of total longitudinal shear force by plastic and strain limited design, new parametric studies have been carried out. Thereby, different parameters related to geometry and material of composite beams and slim-floor beams have been considered. The parameters for slim-floor beams are listed in Table 6.5. In total, 289 different steel profiles, including both open forms and close-forms, which are available in European markets, are considered. The effective width to height (b_{eff}/h) ratio is set to be 4 to 10 for slim-floor beams and minimum one meter is required. All possible combinations of the listed parameters have been calculated, which results in around 500,000 cross-sections.

For the design, instead of the non-linear curves of partial shear diagram (Fig. 6.18 $\widehat{ABC}$), usually the simplified linear curves (Fig. 6.18 $\overline{AC}$) are used. Two points determine the simplified curve. The first point is at zero shear connection, where the bending moment resistance equal to the steel beam resistance (M_a) alone if no longitudinal reinforcement considered, and the total longitudinal shear force equal to zero ($N_{cf} = 0$). The second point is at full shear connection, where bending moment resistance ($M_{sl,Rd}, M_{pl,Rd}$) and total longitudinal shear forces ($N_{cf,sl}, N_{cf,pl}$) can be obtained by the two methods. As the first point A is same for both methods, it is more important to calculate point C at the end. For each cross-section, at full shear connection the total force in concrete by plastic design $N_{cf,pl}$, by strain-limited bending $N_{cf,sl}$, the ratio between them $\beta_N = N_{cf,sl}/N_{cf,pl}$, the bending moments reduction ratio $\beta = M_{sl,rd}/M_{pl,rd}$ and other parameters have been calculated. For concrete the parabolic-rectangle strain-stress model according to Eurocode 2 [19] is used and for steel a bi-linear model without consider strain-hardening according to EN1993-1-5 [21] is used.

6.2.3.2 Relationship between β and β_N

The ratio of bending moment resistances according to strain-limited design and plastic bending resistance (β) and total longitudinal shear force (β_N) are plotted in Fig. 6.25. The color in the figure represents the relative compression zone height z_{pl}/h. A clear relationship between β and β_N cannot be reached. Thus, it is not able to use β to represent β_N in practices.

Table 6.5 – Parameter sets

h_{ct} (mm)	Profile type	b_{eff}/h	h_c (mm)	Concrete class	Steel grade
50	IFB	4	90	C20/25	S235
100	SFB	6	125	C30/37	S275
150	Delta	8	150	C40/50	S355
	ASB	10	...	C50/60	S420
	SWT		300		S460

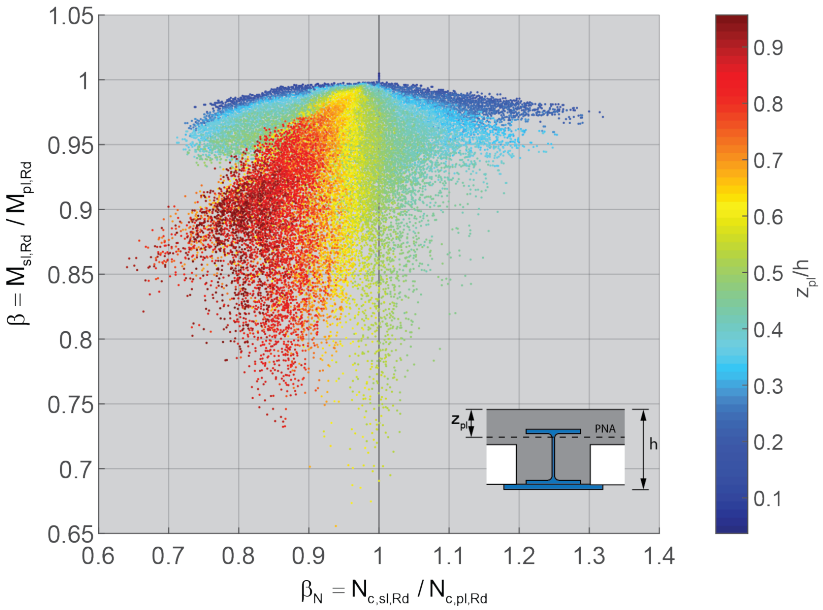

Figure 6.25 – Comparison of reduction factor on bending moment resistance β and on concrete normal force β_N

6.2.3.3 Relationship between β_N and location of PNA

The β_N=$N_{cf,sl}/N_{cf,pl}$ values are related to the relative location of plastic neutral axis to the steel top flanges. Thus another plot in Fig. 6.26 shows the relationship between them. In the vertial direction, the data is split into the following three different zones and the steel top flange is scaled (Fig. 6.26):

- Zone one from 0 to 1 represents concrete slab top surface to the steel top flange upper surface.
- Zone two from 1 to 2 represents steel top flange.
- Zone three from 2 to 3 represents the steel top flange lower surface to bottom of slim-floor beams.

The data also distinguished between if the steel section is below the concrete slab or been encased in it. An approximately linear relationship can be found inside each zone. In zone 1, β_N is smaller than 1.0 indicates by strain-limited design, smaller total longitudinal shear forces are resulted compared to plastic design. In zone 2, the β_N is smaller than one when PNA is in the top half part of the steel top flange and then can be bigger than one if it is in the bottom half part. As PNA is near to the steel top flange lower surface,

the value of β_N increases quickly. In zone 3, the value of β_N decreases with the distance to the steel top flange bottom surface.

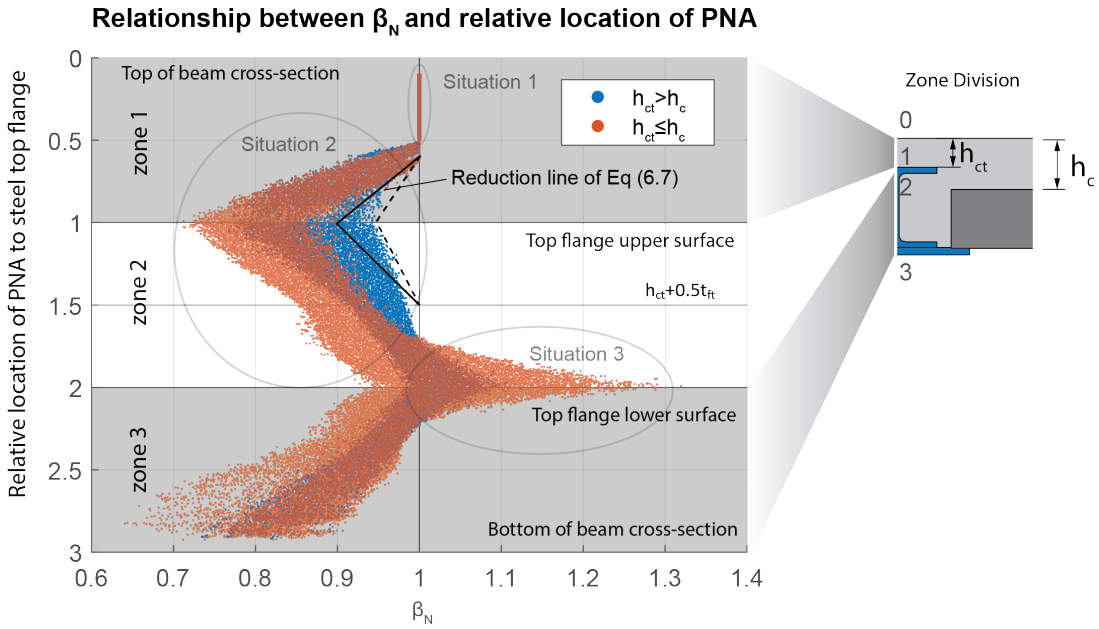

Figure 6.26 – Relationship between β_N and relative location of PNA

6.2.4 Limitations of application of current partial shear diagram based on plastic method

As explained above, if the beam cross-section has big enough rotation capacity, plastic cross-section resistance can yield similar results as strain limited resistance (without considering strain-hardening). Otherwise, the partial shear diagram can be different and plastic resistance may lead to unsafe design results. Thus a few limitations should be set for slim-floor beams when using the current Eurocode 4 partial shear diagram. Of all the three situations explained in section 6.2.2, the first situation allows the directly using the current Eurocode 4 partial shear diagram, as both methods yield very similar results. The second situation plastic resistance gives conservation results of N_c; however, it is still safe to apply. Form Fig. 6.26. It is noticed that if the PNA is above the middle of steel top flanges, the required total longitudinal shear force by strain-limited resistance is equal or smaller than plastic resistance, for which plastic resistance still provides safe design results. Thus, to use the partial shear diagram according to current Eurocode 4 for slim-floor beams, it is proposed to fulfil the following two conditions:

- The reduction factor β=1
- The Plastic neutral axis lays above middle of steel top flange: $z_{pl} < h_{ct} + 0.5t_{ft}$

The limitation can cover most engineering practices. If it is exceeded, more advanced design methods can be applied. On the other hand, when PNA is near the steel top flange upper surface, more economical design results are expected by strain-limited design or other advanced non-linear design methods is used.

6.2.5 Proposal of a simplification method of partial shear design when plastic resistance is not suitable

For slim-floor beams, if the condition in section 6.2.4 is partially exceeded, a simplified design rule can be useful. If the reduction of plastic bending moment resistance is necessary ($\beta<1$), on the condition of $z_{pl} < h_{ct} + 0.5t_{ft}$, the partial shear diagram can be modified by replacing $M_{pl,Rd}$, with $\beta M_{pl,Rd}$, while the required total longitudinal shear force $N_{c,pl}$ keep unchanged. The design by this method gives conservative, however easy to use.

As shown in Fig.6.26. When the PNA is located near the upper surface of the steel top flange, the required total longitudinal shear force by strain-limited design is, in fact, smaller than calculated according to plastic resistance. Thus a reduction factor on it can be defined by using the boundary values. If concrete slab thickness above the steel section is smaller or equal to concrete slab thickness ($h_{ct} <= h_c$). The boundary can be defined as follow in Eq. (6.7).

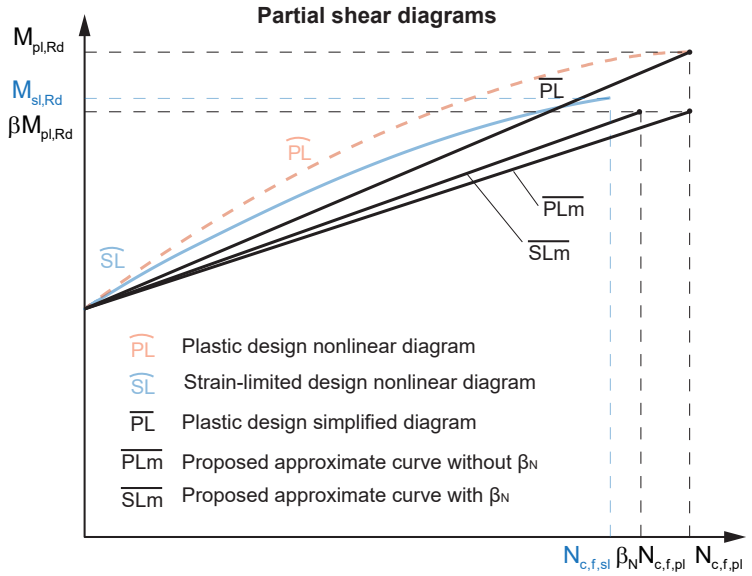

Figure 6.27 – Comparison of partial shear diagram of each method

$$h_{ct} \leq h_c: \qquad (6.7)$$

$$\beta_N = \begin{cases} 1 - \frac{1}{4}(z_{pl} - 0.6h_{ct})/h_{ct} & 0.6h_{ct} < z_{pl} < h_{ct} \\ 1 - \frac{1}{5}(h_{ct} + 0.5t_{ft} - z_{pl})/t_{tf} & h_{ct} < z_{pl} < h_{ct} + 0.5t_{ft} \end{cases}$$

$$h_{ct} > h_c:$$

$$\beta_N = \begin{cases} 1 - \frac{1}{8}(z_{pl} - 0.6h_{ct})/h_{ct} & 0.6h_{ct} < z_{pl} < h_{ct} \\ 1 - \frac{1}{10}(h_{ct} + 0.5t_{ft} - z_{pl})/t_{tf} & h_{ct} < z_{pl} < h_{ct} + 0.5t_{ft} \end{cases}$$

For other situation or to get more accurate calculation results, strain-limited design or other advanced non-linear calculation methods can be applied.

6.3 Chapter summary

This chapter discusses the sagging bending resistance of composite beams for both full and partial shear connection situation. For the full shear connection in section 6.1, the β reduction factor applied on plastic bending moment resistance according to Eurocode 4 [22] is improved using a vast amount of parametric studies considering different types of composite beam cross-sections. In subsection 6.1.1, comparisons of plastic and strain-limited design resistance shows that a deep neutral axis position causes overestimation of bending moment resistance by plastic design. The reasons are further investigated through parametric studies in subsection 6.1.4, and a few key parameters with important influences are selected out. Among them are the steel grades, the effective width of concrete slab, the ratio of steel top flange size to whole steel profile size and the choices of material non-linear strain-stress relationships. The concrete classes until C50/60 have limited influences, for high strength concrete over C50/60, according to current EN1992-1-1 [19] the ultimate compression strain is reduced, thus the strain-limited design resistance can be much smaller compared to the plastic bending resistance results. Based on statistic results, improved β reduction factor functions are proposed in subsection 6.1.5 for all composite beams and only slim-floor beams, which use similar approaches according to Eurocode 4 based on the value of relative compression zone height "z_{pl}/h". Subsection 6.1.6 provides in addition a new reduction function based on the strain stage of steel profile bottom flange. It provides more economical solutions and gives an uniform expression for all steel grades.

For the partial shear connection in section 6.2, considering the deep neutral axis position of slim-floor beams, additional design rules to use the partial shear diagram for slim-floor beams are proposed. In subsection 6.2.1 partial shear diagrams obtained by plastic and strain limited methods are compared. The influences of the neutral axis position on partial shear diagrams are discussed in subsection 6.2.2. For which three different situations are classified: Situation 1 with small relative compression zone height shows similar partial shear diagrams obtained by plastic and strain-limited method. Situation 2 indicates the compression force in the concrete slab calculated by strain-limited design is smaller than the plastic design method. And situation 3 is opposite to situation 2. The full shear connection, which indicates the maximum bending moment resistance and full shear interaction, which indicates no slip at the composite joint, are not necessarily the same. "End-drop" effects are noticed in the strain-limited partial shear diagrams with deep neutral axis position. It means after the full shear connection point, further increase of shear connectors can lead to a reduction of bending moment resistance. It is due to constraining of concrete strain limits reduces the strain in steel section with full shear interaction. Based on a vast amount of parametric study results, the limitations of the plastic partial shear diagram for slim-floor beams are drawn in subsection 6.2.4 based on the neutral axis position. The difference of the concrete compression force according to strain-limited design and plastic design ($\beta_N = N_{c,sl}/N_{c,pl}$) has been analysed. It is found the value of β_N is more related to the relative neutral axis position to steel top flange location than the relative compression zone height z_{pl}/h. It is because that the stress distribution in steel top flange causes major difference in strain limited and plastic design for most of the cross-section. Beyond the limitation, a simplified engineering approach is proposed in subsection 6.2.5 to simplify the design of slim-floor beam.

Chapter 7

Longitudinal shear force in composite beams

Eurocode 4 allows equal distance arrangement of shear connectors on the condition of class 1 and 2 cross-sections, ductile shear connectors and sufficient moment allowance over the whole length of the beam (Fig. 7.1). With class 1 and 2 cross-sections, for a simply supported beam under uniform distributed load, most parts of the steel cross section at mid-span are assumed to reach plastic at failure as shown in Fig. 7.1 B). On the condition of full shear interaction, plastic development in the steel beam results in a non-linear longitudinal shear force distribution along the composite joint. In addition, with ductile shear connectors, due to non-linear redistribution of the longitudinal shear force, an equal distance arrangement of shear connectors is possible as shown in Fig. 7.1 C) providing the moment allowance over the length of the beam is sufficient. Otherwise, the shear connectors should be arranged based on the longitudinal shear force distribution, such examples and design guidance can be found in [33].

However, the analysis in chapter 6 still shows with deep laying neutral axis position, even with class 1 or 2 cross-sections, due to the limitation of concrete compression strain, essential parts of steel sections can not reach plastic strains at concrete failure. It raises the question of whether a uniform arrangement of shear connectors is still suitable for this case. To answer it, a look into the impacts of both plastic development in composite beam (especially in the steel beam part) and longitudinal shear redistribution due to shear connectors becomes necessary. Thus this chapter is divided into the following three main sections:

Section 7.1 discusses the influence of plastic development in the composite beam on longitudinal shear. It is further divided into two sub-sections: Subsection 7.1.1 explains the mechanic background of longitudinal shear force in elastic and post-elastic stage with the help of a simple rectangle beam based on an elastic perfect-plastic material model. The system is simple enough to derive analytical solutions for the plastic zone and the longitudinal shear force distribution at any height. For more complex composite beams explained section 7.1.2, it is difficult and impractical to derive exact analytical solutions. Numerical solutions can be used instead, and simplified engineering approaches are investigated based on parametric studies.

Section 7.2 shows the impact of longitudinal shear force redistribution due to shear connector stiffness and non-linear redistribution for ductile shear connectors. The analysis is based on the FEM calculation results and related parametric studies. The sub-section

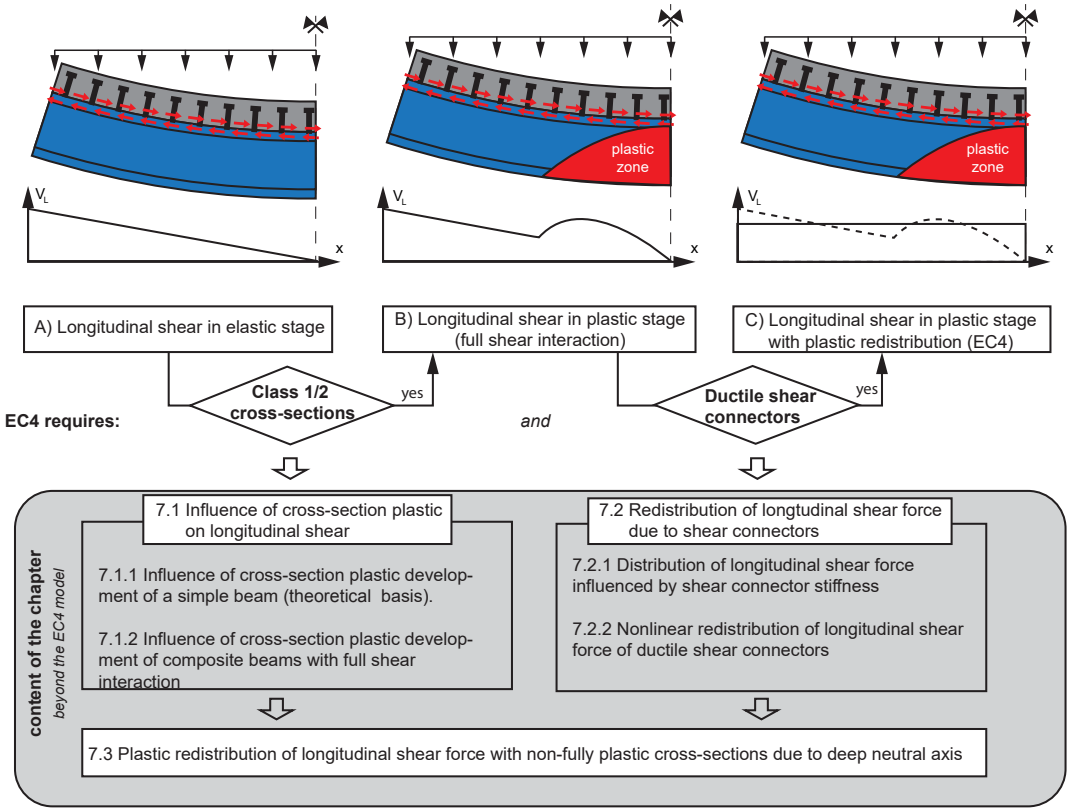

Figure 7.1 – Introduction of chapter 7

7.2.1 summarizes the shear connectors based on their load-deformation behavior. The longitudinal shear force distribution effected by shear connector stiffness is discussed in subsection 7.2.2. In it, linear elastic shear connector load-deformation relationship is assumed. In subsection 7.2.3 non-linear redistribution of longitudinal shear force with ductile shear connectors is analysed. A bi-linear load-deformation relationship of shear connector is assumed in this subsection, based on it, the related topics such as slip development stages, partial and full non-linear longitudinal shear distribution and bending moment resistance envelope based on degree of shear connection are explained.

Section 7.3 explains the influence of deep neutral axis position on the longitudinal shear design with ductile shear connectors. The potential problems related to bending moment envelop and slip development caused by the not-fully plastic development in critical cross-sections are discussed.

7.1 Influence of neutral axis position in critical cross-section on longitudinal shear force

The plastic development inside the beam cross-section influences the longitudinal shear force. In this section, the influence is firstly explained with the help of a simple rectangle beam using bi-linear material stress-strain relationship. With it, the basic concepts can be analytically obtained. Afterwards, more complex composite beam cross-sections are analysed, and simplified calculation approaches are provided.

7.1.1 Influence of cross-section plastic development of a simple beam

Before jumping into the analysis of complex composite beams, it is important first to investigate the basic mechanic concept of longitudinal shear and how plastic development effects it. Thus as a starting point, longitudinal shear in a simple rectangle beam with an ideal bi-linear material model is calculated. In the elastic stage, there is already well-known theoretical solution. However, for the elastic-plastic stage, more analysis is still required. In this part, analytical equations of longitudinal shear force in the simply supported beam are developed. However, due to limitation of pages, only the results are provided, the details are available in Appendix D.

The simply supported beam under symmetric concentrated loads in the middle is shown in Fig 7.2, which results in pure bending between the concentrated loads (zone B) and constant shear force between support and loads (zone A). For simplification, the influences of stress concentration at the support and loading area are neglected.

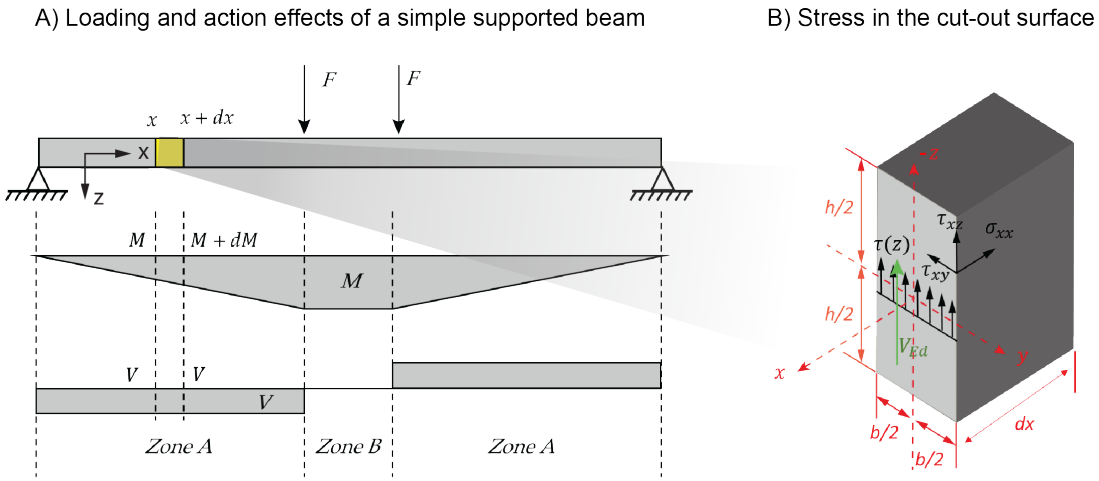

Figure 7.2 – Action effects of a beam under concentrated load and stress at the cut surface

Considering to cut out a infinite small slice of beam length of d_x as shown in Fig 7.2 B). Based on the well-known equilibrium of shear stress, $\tau_{xy} = \tau_{yx}$. At side surfaces if there is no external shear stress applied, shear stress should equal to zero ($\tau_{yx} = 0$), shear stress transverse to the side edges is also equal to zero ($\tau_{xy} = 0$). Thus shear stress $\tau(z)$ must parallel to the side edge. Experiments proved, if the cross-section is slim (h/d is big), the shear stress can be considered to keep constant along the beam width direction. According to the statement above, the following assumptions can be made:

- Plane cross-section keeps plane.

- All the shear stress on the cross-section parallel to the side edges and shear stress does not change along the z-axis of the beam (along the direction of beam width).
- Stress concentration near supports and the concentrated load's applied area is not considered

7.1.1.1 Review of longitudinal shear stress distribution in elastic stage

First to review the beam in the elastic stage. Based on the well established elastic theory, the longitudinal shear stress can be calculated as follow:

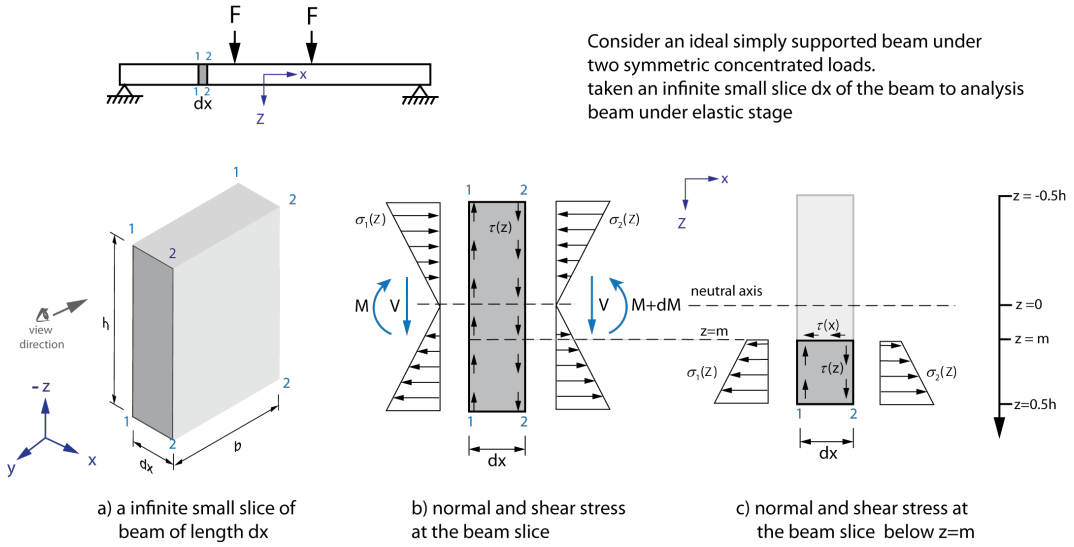

Figure 7.3 – Shear stress at elastic stage

As shown in Fig. 7.3 b), assuming to take out an infinitely small slice of the beam of length d_x between cross-section 1-1 and 2-2. The bending moment M at each side will be different:

For 1-1: $M_1 = M$ and for 2-2: $M_2 = M + dM = M + V d_x$.
The stress at each side $\sigma_1(z), \sigma_2(z)$ will also be different. Separate the lower part of the slice at $z = m$, the following equilibrium of stress in the x-direction can be made:

$$\tau(m)dx = \int_{h/2}^{m} \sigma_2(z)dz - \int_{h/2}^{m} \sigma_1(z)dz \tag{7.1}$$

For beam in elastic stage by solving the equilibrium, we will get the well-known equations to calculate the shear stress at certain height $z = m$ as follow:

$$\sigma(z) = \frac{Mz}{I_y} \tag{7.2}$$

$$\tau(m) = \frac{VS_y(m)}{I_y b} \tag{7.3}$$

7.1.1.2 Longitudinal shear stress distribution in elastic-plastic stage

Assuming the beam is made of an ideal bi-linear material with yielding strength of f_y and has not reached the ultimate strain-limit. When bending moment exceeds the elastic

bending moment resistance, part of the beam cross section will enter the plastic stage. The elastic longitudinal shear stress in Eq. 7.3 can no longer be used, however the basic equilibrium of stress in Eq. 7.1 is still valid. In the stage the calculation can be performed with the following additional assumptions:

- Beam made of a ideal bi-linear material with yielding strength of f_y.
- Ultimate strain-limit is not reached.
- The beam is in elastic-plastic stage.

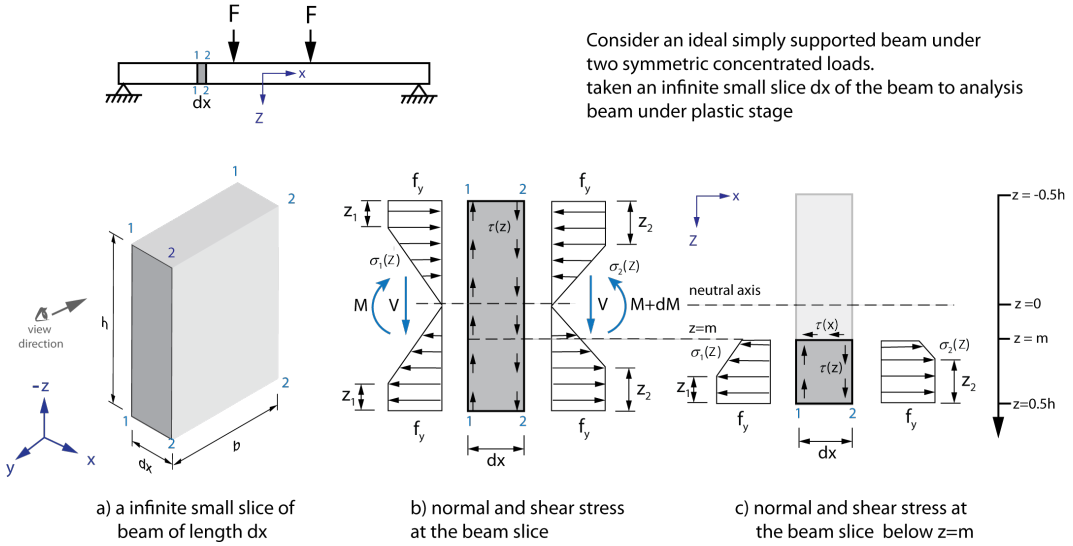

Figure 7.4 – Stress distribution at elastic-plastic stage

By solving the Eq. 7.1 in elastic-plastic stage we can get the the plastic zone height z_{pl} with a given bending moment M at calculated cross-section as shown in Eq. 7.4. Afterwards, the Longitudinal shear stress $\tau(z)$ at height z can be calculated by Eq. 7.5 as "V" is the shear force. Other nominations are provided in Fig. 7.4 The detailed derivation processes of these equations and benchmarks with FEM calculation are given in Appendix D. The equation is developed for a beam under the concentric load condition. However, they are also validated for the situation with the uniformly distributed load.

$$z_{pl} = \sqrt{\frac{3}{4}h^2 - 3\frac{M}{f_y b}} \leq h/2 \tag{7.4}$$

$$\tau(z) = \begin{cases} \frac{2V}{\sqrt{3}b} \cdot \frac{\frac{3}{4}h^2 - 3\frac{M}{f_y b} - z^2}{(h^2 - 4\frac{M}{f_y b})^{3/2}} & ; \mid z \mid \leq z_{pl} \\ 0 & ; z_{pl} < \mid z \mid \leq h/2 \end{cases} \tag{7.5}$$

The maximum shear stress is at z=0

$$\tau_{max} = \tau(0) = \frac{\sqrt{3}V}{2b \cdot \sqrt{h^2 - 4\frac{M}{f_y b}}} \tag{7.6}$$

It is to note that, in Eq. 7.4 to Eq. 7.6 the parameter z_{pl} and z are all based the $z = 0$ at middle of the cross-section, where the neutral axis lays.

7.1.1.3 Development of plastic zone

Plastic zone area can be calculated from Eq. 7.4, after the bending moment at each section is obtained. The results for a rectangle beam under uniform distributed load is given in Fig 7.5 for different load stages. After reaches elastic resistance, a nonlinear plastic zone appears in the centre, and it expended into a triangle shape at failure.

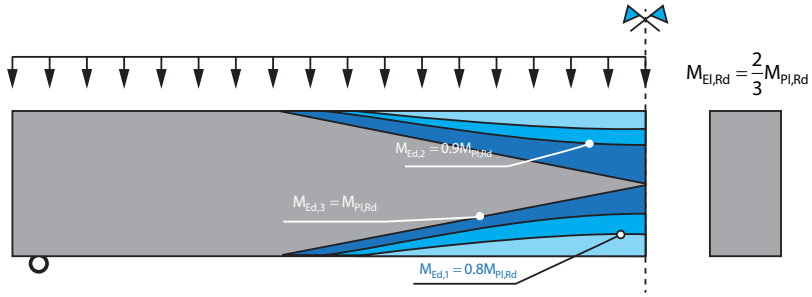

Figure 7.5 – Develop of plastic zone in a rectangle beam

7.1.1.4 Distribution of longitudinal shear stress in elastic-plastic stage

Fig. 7.6 illustrates the theoretical shear stress distribution of post-elastic stage calculated according to Eq. 7.5. Before reaching full plastic resistance, the plastic zone boundary is a curved line with the maximum height at mid-span. The shear stress inside the plastic zones equal to zero. For longitudinal shear stress at each horizontal cross-section (O-O: at the Plastic Neutral Axis), it can be concluded:

- Longitudinal shear stress keeps linear outside the plastic region and is nonlinear inside.
- If part of the horizontal cross-section is inside the plastic zone, the longitudinal shear only starts at the end of the plastic zone with an increased nonlinear part and then changes into a linear distribution.

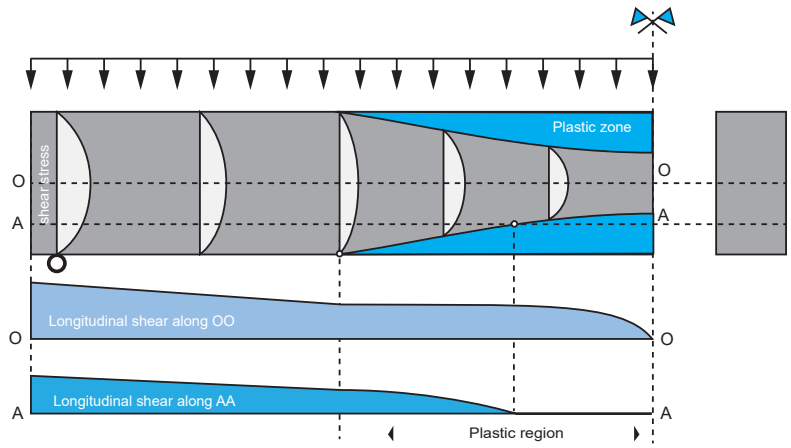

Figure 7.6 – Theoretical shear stress distribution inside the calculated beam and longitudinal shear at different height

Fig 7.7 illustrate changes of longitudinal shear stress with increasing loads. The calculated beam is simply supported with uniform distributed load. It has span length of 8.0m and rectangle cross-section of 200mm x 400mm Four curves are plotted in each subfigure represent the horizontal layers of z= 0mm, 60mm, 120mm, 200mm, with z=200mm representing the middle. The loads change from the elastic stage (a) to elastic-plastic stages (b to f).

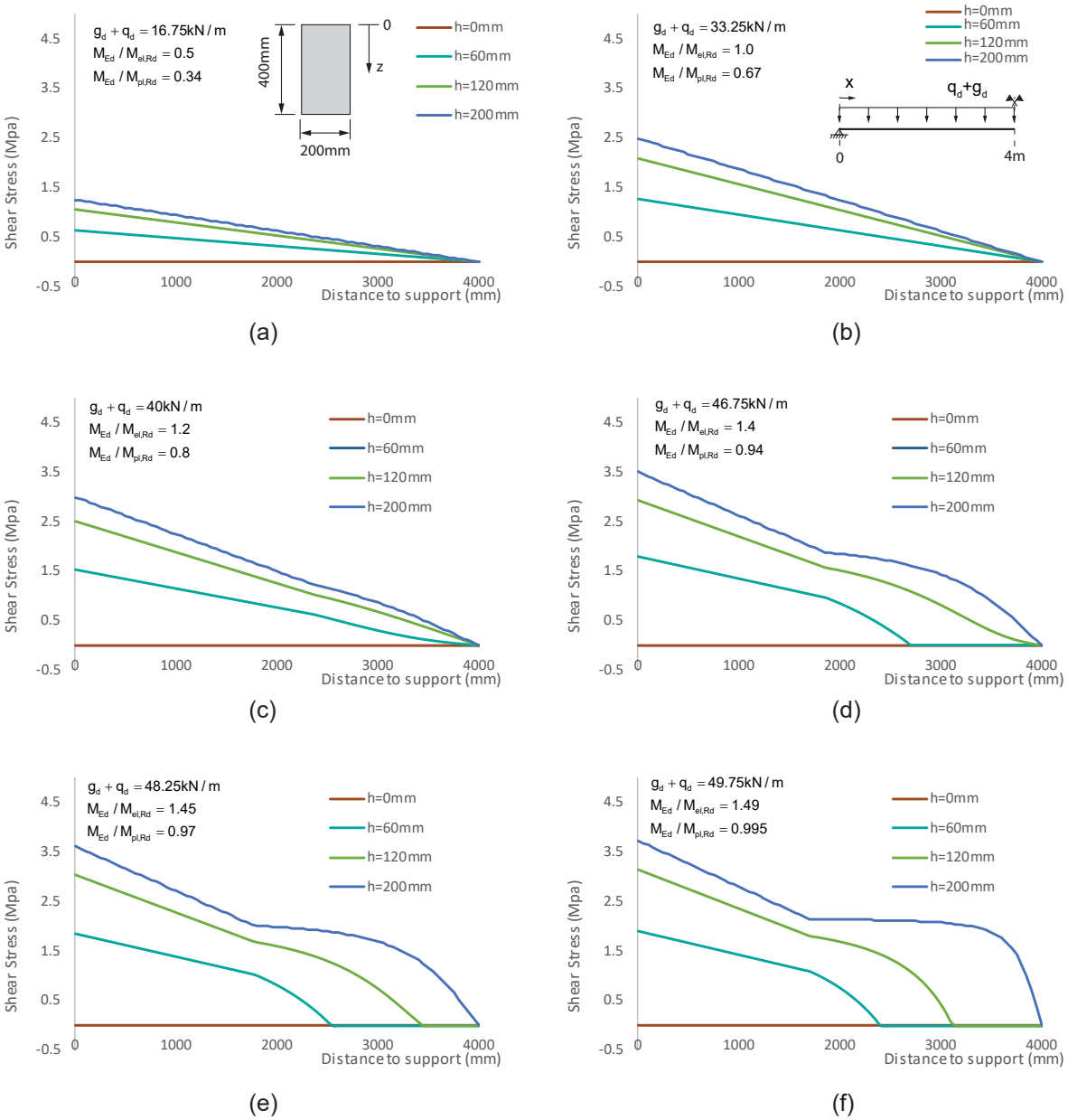

Figure 7.7 – Longitudinal shear stress development with increasing loads

In the elastic stage, longitudinal shear stress increases in portion to the shear force, which is also linear along the beam axis direction. After entering the plastic stage, a "hump" appears near mid-span area and increases with the load. Except for the layer at the neutral axis (z=200mm), longitudinal shear stress reduces to zero before mid-span.

7.1.2 Influence of cross-section plastic development of composite beam with full shear interaction

For full shear interaction, no slip at the composite joint is assumed. Thus only one neutral axis exists in the composite cross-section. As explained in chapter 3, with full interaction assumption, the M-κ curve of a composite beam can be obtained by step-wisely changing the controlling strain values and solving each step. At the same time, the compression force in concrete slab "N_c" can also be calculated. Moreover, the longitudinal shear force "V_L" which is a derivation of the "N_c" at longitudinal direction is able to be calculated.

In this section, the longitudinal shear force in conventional composite beams and slim-floor beams are calculated with the strain-limited design numerical software "SL.com" developed based on the theory of chapter 3. The results of different cases are shown first and based on which simplified engineering approaches for the situation steel section reaches full plastic was developed later on.

7.1.2.1 Longitudinal shear force in traditional composite beams

Beams lists for convential composite beams:

Beam ID	b_{eff}	Concrete	Steel	z_{sl}/h	$M_{sl,Rd}$ (kNm)	$M_{pl,Rd}$ (kNm)	$N_{sl,Rd}$ (kN)
NC1	2m	C30/37	S235	0.09	294	294	1264
NC2	2m	C20/25	S355	0.17	388	399	1587
NC3	2m	C20/25	S460	0.25	474	487	1769
NC4	1m	C20/25	S600	0.34	488	531	1133

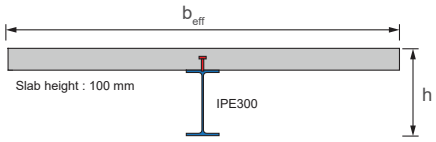

Stress distribution of mid-span at ultimate stage of the beams

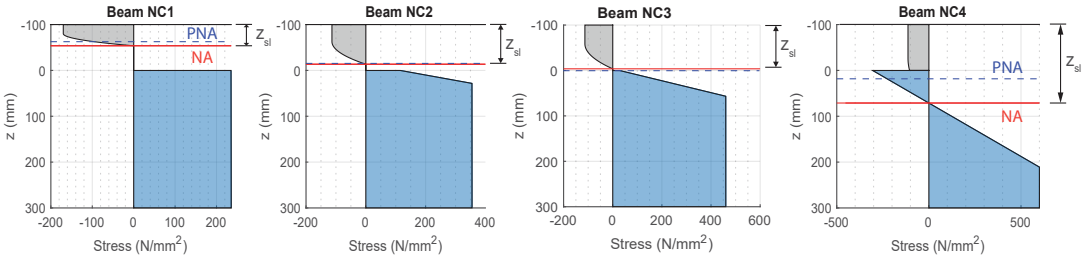

* Stress of concrete scaled 10 times for better visualization.
PNA: Plastic neutral axis. NA: Strain limited design neutral axis

Figure 7.8 – Beam table and stress distribution at failure of traditional composite beams

First, a series traditional composite beams with different relative compression zone height (z_{sl}/h) are given in Fig. 7.8. The beams are designed as simply supported with 8m length. The parabolic-rectangle concrete strain-stress relationship (section 3.1.3.1) and a bilinear steel strain-stress relationship without strain-hardening (section 3.1.3.3) is adopted in the calculation, concrete in tension is neglected. The concrete and steel parts are ideally bond together with zero slip. The stress distribution in mid-span at failure is also illustrated in the figure.

Fig. 7.10 to Fig. 7.13 show the position of neutral axis, plastic zone development and the longitudinal shear distribution of each beam at different load ratios. Fig. 7.9 provides an explanation of different curves shown in these figures. The plastic zone boundary in concrete is assumed to be the area with strain over ε_{c2}.

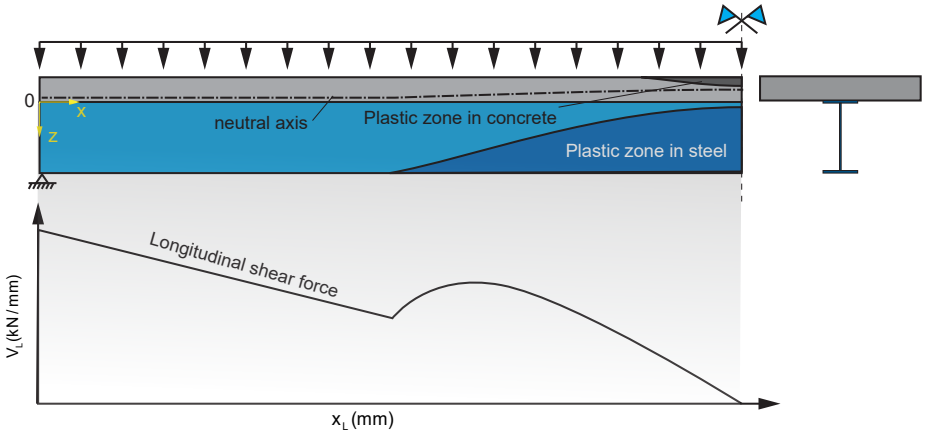

Figure 7.9 – The explanation of information shown in Fig. 7.10 to Fig. 7.13 for uniform distributed load situation

The calculation results with uniform distributed loads are given. The load ratios are taken as 0.2 ,0.4, 0.6, 0.8, 0.9, 0.95 and 1.0 times of the maximum bending moment resistance ($M_{sl,Rd}$). Near failure, the longitudinal shear increases faster than elastic stage, thus smaller step increase value is taken.

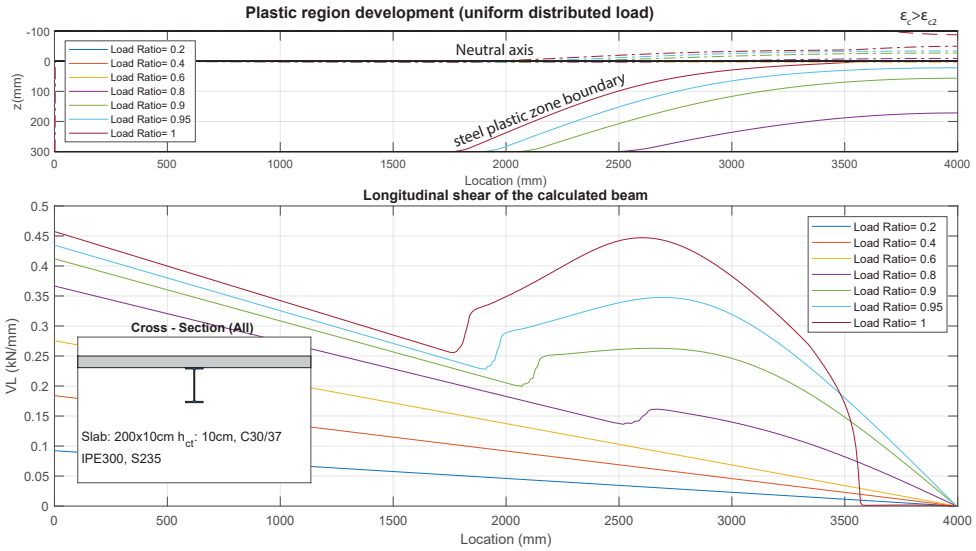

Figure 7.10 – Plastic zones development and longitudinal shear force distribution of beam NC1

Beam: NC1: Fig. 7.10 shows some similarities of longitudinal shear redistribution with the simply rectangle beam investigated in section 7.1.1.4: Non-linear longitudinal shear redistribution only happens when the part of steel beam reaches plastic, and longitudinal shear equal to zero after the steel reaches full plastic if strain-hardening is not considered. Out of the plastic region, the longitudinal shear linear increases similar as the elastic situation.

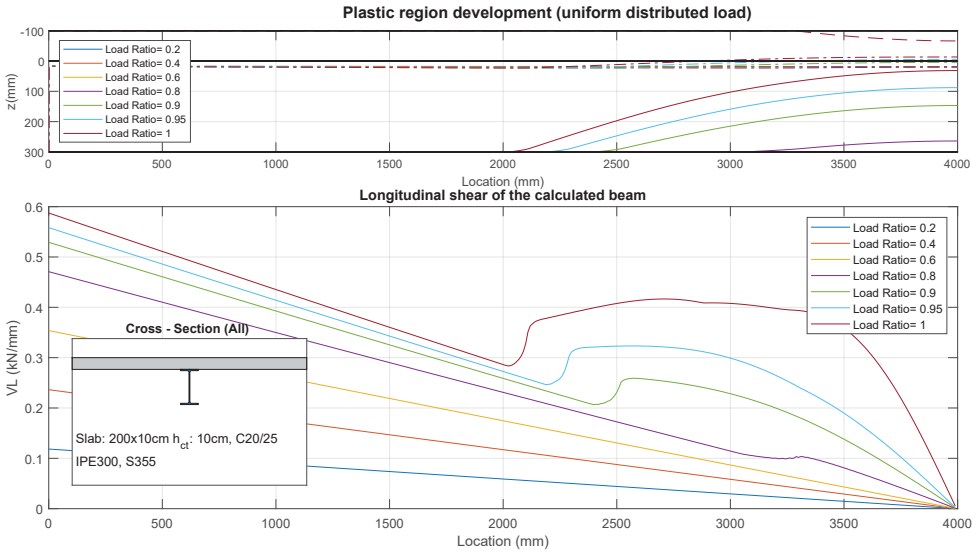

Figure 7.11 – Plastic zones development and longitudinal shear force distribution of beam NC2

Beam NC2: Results from the second beam shown in Fig. 7.11 has a similar longitudinal shear non-linear redistribution pattern as beam NC1. Most part of the steel section reaches plastic at the beam mid-span, however full-plastic of the steel beam has not been reached.

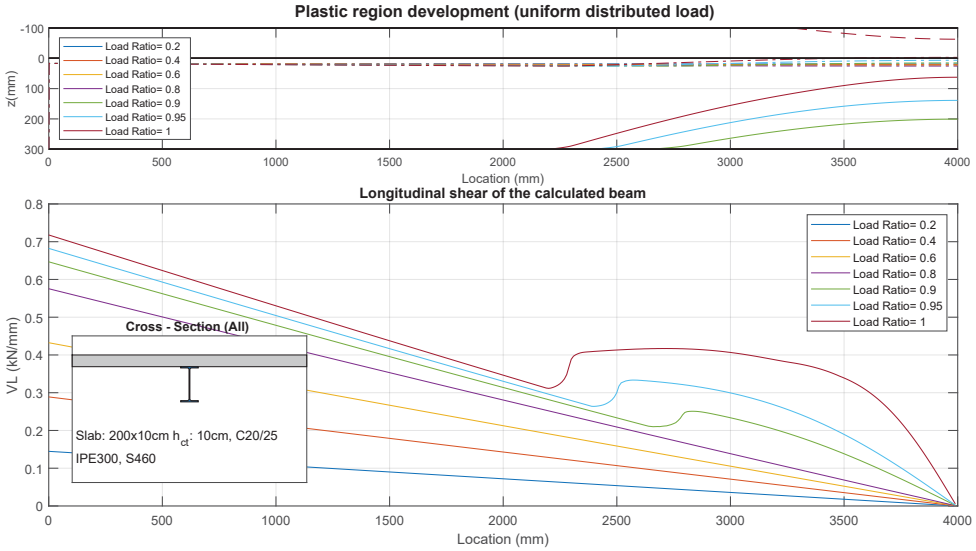

Figure 7.12 – Plastic zones development and longitudinal shear force distribution of beam NC3

Beam NC3: The neutral axis of the third beam shown in Fig. 7.12 is partly inside the steel top flange at the mid-span cross section at failure. The amount of longitudinal shear non-linear redistribution has been reduced compared to the first two situations. Although the steel grade is increased from S355 to S460, the longitudinal shear force does not increase very much.

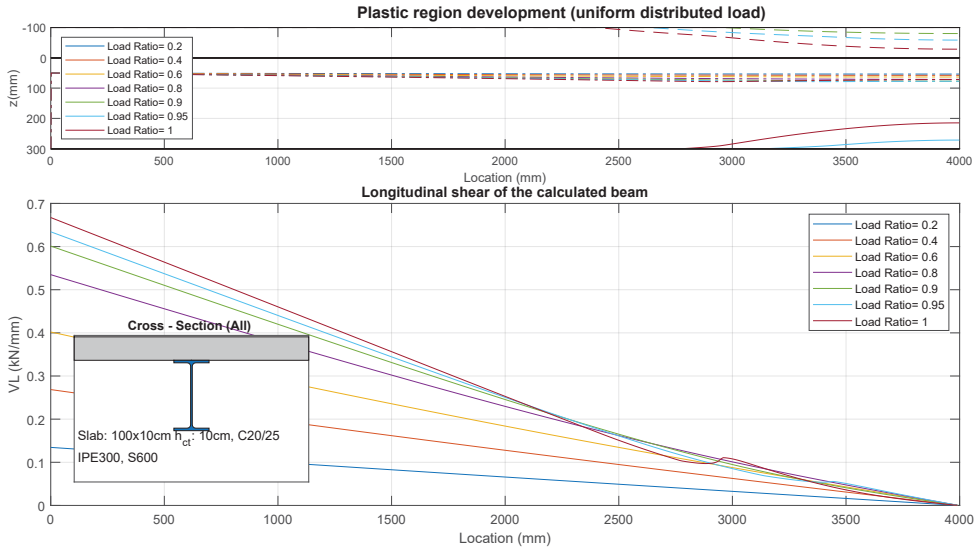

Figure 7.13 – Plastic zones development and longitudinal shear force distribution of beam NC4

Beam NC4: The last beam shown in Fig. 7.13 has very little amount of longitudinal shear non-linear development as a limited region of the steel beam reaches plastic. The neutral axis is located in the steel section only. The beam behaves mostly similar to elastic longitudinal shear distribution.

7.1.2.2 Longitudinal shear force in slim-floor beams

A similar analysis of slim-floor beams has been carried out. The "SFB" type slim-floor beams which have a standard steel profile welded with a bottom plate are used for demonstration. The beam information and stress distribution at ULS are given in Fig. 7.14. The parabolic-rectangle concrete strain-stress relationship (section 3.1.3.1) and a bilinear steel strain-stress relationship without strain-hardening (section 3.1.3.3) is adopted in the calculation, concrete in tension is neglected. The beams are designed with different relative compression zone height z_{pl}/h at mid-span, Beam SF1 and SF2 have neutral axis above the steel section, and the Beam SF3 and SF4 have neutral axis in the steel section at ultimate loads.

The results are presented in a similar way as the conventional composite beams in section 7.1.2.1. The plastic zone, neutral axis position in the beam, as well as the longitudinal shear force distribution are given. Explanation of the information are given in Fig. 7.14. In the vertical direction, z=0 is set as the upper surface of the steel top flange. The results at different load ratios are provided.

Beams lists for slim-floor composite beams:

Beam ID	h_{ct}	Profile	Plate	Concrete	Steel	z_{sl}/h	$M_{sl,Rd}$
SF1	100mm	IPE200	350×10	C50/60	S235	0.08	370
SF2	100mm	HEA200	450×15	C50/60	S235	0.16	661
SF3	50mm	HEM200	450×20	C50/60	S235	0.23	897
SF4	50mm	HEM200	450×20	C30/37	S355	0.39	1190

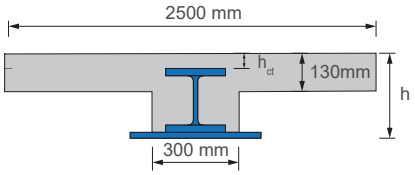

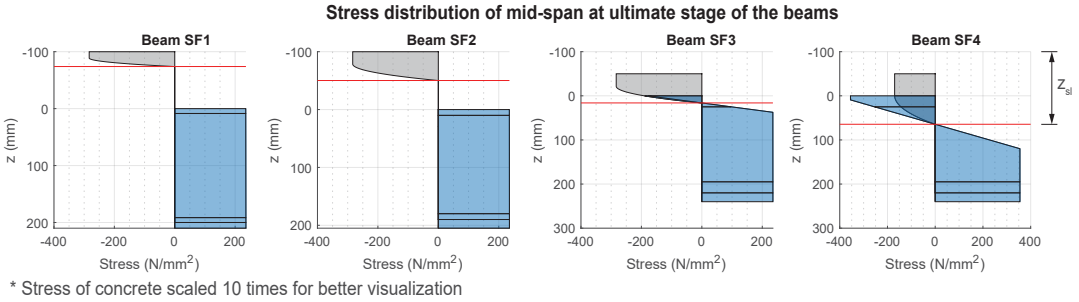

* Stress of concrete scaled 10 times for better visualization

Figure 7.14 – Beam lists and stress distribution at ULS of slim-floor composite beams

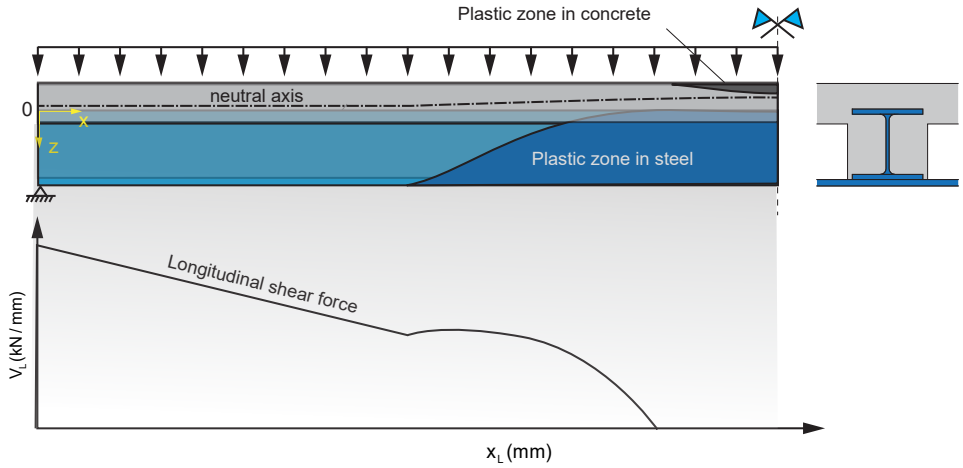

Figure 7.15 – The explanation of information shown in Fig. 7.16 to Fig. 7.19 for uniform distributed load situation

The longitudinal shear force distribution and plastic zone development of the slim-floor beams under uniform distributed loads are given below. The beam span is 8m and simply supported. Only half span is plotted as it is symmetric. The load ratios are taken as 0.2 ,0.4, 0.6, 0.8, 0.9, 0.95 and 1.0 times of the maximum bending moment resistance ($M_{sl,Rd}$). Near failure, the longitudinal shear increases faster than elastic stage, thus smaller step increase value is taken.

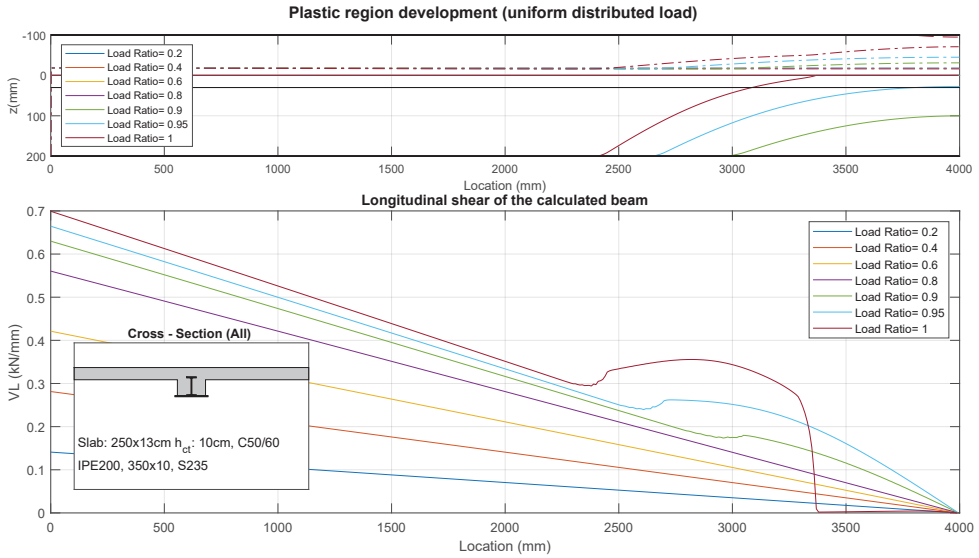

Figure 7.16 – Plastic zones development and longitudinal shear force distribution of beam SF1

Beam SF1: Beam SF1 has a z_{sl}/h ratio of 0.08, which is similar as the conventional composite beam NC1. However, the non-linear longitudinal shear force development near the mid-span of beam is rather limited compared to the beam N1. For slim-floor beams, it is usually found that a smaller beam section showing a non-linear increase.

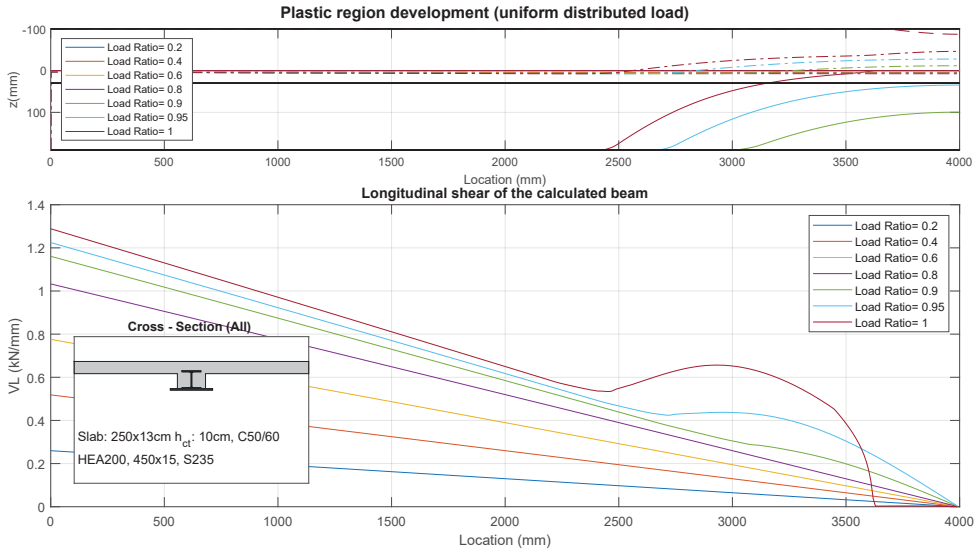

Figure 7.17 – Plastic zones development and longitudinal shear force distribution of beam SF2

Beam SF2: Beam SF2 shows similar response as Beam SF1, both beams have the neutral axis at mid-span above the steel section at failure load. The non-linear increase of longitudinal shear forces due to plastic development is similar with SF1, which shows steel beam section near the mid span reaches full plastic, resulting zero longitudinal shear force near the mid-span.

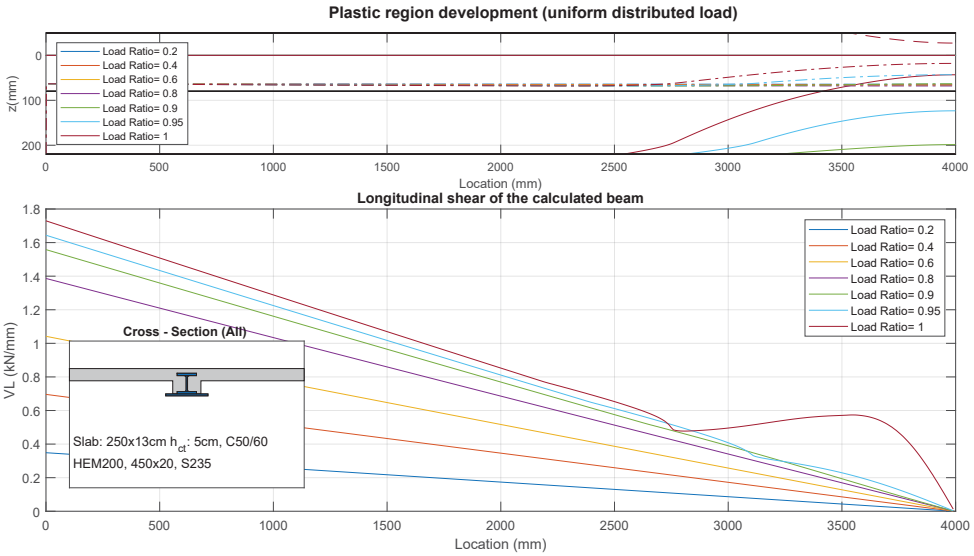

Figure 7.18 – Plastic zones development and longitudinal shear force distribution of beam SF3

Beam SF3: Beam SF3 has a smaller concrete thickness above the steel section and the neutral axis at ULS is inside the steel upper flange, thus the steel beam section did not reach full plastic. The nonlinear longitudinal shear increase is relatively smaller.

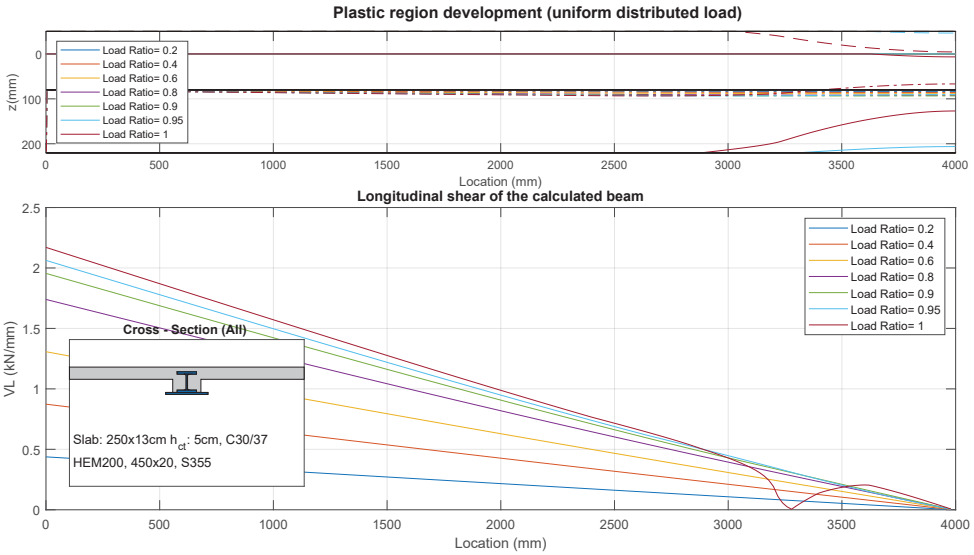

Figure 7.19 – Plastic zones development and longitudinal shear force distribution of beam SF4

Beam SF4: Beam SF4, similar as the conventional composite beam NC4, has a deep neutral axis located in the steel web. The longitudinal shear distribution is mostly linear at failure, with only a small part of steel section reach plastic.

7.1.2.3 Proposal of engineering simplification of longitudinal shear distribution when steel section in full plastic

The above analysis shows similar longitudinal shear force distribution shape if steel section is in full plastic: A non-linear increase happens in the plastic region. Further parametric

study results also confirmed this pattern. The longitudinal shear force distribution is important for design with non-ductile shear connectors as the shear connectors need to be arranged in regions according to the longitudinal shear force value. However, such calculation of the longitudinal shear force requires applying complex non-linear advanced design methods. In this section, a simplified method is proposed to allow engineering to calculate it easily by hand if steel section reaches full plastic at failure.

The $M-N_c$ curve of the composite beams

Because both the bending moment M and the concrete compression force N_c are related to the stress distribution inside a cross-section. With a given strain stage, the bending moment to the concrete compression force relationship ($M-N_c$) can be obtained from the cross-section analysis. It is a cross-section property and not influenced by loading unless the influences from multi-axis stresses, such as bending moment - shear interaction are important. Similar to the use of $M-\kappa$ curve to predict the beam ductility, without the detailed loading information, the beam longitudinal shear behaviour can still be verified from the $M-N_c$ diagram.

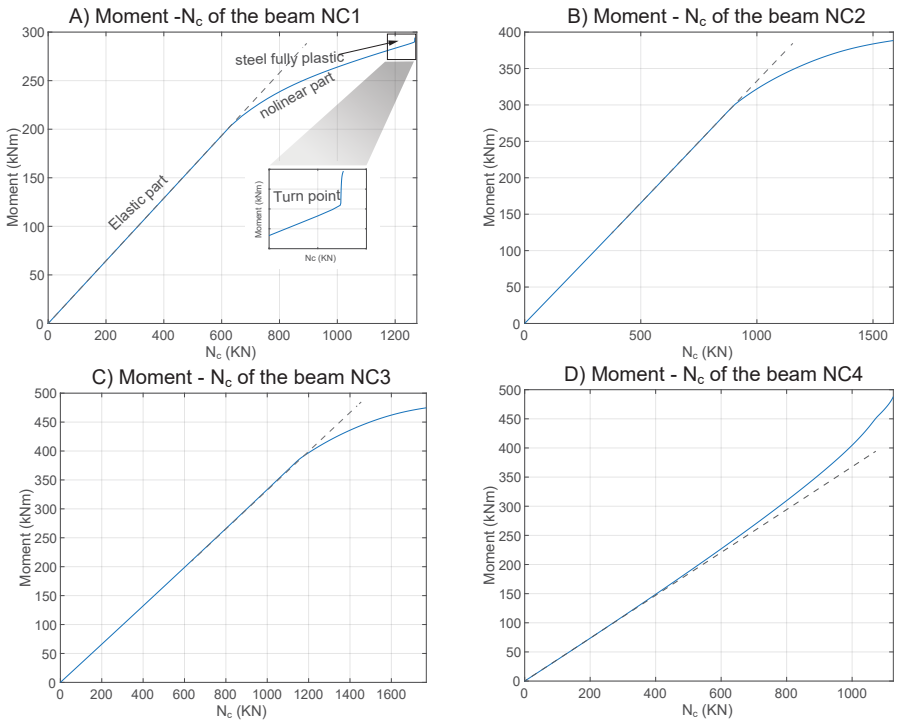

Figure 7.20 – $M-N_c$ relationship of the calculated composite beams

The related $M-N_c$ diagrams of the four calculated conventional beam cross-sections NC1 to NC4 are shown in Fig. 7.20. Generally, the curves compose of three parts: The first part (elastic part) is nearly linear, representing the elastic stage of concrete and steel beam. When steel beam yields, the non-linear part initiates. When steel reaches fully plastic, a sudden turning point is observed with no further increases of N_c (Fig. 7.20 A) if strain hardening is not considered. Steel section not always reaches full plastic at failure, for beam NC2 to NC4 (Fig. 7.20 B, C and D), this turning point is not seen. For the Beam NC4, due to only a small portion of steel section reaches plastic, the curve bends to the opposite side compared to the other three, which indicates smaller longitudinal shear force near mid-span of a simply supported beam under uniform distributed loading.

The $M - V_{L,M}$ curve of the composite beams

The longitudinal shear force V_L is the first derivative of the concrete compression force N_c on longitudinal direction x (Eq. 7.7). For cross-section analysis the beam length is unknown, however with full shear interaction, the relationship between the N_c and bending moment M can be obtained only through the cross-section analysis as explained before. Thus the longitudinal shear force V_L can be alternatively formulated as function to M instead of the length x. This function is noted as $V_{L,M}$ in the following analysis:

$$
\begin{aligned}
set: N_c(x) &= f(M(x)) \\
V_L(x) &= \frac{dN_c(x)}{dx} = \frac{df(M(x))}{dx} = \frac{df(M(x))}{dM(x)} \cdot \frac{dM(x)}{dx} \qquad (7.7) \\
V_L(x) &= \frac{df(M(x))}{dM(x)} \cdot V(x) \qquad (7.8) \\
set: \frac{df(M(x))}{dM(x)} &= V_{L,M}(M(x))
\end{aligned}
$$

$$
\boxed{V_L(x) = V_{L,M}(M(x)) \cdot V(x)} \qquad (7.9)
$$

Thus the longitudinal shear $V_L(x)$ at the composite joint is linked with the vertical shear force $V(x)$ from global analysis through the parameter $V_{L,M}$ given in Eq. 7.9. The function $V_{L,M}$ represents the change of longitudinal shear force with the change of each unit of bending moment. $V_{L,M}$ is not a constant value, it relates to many different parameters of the cross-section shape and materials, numerically it is possible to be obtained. The $V_{L,M}$ of the beam NC1 to NC4 are shown in Fig. 7.21. In these figures, the horizontal axis is the bending moment of the cross-section with full shear interaction, and the vertical axis gives the value of $V_{L,M}$.

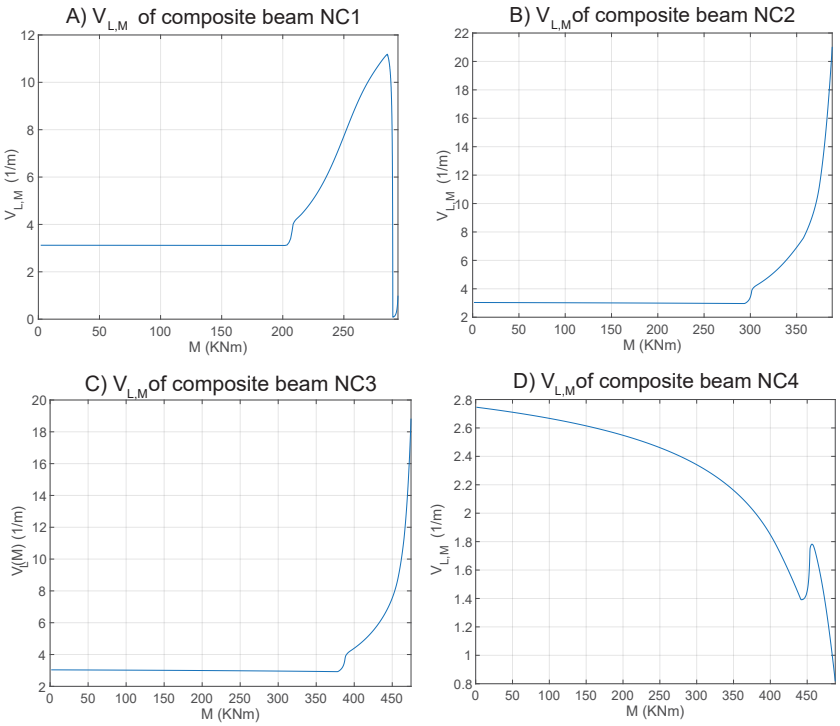

Figure 7.21 – The $V_{L,M} - M$ diagram of composite beam NC1 to NC4

From the Fig. 7.21 it is observed that different shapes of the $M - V_{L,M}$ are possible. Parametric studies show when the neutral axis is above the steel section, and steel can reach full plastic, the function always follows similar rectangle-triangle shape as shown in Fig. 7.21 A). When the neutral axis is deeper, the situation of Fig. 7.21 B) or C) happens. As for the last situations, the non-linear distribution of longitudinal shear is small, and most of the steel beam still in the elastic stage at failure.

Analytical exact solution of longitudinal shear force distribution is difficult to get due to the non-linear material behaviour and complex cross-section geometries. If the steel beam reaches full plastic at failure, a simplified $M - V_{L,M}$ curve can be obtained as shown in Fig. 7.22. The non-linear curves can be represented with the multi-linear simplifications consisting of four key points. Point A marks the end of the elastic stage, after which, the steel section starts plastic. At point B, the steel section reaches full plastic. If strain hardening is not considered, after point B longitudinal shear force will drop to zero. Thus the value will change to point C' until to reach point C of concrete strain failure.

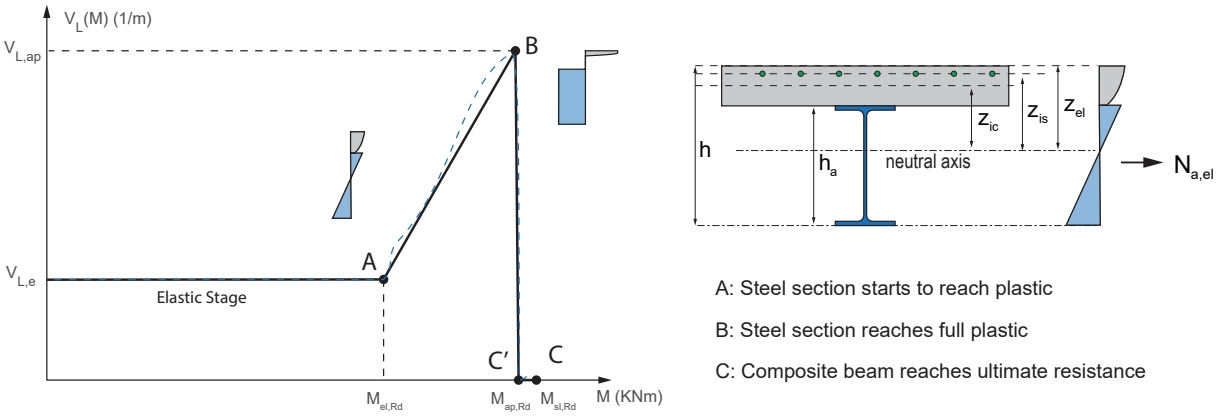

Figure 7.22 – The simplified $V_L - M$ diagram of composite beam when steel section reach full plastic at failure

The corresponding values of parameter $V_{L,M}$ can be obtained by using the equations shown below. It can be divided into elastic and inelastic part. The elastic part can be obtained by using the well-known elastic theory, while the inelastic part is shown in Eq. 7.16.

Elastic part:

$$S_{y,i} = A_i \cdot z_i \tag{7.10}$$

$$\boxed{V_{L,e} = \frac{\sum E_i S_{y,i}}{EI_{eff}}} \tag{7.11}$$

Inelastic part:

$$N_{a,pl} = A_a \cdot f_y \tag{7.12}$$

$$\sigma_{a,tf} = \frac{h_c - z_{el}}{h - z_{el}} \cdot f_y \tag{7.13}$$

$$N_{a,el} = A_f \cdot (f_y + \sigma_{a,tf}) + 0.5A_w \cdot (f_y + \sigma_{a,tf}) \tag{7.14}$$

$$\tag{7.15}$$

$$\boxed{V_{L,ap} = \frac{2(N_{a,pl} - N_{a,el})}{M_{a1,Rd} - M_{el,Rd}} - V_{L,e}} \tag{7.16}$$

Most of the related parameters in the simplified curve shown in Fig. 7.22 can be obtained by conventional elastic and plastic analysis according to Eurocode 4. The point A is defined by the elastic bending moment resistance $M_{el,Rd}$ and the longitudinal shear coefficient $V_{L,e}$ for elastic analysis as shown in Eq. 7.11. The point B and C is defined by the bending moment resistance when steel section at full plastic $M_{ap,Rd}$ and the value $V_{L,ap}$. And the point C' is related the strain-limited resistance $M_{sl,Rd}$. Exact solution of $M_{ap,Rd}$ and $M_{sl,Rd}$ requires non-linear strain-limited analysis. However a simplified method to calculated $M_{ap,Rd}$ in introduced in Appendix E, and a hand-calculation method to get $M_{sl,Rd}$ is provided in section 3.5.

If the steel section reaches full plastic at the ultimate stage. The bending moment increase in part C'C only results from stress redistribution in concrete part, which causes a change of lever arm, it can usually be neglected by using the ultimate resistance $M_{sl,Rd}$ to replace the bending moment resistance when steel just reaches full plastic $M_{ap,Rd}$. Furthermore, if the relative compression zone height (z_{pl}/h) is very small, the strain limited design resistance $M_{sl,Rd}$ is similar as plastic bending resistance $M_{pl,Rd}$. Thus the Eq.(7.16) can be simplified as below in Eq. (7.17). In order to use this simplification, certain limitations must be fulfilled. Further parametric studies on the limitation of this simplified method is still necessary.

$$V_{L,ap} = \frac{2(N_{a,pl} - N_{a,el})}{M_{pl,Rd} - M_{el,Rd}} - V_{L,e} \tag{7.17}$$

$$V_L(M) = \begin{cases} V_{L,e} & M \leq M_{el,Rd} \\ V_{L,e} + \frac{V_{L,ap} - V_{L,e}}{M_{pl,Rd} - M_{el,Rd}}(M - M_{el,Rd}) & M_{el,Rd} \leq M \leq M_{pl,Rd} \end{cases} \tag{7.18}$$

Fig. 7.23 shows the comparison of the longitudinal shear force distribution according to the numerical method and simplified method of beam NC1. Due to the part "C'C" in Fig. 7.22 is neglected, the zero longitudinal shear part is not shown in the theoretical curve. However, if we compare with the results with up to 98% of design ultimate resistance (100% is not reachable due to failure occurs before mid-span), the results still fits well.

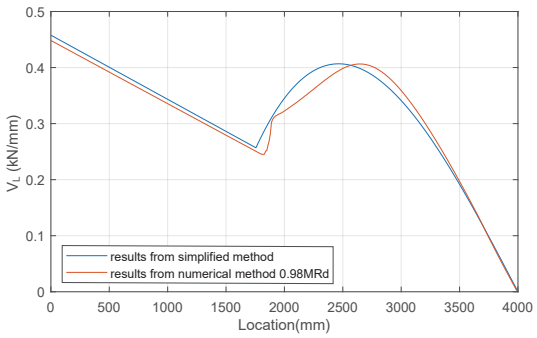

Figure 7.23 – Comparison of longitudinal shear calculated by the simplified method and the numerical method

For bending moment resistance with plastic design, the calculation can be much simplified considering plastic stress distribution in side the cross-section. However for

longitudinal shear distribution with full shear interaction, due to part of the beam are still in elastic stage when the critical cross-section fails. Thus the impacts from long term effects, sequences of loading should not be neglected.

7.2 Longitudinal shear force redistribution due to shear connectors

The full shear interaction is however not common for composite beams with mechanical shear connectors. Slip normally exists at the composite joint, because the mechanical shear connectors need certain deformation to reach the design resistance. Influenced by the shear connectors, the longitudinal shear force can be redistributed in the composite joint. For shear connectors installed with equal distance, if all the shear connectors are in elastic stage, their stiffness influences the longitudinal shear distribution. After the shear connectors reaches the resistance plateau, non-linear redistribution of longitudinal shear force changes the composite beam behavior as well.

7.2.1 Shear connector properties and impact on longitudinal shear

Partial shear interaction is realized when the steel and concrete parts are joint by a limited amount of shear connectors. The beam behaviour is greatly influenced by the shear connector number and their mechanical properties, which can be represented by the shear connector load-deflection curve. For common head-studs in the solid concrete slab, the shear connector load-deflection curve can be simplified to a bi-linear elastic-plastic curve (details in section. 3.1.3). For this model, the initial stiffness and ductility of the shear connector need to be defined. Together with the degree of shear interaction are the key parameters impacts the longitudinal shear force.

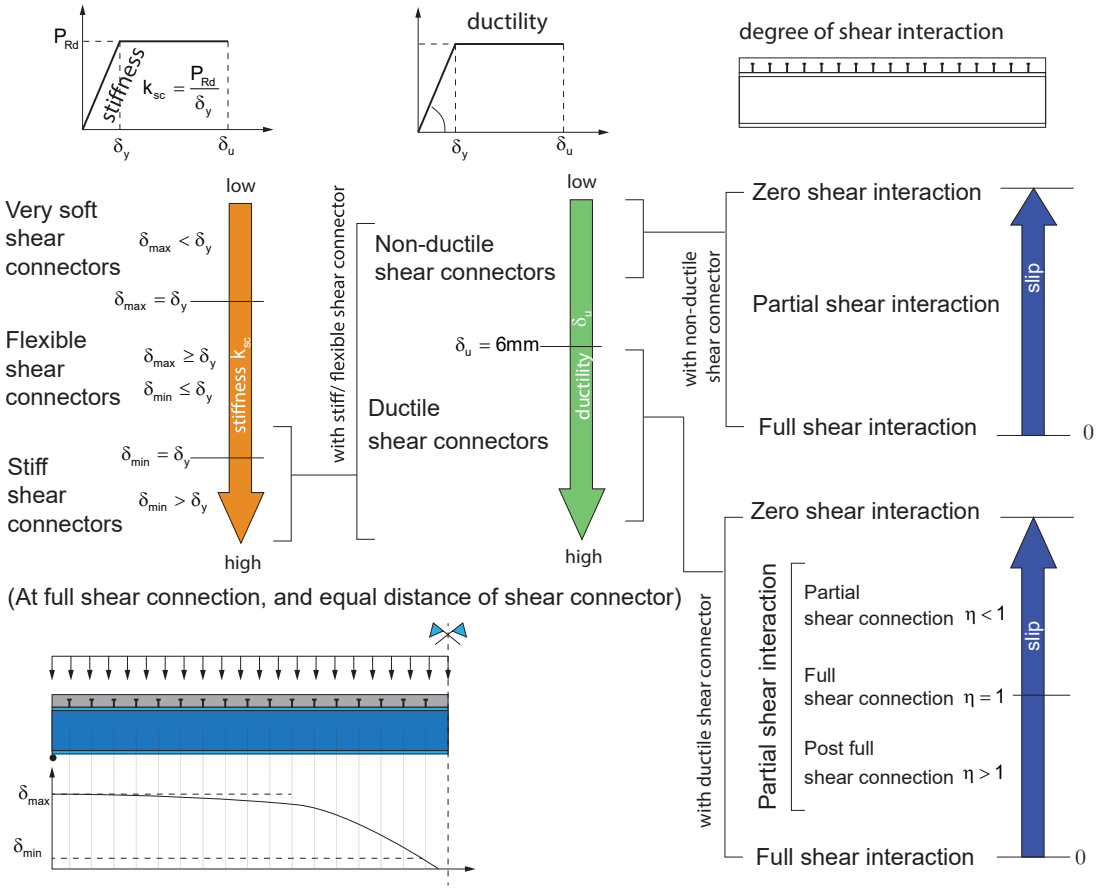

Figure 7.24 – Influence of shear connector stiffness, ductility and shear degree based on a bi-linear shear connector model and equal distance shear connectors distribution

If ductile shear connectors are used for plastic design, often they are installed with equal distance. Based on the shear connector types, amount and installation position, partial shear interaction can be categorized into different types, as shown in Fig. 7.24. The relative stiffness of shear connectors can vary from around 20KN/mm to 300kN/mm from different push-out test results [33]. General universal classification of shear connector stiffness is not available. In this work, it is categorized based on their required deformation to reach design resistance (δ_y) and the minimum and maximum failure slip in the beam with full shear connection (δ_{min}, δ_{max}). Here the minimum failure slip is the boundary slip value with most shear connector slips beyond it (more exact values can be replaced based on further analysis). With too soft shear connectors, the maximum slip δ_{max} in the beam at failure is still smaller than the δ_y, the shear connectors can not reach their design resistance. However, this situation is rare. If only part of shear connectors reaches design resistance ($\delta_{min} \leq \delta_y \leq \delta_{max}$), They are flexible shear connectors. If most of the shear connector can reach the design resistance ($\delta_{min} \geq \delta_y$), the shear connector can be regarded as stiff shear connectors. For this definition, the shear connection stiffness category is a relative value depending on beam cross-section, span length and loading conditions as well.

For plastic design, according to Eurocode 4, ductile shear connectors are required for equal distance arrangement. The shear connectors must have at least 6mm characteristic deformation capacity to be recognized as ductile shear connectors. This value is chosen based on the typical headed studs and consideration of a minimum degree of shear connection [45]. Although shear connector initial stiffness is not mentioned in the definition of ductility of shear connectors, it requires certain stiffness of shear connectors. As for very soft shear connectors, most of them are still in elastic stage at failure, thus it is no use to talk about ductility. In [38], a new definition of ductility consider the plateau length is proposed. It was suggested the ductile shear connector should have at least $5mm$ additional deformation capacity after elastic range. With ductile shear connectors, most of the shear connector can reach design resistance P_{Rd} due to a large plastic range to allow the plastic longitudinal shear force redistribution. Considering longitudinal shear force redistribution, the shear connector arrangement can be more flexible, for which equal distance of shear connectors can be realized. With non-ductile shear connectors, plastic longitudinal shear force redistribution is not allowed. In this case, the shear connectors should be installed according to the longitudinal shear force distribution.

Eurocode 4 distinguishes partial and full shear connection for ductile shear connector based on plastic bending resistance. The partial shear connection is realized when the shear connector number is below the required number $n < N_{c,f}/P_{Rd}$. When the shear connector number reaches $n = N_{c,f}/P_{Rd}$, full shear connection is realized. After full shear connection, further increase of shear connector numbers will not increase the maximum bending moment resistance. However, the longitudinal shear force distribution and the slip further changes. This post-full shear connection stage with $n > N_{c,f}/P_{Rd}$ will only theoretically end with full shear interaction where slip equal to zero at the entire joint.

7.2.2 Longitudinal shear force distribution influenced by shear connector stiffness with elastic shear connector model

The impact of longitudinal shear force distribution influenced by shear connector stiffness have been analyzed in the publication of Bode and Schanzenbach [8]. They used a strain-limited numerical software to calculate the longitudinal shear force distribution, a

more smooth distribution is observed with flexible shear connector, where at the beam end the shear connector force is smaller. However, only one calculation example with flexible shear connector is shown.

In this work, a more detailed parametric study is carried out to show the longitudinal shear force redistribution with flexible shear connectors. Linear elastic spring models with stiffness vary from 1kN/mm to 400kN/mm are used for the FEM calculations. The FEM model details are provided in Fig.7.25. For the FEM model, parabolic rectangle concrete material model and bilinear steel model without strain hardening are used. The calculations are performed with help of the Abaqus-CivilLab add-in, which is explained in Chapter 4.

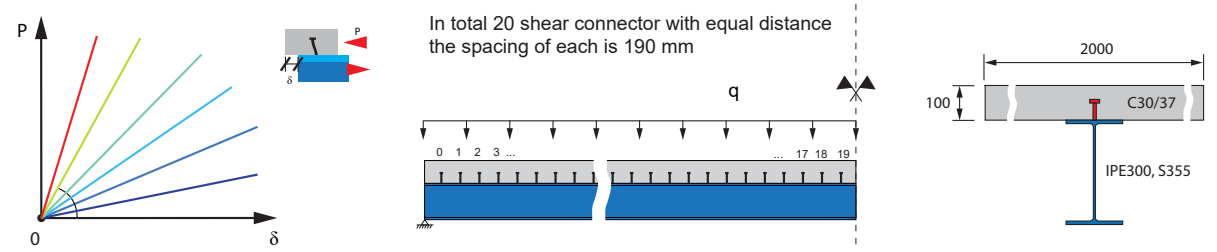

Figure 7.25 – Parametric study settings for different shear connector stiffness

The load-deflection relationship of all beams are compared in Fig.7.26 A). The stiffness of shear connectors impacts both the stiffness and the ultimate resistance of the calculated beams. With very soft shear connectors (stiffness<50kN/mm in this example) full shear connection can not be reached and the maximum bending resistance is lower than the design value. Because shear connector does not have enough slip to provide the required longitudinal shear force to reach full shear connection, regardless there is no limit for the shear connector strength, more longitudinal shear force can not be provided. When the shear connector stiffness is higher, the influence is less important. The load to end-slip relationship is shown in Fig.7.26 B) with high stiffness, a generally linear relationship between load and end-slip is observed. With low stiffness of shear connector, end-slip develops faster when beam fibre starts to yield. The end-slip to deflection curves in Fig.7.26 C) shows almost linear relationship when very soft shear connectors are used.

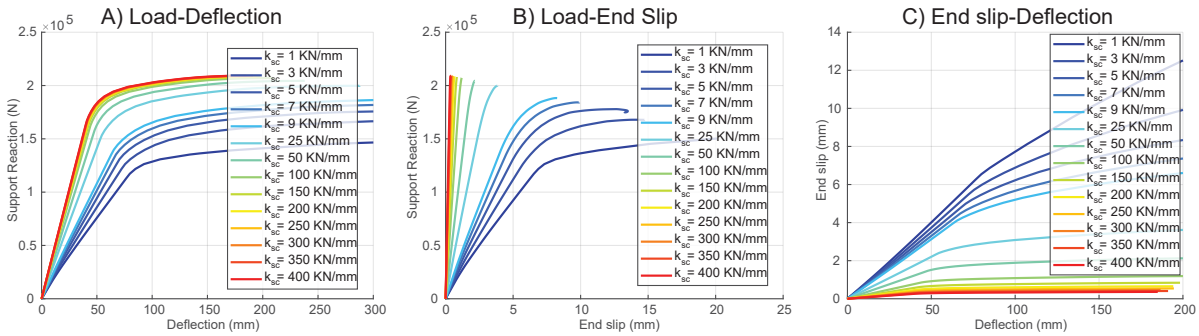

Figure 7.26 – The load-deflection-end slip relationship of the calculated beams with different shear connector initial stiffness

The shear connector relative load ratio of all beams are compared in Fig.7.27 A) at beam deflection equal to 40mm, when the beams are in elastic stage. The relative load

ratios are calculated as the ratio between each shear connector force to the maximum one of the same beam. With very low initial stiffness (blue coloured in the figure), the shear connector forces are more non linearly distributed. The slip development in the cross-section is similar to situation with zero shear interaction. On the other hand, when the shear connector stiffness is very high, the longitudinal shear force turns to be linear. The slip distribution in Fig.7.27 B) shows an increase of slip with softener shear connectors.

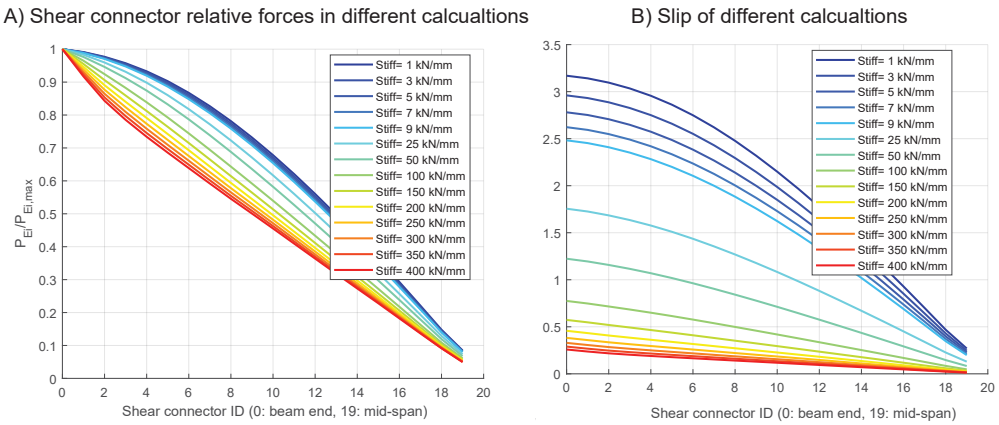

Figure 7.27 – The shear connector forces and slip of the calculated beams when deflection is 40mm in elastic stage

The shear connector forces of all beams are compared in Fig.7.28 A) at beam deflection equal to 180mm, which is close to the failure stage shown in Fig.7.26 A). With very low initial stiffness (blue coloured in the figure), the shear connector forces are more smooth distributed. On the other hand, when the shear connector stiffness is very high, the longitudinal shear force distribution is similar to the theoretical distribution of full shear interaction, for which a nonlinear increase of shear connector force at mid-span is seen.

With the increase of shear connector stiffness, slip decreases. When the deflection at mid-span equal to 180mm, the slip distribution of all beams are compared in 7.28 B). The slip of shear connector stiffness equal to 1kN/mm (near zero shear connection) can reach around 12mm, while if the stiffness of shear connector equal to 50kN/mm, the value reduced to around 2mm. When the stiffness is more than 100kN/mm, the slip is so small that further increase of shear connector stiffness does not really reduce much the slip.

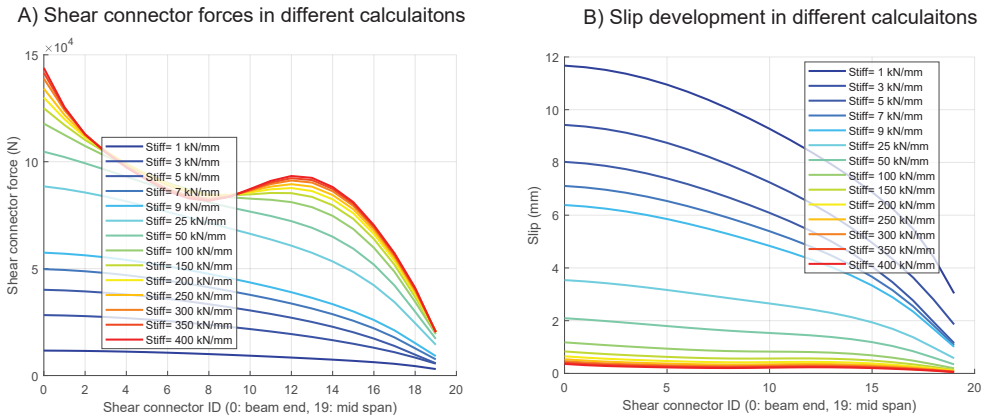

Figure 7.28 – The shear connector forces and slip of the calculated beams when deflection is 180mm

Overall, it can be concluded that the distribution of longitudinal shear force with flexible shear connectors smooths the curve, which reduces the shear connector forces at beam end for a simply supported composite beam. However, with too low stiffness, the shear connectors may provide less longitudinal shear force than required for full shear connection.

7.2.3 Non-linear longitudinal shear force distribution with ductile shear connectors

With elastic-ideal horizontal plateau load-deformation relationship for ductile shear connectors (see Fig. 7.24 and Fig. 7.29), the distribution of the longitudinal shear force can be generally divided into three different stages: **elastic distribution of longitudinal shear forces** happens the first when all shear connectors are in elastic stage. Depending on the shear connector initial stiffness, the longitudinal shear force can be linear or curved as explained in the section before. When the load on a shear connector reaches its design resistance, it can no longer carry extra load, due to the ideal horizontal plateau of the shear connector load-deformation curve. Shear connector can be replaced by an equivalent force pair. With increased loading, overall slip within the composite joint increases, which redistributes the longitudinal shear force to other shear connectors and cause more shear connectors to reach the resistance plateau. This stage is the **partial non-linear redistribution of longitudinal shear force**. After all the shear connectors reach the design resistance and still within the deformation capacity, the beam reaches **full non-linear redistribution of longitudinal shear force**. Their stiffness will no longer impact the beam behaviour and can be all ideally simplified as force pairs. Thus the longitudinal shear force distribution is only determined by the arrangement and resistance of shear connectors and not influenced by the cross-section properties. If shear connectors are installed with equal distance, a constant longitudinal shear force flow can be assumed as shown in Fig. 7.29. In the stage, longitudinal shear force keeps constant, the beam can still carry more loads with slip quickly increases.

The full non-linear redistribution of longitudinal shear force allows calculating the required shear connector numbers simply based on the concrete compression force differences in critical sections (N_c) and design resistance per shear connector (P_{Rd}) as $n = N_c/P_{Pd}$, which is used by many design codes including Eurocode 4.

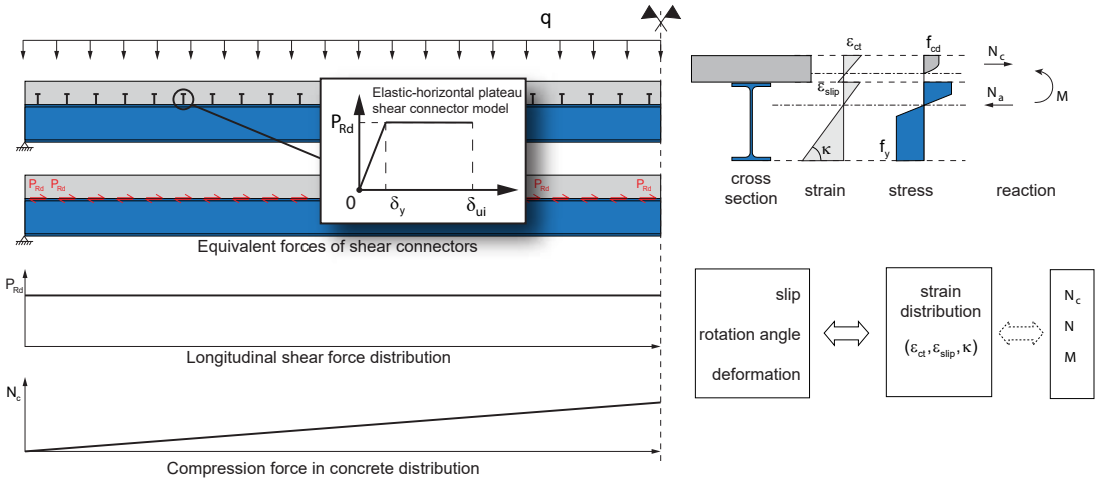

Figure 7.29 – The full non-linear longitudinal shear force redistribution in composite beam with equal distance arrangement of shear connectors

As discussed in section 3, to confirm the strain distribution of a cross-section in partial shear interaction, at least three values (N_{ci}, N_i and M_i) should be provided. Under the circumstance of full non-linear redistribution of longitudinal shear force, $N_{ci} = \sum P_{Rd}$. As for pure bending, the $N_i = 0$. Furthermore, for a structural determined system, the bending moment M_i is only related to the loads. Thus, the strain distribution, as well as the slip and deformation, can be directly calculated without an iterative procedure.

However, the full non-linear longitudinal shear force redistribution and based on which the equal distance arrangement of shear connectors also have their limitations regarding minimum degree of shear connection and bending moment resistance envelope of whole beam, which will be further discussed in following sections.

7.2.3.1 Slip development stages with non-linear longitudinal shear force distribution

When all shear connectors are in the elastic stage, slip is only able to increase slowly. When partial non-linear redistribution happens, part of the shear connectors lose their stiffness, thus slip increases faster with the same amount of additional load. Under the situation of full non-linear redistribution, all shear connector lose their stiffness, the system turns into a similar mechanism with zero shear interaction but with additional surface longitudinal loads applied on the joint. Thus slip quickly increases. Fig. 7.30 shows load-deflection and load-end slip relationship of a simply supported composite beam under uniformly distributed load with the degrees of shear connection η equal to 0.2 and 0.8. The low degree of shear connection $\eta = 0.2$ allows the profile stays in the elastic stage when full non-linear redistribution of longitudinal shear force reaches. Thus in stage 1 to stage 3 in the figure, the changes of beam stiffness are mainly resulted by the shear connectors. Only in stage 4, plastic development inside the cross-section especially the steel section further increases the slip and deflection. With a higher degree of shear connection, as shown in the cases of $\eta = 0.8$ in Fig. 7.30, plastic development of the cross-section is mixed with the non-linear redistribution of longitudinal shear force. Thus a clear boundary of the four stages is not easy to determine.

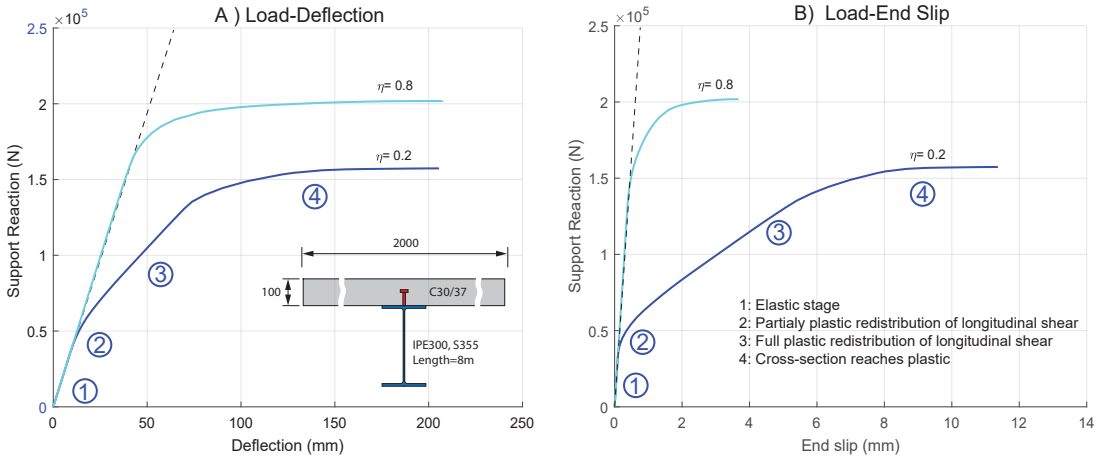

Figure 7.30 – The develop of slip with non-linear redistribution of longitudinal shear force in four different stages

As shown in Fig. 7.30, slip increases much faster at non-linear redistribution stage compared to the elastic stage. Near failure, a small increase in load can significantly increase

the slip amount. The extensive deformation capacity required by ductile shear connectors to accommodate the slip development at the composite joint is therefore mostly to allow the composite beam to have a ductile behaviour rather than to reach cross-section resistance requirement. For example for $\eta = 0.8$, around 95% of bending resistance is reached when end slip reaches 2mm, and the rest 2mm end slip increases only bring less than 5% increase of load but 100% increase of deflection. Thus the slip distribution and end-slip should also be compared with a beam deformation related parameter such as strain values at a certain location or deflection at mid-span, which represents better the beam ductility. Two limitations related to beam ductility are suggested:

- The limitation can be when maximum strain in steel section reaches 10 times of the yielding strain ($\varepsilon_{a,max} = 10\varepsilon_y$). This limit is also used in [4] as a criteria for plastic design.
- The limitation can be related to the deflection limitation. Here a limit of L/80 is suggested as the approximate beam ductility allowance, more exact values need however further investigation.

The slip distributions at the two suggested limitations are shown in Fig.7.31 A) and B) with the slip distribution at load ratio equal to 0.98 plotted in Fig.7.31 C). In the figure, different degree of shear connections have been considered. Due to the ideal horizontal plateau assumption of the shear connector Load-deformation curve, after load ratio reaches 0.98, the Load-slip curve of the composite beam shows nearly horizontal line as shown in Fig.7.30 B) and Fig.7.32 A), the numerical calculation is difficult to give precise slip values.

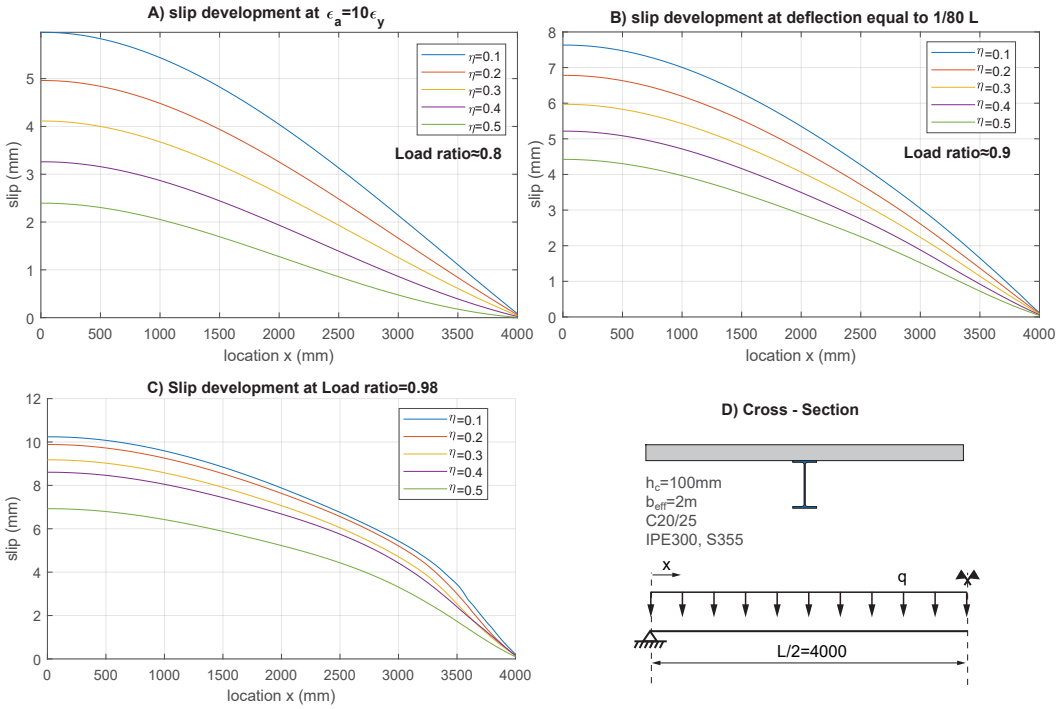

Figure 7.31 – The slip development inside composite joint

Another example from FEM calculation results are shown in Fig. 7.32. The beam is simply supported under uniform distributed load. It has a degree of shear connection equal to 0.5, and the shear connectors are distributed with equal distance. Results of the half

span are plotted as shear connector Nr. 0 is located at beam end, and shear connector Nr. 19 is and mid-span. From the Fig. 7.32 A), a rapid increase of slip after load ratio equal to 0.8 is noticed.

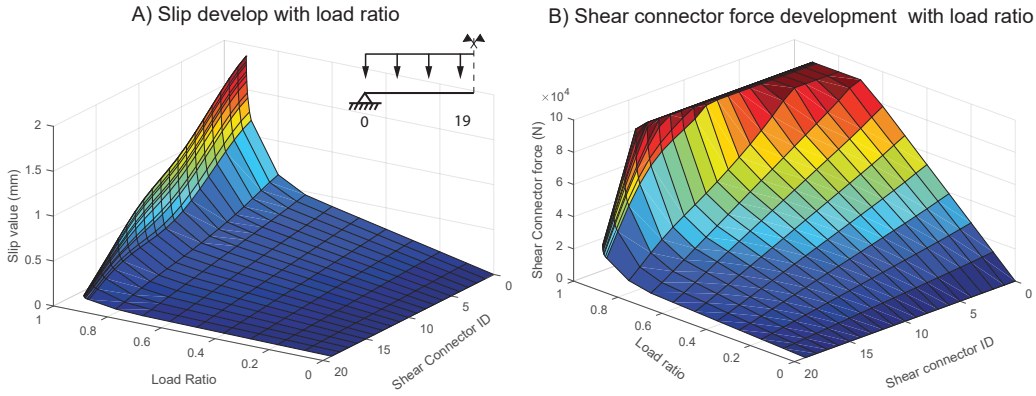

Figure 7.32 – 3D illustration of slip and longitudinal shear development of a composite beam, (Shear connector ID=0 is located at beam end, while ID=19 is mid-span

7.2.3.2 Full non-linear longitudinal shear force redistribution with partial shear connection ($\eta < 1$)

$M-\kappa-N_c$ solution surface introduced in section 3.3.2 is a great tool to explain the impact of degree of shear connection on plastic longitudinal shear force distribution. In Fig. 7.33 a 2D-top view (from axis-κ) of a solution surface is given. The gray area shows the possible solutions range of $M-N_c$ combination of the cross-section with different strain distribution for pure bending, with lower boundary line limited to full shear interaction line. The upper boundary is the partial shear diagram obtained by strain-limited method.

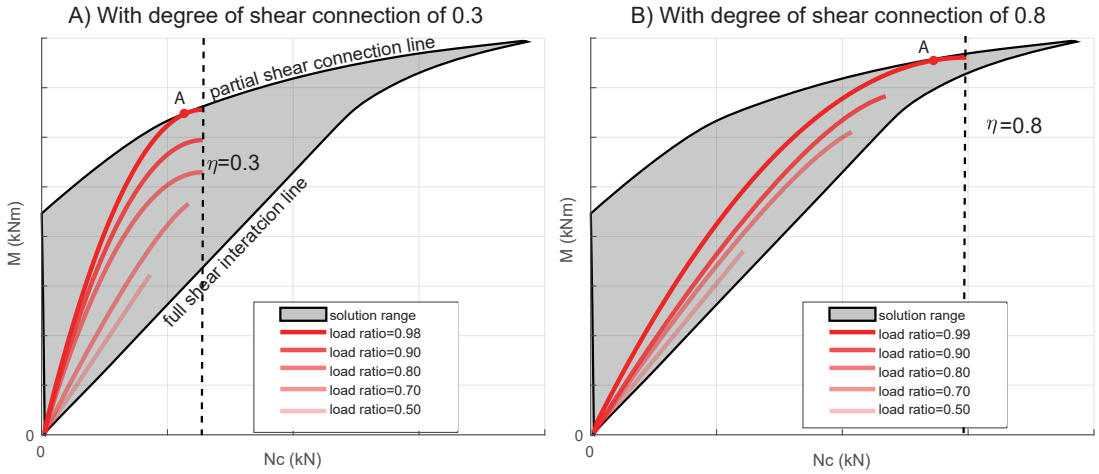

Figure 7.33 – The $M-N_c$ of $\eta = 0.3$ and $\eta = 0.8$ on the $M-N_c$ solution surface of calculated composite beam (principle drawing)

The red curves insides Fig. 7.33 represent $M-N_c$ diagram of a simply support composite beam under uniform distributed loads with different loads steps. It can be obtained as follow: When a certain amount of load is applied, we can calculate the bending moment distribution M and longitudinal shear force distribution V_L, The integral of V_L from

zero point at beam end to mid-span is the N_c values. Then the $M-N_c$ diagram can be obtained and plotted in the solution surface. However, in the figure, it is more a principle drawing considering uniform changes of V_L, in real beams considering explicit positions of shear connectors, the $M-N_c$ diagram is a more like a "stair-shape" as shown in Fig. 3.16 for the solution path.

In the elastic stage, the $M-N_c$ curve shows more linear distribution. With partial non-linear redistribution of longitudinal shear force, the curve starts to bend, and when full non-linear redistribution is reached at $\eta = 0.3$ for Fig. 7.33 A) and $\eta = 0.8$ for Fig. 7.33 B), the $M-N_c$ curves turn into parabolic shapes. That is because, with the full non-linear redistribution of longitudinal shear, the N_c is linearly increase with the distance to the beam end (x) as shown in Fig. 7.29. As the bending moment have a parabolic relationship with x, it also shows the same parabolic relationship with N_c but with a different scale. Further increase of load will not be able to increase the longitudinal shear force; the $M-N_c$ diagram can only vertically change until to reach failure at point A. Compared with $\eta = 0.3$, with a higher degree of shear connection, the full non-linear redistribution part is much reduced. With full shear connection, $\eta = 1.0$ full non-linear redistribution is theoretically only reached at the same time of cross-section failure.

7.2.3.3 Partial non-linear redistribution of longitudinal shear force with full shear connection and beyond ($\eta \geq 1$)

When more shear connector than needed are installed ($\eta > 1$), according to plastic design, the bending moment resistance will not be further increased; however, the slip will be reduced. Part of the shear connectors will not reach their design resistance, resulting non-linear redistribution of the longitudinal shear at failure. As the influence of cross-section plastic development, a non-linear longitudinal shear force distribution is seen in the plastic region. With the increased shear degree, the longitudinal shear force distribution is more similar to that resulting from the full shear interaction situation.

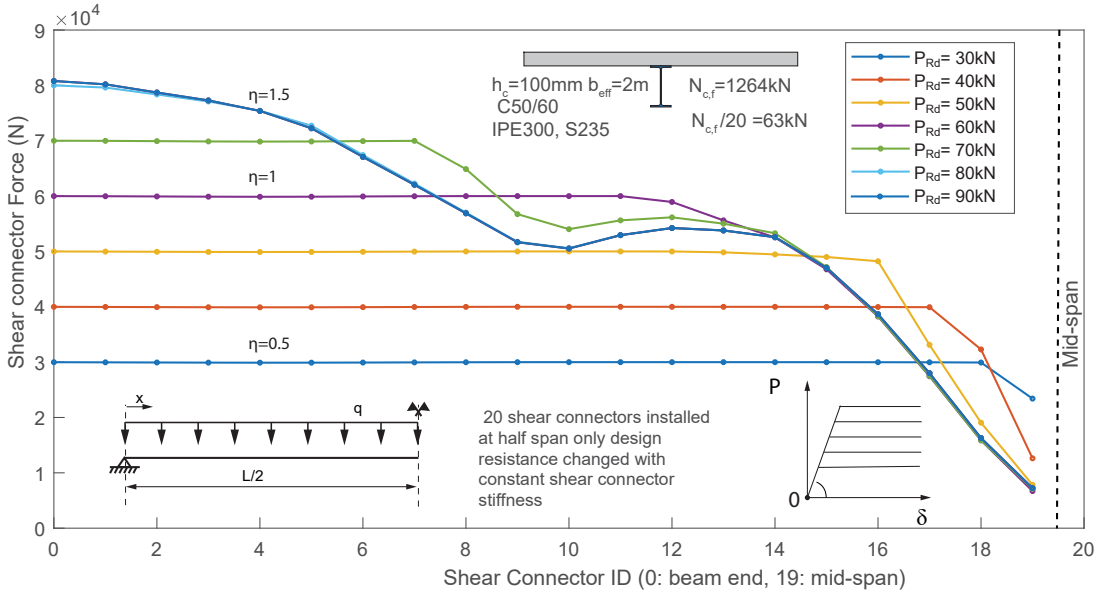

Figure 7.34 – The distribution of longitudinal shear force with increased shear connector resistances

Fig. 7.34 gives one such example calculated with Abaqus FEM model, with the help of

CivilLab add-in (details see chapter 4). The beam cross-section information is given in the figure, in total 20 ductile shear connectors are installed with equal distance inside a half-span. The shear connectors are simulated by the bilinear load-deformation model with a horizontal plateau and without the deformation capacity limits. The concrete is simulated with parabolic-rectangle strain stress relationship and structural steel is simulated with the bilinear model without strain hardening. Design values of materials according to Eurocode are used. For different calculations, the shear connector resistance P_{Rd} is changed with the initial stiffness keeps constant. The compression force at full shear connection is 1264kN, which requires P_{Rd} of 63.15kN to reach the full shear connection (approximately the line "$P_{Pd} = 60kN$" in the drawing).

Due to the small slip values near the mid-span, even with degree of shear connection equal or more than one, the shear connectors near mid-span can not reach their design resistance. After degree of shear connection over around 1.3, the longitudinal shear force distribution will stay identical as the maximum resulting shear connector force is around 80kN which is below the shear connector design resistance. However in this simulation, only the design resistance of shear connector is increased, if the degree of shear connection is increased by adding shear connector numbers and keeps the design shear connector resistance per connector, the total shear stiffness inside the composite joint will increase as well, thus different behaviour is expected.

7.2.3.4 Bending moment resistance envelope based on degree of shear connection

If the ideal ductile shear connectors are installed with equal distance, full non-linear redistribution of longitudinal shear force results in constant value of V_L and a linear increase of N_c along the beam length from the beam end to the adjacent critical section, which is the mid-span ($x = L/2$ in Fig. 7.35) for simply supported beam with uniformly distributed loads. In this case, the partial shear diagram is also the bending resistance envelope limited by the degree of shear connection. As the degree of shear connection is proportional to the distance from end support until the mid-span, we can also plot the bending moment diagram resulted from loading. All the bending diagram should located under the resistance envelope, if the resistance of steel section part is too small, as shown in point A of Fig. 7.35 B), for full shear connection, a premature failure happens before the mid-span reaches its resistance. To avoid it, Eurocode 4 requires the steel section bending moment resistance $M_{pl,a}$ should be at least 40% of the composite beam resistance $M_{pl,Rd}$ to arrange shear connectors with equal distance for the case of full shear connection.

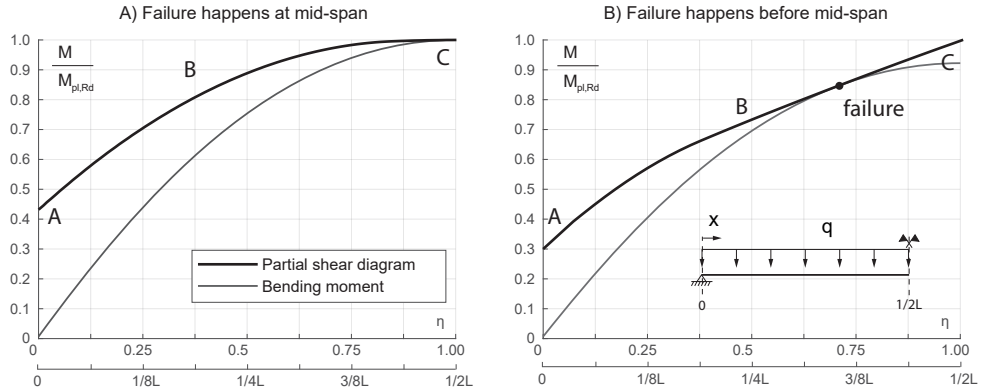

Figure 7.35 – Partial shear diagram as moment resistance envelope with equal distance arrangement of shear connectors and bending moment diagram with uniform distributed load

Because the first part of the partial shear diagram is usually more linear compared to the entire curve, for the composite beam with a low degree of shear connection and uniformly distributed load, the failure may happen ahead of mid-span as shown in Fig. 7.36. In the diagram, although for full shear connection, the failure happens at mid-span, however for a shear degree equal to 0.5, the failure happens before mid-span. This is also shown in Fig.7.36 as failure point is not the maximum bending moment point. FEM calculation also confirms this effect. Thus the maximum bending resistance obtained by the non-linear partial shear diagram ABC can not be reached. However, with the simplified linear curve, it is usually no problem as the line AC is much below the non-linear curve ABC.

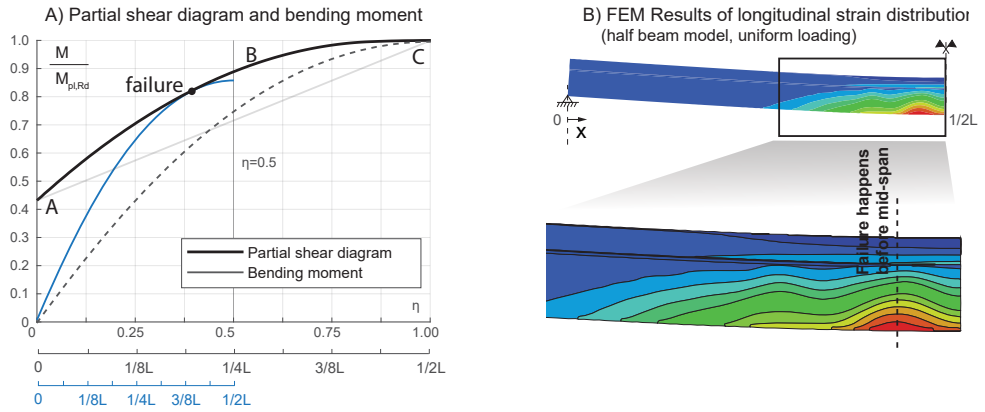

Figure 7.36 – Partial shear diagram and bending moment diagram

7.2.3.5 Influence of shear connector softening / hardening behaviour

The above-mentioned non-linear longitudinal shear redistribution is based on the elastic-ideal horizontal plateau shear connector load-deformation relationship assumption. This assumption is based on the typical behaviour of headed stud in solid concrete slabs, for headed studs with profiled steel sheeting or other types of shear connectors, the behaviour can be different. The post-elastic part can show a softening or hardening behaviour besides the plastic plateau assumption. Leskelä [60] mentioned with extensive softening behavior, a zip-failure of shear connectors is expected. However, with a hardening behaviour, the shear connector forces near beam end can be bigger than

their design resistance, which may cause the concrete shear off failure if the additional amount of longitudinal shear force is not considered.

7.3 Deep neutral axis position with longitudinal shear force non-linear redistribution and ductile shear connectors

While longitudinal shear force distribution influenced by cross-section plastic development depends mostly on the material properties and cross-section geometry, the longitudinal shear force non-linear redistribution is influenced mostly by the shear connector properties. The two factors also influence each other. The sum of longitudinal shear resistances between critical sections N_v influence the strain distribution in the cross-section as it controls the total normal force in concrete and steel part ($N_v = N_c = -N_a$). The plastic development in cross-section, on the other hand, influences the longitudinal shear force distribution and loads in each shear connector.

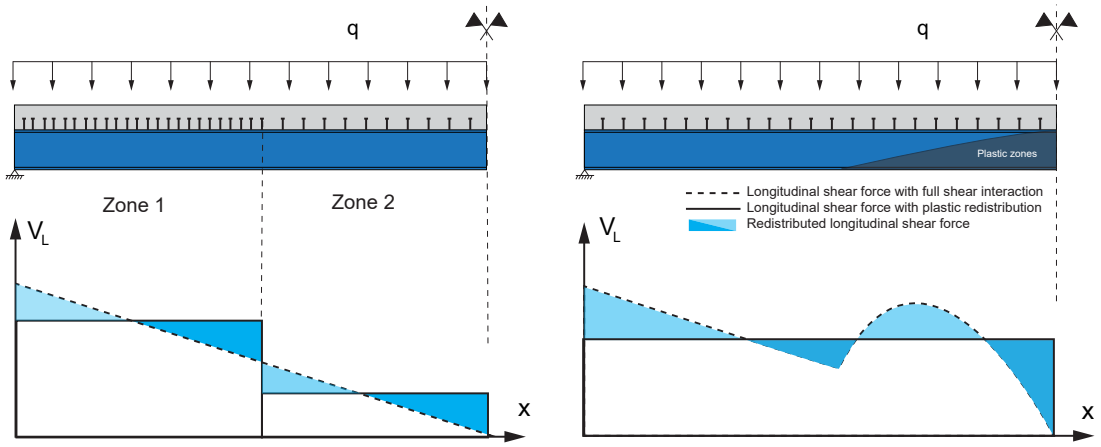

A) Elastic longitudinal shear design with two sub zone

B) Plastic longitudinal shear design with equal distance of shear connectors

Figure 7.37 – The redistribution of longitudinal shear force for elastic design method with sub-zones and equal distance arrangement with plastic method. The beams are assumed to be designed with theoretically full shear connection.

Eurocode 4 [22] allows equal distance arrangement of shear connectors between critical section if plastic cross-section design is followed and ductile shear connectors are used. For a simply supported composite beam with uniform distributed load and full shear interaction, yielding of the cross-section increases longitudinal shear force near mid-span area, as shown in Fig. 7.37. Thus with ductile shear connectors, less amount of longitudinal shear force is needed to be redistributed to keep the total surface area covered by two longitudinal shear diagram the same. For elastic design, equal distance arrangement of shear connectors between critical sections is usually not allowed. Instead, it should be subdivided into a few sub-zones and installed based on the longitudinal shear force values, a 10% carve up into the shear force boundary curve is usually allowed [33].

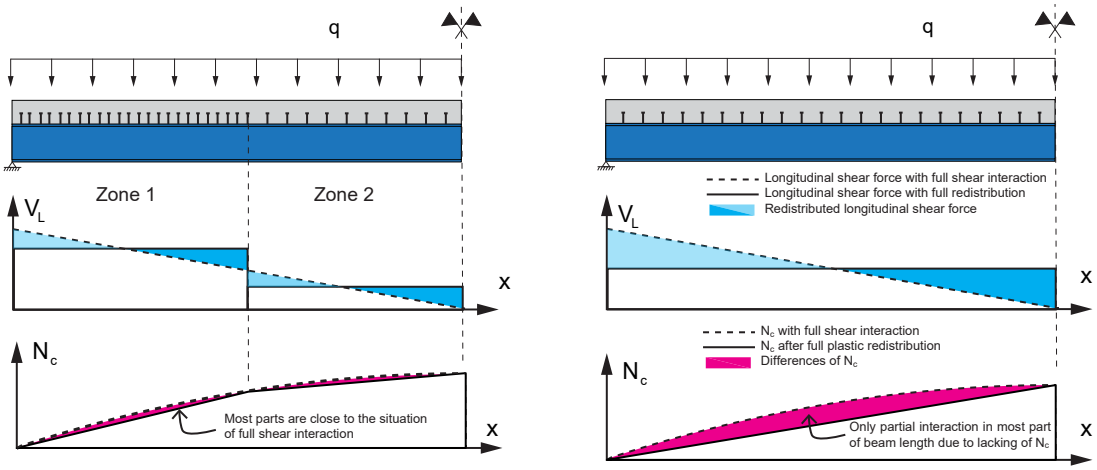

Figure 7.38 – The redistribution of longitudinal shear force at failure for elastic stage with two sub zones and without sub-zones.

As discussed before in section 6 cross-section class 1 or 2 does not automatically guarantee that the cross-section reaches its full plastic resistance at failure. With deep relative compression zone height and high steel yielding strength, an important part of cross-section still stays in the elastic stage. As shown in Fig. 7.13, with (very) deep neutral axis, the longitudinal shear force with full shear interaction is more similar to the linear elastic distribution. It brings the question if the equal distance arrangement of shear connectors between critical sections can still be applied or the subdivision into sub-zones should be used.

As in Fig. 7.38,compared with a linear distribution of longitudinal shear force in full shear interaction situation, a two-zones arrangement allows more similar longitudinal shear force distribution and N_c to the full shear interaction situation. With only one zone, only the critical cross-section have enough N_c force provided by shear connectors to reaches full shear interaction, an important section of the beam is still far below full shear interaction. This will brings a few risks in the design:

- First, as only the critical cross-section reaches its design resistance of full shear interaction, meanwhile the other cross-sections only have reduced design resistance due to only partial shear interaction is realized, thus, may not provide enough resistance in other cross-sections.
- Second, as most parts are with partial shear interaction, bigger slip values are expected. Thus the shear connectors may not have enough deformation capacity.

Analysis of these risks is provided below in different subsection through a few examples.

7.3.1 Bending resistance envelope with full non-linear redistribution of longitudinal shear

The similar bending moment resistance envelope used in section 7.2.3.4 can be used to check the resistance of whole beam length. For the composite beam cross-section with deep laying neutral axis, the increase of bending moment resistance due to composite

effects is usually less compared to a beam with smaller compression zone height. Thus a bigger ratio of $M_{pl,a,Rd}/M_{pl,Rd}$ is expected, and usually, the failure occurred in the critical section. In Fig. 7.39 a comparison of the partial shear diagram of beam NC1 to NC4 in section 7.1.2.1 is given. Although Beam NC4 has very deep laying neutral axis, the failure still occurs at mid-span.

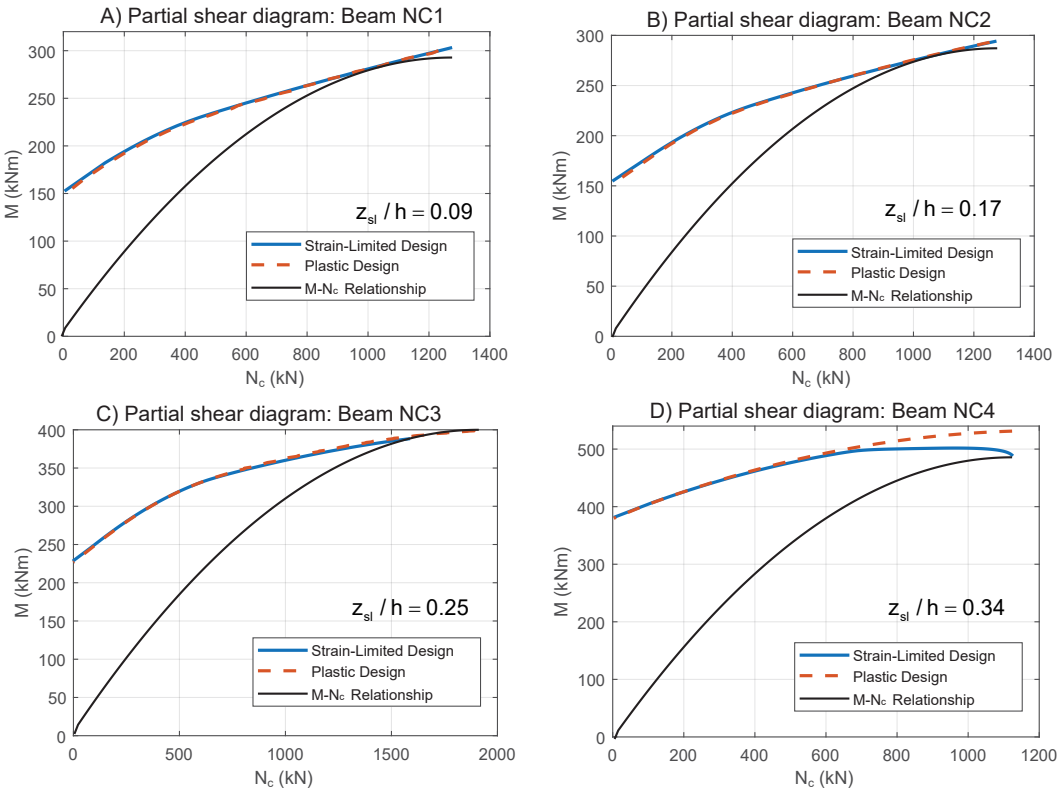

Figure 7.39 – Bending resistance envelope with full non-linear redistribution of longitudinal shear for beam NC1 to NC4

7.3.2 Slip development influenced by the cross-section plastic with full shear connection

The slip distribution for beam beams NC1 to NC4 with full shear connection is compared in Fig. 7.40. The beam cross-sections are the same as the ones in section 7.1.2.1 with details provided in Fig. 7.8. Of the four beam cross-sections from NC1 to NC4, the neutral axis position at failure increases. By cross-section analysis, the beam NC1 shows full plastic of steel section at failure while NC4 shows most steel sections are still in the elastic stage at failure. All the beams are designed for 8m length and simply supported. The shear connectors are simulated as an elastic-ideal plastic spring model with initial stiffness equal to 200kN/mm. Twenty shear connectors are equal distance installed within the half span length. The shear connector design resistance are artificially set to fulfil the requirement of full shear connection. The deformation and shear connector force P_i are monitored. The value $N_c = \sum P_i$ indicates the compression forces in the concrete slab transferred by shear connectors. It is calculated as the accumulated shear connector forces from beam end to mid-span. The Load-deflection curve from FEM calculation shows the beams all plastic range after deflection reaches 100mm. Thus in Fig. 7.40, slip distribution and N_c values are compared at beam deflection equal to 120mm, which is

near to the failure stage.

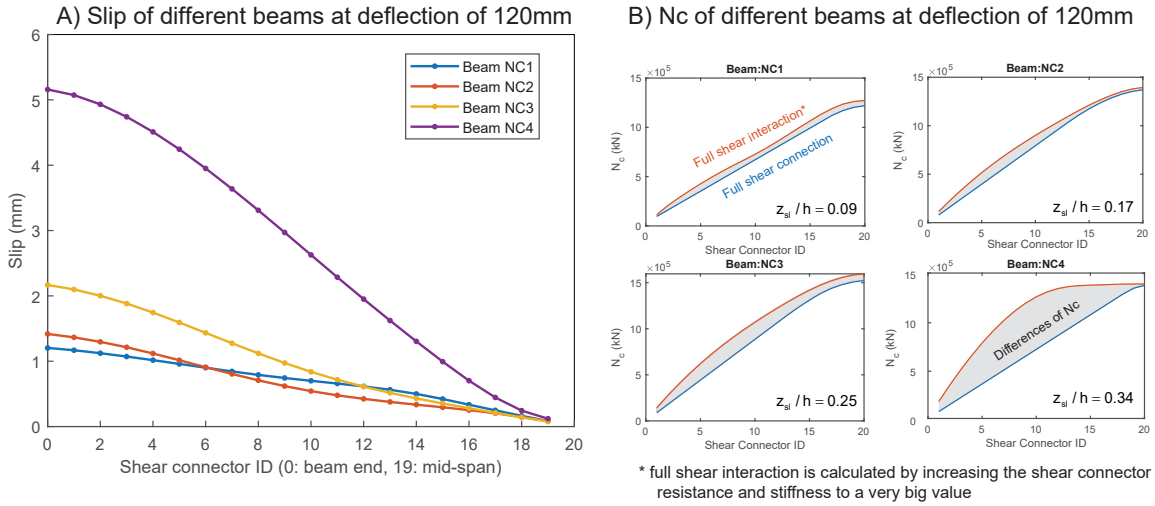

Figure 7.40 – Slip development of beam NC1 to NC4, (beams are simply supported with span length of 8m under uniform distributed load)

The results show significate higher slip value for beam NC4. It is due to other three beams have bigger parts of the beam reach plastic at failure, which create nearly linear N_c force distributions in the critical span at full shear interaction. The comparison of N_c values required to reach full shear interaction and the real N_c values after non-linear redistribution in the calculation shows big differences in beam NC4. For beam NC4, even with shear connector amount fulfils full shear connection at mid-span, big amount of end-slip is still expected, due to other cross-sections do not reach required N_c for full shear interaction. Shear connectors may fail due to big slip.

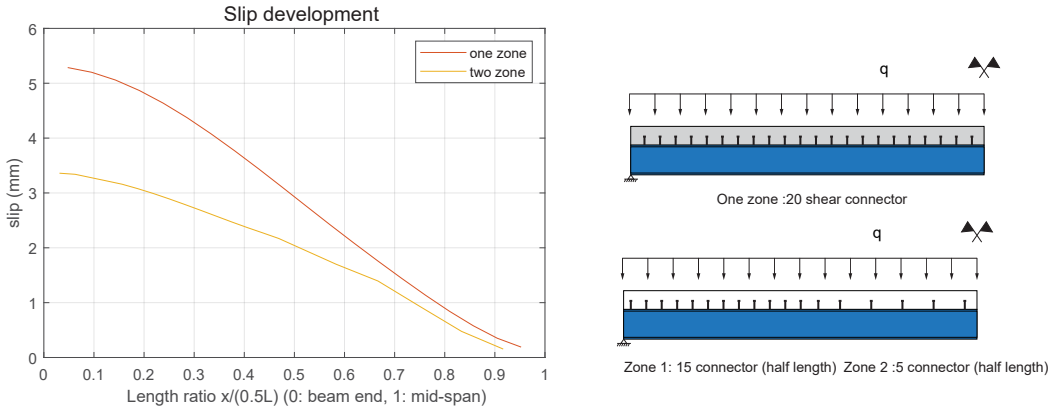

Figure 7.41 – Slip development of beam NC4 with one or two zones of shear connector arrangement

In Fig. 7.41, slip development of beam NC4 for a two zones set-up and equal distance arrangement of shear connectors are compared. For the two zones set-up, the first half of the beam has 15 shear connectors and the second half near mid-span has five shear connectors. The results show a much smaller slip if the shear connectors are arranged following the longitudinal shear force distribution calculated at full shear interaction.

7.3.3 Suggestions for longitudinal shear design with deep neutral axis position and ductile shear connector

As shown above, for composite beams with very deep neutral axis position and ductile shear connectors, the resistances of non-critical sections usually have no problem to be reached. It is because only limited bending moment resistance increase in the composite section compared to the steel beam section only, thus a high $M_{pl,a,Rd}/M_{pl,Rd}$ is usually expected. However, on the other hand, slip in the join may be significantly larger compared to composite beams with small compression zone height. Thus shear connector failures are possible. Thus it is suggested to perform advanced analysis for this situation for the design of shear connectors.

7.4 Chapter summary

With the assumption of full shear interaction, longitudinal shear force distribution can be easily calculated in the elastic stage. In the elastic-plastic stage, however, is complex to be analytically calculated. Based on a rectangle cross-section and bi-linear material strain-stress relationship, analytically solutions of longitudinal shear force distribution are provided in section 7.1.1. It shows a non-linear increase of longitudinal shear force if part of the section is in the plastic stage. For composite beams, section 7.1.2 provides numerical solutions based on the strain-limited design for a simply supported composite beam with full shear interaction. The numerical parametric studies show slim-floor beams usually have smaller non-linear redistribution of longitudinal shear forces compared to conventional composite beams. Furthermore, a simplified engineering approach to calculate longitudinal shear distribution, for the case that the steel section reaches full plastic at mid-span, is given. This approach can be used for longitudinal shear design with non-ductile shear connectors.

The bi-linear shear connector load-deformation relationship with a horizontal resistance plateau is widely used in the design. The parametric study in section 7.2.2 with linear shear connector load-deformation relationship shows, that under uniform distributed load, the longitudinal shear distribution has a curved shape with low stiffness shear connector. And only with ideal stiff shear connector to reach full shear interaction, a typical linear distribution can be achieved. Non-linear longitudinal shear force redistribution with ductile shear connectors are investigated in section 7.2.3 based on the bi-linear shear connector load-deformation relationship. Based on the number of shear connectors reaches the resistance plateau, the non-linear distribution of longitudinal shear force can be divided into "elastic distribution","partial non-linear distribution" and "full non-linear distribution". The three stages show increasing slip development ratio with the load. The full non-linear distribution may happen with partial shear connection, while full and post-full shear connection enables partial non-linear distribution at failure. It is found that with a low degree of shear connection, the bending failure may happen at the cross-section other than the mid-span with an equal-distance arrangement of shear connectors and uniformly distributed load.

If the cross-section has deep laying neutral axis, even if it is cross-section 1 or 2 according to Eurocode 4, with ductile shear connectors, uniform distribution of shear connectors is not suggested. It is due to lack of cross-section plastic development more longitudinal shear force needs to be redistributed, the potential of extensive slip development can cause shear connector failure; the details are provided in section 7.3.

Chapter 8

Conclusions

With full shear connection, deep neutral axis position in composite beams of steel and concrete under sagging bending may cause important part of the steel section stay elastic at concrete failure. In this case, plastic bending resistance calculated based on rectangle stress blocks can result in an overestimation of the resistance and therefore leads to unsafe design for those sections. Therefore, according to Eurocode 4 [22], a reduction factor β on plastic bending resistance ($M_{pl,Rd}$) needs to be applied for cross-sections with steel grade S420 and S460 and relative compression zone height x_{pl}/h exceeds 0.15. While the conventional plastic design method has its limitations and only applicable when the beam cross-section has enough rotation capacity to allow full plastic development, the more advanced strain-limited numerical calculation and FEM can be used for a much wider range regardless the position of neutral axis.

The investigations in this dissertation have confirmed that beside the cross-sections with high steel grades, also certain cross-section with lower steel grades but important relative compression zone height can cause an overestimated plastic bending moment resistance. At least this effect is more important for more compact cross-section types such as slim-floor sections or composite beams with asymmetrical structural steel profiles or with a small concrete slab effective width. Therefore vast amount of parametric studies based on strain-limited method and FEM have been developed to check the limitation of plastic design methods for conventional composite beams, its variations with asymmetrical structural steel profiles as well as slim-floor beams. Furthermore new reduction β functions on $M_{pl,Rd}$ for engineering practise considering much wider variates of composite beam cross-sections have been developed based on statistical analysis.

For design with partial shear connection, partial shear diagram developed based on plastic analysis has been widely used. As discussed above, the plastic design may be unsafe when the relative compression zone height is big enough to cause important part of steel section still in elastic at failure. This problem is especially important for slim-floor beams, for which due to the compact cross-section, the relative compression zone height is usually much bigger than conventional composite beams. Thus the limitation of using partial shear diagram for slim-floor beams are analysed and provided based on the neutral axis position and additional simplified engineering design rules are proposed.

Plastic development inside the cross-section increases the longitudinal shear force in the composite joint, where the steel section turns plastic and furthermore with ductile shear connectors and respecting the minimum degree of shear connection, the plastic redistribution of longitudinal shear force allows equal distance arrangement of

shear connectors by the conventional design. For which, the full plastic development of the cross-section and non-linear redistribution of longitudinal shear force are two fundamental conditions. The deep neutral axis position brings questions directly to the first assumption, as full plastic development of cross-section may not be able reached. Thus the impact of neutral axis position at critical cross-section and its impact on stress distribution and yielding of section on longitudinal shear force distribution has been analysed.

8.1 Summary of outcomes

The outcomes regarding to the initial objectives listed in the introduction in section 1.1 are summarized as follow:

- The non-linear strain-limited design principles and numerical approaches for composite beam are systemically summarized in chapter 3. And new developed simplified numerical approaches such as the finite cell method, integral stain method in section 3.4 allow much easier strain limited design, furthermore strain-limited design based simplified hand-calculation approach is provided in section 3.5. strain-limited design still has its limitations, thus simplified FEM models for traditional composite beams and slim-floor beams (explained in section 4.3) have been developed as part of the "CivilLab" Add-in, which enhances the FEM analysis of composite structures with Abaqus CAE. Benchmarks with various existing test results including both conventional composite beams and slim-floor beams in chapter 5 proof the reliability of these numerical calculation methods.
- The limitations of plastic design can be determined by comparing the results from non-linear advanced calculation methods and plastic design results at where $\beta = M_{sl,Rd}/M_{pl,Rd} = 1$. It can be defined regarding to relative compression zone height (z_{pl}/h) for different steel grades. For conventional composite beams and slim-floor beams the results are different, furthermore the choice of material strain-stress relationship types have a big influence. For example as shown in section 6.1.4.2 with considering strain hardening of a bi-linear steel relationship the boundary value of z_{pl}/h to reach $\beta = 1$ is much bigger than that without strain hardening. Other parameters such as effective width of concrete slab and the steel profile shapes also impact the results. To get an economical design, at least the effective width of concrete slab is suggested to be no less than $1m$ and the size of steel upper flange should be limited as well. Under the limitations provided in section 6.1.5, based on the non-linear concrete strain-stress relationship and quart-linear steel strain-strain relationship, plastic design without reduction ($\beta = 1$) necessary is overall allowed at around $z_{pl}/h \leq 0.1$ for conventional composite beams and slim-floor beams. However, the reduction is small with further increase of z_{pl}/h value to certain values, for example, it can be extended to around $z_{pl}/h \leq 0.15$ for only $\beta = 0.97$. More details of the limitations related to each steel grades are provided in section 6.1.5.2 and 6.1.5.3.

  With further deeper neutral axis position until $z_{pl}/h \leq 0.6$, the reduction factor β according to Fig. **??** defined based on z_{pl}/h and different steel grades can be used. For slim-floor beams, separated reduction functions have been developed to reach more economical design results. The new proposed reduction functions in this research are in the discussion to be integrated for the second generation of

Eurocode 4. Alternatively a new reduction β based on lower flange strain stage according section 6.1.6 is expected to give more economical results, however requires a few more steps of calculation.

- Regarding to slim-floor beams, partial shear diagram defined by plastic design is suggested to be directly used only when reduction of plastic resistance is not necessary ($\beta = 1$), and the compression zone height is above half of the distance of steel upper flange ($z_{pl} \leq h_{ct}/2$). In this situation, the partial shear diagrams calculated by plastic design and non-linear strain limited design (without steel strain hardening) are similar. Beyond the limitation, strain limited design and plastic design may yields different results, for which plastic design may not be accurate. For simplification, until the neutral axis lays within top half of steel upper flange ($z_{pl} \leq h_{ct} + t_{ft}/2$) simplified design rules are provided in section 6.2.5 Fig.6.27 for an approximate design based on the partial shear diagram. If the neutral axis is located at a deeper position, advanced design methods are suggested to be applied.

- The longitudinal shear force distribution at full shear interaction is affected by plastic development of the cross-section. While it is possible to analytically solve the longitudinal shear force for a simple supported rectangle beam with a bi-linear material model as shown in section 7.1.1, for more complex composite beam cross-section, numerical solution is much easier to obtain. Parametric study in section 7.1.2 shows more linear distribution of longitudinal shear force when the neutral axis is deeply laying within the steel section, meanwhile increased non-linear distribution for cross-section with more part reaches plastic. For the cross-section where the steel section can nearly reaches full plastic at ULS, a simplified approach to calculate the non-linear longitudinal shear force distribution with full shear interaction is proposed for simply supported composite beam in section 7.1.2.3. With shear connectors installation based on the calculated longitudinal shear force distribution, non ductile shear connectors are also possible to be used.

  With partial shear iteration, the distribution of longitudinal shear force and slip inside the composite joint are however further influenced by the shear connectors. The influence of shear connector stiffness on longitudinal shear force distribution is discussed in section 7.2.2. With ductile shear connectors, non-linear redistribution of longitudinal shear force is possible. The different stages of non-linear redistribution of longitudinal shear force are analysed based on numerical calculation results in section 7.2.3 . Afterwards, the longitudinal shear design with deep laying neutral axis and ductile shear connector is shown in section 7.3. It is generally not suggested to use equal distance arrangement of shear connectors for such situation due to the extensive slip developed in the joint may cause shear connector failure.

8.2 Outlooks on further research

This work focuses on the influence of deep neutral axis position on sagging bending moment resistance and longitudinal shear design. Numerical analyses based on strain limited design and FEM are compared with the plastic design method. However, there are limited existing experimental tests with very deep neutral axis. Thus further experimental tests on conventional composite beams and slim-floor beams with high strength steel and big compression zone height to prove the theoretical results are welcome.

For strain-limited design, determination of strain-limitation is fundamental for the strain

limited design resistance. With the parabolic-rectangle concrete stress-strain relationship, current Eurocode 2 [19] requires the strain-limited points to be limited to $\varepsilon_{c,2}$ if concrete flange mostly under compression. This rule has been suggested to be removed in the new draft proposal [72] to allow simpler and more economical strain-limited design. More comparison of these two strain limitations are provided in section 3.2.1 and for the situation with deep neutral axis position, where big differences in calculation results are expected. However both models have not been proofed by experimental tests for this situation, thus more investigation on concrete strain limitations of composite beams with deep neutral axis position are necessary.

For longitudinal shear design, the longitudinal shear force distribution is influenced by both the cross-section and shear connectors. With the new developments of various shear connector types. Their behaviour may much different from the conventional head-studs, thus the influence of shear connectors onto longitudinal shear distributions also need to be further analysed.

List of Figures

List of Tables

Bibliography

[1] Abaqus-GUI. Abaqus 6.11 users manual, 2011. (Cited on pages 87, 88, 90, 181, 185, 204, and 205).

[2] A. Adekola. Partial interaction between elastically connected elements of a composite beam. *International Journal of Solids and Structures*, 4(11):1125–1135, 1968. (Cited on page 36).

[3] P. Ansourian. Plastic rotation of composite beams. *Journal of the Structural Division*, 108(ST3), 1982. (Cited on pages 30 and 120).

[4] P. Ansourian. Beitrag zur plastischen Bemessung von Verbundträgern. *Bauingenieur*, 59(7), 1984. (Cited on pages 162 and 207).

[5] ArcelorMittal. *Slim-Floor an innovative concept for floors - ArcelorMittal Europe -Long Products* (*Products Catalog*). ArcelorMittal, 2017. (Cited on pages 28 and 113).

[6] A. Ayoub and F. C. Filippou. Mixed formulation of nonlinear steel-concrete composite beam element. *Journal of Structural Engineering*, 126(3):371–381, 2000. (Cited on page 36).

[7] H. Ban, M. A. Bradford, B. Uy, and X. Liu. Available rotation capacity of composite beams with high-strength materials under sagging moment. *Journal of Constructional Steel Research*, 118:156–168, 2016. (Cited on page 30).

[8] H. Bode and J. Schanzenbach. Das Tragverhalten von Verbundträgern bei Berücksichtigung der Dübelnachgiebigkeit. *Der Stahlbau*, 58(3):65–74, 1989. (Cited on pages 32, 33, 41, and 157).

[9] H. Bode, J. Stengel, G. Sedlacek, M. Feldmann, and C. Müller. *Untersuchung des Tragverhaltens bei Flachdecken-Systemen* (*Slim-Floor Konstruktionen*) *mit verschiedener Ausbildung der Platten und verschiedener Lage der Stahlträger: Forschungsbericht*. Verlag und Vetriebsges., 1997. (Cited on page 35).

[10] M. Braun. *Investigation of the load-bearing behaviour of CoSFB-Dowels*. Dissertation, University of Luxembourg, 2018. (Cited on page 28).

[11] M. Braun, O. Hechler, R. Obiala, U. Kuhlmann, F. Eggert, G. Hauf, and M. Konrad. Experimentelle Untersuchungen von Slim-Floor-Trägern in Verbundbauweise: Anwendung von tiefliegenden Betondübeln bei Slim-Floor-Konstruktionen- CoSFB. *Stahlbau*, 83(10):741–749, 2014. (Cited on pages 31, 95, 97, and 98).

[12] M. Classen. Limitations on the use of partial shear connection in composite beams with steel t-sections and uniformly spaced rib shear connectors. *Journal of Constructional Steel Research*, 142:99–112, 2018. (Cited on page 27).

[13] Corus. *Advance sections, CE marked structural sections* (*Products Catalogue*). Corus, 2007. (Cited on page 113).

[14] C. Culver, P. Zarzeczny, and G. Driscoll Jr. *Tests of composite beams for buildings, June 1960*. Fritz Laboratory Reports, 1960. (Cited on pages 27, 40, 56, 58, 95, 96, 181, and 187).

[15] S. De Nardin and A. L. El Debs. Composite connections in slim-floor system: An experimental study. *Journal of Constructional Steel Research*, 68(1):78–88, 2012. (Cited on page 27).

[16] P. Döinghaus. *Zum Zusammenwirken hochfester Baustoffe in Verbundträgern*. Dissertation, Lehrstuhl und Institut für Massivbau der RWTH, 2002. (Cited on pages 27, 32, and 39).

[17] F. Eggert. *Einfluss der Verdübelung auf das Trag- und Verformungsverhalten von Verbundträgern mit und ohne Profilblech*. Dissertation, Universität Stuttgart, 2018. (Cited on pages 27 and 97).

[18] EN12390-13:2013. *Testing hardened concrete. Determination of secant modulus of elasticity in compression*. CEN, 2012. (Cited on page 47).

[19] EN1992-1-1:2004. *Design of concrete structures. Part 1-1: EN1992-1-1:2004, General rules for buildings*. CEN, 2004. (Cited on pages 30, 32, 45, 47, 51, 52, 87, 109, 114, 127, 132, 136, 178, 179, 180, 185, 199, and 200).

[20] EN1993-1-1:2004. *Design of steel structures: Eurocode 3: Design of steel structures, Part 1-1: General rules and rules for buildings*. CEN, 2005. (Cited on page 29).

[21] EN1993-1-5:2006. *Design of plated structures: Eurocode 3: Design of steel structures, Part 1-5: Design of plated structures*. CEN, 2012. (Cited on pages 48, 98, 127, 132, and 180).

[22] EN1994-1-1:2004. *Design of composite steel and concrete structures. Part 1-1: EN1994-1-1, General rules for buildings*. CEN, 2004. (Cited on pages 7, 14, 19, 21, 25, 29, 32, 33, 35, 39, 40, 41, 45, 107, 109, 126, 127, 136, 168, and 175).

[23] G. Fabbrocino, G. Manfredi, and E. Cosenza. Analysis of continuous composite beams including partial interaction and bond. *Journal of structural Engineering*, 126(11):1288–1294, 2000. (Cited on pages 36 and 61).

[24] Fielders. *Asymmetric beams for fielders slimflor construction-beam selection tables* (*Fielders Fact File: F3.5*). Fielders, 2018. (Cited on page 113).

[25] J. Fries. *Tragverhalten von Flachdecken mit Hutprofilen. Mitteilungen des Instituts für Konstruktion und Entwurf, Nr. 2002-1*. Dissertation, Institut für Konstruktion und Entwurf, Universität Stuttgart, 2001. (Cited on page 31).

[26] L. Gardner, X. Yun, L. Macorini, and M. Kucukler. Hot-rolled steel and steel-concrete composite design incorporating strain hardening. In *Structures*, volume 9, pages 21–28. Elsevier, 2017. (Cited on page 38).

[27] GB50010-2010. *Codes for design of concrete structures*. 2015. (Cited on pages 87, 185, and 200).

[28] J. A. Grant Jr. Determination of connector and beam behavior for composite beams with deck formed slabs, phd dissertation, 1980. 1980. (Cited on pages 101, 103, and 223).

[29] M. Gündel, M. Kopp, M. Feldmann, J. Gallwoszus, J. Hegger, and G. Seidl. Die Bemessung von Verbunddübelleisten nach neuer Allgemeiner bauaufsichtlicher Zulassung. *Stahlbau*, 83(2):112–121, 2014. (Cited on page 27).

[30] G. Haaijer and B. Thürlimann. On inelastic buckling in steel. *Journal of the Engineering Mechanics Division*, 84(2):1–48, 1958. (Cited on page 29).

[31] G. Hanswille. Zur Rißbreitenbeschränkung bei Verbundträgern. *Technisch-Wissenschaftliche Mitteilungen*, 86(1), 1986. (Cited on page 27).

[32] G. Hanswille and M. Schäfer. Zur praktischen Ermittlung der Verformungen von Verbundträgern und Flachdeckensystemen unter Berücksichtigung der Nachgiebigkeit der Verbundfuge. *Stahlbau*, 76(11):845–854, 2007. (Cited on pages 29, 31, and 179).

[33] G. Hanswille, M. Schäfer, and M. Bergmann. *Verbundtragwerke aus Stahl und Beton - Bemessung und Konstruktion - Kommentar zur DIN EN 1994-1-1*. Ernst & Sohn, 2018. (Cited on pages 28, 30, 32, 34, 41, 137, 157, 168, and 179).

[34] G. Hanswille, G. Sedlacek, and D. Anderson. The use of steel grades s460 and s420 in composite structures. *ECCS-EUROFER improvements by TC11 to EUROCODE 4 report*, 1996. (Cited on pages 32, 33, 39, 51, 111, and 115).

[35] G. Hauf. *Trag-und Verformungsverhalten von Slim-Floor Trägern unter Biegebeanspruchung*. Dissertation, University of Stuttgart, 2010. (Cited on pages 35 and 39).

[36] J. Hegger, G. Sedlacek, P. Doeinghaus, and H. Trumpf. Untersuchungen zur Duktilität der Verbundmittel bei Anwendung von hochfestem Stahl und hochfestem Beton. *Stahlbau*, 70(7):436–446, 2001. (Cited on page 27).

[37] S. Heinemeyer. *Zum Trag- und Verformungsverhalten von Verbundträgern aus ultrahochfestem Beton mit Verbundleisten*. Dissertation, Eigenverl. Aachen, 2011. (Cited on pages 27, 33, 39, 61, 111, and 115).

[38] S. J. Hicks. Ductility of headed stud connectors assumed in the development of proposed sc4.t3 design model with existing en 1994-1-1, 6.6.1.2 for limits on the use of partial shear connection in beams for buildings. Technical report, CEN, SC4.T3, 2018. (Cited on page 157).

[39] S. J. Hicks and A. L. Smith. Stud shear connectors in composite beams that support slabs with profiled steel sheeting. *Structural Engineering International*, 24(2):246–253, 2014. (Cited on page 27).

[40] A. Jähring. *Zum Tragverhalten von Kopfbolzendübeln in hochfestem Beton*. Dissertation, Technische Universität München, 2008. (Cited on page 27).

[41] N. Jasim. Computation of deflections for continuous composite beams with partial interaction. *Proceedings of the Institution of Civil Engineers-Structures and Buildings*, 122(3):347–354, 1997. (Cited on page 36).

[42] JGJ138-2016. *Code for design of composite structures*. Chinese standards, 2016. (Cited on page 33).

[43] R. P. Johnson. *Composite Structures of Steel and Concrete: beams, slabs, columns and frames for buildings*. John Wiley & Sons, 2018. (Cited on pages 14, 37, 41, and 127).

[44] R. P. Johnson and I. May. Partial-interaction design of composite beams. *Structural Engineer*, 8(53), 1975. (Cited on pages 32 and 33).

[45] R. P. Johnson and N. Molenstra. Partial shear connection in composite beams for buildings. *Proceedings of the Institution of Civil Engineers*, 91(4):679–704, 1991. (Cited on pages 40 and 157).

[46] A. Kemp. Slenderness limits normal to the plane of bending for beam-columns in plastic design. *Journal of Constructional Steel Research*, 4(2):135–150, 1984. (Cited on page 29).

[47] A. R. Kemp. Interaction of plastic local and lateral buckling. *Journal of Structural Engineering*, 111(10):2181–2196, 1985. (Cited on page 32).

[48] A. R. Kemp and N. Dekker. Available rotation capacity in steel and composite beams. *Structural engineer*, 69:88–97, 1991. (Cited on page 30).

[49] A. R. Kemp and D. A. Nethercot. Required and available rotations in continuous composite beams with semi-rigid connections. *Journal of Constructional Steel Research*, 57(4):375–400, 2001. (Cited on page 30).

[50] J.-S. Kim, J. Kwark, C. Joh, S.-W. Yoo, and K.-C. Lee. Headed stud shear connector for thin ultrahigh-performance concrete bridge deck. *Journal of Constructional Steel Research*, 108:23–30, 2015. (Cited on page 27).

[51] P. Kmiecik and M. Kamiński. Modelling of reinforced concrete structures and composite structures with concrete strength degradation taken into consideration. *Archives of civil and mechanical engineering*, 11(3):623–636, 2011. (Cited on pages 187, 200, and 201).

[52] M. Konrad. *Tragverhalten von Kopfbolzen in Verbundträgern bei senkrecht spannenden Trapezprofilblechen*. Dissertation, Universitat Stuttgart, 2011. (Cited on page 27).

[53] U. Kuhlmann. Definition of flange slenderness limits on the basis of rotation capacity values. *Journal of Constructional Steel Research*, 14(1):21–40, 1989. (Cited on pages 28, 29, and 38).

[54] U. Kuhlmann, G. Hauf, and M. Konrad. Push-out and girder tests for the determination of the bending capacity and longitudinal shear capacity of composite slim-floor girder with cofradal 200 deck elements. *Versuchsbericht* (*unveröffentlicht*). *Institut für Konstruktion und Entwurf, Universität Stuttgart*, 2010. (Cited on page 111).

[55] U. Kuhlmann, D. Lam, R. Zandonini, J. Schorr, T. Sheehan, and N. Baldassino. Experimentelle Untersuchungen an Slim-Floor-Trägern. *Stahlbau*, 88(7):633–641, 2019. (Cited on page 97).

[56] D. Lam, X. Dai, U. Kuhlmann, J. Raichle, and M. Braun. Slim-floor construction–design for ultimate limit state. *Steel Construction*, 8(2):79–84, 2015. (Cited on page 35).

[57] R. Lawson, H. Bode, J. Brekelmans, P. Wright, and D. Mullett. Slimflor and slimdek construction: European developments. *Architecture and Building*, 1999. (Cited on pages 28 and 35).

[58] R. M. Lawson, E. Aggelopulos, R. Obiala, F. Hanus, C. Odenbreit, Nellinger.S, U. Kuhlmann, F. Eggert, D. Lam, and T. Sheehan. *Development of improved shear connection rules in composite beams (DISCCO) final report*. RFCS Publications, 2017. (Cited on pages 27, 95, 96, 97, 101, 182, 187, and 224).

[59] R. M. Lawson, D. L. Mullett, and J. Rackham. *Design of asymmetric slimflor beams using deep composite decking*. Steel Construction Institute Berkshire, 1997. (Cited on pages 95, 97, 98, and 111).

[60] M. Leskelä, J. Aribert, A. Ciutina, M. Hjiaj, R. P. Johnson, U. Kuhlmann, D. Lam, J. Lebet, I. Mangerig, L. Neves, et al. *Shear connections in composite flexural members of steel and concrete*. ECCS-European Convention for Constructional Steelwork, 2017. (Cited on pages 35, 40, and 166).

[61] T. Li, B. Choo, and D. Nethercot. Determination of rotation capacity requirements for steel and composite beams. *Journal of Constructional Steel Research*, 32(3):303–332, 1995. (Cited on page 30).

[62] K. S. Naraine. *Slip and uplift effects in composite beams*. Dissertation, McMaster University, 1984. (Cited on page 36).

[63] S. Nellinger. *On the behaviour of shear stud connections in composite beams with deep decking*. Dissertation, University of Luxembourg, 2015. (Cited on pages 97, 101, and 103).

[64] D. Nethercot, T. Li, and B. Choo. Required rotations and moment redistribution for composite frames and continuous beams. *Journal of Constructional Steel Research*, 35(2):121–163, 1995. (Cited on page 30).

[65] G. M. Newman. Fire resistance of slim floor beams. *Journal of constructional steel research*, 33(1-2):87–100, 1995. (Cited on page 27).

[66] N. M. Newmark. Test and analysis of composite beams with incomplete interaction. *Proceedings of society for experimental stress analysis*, 9(1):75–92, 1951. (Cited on pages 32 and 36).

[67] J. Nie, Y. Xiao, and L. Chen. Experimental studies on shear strength of steel–concrete composite beams. *Journal of Structural Engineering*, 130(8):1206–1213, 2004. (Cited on pages 13, 185, 215, 216, 217, 218, 219, 220, 221, 222, and 223).

[68] D. J. Oehlers, N. T. Nguyen, M. Ahmed, and M. A. Bradford. Partial interaction in composite steel and concrete beams with full shear connection. *Journal of*

Constructional Steel Research, 41(2-3):235–248, 1997. (Cited on pages 14, 37, 41, 42, and 128).

[69] H. Othman and H. Marzouk. Applicability of damage plasticity constitutive model for ultra-high performance fibre-reinforced concrete under impact loads. *International Journal of Impact Engineering*, 114:20–31, 2018. (Cited on pages 87, 88, and 181).

[70] PeikkoSteel. *DeltaBeam slim floor structure* (*Technical Manual*). Peikko Steel, 2014. (Cited on pages 28 and 113).

[71] D. Plum and M. Horne. The analysis of continuous composite beams with partial interaction. *Proceedings of the Institution of Civil Engineers*, 59(4):625–643, 1975. (Cited on page 36).

[72] prEN1992 1-1:2019. *Design of concrete structures. Part 1-1: prEN1992-1-1:2019, General rules for buildings* (*draft version*). CEN, 2019. (Cited on pages 33, 47, 51, 52, 113, 178, 180, 199, and 200).

[73] prEN1993 1-14:2019 (draft). *Design of steel structures. Part 1-14: prEN1993-1-14:2019,* (*draft version document AHGFE2017-019*). CEN, 2019. (Cited on pages 48, 49, 180, 185, 207, and 208).

[74] J. Qureshi, D. Lam, and J. Ye. Effect of shear connector spacing and layout on the shear connector capacity in composite beams. *Journal of constructional steel research*, 67(4):706–719, 2011. (Cited on page 27).

[75] G. Ranzi. *Partial-interaction analysis of composite beams using the direct stiffness method*. University of New South Wales, 2003. (Cited on page 36).

[76] A. Rieg. *Verformungsbezogene mittragende Betongurtbreite niedriger Verbundträger. Mitteilungen des Instituts für Konstruktion und Entwurf, Nr. 2006-2*. Dissertation, Dissertation, Institut für Konstruktion und Entwurf, Universität Stuttgart, 2006. (Cited on page 27).

[77] A. Rieg and U. Kuhlmann. Verformungsbezogene mittragende Breite niedriger Verbundträger. *Stahlbau*, 76(11):794–804, 2007. (Cited on pages 27 and 31).

[78] k. Roik, H. Bode, and J. Haensel. Erläuterungen zu den richtlinien für die Bemessung und Ausführung von Stahlverbundträgern, 1975. (Cited on pages 27, 33, 37, and 41).

[79] J. Rotter and P. Ansourian. Cross-section behaviour and ductility in composite beams. *Proceedings of the Institution of Civil Engineers*, 67(2):453–474, 1979. (Cited on page 30).

[80] Scandinavian-WeldTech. *SWT-beam standard-details and best practice* (*Products Catalogue*). SWT, 2016. (Cited on pages 28 and 113).

[81] M. Schäfer. *Zum Tragverhalten von Flachdecken mit integrierten hohlkastenförmigen Stahlprofilen*. Dissertation, Universität Wuppertal, Fakultät für Architektur und Bauingenieurwesen . . . , 2007. (Cited on pages 28, 31, 32, 35, 39, 41, and 179).

[82] M. Schäfer. Schubtragfähigkeit und M-V-Interaktion von Flachdecken mit integrierten hohlkastenförmigen Stahlprofilen: Ansatz eines hybriden Fachwerkmodells zur Querkraftbemessung. *Stahlbau*, 84(5):314–323, 2015. (Cited on page 35).

[83] M. Schäfer and M. Banfi. Plastic moment resistance of composite beams - harmonization of eurocode 4 with eurocode 2, background report to en 1994. In *CEN, Project Team CEN/TC250/SC4*, 2017. (Cited on pages 39, 115, and 120).

[84] M. Schäfer, M. Braun, and G. Hauf. Flachdecken in Verbundbauweise: Bemessung und Konstruktion von Slim-Floor-Trägern. *Stahlbau Kalender 2018: Verbundbau Fertigung*, 20:631–741, 2018. (Cited on page 35).

[85] M. Schäfer and Q. Zhang. Zur dehnungsbegrenzten Momententragfähigkeit von Flachdecken in Verbundbauweise. *Stahlbau*, 88(7):653–664, 2019. (Cited on pages 39 and 110).

[86] M. Schäfer, Q. Zhang, and M. Banfi. Plastic moment resistance for composite cross-sections with deep position of plastic neutral axis, backgroud report to prEN1994-1-1: 2020 for CEN/TC250/SC4.T6 and SC4.T5: in preparation. Technical report, University of Luxembourg, 2020. (Cited on pages 39, 52, and 120).

[87] M. Schäfer, Q. Zhang, M. Braun, and M. Banfi. Plastic design for composite beams - are there any limits? In *Conference-ICSAS2019, Bradford*, 2019. (Cited on pages 37, 39, and 120).

[88] M. Schäfer, Q. Zhang, M. Braun, and M. Banfi. Plastic design for composite beams - are there any limits? *proceeding of 9th International Conference on Steel and Aluminium Structures,Bradford*, 2019. (Cited on page 115).

[89] G. Sedlacek and B. Hoffmeister. *Untersuchunge n zur Rotationsanforderung bei Anwendung des Fließgelenkverfahrens bei Verbundträgern*. Bauforschung, 1998. (Cited on pages 28 and 30).

[90] Y.-j. SHI, Q.-z. LI, Y.-q. WANG, and Q. CHEN. Loading capacity of composite slim beam in the sagging moment region [j]. *Journal of Harbin Institute of Technology*, 11, 2004. (Cited on pages 97, 98, and 111).

[91] W. Siokola and E. Ringsmuth. Trapezblechbogen-Verbunddecke Eine altbekannte Bauweise mit modernen Baustoffen neu entdeckt. *Stahlbau Rundschau*, 89:33–34, 1997. (Cited on page 28).

[92] J. Stark and J. Brekelmans. Plastic design of continuous composite slabs. *Journal of Constructional Steel Research*, 15(1-2):23–47, 1990. (Cited on page 32).

[93] J. Stark and B. Van Hove. Statistical analysis of pushout tests on stud connectors in composite steel and concrete structures, 1991. (Cited on page 27).

[94] L. Taerwe and S. Matthys. Fib model code for concrete structures 2010, 2013. (Cited on page 200).

[95] H.-T. Thai, T.-K. Nguyen, S. Lee, V. I. Patel, and T. P. Vo. Review of nonlinear analysis and modelling of steel and composite structures. *International Journal of Structural Stability and Dynamics*, 2020. (Cited on page 36).

[96] Y. Wang, L. Yang, Y. Shi, and R. Zhang. Loading capacity of composite slim frame beams. *Journal of Constructional Steel Research*, 65(3):650–661, 2009. (Cited on pages 97, 98, and 111).

[97] Westok. Ultra shallow floor beams-products catalogue, 2010. (Cited on page 28).

[98] Westok. *The cellular beam - pocket guide - entrusted to design and deliver metal solutions* (*Products Catalogue*). Westok, 2018. (Cited on page 28).

[99] L. Yam and J. Chapman. The inelastic behavior of continuous composite beams of steel and concrete. *Institution of Civil Engrs, Pt2, Research & Theory*, 53(Proceeding), 1972. (Cited on page 36).

[100] H. Yuan. *The resistances of stud shear connectors with profiled sheeting*. Dissertation, University of Warwick, 1996. (Cited on page 27).

[101] J. A. Yura, M. K. Ravindra, and T. V. Galambos. The bending resistance of steel beams. *Journal of the Structural Division*, 104(9):1355–1370, 1978. (Cited on page 29).

[102] C. Zapfe. *Trag-und Verformungsverhalten von Verbundträgern mit Betondübeln zur Übertragung der Längsschubkräfte*. Dissertation, Universität der Bundeswehr München, 2001. (Cited on page 27).

[103] Q. Zhang and M. Schäfer. Slim-floor beams bending moment resistance considering partial shear connection. In *Conference-SDSS2019, Prague*, 2019. (Cited on pages 32, 33, 38, and 126).

[104] Q. Zhang, M. Schäfer, K. Santos Ferreira, M. Bender, S. Wong, H. Luc, and et al. *Comparison of European and Chinese design codes for concrete structures and composite structures of steel and concrete*. AVEC-BNT,final report, available at http://www.avec-bnt.de/, 2018. (Cited on page 5).

[105] K. Zilch and G. Zehetmaier. *Bemessung im konstruktiven Betonbau: Grundlagen und Tragfähigkeit*. Springer, 2006. (Cited on pages 51 and 52).

Appendices

Appendix A

Non-linear material models for numerical calculation

A.1 Concrete

A.1.1 Concrete uni-axis strain-stress relationship

The concrete strain-stress relationship used in the analysis is based on Eurocode 2. The parabolic-rectangle stress-strain relationship in EN1992-1-1 3.1.7 as well as the non-linear stress-strain relationship defined in EN1992-1-1 3.1.6 are adopted in this work. The models are shown as below. The compression strain limits for the parabolic-rectangle model is $\varepsilon_{cu,2}$ and for non-linear model is $\varepsilon_{cu,1}$. They are related to concrete classes, below C50/60 the value 3.5 ‰ is used in the current code. While with high strength concrete, the ductility is reduced for which a smaller strain limit is expected. However, test results show for many cases the concrete strain limit can go much beyond the given value in the code, thus the draft version of next generation prEN1992-1-1:2019 [72] suggests to use 3.5 ‰ for all concrete classes. Meanwhile, the concrete compressional strength is reduced.

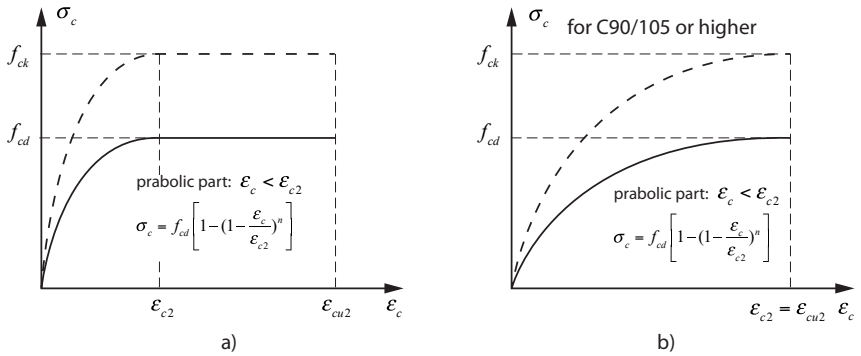

Figure A.1 – Parabolic stress-strain relationship of concrete according to Eurocode 2 [19]

For the non-linear concrete model, it is based of the mean concrete strength (f_{cm}), which can be represented by strength values by tests. However if the model is used for design purpose, according to EN1992-1-1 5.8.6, the f_{cm} should be substituted by f_{cd}, and the E_{cm} should be replaced by E_{cd}, with $E_{cd} = E_{cm}/\gamma_{cE}$. In the draft new version of code

prEN1992-1-1:2019 [72] this model still have been partly modified due to new concrete stiffness values.

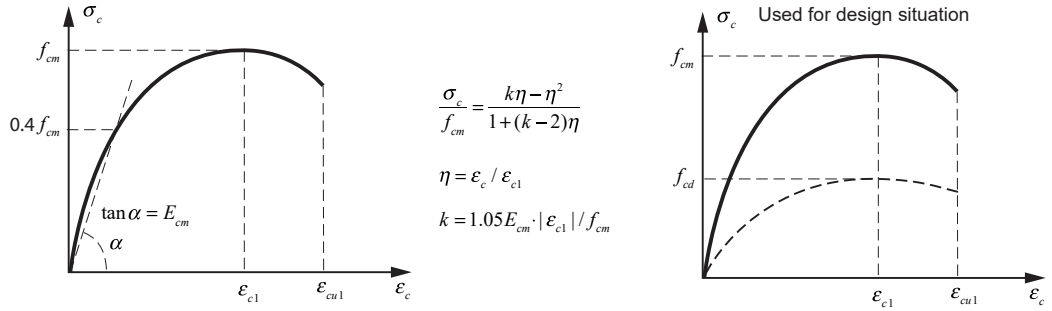

A) The nonlinear concrete model according to EN1992-1-1:2004

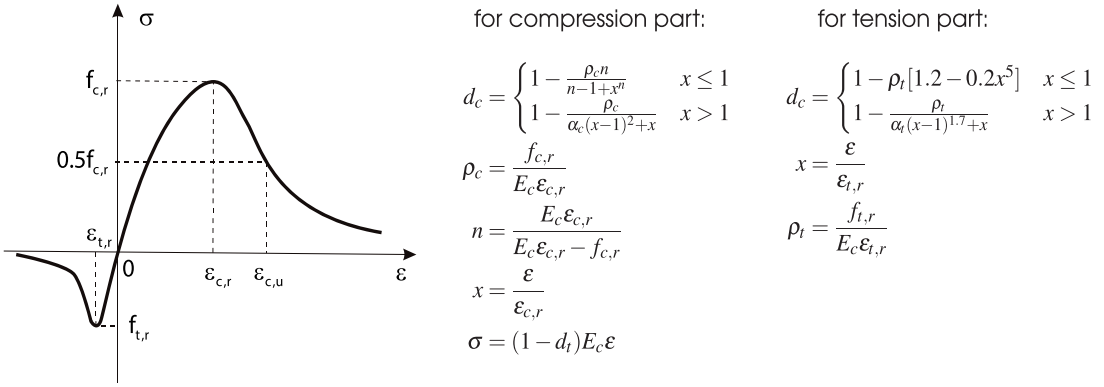

B) The nonlinear concrete model according to GB50010

C

Figure A.2 – Non-linear stress-strain relationship of concrete according to EN1992-1-1:2004 [19] and GB50010 [27]

Other non-linear material models from literature can also be applied, such as the non-linear curve from Chinese national code GB50010 [27] which include also the tensile parts, the fib model code nonlinear curve [94] which is the base of Eurocode 2 models. In [51] a collection of varies other concrete non-linear models such as the Madrid parabola model, Desay& Krishnan model, Wang & Hsu models are given. The formula in [51] are summarized in the Table A.1, the details can be found in the references. However it should be noticed most of the following models are based on the initial value of modulus of elasticity.

Table A.1 – Summary of non-linear stress-strain relationship of concrete from literature [51]

Formula name/ source	Formula form	Variables
Madrid parabola	$\sigma_c = E_c\varepsilon_c\left[1-\frac{1}{2}\left(\frac{\varepsilon_c}{\varepsilon_{c1}}\right)\right]$	$\sigma_c = f\left(E_c, \varepsilon_{c1}\right)$
Desay & Krishnan formula	$\sigma_c = \frac{E_c\varepsilon_c}{1+\left(\frac{\varepsilon_c}{\varepsilon_{c1}}\right)^2}$	$\sigma_c = f\left(E_c, \varepsilon_{c1}\right)$
EN 1992-1-1	$\sigma_c = f_{cm}\frac{k\eta-\eta^2}{1+(k-2)\eta}$ $k = 1.05E_{cm}\frac{\varepsilon_{c1}}{f_{cm}},\quad \eta = \frac{\varepsilon_c}{\varepsilon_{c1}}$	$\sigma_c = f\left(E_{cm}, f_{cm}, \varepsilon_{c1}\right)$
Majewski formula	$\sigma_c = E_c\varepsilon_c$ if $\sigma_c \le e_{\lim} f_{cm}$ $\sigma_c = f_{cm}\frac{(e_{\lim}-2)^2}{4(e_{\lim}-1)}\left(\frac{\varepsilon_c}{\varepsilon_{c1}}\right)^2 - f_{cm}\frac{(e_{\lim}-2)^2}{2(e_{\lim}-1)}\left(\frac{\varepsilon_c}{\varepsilon_{c1}}\right) + f_{cm}\frac{e_{\lim}^2}{4(e_{\lim}-1)}$ *if* $\sigma_c > e_{\lim} f_{cm}$ $e_{\lim} = 1-\exp\left(\frac{-f_c}{80}\right),\qquad E_c = \frac{f_{cm}}{\varepsilon_c}\left(2-e_{\lim}\right),$	$\sigma_c = f\left(E_c, f_{cm}, \varepsilon_{c1}\right)$
Wang & Hsu formula	$\sigma_c = \zeta f_{cm}\left[2\left(\frac{\varepsilon_c}{\zeta\varepsilon_{c1}}\right)-\left(\frac{\varepsilon_c}{\zeta\varepsilon_{c1}}\right)^2\right]$ if $\frac{\varepsilon_c}{\zeta\varepsilon_{c1}} \le 1$ $\sigma_c = \zeta f_{cm}\left[1-\left(\frac{\varepsilon_c/\zeta\varepsilon_{c1}-1}{2/\zeta-1}\right)^2\right]$ if $\frac{\varepsilon_c}{\zeta\varepsilon_{c1}} > 1$	$\sigma_c = f\left(f_{cm}, \varepsilon_{c1}\right)$
Sáenz formula	$\sigma_c = \frac{\varepsilon_c}{A+B\varepsilon_c+C\varepsilon_c^{\,2}+D\varepsilon_c^{\,3}}$ $A = \frac{1}{E_c},\quad B = \frac{P_3+P_4-2}{P_3 f_{cm}}$ $C = -\frac{2P_4-1}{P_3 f_{cm}\varepsilon_{c1}},\quad D = \frac{P_4-1}{P_3 f_{cm}\varepsilon_{c1}}$ $P_1 = \frac{\varepsilon_{cu}}{\varepsilon_{c1}},\quad P_2 = \frac{f_{cm}}{f_{cu}}$ $P_3 = \frac{E_c\varepsilon_{c1}}{f_{cm}},\quad P_4 = \frac{P_3(P_2-1)}{(P_1-1)^2}-\frac{1}{P_1}$	$\sigma_c = f\left(\begin{matrix}E_c, f_{cm}, f_{cu},\\ \varepsilon_{c1}, \varepsilon_{cu1}\end{matrix}\right)$

A.1.2 Concrete multi-axial behavior and CDP model in Abaqus

Usually concrete members are designed based on their uniaxial strength. In some situations, concrete members exhibit stresses coming from different directions. In these situations it is important to predetermine biaxial and triaxial strength of the concrete.

For normal structures, triaxial stress situation is not very common. More often concrete member is under biaxial stress, such as beam under shear and bending at the same time. For biaxial concrete strength, GB50010-2010 gives a stress-strain relationship curve

consisting of 4 parts, as shown below in Fig. A.3

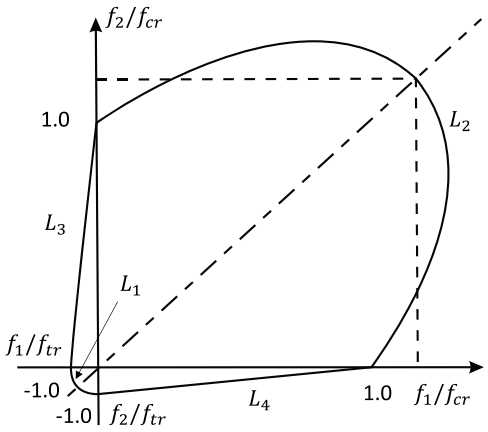

$$L_1: f_1^2 + f_2^2 - 2\upsilon f_1 f_2 = f_{\tau,r}^2$$

$$L_2: \sqrt{f_1^2 + f_2^2 - f_1 f_2} - \alpha_s(f_1 + f_2) = (1 - \alpha_s)\left|f_{c,r}\right|$$

$$L_3: \frac{f_2}{f_{c,r}} - \frac{f_1}{f_{t,r}} = 1$$

$$L_4: \frac{f_1}{f_{c,r}} - \frac{f_2}{f_{t,r}} = 1$$

$$\alpha_s = \frac{r-1}{2r-1}$$

T-C	f_2/f_{tr}	0	-0.1	-0.2	-0.3	-0.4	-0.5	-0.6	-0.7	-0.8	-0.9	-1.0
	f_1/f_{cr}	1.0	0.9	0.8	0.7	0.6	0.5	0.4	0.3	0.2	0.1	0
C-C	f_1/f_{cr}	1.0	1.05	1.10	1.15	1.20	1.25	1.29	1.25	1.20	1.16	
	f_2/f_{cr}	0	0.074	0.16	0.25	0.36	0.50	0.88	1.03	1.11	1.16	
T-T	f_1/f_{tr}	-0.79	-0.7	-0.6	-0.5	-0.4	-0.3	-0.2	-0.1	0		
	f_2/t_{cr}	-0.79	-0.86	-0.93	-0.97	-1.00	-1.02	-1.02	-1.02	-1.00		

Figure A.3 – Biaxial stress of concrete based on GB50010-2010

Concrete triaxial strength is important to determine when a concrete member is loaded in the directions of three non-complanary axes. It is mainly used for the analysis in the case of massive concrete volume, confined concrete and in some other situations. In triaxial stress situation, the member can be loaded in one of the four combinations: compression-compression-compression (C-C-C), tension-compression-compression (T-C-C), tension-tension-compression (T-T-C), tension-tension-tension (T-T-T). Unlike the uniaxial situation, concrete member may not exhibit failure when the design strength f_c is reached. Triaxial strength of concrete can be described in a three-dimensional stress / strain space. Fig. A.4 shows the plots of the stress envelop surface in the case of triaxial concrete strength. It usually has the shape of convex cone and is tri-symmetrical about the hydrostatic axis. In Fig. A.4 b) c) d) the typical yield surface of the deviatoric plan envelop, the compression-tension meridian surface as well as the hydrostatic stress-deviatioric stress surface are shown respectively.

A.1.2.1 Introduction to Concrete Damage Plasticity model

One of the earliest concrete plasticity model is the "Drucker-Prager" model, which has a cone shape stress space. Due to the smoothness of the surface, it is easy to apply this model in numerical applications. However, the model itself is not fully consistent with the real concrete behaviour. Thus, many modified material models, based on the DP model, were developed since with the intention of faithful representation of concrete behaviour in FEA.

Concrete Damaged Plasticity model is a modification of Drucker-Prager model. The roundness of failure surface in deviatoric plan is controlled by the input parameter K_c which is usually chosen as $K_c = 2/3$. (if $K_c = 1$, the failure surface will be a circle which is same as Drucker-Prager model). The meridian surface of concrete is usually a curve instead of a straight line - CDP model reflects this through a hyperbolic plastic potential surface, adjusted by parameter "plastic potential eccentricity". It can be calculated as a ratio of tensile strength to compressive strength, usually taken as 0.1. (if plastic potential eccentricity is taken as 0, the meridional plane becomes a straight line as in DP-model). Another parameter which needs to be determined in the CDP model is the ratio of the strength in bi-axial stage to uni-axial one, which is suggested to be taken as 1.16. The last

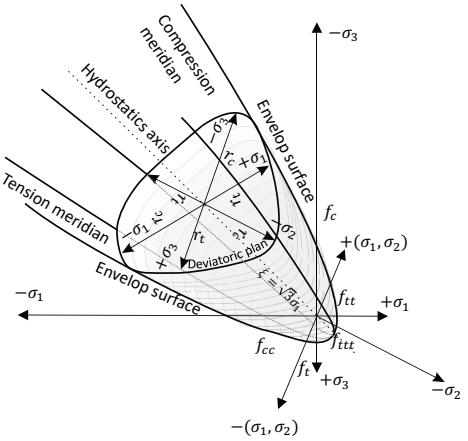

a. Envelop surface in three-dimensional space

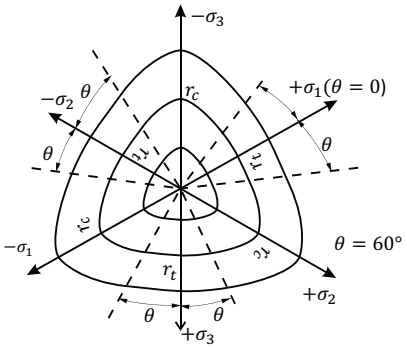

b. Deviatoric plan

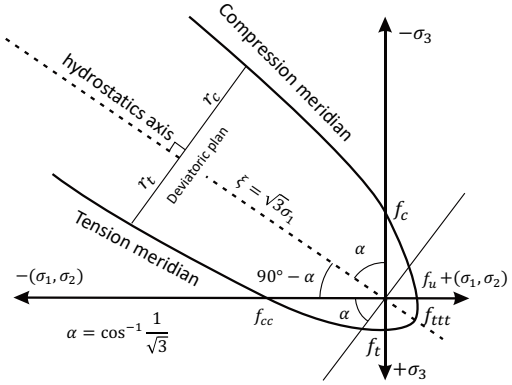

c. Compression-Tension meridian surface

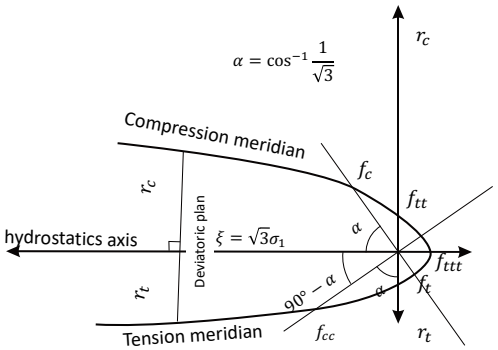

d. Hydrostatics stress-deviatioric stress surface

Figure A.4 – The general multi-axial behavior of concrete

input parameter is the dilatation angle which reflects an amount of the plastic volumetric strain developed during plastic shearing and is often assumed to be 36 degrees. The General inputs are summarized in the table below:

Parameter name	Dilatation angle	Eccentricity	fbo/fco	κ	Viscosity parameter
Values	36	0.1	1.16	0.667	0

Table A.2 – The general inputs for CDP model in Abaqus

The stress-strain relationship can be obtained from uni-axial test results. If test results are not available, theoretical values from design codes or literature can also be used. However, in Abaqus software the required input is based on the inelastic strain values $\widetilde{\varepsilon_c^{in}}$ instead of the total strain (elastic strain + plastic strain). Thus the model will start with a elastic part until reach σ_{c0} which is the first input point and afterwards continues with the non-linear inputs. As concrete shows nonlinear stress-strain behaviour almost from the beginning of the loading phase, the initial stage can often be neglected. However, in order to simplify the calculation procedure and improve convergence of the process, a linear stage up until to $0.4f_{cm}$ is suggested by Eurocode 2. The CDP model for the compression part defined in Abaqus [1] is shown below in Fig. A.5.

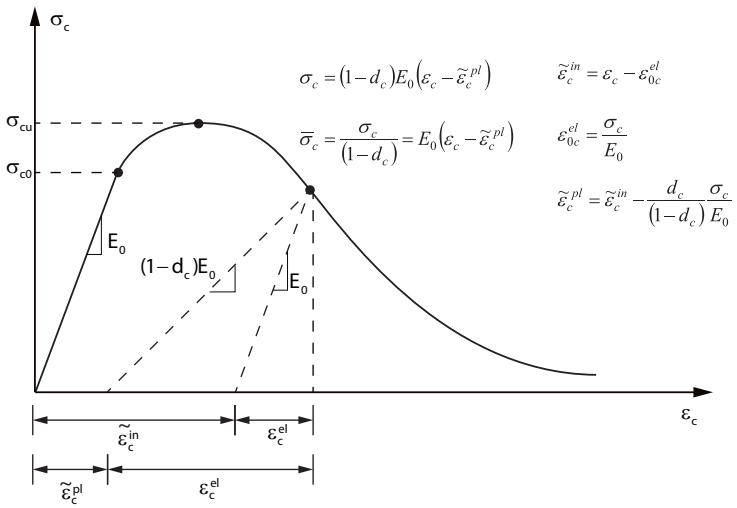

Figure A.5 – Definition of inelastic strains [1]

The stress-strain relationship for the tensile part can be obtained by tests. If test results are not available theoretical values can be used instead. The CDP model for the tension part defined in Abaqus [1] is shown below in Fig. A.6. The craking strain is used in the model to simulate tension stiffening (reinforcement is modelled separately). Instead of a brittle failure, after cracking of the concrete stress usually drops in resistance gradually due to the interlocking of the cracks and other effects.

A.1.2.2 Parameter settings for CDP model and automation with CivilLab add-in

With the help of the "CivilLab-Abaqus" the above mentioned theoretical concrete CDP model can be automatically generated by specifying a few parameters. The resistance values are taken from Eurocode 2 by default but if some other strength values are

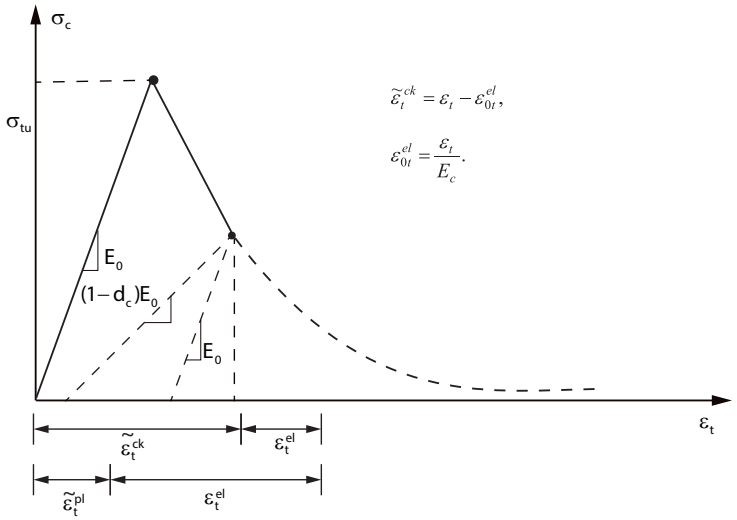

Figure A.6 – Definition of strain after cracking – tension stiffening [1]

provided, the original values will be overwritten. Different compression and tension stress-strain models can be used as shown in the Table A.3 below.

An input example:

```
from ABfoos import *
# to add concrete grade C20/25 in the model by using parabolic rectangle
# compression model and Wang&Hsu tensile model.
mycon=AddConcrete(Grade='C20/25',Model_C='EC2_parabolaRec',Model_T='Wang&Hsu',
    alphacc=0.85,Rows_C=10,Rows_T=5)
```

With this input, a concrete model with concrete grade name will be generated. If test data is used additional arguments for test values can be added to overwrite the original values. Due to page limitations, the details will not be shown here.

Compression models	keywords
Bilinear-fcd	fcd
Bilinear-fcm	fcm
Bilinear-fck	fck
Parabolic-Rectangle (EC2)	EC2_parabolaRec
EC2 nonlinear	EC2
GB50010 nonlinear	GB50010
Madrid parabola	Madrid_parabola
Desay & Krishnan	D&K
Wang & Hsu	Wang & Hsu

Tension models	keywords
Bilinear-ftm	Non
GB50010 nonlinear	GB50010
Wang & Hsu	Wang & Hsu

Table A.3 – The concrete compression and tension models for CDP model with CivilLab

A.2 Reinforcement

The bilinear stain-stress relationships by Eurocode 2 with and without strain-hardening is used in the analysis, the mechanical models are shown below:

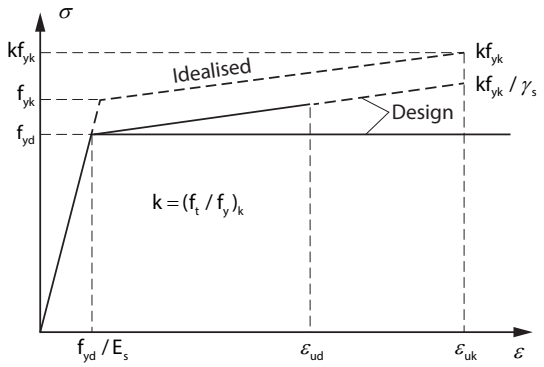

Figure A.7 – Reinforcement stress-strain relationship by Eurocode 2

The strain-hardening is considered by a factor k of the ratio between ultimate tensile strength to characteristic yielding strength. The yielding strain values can be calculated based on the strength and the elastic modulus E_s is 200GPa. The k values and the characteristic ultimate strain values "ε_{uk}" are given in EN1992-1-1.

Table A.4 – The suggestion values of f_{yk} and ε_{uk} for reinforcement according to EN1992-1-1

class	A	B	C
f_{yk} or $f_{0.2k}$	400 to 600Mpa		
k	$\geq$1.05	$\geq$1.08	1.15 to 1.35
ε_{uk} (‰)	$\geq$2.5	$\geq$5.0	$\geq$7.5

A.3 Structural steel

A.3.1 Bi-linear relationship defined by EN1993-1-5, Annex C

The following stress-strain relationship from EN1993-1-5 Annex C can be used. Four different models are provided: The model a is the design model without strain hardening. Model b considers a nominal plateau slop with a very small value, which can be similar to the model a. The model c is bilinear curve with strain hardening. The model d is the stress-strain curve modified from tests as:

$$\sigma_{true} = \sigma(1+\varepsilon)$$
$$\varepsilon_{true} = ln(1+\varepsilon)$$

The stress-strain relationship models are illustrated in figure below:

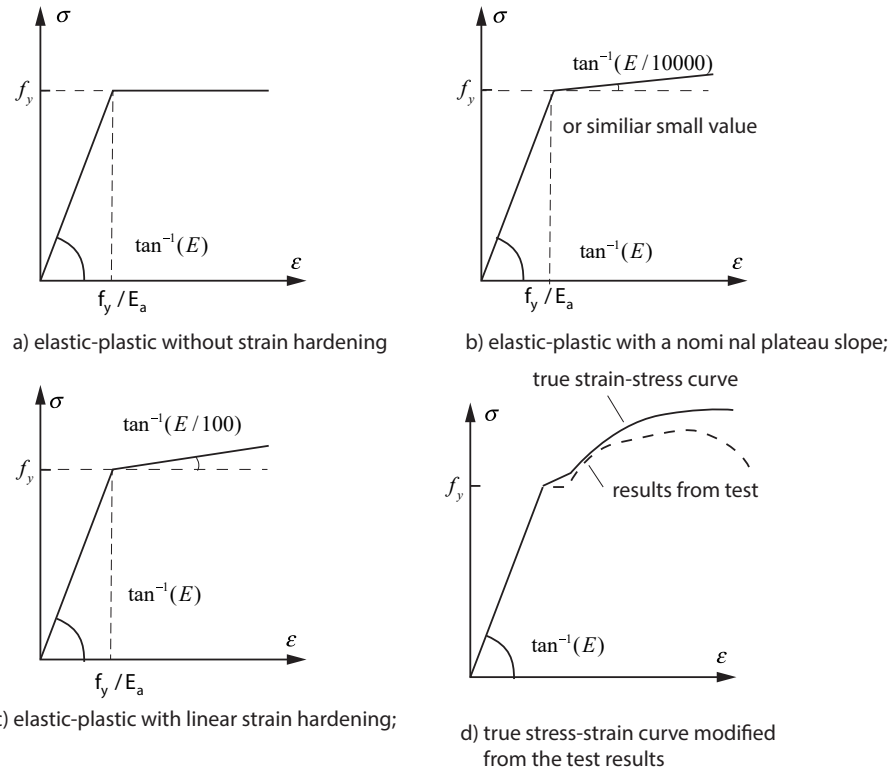

Figure A.8 – Steel stress-strain relationship by EN1993-1-5, Annex C

A.3.2 Tri-linear relationship

To consider both the plastic plateau as well the strain hardening of typical structural steel behaviour, often the tri-linear strain-stress relationship can be used. The model used in [4] is shown as below in Fig. A.9. After the initial elastic part, a horizontal line follows until reach strain hardening strain ε_{sh}. Afterwards a strain hardening part with modulus of E_{sh} is followed until to reach the ultimate strain ε_u. In [4] the value of ε_{sh} is taken as ten times of the elastic strain limit $\varepsilon_{sh} = 10 f_y / E_a$, and the $E_{sh} = 1/33 E_a$.

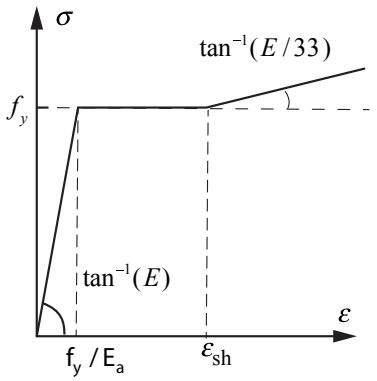

Figure A.9 – Steel stress-strain relationship by tri-linear model

A.3.3 Quart-linear relationship defined by prEN1993-1-14 (draft)

In the case of the more advanced analysis a non-linear curve from experimental tests or a multi-linear approximation according to the draft version of new prEN1994-1-14 [73]

can be used (The document is currently not yet the prEN1993-1-14 stage,only based on the draft document AHGFE-2018-014 Code version v6.6, further modification is possible in the final version draft). For the multi-linear curve the following parameters provided in the Fig. A.10 can be applied. These values are only suitable for hot-rolled steel sections. In the case of cold-formed steel and stainless steels sections other models should be applied.

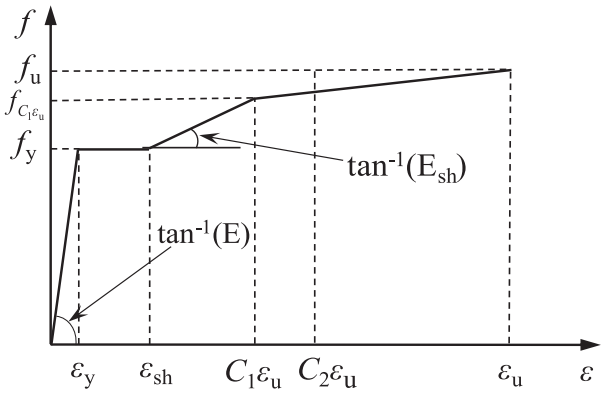

$$f(\varepsilon)=\begin{cases} \mathrm{E}\varepsilon & \text{for } \varepsilon \le \varepsilon_y \\ f_y & \text{for } \varepsilon_y < \varepsilon \le \varepsilon_{sh} \\ f_y + \mathrm{E}_{sh}(\varepsilon-\varepsilon_{sh}) & \text{for } \varepsilon_{sh} < \varepsilon \le C_1\varepsilon_u \\ f_{C_1\varepsilon_u} + \dfrac{f_u - f_{C_1\varepsilon_u}}{\varepsilon_u - C_1\varepsilon_u}(\varepsilon - C_1\varepsilon_u) & \text{for } C_1\varepsilon_u < \varepsilon \le \varepsilon_u \end{cases}$$

$$\varepsilon_{sh} = 0.1\frac{f_y}{f_u} - 0.055, \quad \text{but } 0.015 \le \varepsilon_{sh} \le 0.03$$

$$\varepsilon_u = 0.6\left(1 - \frac{f_y}{f_u}\right), \quad \text{but } 0.06 \le \varepsilon_u \le \mathrm{A}$$

$$\mathrm{E}_{sh} = \frac{J_u - J_y}{C_2\varepsilon_u - \varepsilon_{sh}}$$

$$C_1 = \frac{\varepsilon_{sh} + 0.25(\varepsilon_u - \varepsilon_{sh})}{\varepsilon_u} \qquad C_2 = \frac{\varepsilon_{sh} + 0.4(\varepsilon_u - \varepsilon_{sh})}{\varepsilon_u}$$

A is the elongation after fracture defined in the relevant material specification

Figure A.10 – Steel stress-strain relationship by multi-linear model according to prEN1993-1-14 (draft) [73]

Appendix B

Example of simplified strain-limited design approach with hand calculation and benchmarks with exact numerical methods

In this section, example of calculations according to the simplified strain-limited design method shown in section 3.5 is presented. In the example a slim-floor beam is shown. The steel profile is formed by a HEM220 beam weld with an additional 450×20 mm steel plate at bottom. The concrete slab has 13.5cm thickness above the profiled sheeting with effective width of 2.5m. the thickness of concrete above the top of steel profile is 5cm. All the steel parts has steel grade of S355 and C30/37 concrete is used. The cross-section is shown in Fig. B.1.

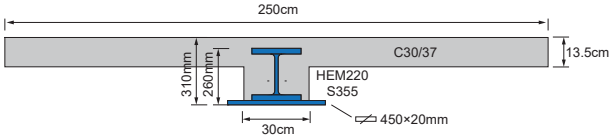

Figure B.1 – Cross-section of calculated beam in the example

B.1 Calculation results with the SL.com software

The calculation results with the software "SL.com" is shown below in Fig. B.2. The parabolic-rectangle strain-stress relationship as well as the bilinear steel strain-stress relationship without strain hardening is used. The software considers the exact steel profile shape including the curved fillet between steel web and flange. It also considers the reduction of concrete area taken by the steel profile. For the calculation the results are: $x_{sl} = \mathbf{117.52}\,mm$ and $M_{sl,Rd} = \mathbf{1361}\,kNm$.

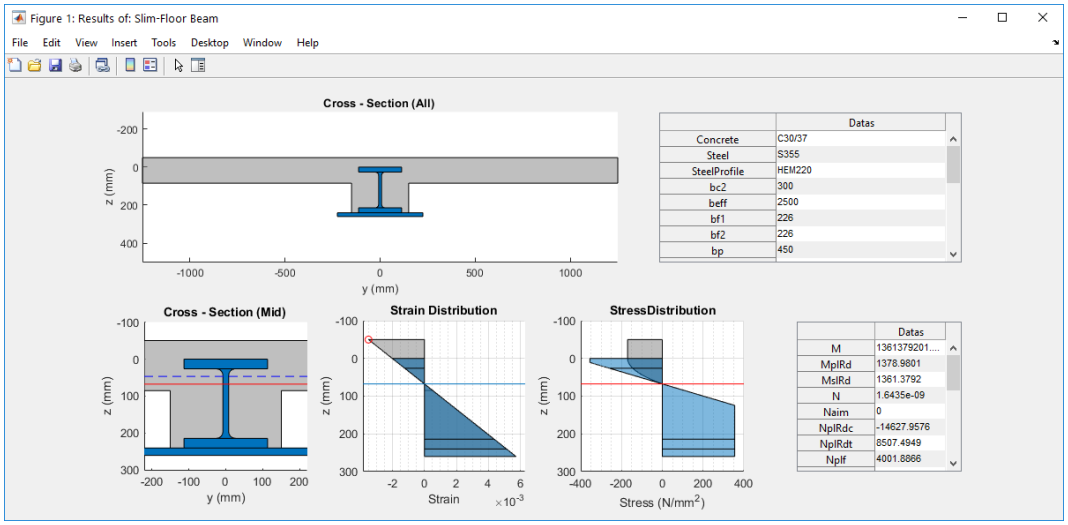

Figure B.2 – Calculation result of the slim-floor beam with SL.com

B.2 Calculation according to the simplified method in section 3.5

In this subsection, the calculation procedure according to the simplified method in section 3.5 is shown. First the key-points of steel section and concrete section need to be obtained and plotted. At the intersection of the two curves, the position of neutral axis x_{sl} can be found. And afterwards the resulting normal forces and bending moment at x_{sl} can be checked.

- Step 1: calculate points "ABCDE" and 'abcd'

$$0.85 \cdot f_{cd} = 0.85 \cdot \frac{30}{1.5} = 17N/mm^2; \qquad \varepsilon_{cu2} = 0.0035$$

$$f_y = 355N/mm^2; \qquad \varepsilon_y = \frac{f_y}{E_a} = 0.0017$$

$$h = 310mm; \qquad h_c = 145mm$$

$$b_{eff} = 2500mm; \qquad b_{c2} = 300mm$$

$$h_1 = h_{ct} + t_{f,t}/2 = 50 + 26/2 = 63mm$$

$$h_2 = h_{ct} + h_a = 50 + 240 = 290mm$$

$$z_{t,t} = h_1 \cdot \frac{\varepsilon_{cu}}{\varepsilon_{cu} + \varepsilon_y} = 50 \cdot \frac{0.0035}{0.0035 + 0.0017} = 42.48mm$$

$$z_{c,t} = h_1 \cdot \frac{\varepsilon_{cu}}{\varepsilon_{cu} - \varepsilon_y} = 121.8mm$$

$$z_{t,b} = h_2 \cdot \frac{\varepsilon_{cu}}{\varepsilon_{cu} + \varepsilon_y} = 195.5mm$$

$$A_{f,t} = b_f \cdot t_f = 226 \cdot 26 = 5876mm^2$$

$$A_w = (h_a - 2t_f) \cdot t_w = (240 - 52) \cdot 15.5 = 2914mm^2$$

$$A_{f,b+p} = A_{f,b} + A_p = 5876 + 450 \cdot 20 = 14876mm^2$$

- Step 2: calculate x_{sl} and $N_{v,sl}$

Results of Points "ABCDE" according to table.3.2

Points	x_i mm	f_t N/mm^2	f_b N/mm^2	N_w kN	$N_a - N_w$ kN	N_a kN
A	42.8	-355	355	1035	7367	8401
B	63	0	355	950	5281	6232
C	121.8	-355	355	601	3195	3796
D	195	-355	355	-209	3195	2985
E	290	355	0	-660	-2086	-2746

Points "abcd" according to Table.3.3

Points	x_i (mm)	N_c (kN)
a	135	4647
b	202	5782
c	310	6331
d	290	6245

After get all the points, the $N_i - x_i$ curves of concrete and steel beams can be plotted as shown in Eq. B.3 in solid line. The intersection points is the results for pure bending. From the Figure, x_{sl} is 116.6mm and the resulting total longitudinal shear force between concrete and steel $N_{v,sl}$ is **4014** kN.

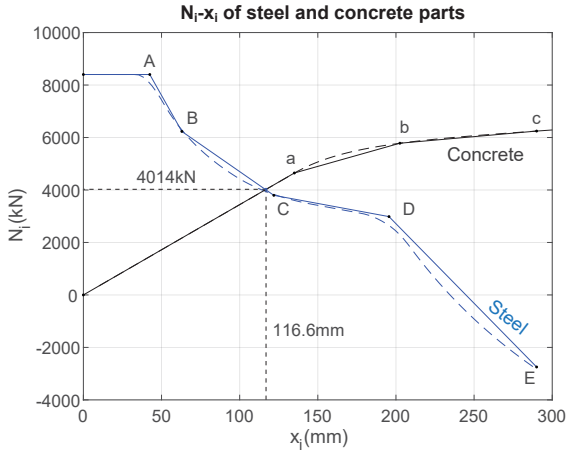

Figure B.3 – $N_i - x_i$ of the steel and concrete part

• Step 3.a: Calculate M_{sl}, N_a, N_c by direct analytical method

As the position of neutral axis x_{sl} has been obtained, now the normal forces and bending moment of $x_i = x_{sl}$ can be calculated by the direct analytical method in section 3.4.4. The calculated N_a and N_c should be compared with the $N_{v,sl}$ calculated from the simplified method. If the difference is more than 5% then the value (x_{sl},N_a) and (x_{sl},N_c) should be used as additional points in $N_i - x_i$ lines, then repeat from the Step 2 to calculate the new position of neutral axis x_{sl}, until the limits is fulfilled.

$$x_{sl} = 116.6mm; \quad x_{sl} < z_{ct}; \; x_{sl} < z_{tb}$$
$$f_{f,t} = (\frac{z_i}{x_i} - 1)\frac{\varepsilon_{cu2}}{\varepsilon_y} = (\frac{63}{116.6} - 1)\frac{3.5}{1.7} = -335.9N/mm^2$$
$$N_{f,t} = f_{f,t}A_f = -1974kN$$

$$f_{f,b} = fy = 355N/mm^2; \quad N_{f,b+p} = f_{f,b}(A_{f,b+p}) = 5280kN$$
$$h_t = (1+\frac{\varepsilon_y}{\varepsilon_{cu}})\cdot x_{sl} - (h_{ct}+t_f) = 97.23;$$
$$h_c = h - t_p - t_{f2} - (1-\frac{\varepsilon_y}{\varepsilon_{cu}})\cdot x_{sl} = 204.03;$$
$$N_w = f_y t_w (h_c - h_t) = 588kN$$
$$M_{f,t} = N_{f,t}(h_1 - x_{sl}) = -1974 * (63 - 116.6) = 105.8kNm;$$
$$M_{f,b+p} = N_{f,b+p}(h_2 - x_{sl}) = -5280 * (290 - 116.6) = 915.5kNm;$$
$$d = h_a - 2\cdot t_f = 240 - 26\cdot 2 = 188;$$
$$a_m = 3h_t(d-h_t) + 3h_c(d-h_c) + (h_c + h_t - d)^2 = 29573mm^2$$
$$M_w = N_w(h_c - h_t) + \frac{f_{f,b} - f_{f,t}}{12} a_m = 64.5kNm$$
$$N_a = N_{f,t} + N_{f,b+p} + N_w = \mathbf{3894}kN$$
$$M_a = M_{f,t} + M_{f,b+p} + M_w = \mathbf{1085.8}kNm$$

$$x_0 = 1 - \frac{h_c}{x_{sl}} = 1 - \frac{135}{116.6} = -0.16 < 0;$$
$$check\ \alpha_{N1}, \alpha_{N2}, \alpha_{M1}, \alpha_{M2}\ from\ Fig.\ 3.32$$
$$N_{c1} = 0.8095 \cdot f_{cd} b_{eff} x_i = 4011kN$$
$$N_{c2} = 0 \cdot f_{cd} b_{c2} x_i = 0kN$$
$$M_{c1} = \alpha_{M1} \cdot f_{cd} b_{eff} x_i^2 = 273.2kNm$$
$$M_{c2} = 0 \cdot f_{cd} b_{c2} x_i^2 = 0kNm$$
$$N_c = N_{c1} + N_{c2} = \mathbf{4011}kN$$
$$M_c = M_{c1} + M_{c2} = \mathbf{273.2}kNm$$

$$\frac{|N_a - N_{vsl}|}{N_{vsl}} = \frac{|3894 - 4014|}{4014} = 3.0\% < 5\%$$
$$\frac{|N_c - N_{vsl}|}{N_{vsl}} = \frac{|4011 - 4014|}{4014} = 0.1\% < 5\%;$$
$$\Rightarrow no\ need\ for\ addtional\ points$$
$$M_{sl,Rd} = M_a + M_c = \mathbf{1359}kNm$$

• Step 3.b: Integral strain method

Similarly as Step 3.a, the M_{sl}, N_a, N_c can also calculated by the Integral strain method according to section 3.4.3. This method do not need to simplify the flanges and additional plates as line member, thus gives more accurate results.

Steel parts (T.F: top flange, B.F : bottom flange)

Layers	1	2	3	4	5
z_i(mm)	50	76	264	290	310
ε_i (‰)	-1.9	-1.2	4.4	5.2	5.8
$n_s(\varepsilon_i)$ (N/mm^2)	0.409	0.156	1.270	1.548	1.761
$m_s(\varepsilon_i)$ (kN/mm^2)	-0.540	-0.127	3.306	4.640	5.813
	T.F (1-2)	Web (2-3)	B.F (3-4)	Plate (4-5)	Σ
b_i (mm)	226	15.5	226	450	
N_i(kN) $^{Eq.3.6}$	-1910	575	2086	3195	**3946**
M_i(kNm) $^{Eq.3.7}$	103.7	59.0	334.6	586.0	**1083.3**

Concrete parts:

Layers	1	2	3
z_i(mm)	0	135	290
ε_i (‰)	-3.5	0.55	5.21
$n_s(\varepsilon_i)$ (N/mm^2)	0.0482	0	0
$m_s(\varepsilon_i)$ (kN/mm^2)	0.0985	0	0
	Top part	Chamber part	Σ
b_i (mm)	2500	300	
N_i(kN) $^{Eq.3.6}$	4011	0	**4011**
M_i(kNm) $^{Eq.3.7}$	273.2	0	**273.2**

$$\frac{|N_a - N_{vsl}|}{N_{vsl}} = \frac{|3946 - 4014|}{4014} = 1.7\%; < 5\%;$$
$$\frac{|N_c - N_{vsl}|}{N_{vsl}} = \frac{|4011 - 4014|}{4014} = 0.1\%; < 5\%;$$
$$\Rightarrow no\ need\ for\ addtional\ points$$
$$M_{sl,Rd} = M_a + M_c = 1083.3 + 273.2 = \mathbf{1356.5} kNm$$

Compared to the SL.com numerical results, the results by simplified method are very similar. If the cross-section geometry is simplified, for which the steel profile fillet radius is neglected and the concrete area taken by steel profile is not considered. The numerical results are $x_{sl} = \mathbf{115.48} mm$ and $M_{sl,Rd} = \mathbf{1355} kNm$, which are even closer.

B.3 Verification of the simplified design methods

To check the reliability of the simplified method, parametric studies on different slim-floor cross-sections and material properties has been carried out. The parameter sets are shown in Table.B.1. In total more than 240,000 cross-sections have been calculated. For each cross-section, the bending resistance ($M_{sl,nl}$) and neutral axis location ($x_{sl,nl}$) calculated by numerical procedures (finite fiber method) considering the exact cross-sections including the round corners between the steel web and flange as well the reduction of concrete areas due to embedded steel sections are used as reference. The results ($M_{sl,e}$, $x_{sl,e}$) calculated by the exact procedure in section 3.4.4, the results ($M_{sl,m}$, $x_{sl,m}$) by the strain integral method in section 3.4.3 and the simplified method ($M_{sl,s}$, $x_{sl,s}$) are compared with the numerical calculation results.

Compared to the numerical calculation results by finite fiber method, the exact methods and the simplified method give usually smaller values of bending moment resistance

Table B.1 – Parameter sets for verification

h_{ct}	Profile*	Concrete	Steel	b_{eff}/h	h_p
50	IFB, SFB	C20/25	S235	4	75
100	ASB, UPE	C30/37	S275	6	100
150	Delta	C40/50	S355	8	150
	USFB	C50/60	S420	10	200
	SWT		S460		250

*: In total 327 different steel profiles for slim-floor beams are considered. In the list only their general groups are given. The units of h_{ct}, h_p is mm

and location of neutral axis. It is due to by these methods, the steel rounded corner is not considered, which reduced the effective cross-section area. Although without reduction of the embedded steel sections area, the concrete area by these methods are bigger, the increase is comparably small for most of the time. The differences in bending resistance compared to the nonlinear method is less than 4% (0.5% in average) and mostly towards the safe side. The the differences in location of neutral axis is also less than 5% (1% in average). Thus they are still reliable to use for the design

Compare the results of the simplified method and the exact methods, the maximum

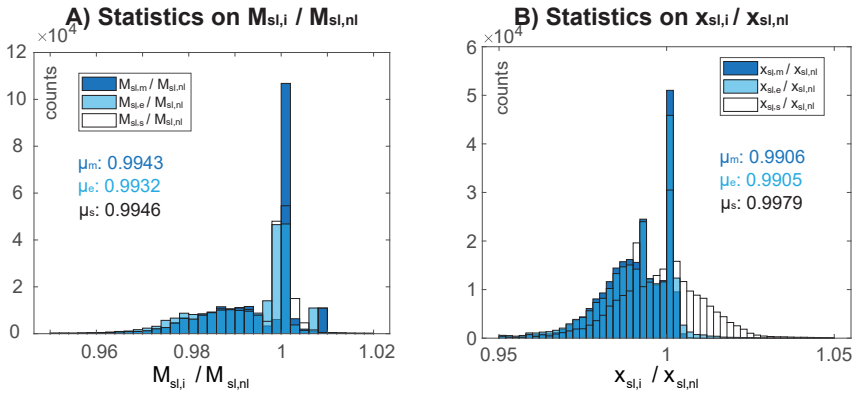

Figure B.4 – Statistics for comparison of different methods

difference of bending moments is around 2%, and more than 98% of all the 240,000 data shows the differences of $M_{sl,s}$ and $M_{sl,m}$ are smaller than 0.5%. The location of neutral axis according to the two methods shows mostly differences less than 5%. Usually the simplified methods slightly overestimated the compression zone height. The compression results are shown below in Fig. B.5.

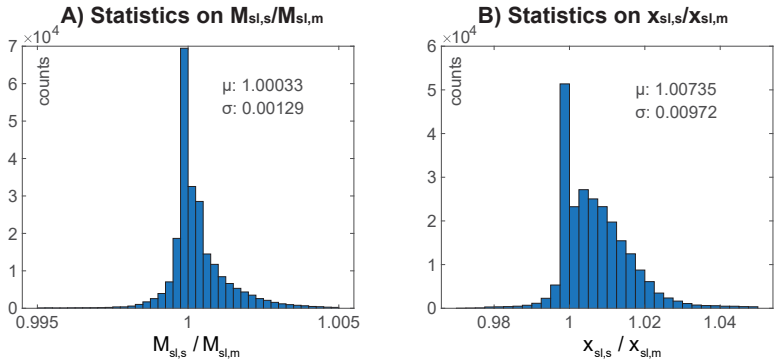

Figure B.5 – Statistics for comparison of simplified and exact method

Appendix C

Calibration and sensitivity test for FEM models

In order to benchmark the FE-model of composite beams with regard to the load-deflection curve, several parameters are evaluated by performing analysis with the FEM software Abaqus. The impact of these parameters on the results, mainly on properties such as the stiffness or resistance, is examined. In the next few pages the parametric studies of the following parameters will be presented.

- Mesh density
- Shear connector radius
- Load pad size
- Friction
- Material behaviour (Steel and concrete)
- Shear connector stiffness

C.1 Referenced existing tests in [67]

In this chapter, the FEM models from section C.2 to section C.9 are benchmarked with the static loading tests from Nie and Yuan [67]. In total 16 simply supported composite beams (CBS-1 to CBS-16) were tested with different shear span aspect ratio from 1.0 to 4.0. Here only the ones designed for bending failure with high shear span ratios are used for benchmark as bending failure is main focus in the research. The beams are reported to be designed with full shear connection, however the push-out results of shear connectors are not provided. Thus theoretical values are taken for the simulation of shear connectors.

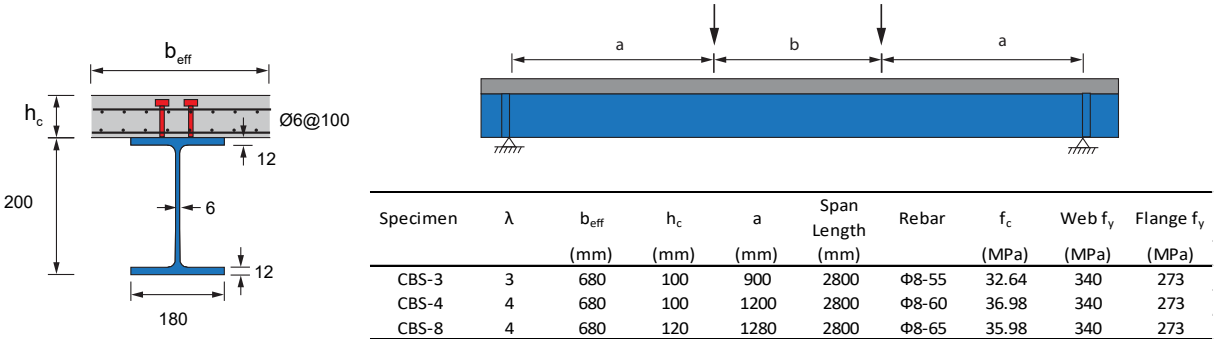

Specimen	λ	b_{eff} (mm)	h_c (mm)	a (mm)	Span Length (mm)	Rebar	f_c (MPa)	Web f_y (MPa)	Flange f_y (MPa)
CBS-3	3	680	100	900	2800	Φ8-55	32.64	340	273
CBS-4	4	680	100	1200	2800	Φ8-60	36.98	340	273
CBS-8	4	680	120	1280	2800	Φ8-65	35.98	340	273

note: λ=a/h, h is height of composite beam

Figure C.1 – The parameters of composite beam tests from Nie and Yuan [67]

C.2 Mesh density

The first parameter to benchmark is the mesh density. To evaluate the influence of the mesh density, FE-models with three different mesh densities are performed and compared with each other.

- Uniform mesh density of the concrete slab
- Higher mesh density in the center of the concrete slab near the area of the shear stud
- Double mesh density in the concrete slab

The following Figure shows the curves for different mesh densities obtained from the FE-analysis.

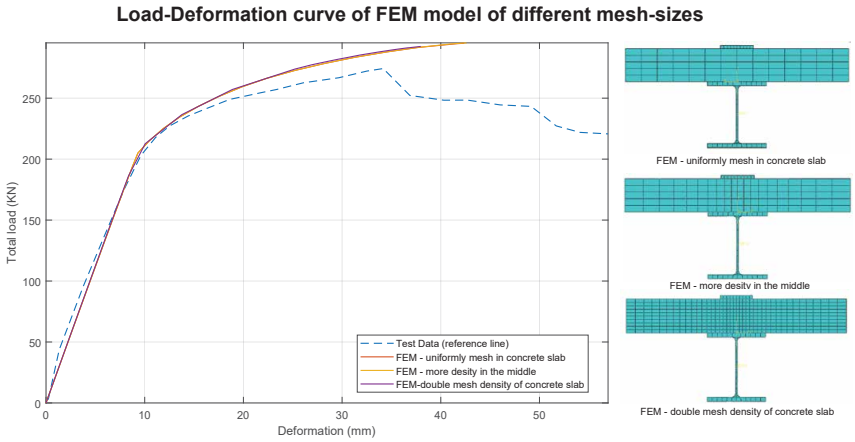

Figure C.2 – Parameter study on different mesh densities (Test data CBS-3 from [67])

Besides the three curves representing the results obtained for the different mesh densities, the fourth dashed curve, given in Fig. C.2, represents the results of an experiment and serves only as a general reference, given that the calculation parameters were not yet calibrated. By analyzing the three different curves, it can be noticed that the mesh density does not have an important impact on the results. This can be deducted from the fact that the stiffness of all the three curves is almost equal. Moreover, only a very

small difference in the resistance can be noticed. The yellow curve, which represents the double mesh density in the concrete slab, shows a remotely smaller resistance compared to the two other curves. Given all of the above, it can be concluded that the original mesh is still appropriate for the simulation, as mesh density does not impact the results significantly.

C.3 Load pad size

Due to the fact that model was loaded with concentrated loads, the concrete near the load introduction area exhibits very big compression stress. In order to avoid local failure, usually a steel load pad can be modelled so as to distribute the compression load to a bigger area. With the aim of evaluating the influence of the load pad size on the results, three different sizes of the load pad are set and analyzed with the FEM software Abaqus. The following pad sizes are used for the comparison. All the load pads are modeled with 10mm thickness.

- Load pad size 100 mm
- Load pad size 150 mm
- Load pad size 200 mm

The following Figure shows the curves for different load pad sizes obtained from the FE-analysis.

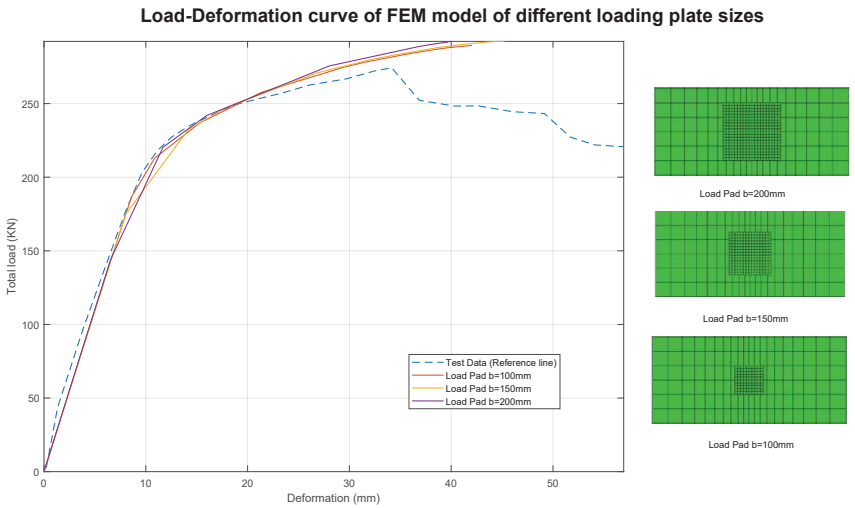

Figure C.3 – Parameter study on different load pad sizes (Test data CBS-3 from [67])

As it can be noticed from the Fig. C.3, the load pad size has not an important influence on the stiffness or resistance when the size is above certain level - another load pad of 50mm length was being examined and have induced local failure of the concrete causing the simulation to stop at very early stage.

C.4 Friction between steel and concrete beam

Another benchmarked parameter is the friction factor, which describes the friction in the composite joint between the steel beam and concrete slab. To evaluate the influence

of the friction factor on the results, the following five different friction factors are used for the FE-analysis.

- Friction factor 0
- Friction factor 0.2
- Friction factor 0.4
- Friction factor 0.6
- Friction factor 0.8

The following Figure shows the curves for different friction coefficients obtained from the FE-analysis.

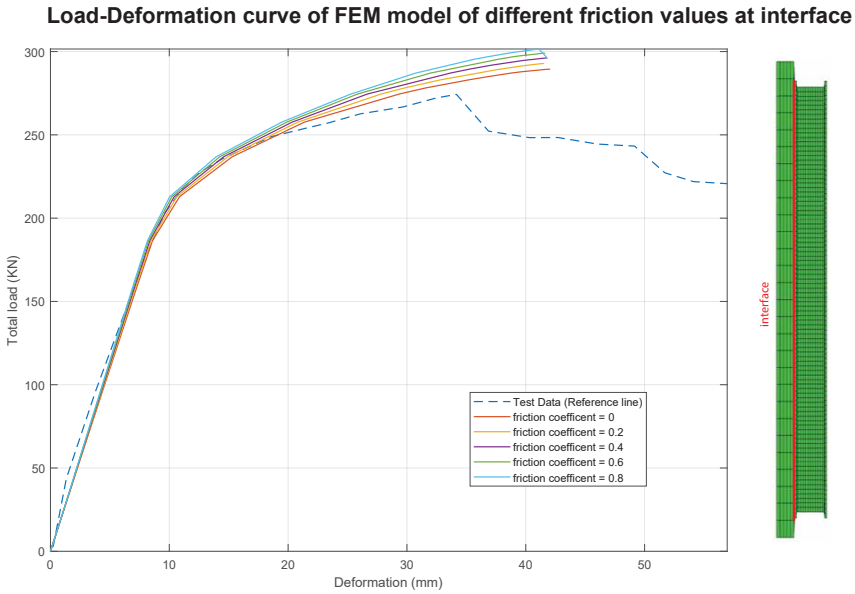

Figure C.4 – Parameter study on different friction factors (Test data CBS-3 from [67])

By comparing the curves from the Fig. C.4, it can be noticed that the stiffness in the plastic range is dependant on the friction factor. The stiffness is affine to the friction factor, which means that a higher friction factor generates a higher stiffness. Due to this fact, it can be deducted that a higher friction factor has the same effect as an increase in the number of the shear connectors, which is expected.

C.5 Influence of different steel material models

For the benchmark of the steel material model, the following material behaviour models provided in EN1993-1-5 are analysed. The bilinear model without strain hardening suggests post yielding stiffness as 1/100000 of the Ea. The bilinear model with strain hardening suggests post yielding stiffness as 1/100 of the Ea.

- Bi-linear material behaviour model
- Bi-linear material behaviour model with strain hardening
- Bi-linear material behaviour model with strain limitations

The following Figure shows the curves for differentmaterial models obtained from the FE-analysis.

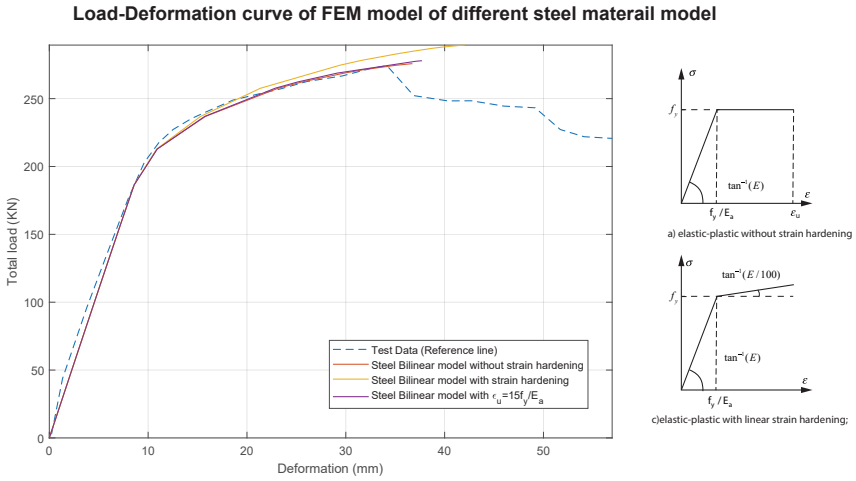

Figure C.5 – Parameter study on different steel material models (Test data CBS-3 from [67])

From the Fig. C.5 a difference in the post yielding stiffness and overall resistance can be observed. The strain-limits do not make a difference in this model as the failure type is not controlled by the steel beam.

C.6 Influence of different concrete material models

For the benchmark of the concrete material model, the following material behaviour models, provided in EN1992-1-1, are analysed. The tensile resistance is modeled as f_{ctm} according to Eurocode 2 if tension softening/stiffening is not considered. Otherwise it is modelled as suggested by "Wong&HSu", which explained before.

- Non-linear material behaviour model
- Non-linear material behaviour model with tension softening
- Bi-linear material behaviour model
- Parabolic rectangle material behaviour model
- Parabolic rectangle material behaviour model with tension softening

The following Figure shows the curves for different concrete material models obtained from the FE-analysis.

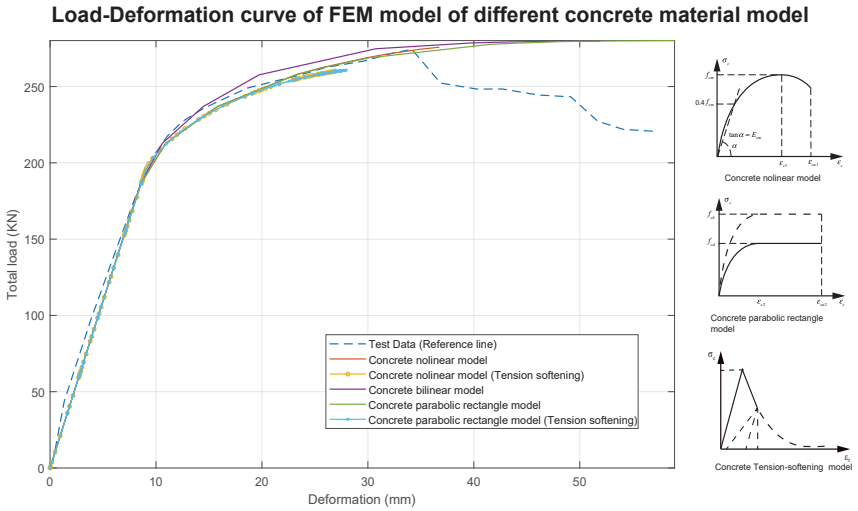

Figure C.6 – Parameter study on different concrete material models (Test data CBS-3 from [67])

The non-linear model and parabolic model predict generally similar results in terms of the stiffness while the bi-linear model shows a bigger difference (Fig. C.6). The parabolic model without strain-limitations overestimate the deflection, while the non-linear model gives the best results. If tension softening is considered, the stiffness in plastic stages is smaller compared to the case when tensile resistance is assumed as constant value. However detailed reinforcement is necessary in this case in order to avoid local failure.

C.7 Influence of different shear connector stiffness

The influence of the shear connector's stiffness is also analysed with the FEM software Abaqus, in order to evaluate its impact on the results. Shear connectors based on a bilinear model with different stiffness and behaviour are evaluated.

- Bilinear model with intial stiffness of 35kN/mm
- Bilinear model with intial stiffness of 70kN/mm
- Bilinear model with intial stiffness of 140kN/mm
- Bilinear model with non-linear model

The following Figure shows the curves for different stiffness of the shear connectors obtained from the FE-analysis.

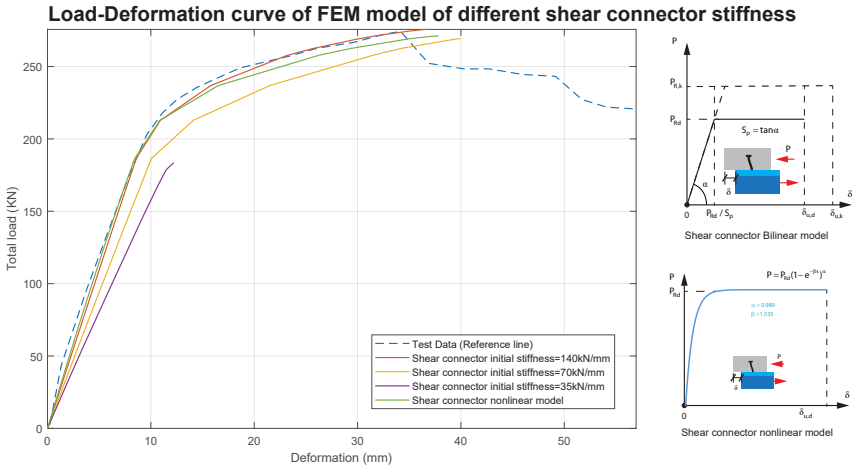

Figure C.7 – Parameter study on different shear connector stiffness (Test data CBS-3 from [67])

Calculation with stiffness equal to 35 kN/mm predicts a buckling failure of the steel beam due to the steel upper flange being subjected to compression in both longitudinal and vertical direction (Fig. C.7). The stiffness of each curve is different in the elastic range. Due to this fact, it can be deducted that the stiffness of the shear connectors has a big impact on the stiffness of the composite section in the elastic range. Also the stiffness can reduce the bending resistance if the shear connectors are too soft, due to the fact that shear connectors near mid-span do not have enough deformation to reach their resistance.

C.8 Influence of different shear connector influence radius

The impact of the radius around the shear connector is evaluated by performing FE-analysis with different radius sizes around the shear connector. Moreover, the load sharing between the nodes is defined either by the types Uniform or Linear. The type Uniform distributes the loads equally on all the nodes, whereas with type Linear the load decreases with the increasing distance to the shear connector. By changing this parameter the local impact of shear connectors on the concrete slab and steel beam can be changed - if the value is too small, the calculation may stop due to stress concentration near the shear connectors. On the other hand if it is too big, the local impact will not be represented correctly.

- Uniform 100 mm
- Uniform 150 mm
- Uniform 200 mm
- Uniform 500 mm
- Liner 100 mm
- Liner 150 mm
- Liner 200 mm
- Liner 500 mm

The following Figure shows the curves for different mesh densities obtained from the FE-analysis.

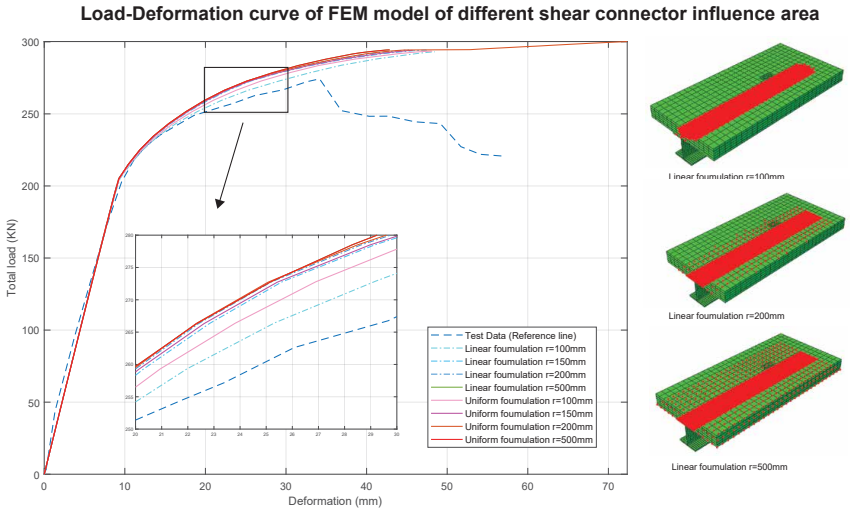

Figure C.8 – Parameter study on different shear connector radius (Test data CBS-3 from [67])

In Fig. C.8 the test data is only given as a general reference and is not used for the evaluation. In the case of the Linear option the loads are more concentrated near the shear studs compared with the Uniform ones. Due to this fact it can be deducted that the type, which defines the load sharing between the nodes, has not a big impact on the results. In contrast, the size of the radius has a greater impact on the results. The initial stiffness in the elastic range is independent of the radius, whereas the stiffness in the plastic range depends on the size of the radius. For a radius smaller than 150 mm, an increase of the radius will increase the stiffness in the plastic range. By increasing a radius of 200 mm, the increase of the stiffness in the plastic range will be smaller. Due to the fact that the push-out results represent the overall stiffness of shear connectors, if the radius is too small, additional concrete deformation will reduce the shear connector stiffness, which is not ideal. Therefore, a bigger radius is more suitable as it prevents the local failure of the concrete around the shear studs.

C.9 Choice of the parameters and benchmark with tests results

After these parametric studies, it can be concluded that a combination of the following settings should give the best representation of the test results:

- Mesh size : default
- Load pad size : 100mm
- Steel model : bi-linear with strain-hardening
- Concrete : nonlinear model considering tension-softening
- Friction : 0.2
- Shear studs : non-linear model with influence area of 300mm

Benchmark with different test groups by using the same parameter settings are shown below in the figure:

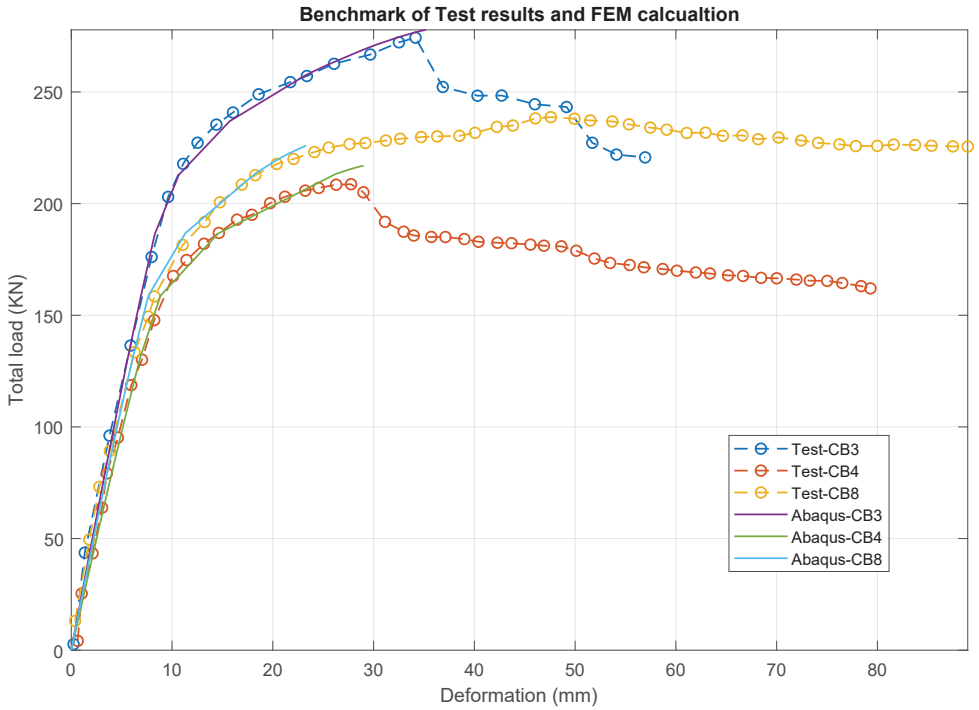

Figure C.9 – Parameter study on different shear connector radius (Test data from [67])

All of the three simulations show very similar results with the tests regarding the stiffness and the resistance. The test CB8 shows greater deflection capacity than the FEM simulation. However, the rest two simulations predict precisely the deflection at failure. With the Abaqus standard solver it is not possible to calculate the post-failure behavior - an explicit simulation may give better results. However, it should be noted that it requires greater numerical demand.

C.10 The modified shear connector model for headed studs together with profiled sheeting

In the benchmark of load-deflection test curve from composite beam in combination of profiled sheeting in section 5.2.2 shows a softening decrease of resistance after reaching the peak value. If the push-out results are directly used as shear connector load-deformation relationship in the simulation, usually the higher resistances are obtained compared with the tests and the softening behavior can not be simulated. Research work in [28] suggested it is caused by the different behavior of shear connectors in push-out tests and beam tests, thus a non-linear part in shear connector load-deflection curve is suggested. Here a similar tri-linear model shear connector load-deflection model is proposed as shown in Fig. C.12.

To better evaluate the influence of the drop in the tri-linear model, further analyses were performed with different percentages of drop in the resistance. The tri-linear models with different percentages of drop in the resistance are shown in Fig. C.10 A). Further analyses were performed to investigate the influence of different decreasing ratios of the drop part in the tri-linear model. The tri-linear models with different decreasing ratios for the drop are shown in Fig. C.10 B), whereas the corresponding load-deflection curves are shown in Fig. C.12.

To get the post-failure behavior, the deformation controlled method is used in Abaqus, with symmetrical point loads applied near mid span. The beam cross-section and material proprieties are base the beam specimen 2-02 from DISSCO test program [58]. The beam has IPE300 profile, with 5m span and b_{eff} equal to 1.25m, the concrete slab is 130mm with CP60 decking.

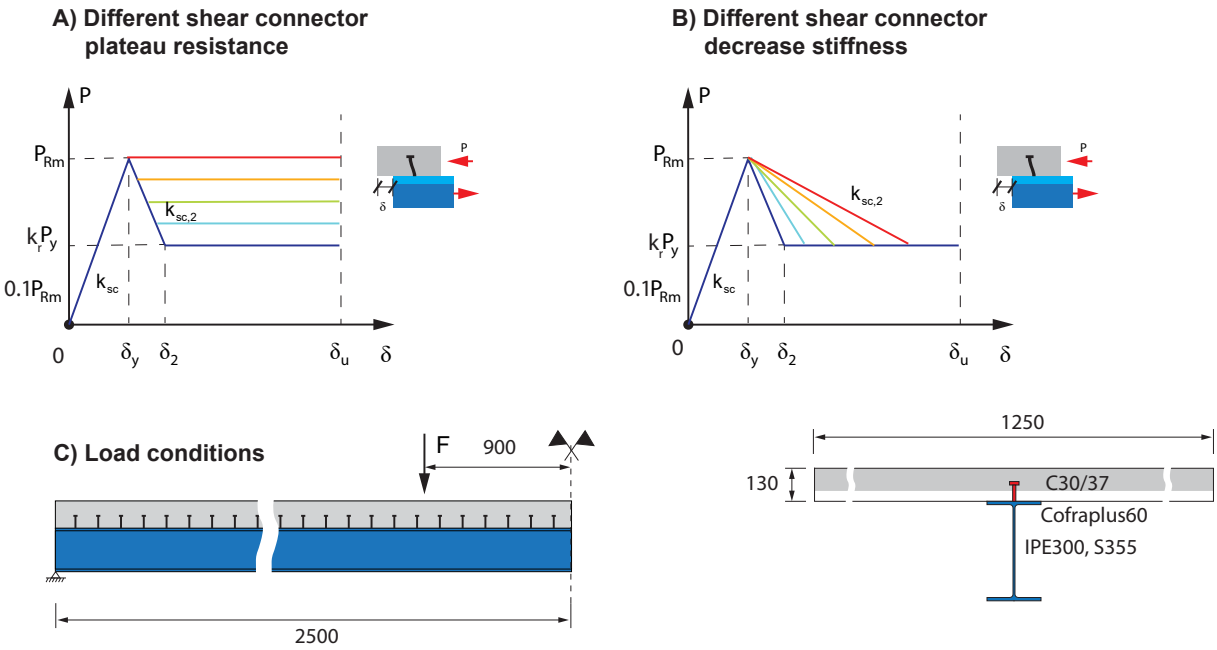

Figure C.10 – Load-slip curves for tri-linear models with different drop percentages and plateau height

By comparing the load-deflection curves from Fig. C.11, it is obvious that the drop of the resistance in the tri-linear model has an impact on the bearing capacity. The bearing capacity of the composite beam decreases with increasing drop percentage in the tri-linear model.

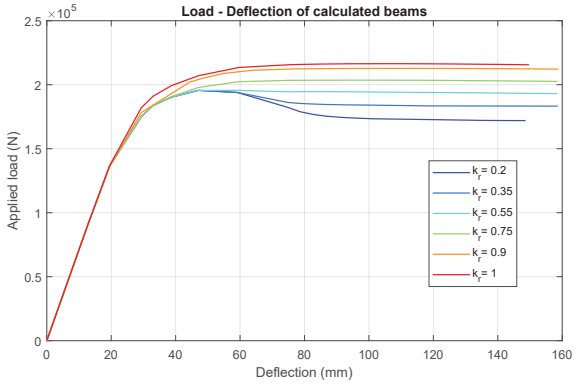

Figure C.11 – Load-deflection curves for tri-linear models with different decreasing part

Figure C.12 shows that the decreasing ratio of the drop impacts even more the bearing capacity. Especially for high decreasing ratios the composite beam loses earlier stiffness and consequently the bearing capacity decreases.

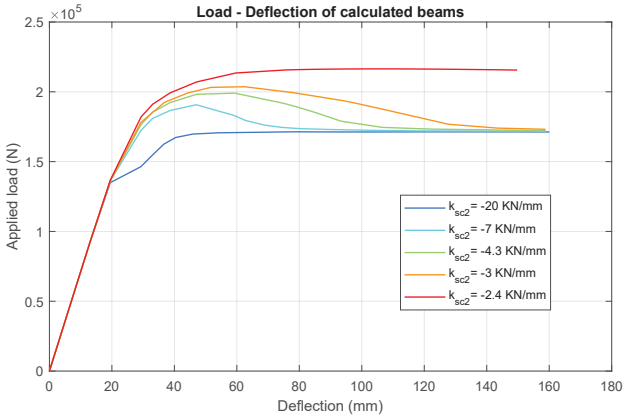

Figure C.12 – Load-deflection curves for tri-linear models with different decreasing part

The parametric studies shows the impact of the softening part of shear connector load-deflection relationship based on a tri-linear model. However to link the simplified model with the real composite beam, further analysis are still necessary.

Appendix D

The longitudinal shear force distribution of a simply beam in elastic-plastic stage

In this appendix, the details about the analytical equations related to the plastic zone development and longitudinal shear force in section 7.1.1 are provided. The basic mechanical model, differential equations and the detailed mathematical solutions are given first. Then the benchmark with FEM calculation using ANSYS are given as proof of the analytical solution.

D.1 Longitudinal shear stress distribution in elastic stage

A beam is under two same concentrated loads "F" near middle span, which has the symmetric location. It is known that, between the loads and end-support, shear stress keeps constant and bending moment increases linearly. Considering the beam is in the elastic stage, normal stress keeps linear. Assuming to take out an infinitely small slice of the beam of length d_x between cross section 1-1 and 2-2. Because of shear force V, the moment at each side will be different. For 1-1: $M_1 = M$ and for 2-2: $M_2 = M + dM = M + V d_x$. The stress at each side$\sigma_1(z), \sigma_2(z)$ will also be different. Separate the lower part of the slice at $z = m$, (Fig.D.1 b)) the following equilibrium can be made:

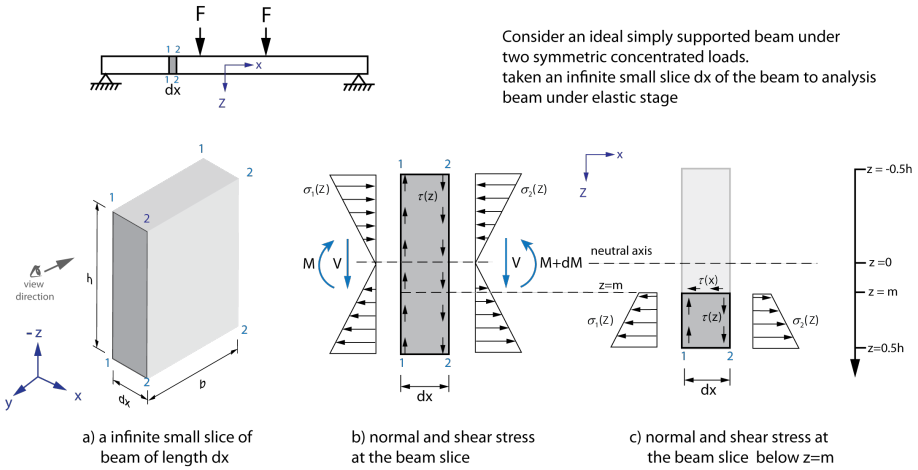

Figure D.1 – Shear stress at elastic stage

$$
\begin{aligned}
\sum F(x) &= 0 \\
\tau(m)bdx &= \int_{h/2}^{m} \sigma_2(z)b \cdot dz - \int_{h/2}^{m} \sigma_1(z)b \cdot dz \\
\tau(m)bdx &= (\int_{h/2}^{m} \sigma_2(z)dz - \int_{h/2}^{m} \sigma_1(z)dz)b \\
\tau(m)dx &= \int_{h/2}^{m} \sigma_2(z)dz - \int_{h/2}^{m} \sigma_1(z)dz \\
For\,beam\,in\,elastic\,stage: \sigma(z) &= \frac{Mz}{I_y} \\
\tau(m)dx &= \int_{h/2}^{m} \frac{M_2 z}{I_y}dz - \int_{h/2}^{m} \frac{M_1 z}{I_y}dz \\
\tau(m)dx &= \int_{h/2}^{m} \frac{V dx \cdot z}{I_y}dz \\
set: S_z(m) &= b\int_{h/2}^{m} z \cdot dz \\
\tau(m) &= \frac{V S_y(m)}{I_y b}
\end{aligned}
\tag{D.1}
$$

D.2 Longitudinal shear stress distribution in inelastic stage

Assuming the beam is made of an ideal bi-linear material with yielding strength of f_y and has unlimited deformation ability as shown in Eq. D.3 and Eq. D.4, when bending moment exceeds the elastic bending moment resistance, part of the beam cross section will enter the plastic stage. However the basic equilibrium of stress in Eq. D.2 is still valid. In the stage the calculation can be performed with the following additional assumptions:

- Beam made of a ideal bi-linear material with yielding strength of f_y.
- Unlimited strain and unlimited deformation ability.
- Applied bending moment between the elastic bending resistance and plastic moment resistance.

- stress concentration near supports and concentrated loads applied area is not considered

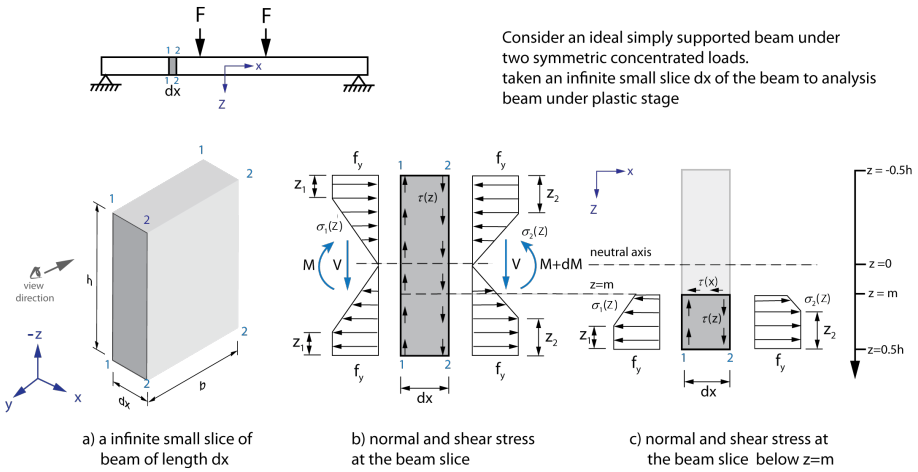

Figure D.2 – Stress distribution at elastic-plastic stage

$$\tau(m)dx = \int_{h/2}^{m} \sigma_2(z)dz - \int_{h/2}^{m} \sigma_1(z)dz$$

$$\tau(m)dx = \int_{h/2}^{m} (\sigma_2(z) - \sigma_1(z))dz \tag{D.2}$$

for stress:

$$\sigma_1(z) = \begin{cases} f_y & ; h/2 - z_1 < z \leq h/2 \\ f_y \cdot \frac{z}{h/2 - z_1} & ; -(h/2 - z_1) < z \leq h/2 - z_1 \\ -f_y & ; -h/2 < z < -(h/2 - z_1) \end{cases} \tag{D.3}$$

$$\sigma_2(z) = \begin{cases} f_y & ; h/2 - z_2 < z \leq h/2 \\ f_y \cdot \frac{z}{h/2 - z_2} & ; -(h/2 - z_2) < z \leq h/2 - z_2 \\ -f_y & ; -h/2 < z \leq -(h/2 - z_2) \end{cases} \tag{D.4}$$

then:

$$\sigma_1(z) - \sigma_2(z) = \begin{cases} 0 & ; h/2 - z_1 < \mid z \mid < h/2 \\ f_y(1 - \frac{z}{h/2 - z_2}) & ; h/2 - z_2 \leq z < h/2 - z_1 \\ -f_y(1 + \frac{z}{h/2 - z_2}) & ; -(h/2 - z_1) \leq z < (h/2 - z_2) \\ f_y \frac{(z_2 - z_1)z}{(h/2 - z_1)(h/2 - z_2)} & ; 0 \leq \mid z \mid < h/2 - z_2 \end{cases} \tag{D.5}$$

Taken **Eq.** D.5 into **Eq**.D.2 :

To calculate $\tau(m)$, for situation $h/2 - z_2 < \mid m \mid \leq h/2$, $\sigma_1(z) - \sigma_2(z) = 0$, thus it can be easily concluded that no shear stress exist ($\tau(m)$ = 0).

For situation $h/2-z_1 \geq \mid m \mid$ where m is the calculation point. Because $\sigma_1(z)-\sigma_2(z)$ is not continuous, the formula can be solved by subsection integral. When m>0 the integral area can be divided into three parts as shown in Fig D.3 (b). For the case of m<0 same results can be found by following the same calculation steps, the detailed calculation is not shown to avoid repetition.

$$\tau(m)dx = \int_m^{h/2-z_2}(\sigma_2(z)-\sigma_1(z))dz + \int_{h/2-z2}^{h/2-z1}(\sigma_2(z)-\sigma_1(z))dz + \int_{h/2-z1}^{h/2}(\sigma_2(z)-\sigma_1(z))dy$$

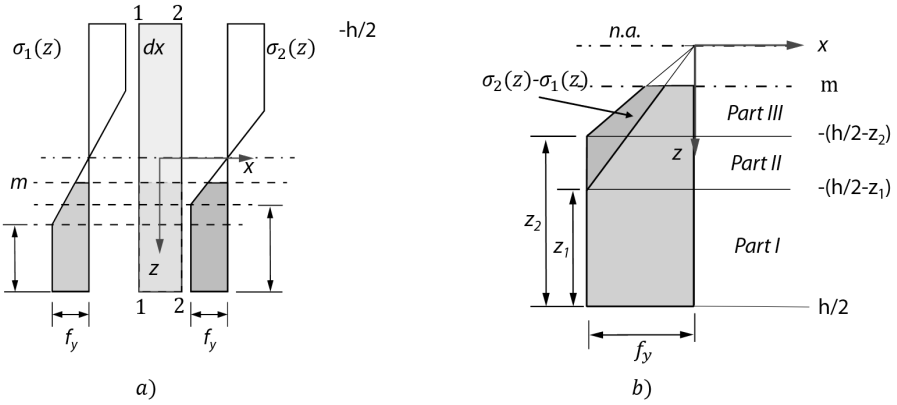

Figure D.3 – Stress at surface 1-1 and 2-2

Part 1: for $h/2-z_1 < z < h/2$:

$$\begin{aligned}\int_{h/2-z_1}^{h/2}(\sigma_2(z)-\sigma_1(z))dz &= \int_{h/2}^{h/2-z1} 0dz \\ &= 0\end{aligned}$$

Part2: for $h/2-z_2 \leq z < h/2-z_1$:

$$\begin{aligned}\int_{h/2-z_2}^{h/2-z_1}(\sigma_2(z)-\sigma_1(z))dz &= \int_{h/2-z_1}^{h/2-z_2}(f_y(1-\frac{z}{h/2-z_2}))dz \\ &= f_y\int_{h/2-z_1}^{h/2-z_2}(1-\frac{z}{h/2-z_2})dz \\ &= f_y(z-\frac{z^2}{h-2z_2})\mid_{h/2-z_1}^{h/2-z_2} \\ &= f_y[(z_2-z_1)-\frac{(h/2-z_1)^2-(h/2-z_2)^2}{h-2z_2}] \\ &= f_y\frac{(z_2-z_1)^2}{h-2z_2}\end{aligned}$$

Part 3: for $h/2-z_2 \geq z > m$:

$$\begin{aligned}\int_{m}^{h/2-z_2}(\sigma_2(z)-\sigma_1(z))dz &= \int_{h/2-z_2}^{m}(f_y\frac{(z_2-z_1)z}{(h/2-z_1)(h/2-z_2)})dz \\ &= f_y\frac{2(z_2-z_1)z^2}{(h-2z_1)(h-2z_2)}\,|_{h/2-z_2}^{m} \\ &= f_y\frac{2(z_2-z_1)}{(h-2z_1)(h-2z_2)}((h/2-z_2)^2-m^2)\end{aligned}$$

then:

$$\begin{aligned}\tau(m)dx &= \int_{m}^{h/2-z_2}(\sigma_2(z)-\sigma_1(z))dz+\int_{h/2-z_2}^{h/2-z_1}(\sigma_2(z)-\sigma_1(z))dz+\int_{h/2-z_1}^{h/2}(\sigma_2(z)-\sigma_1(z))dz \\ &= f_y\frac{(z_2-z_1)^2}{h-2z_2}+f_y\frac{2(z_2-z_1)}{(h-2z_1)(h-2z_2)}((h/2-z_2)^2-m^2) \\ \tau(z) &= f_y\cdot\frac{(z_2-z_1)}{(h-2z_2)dx}[(z_2-z_1)+2\frac{(h/2-z_2)^2-z^2}{(h-2z_1)}]\end{aligned} \tag{D.6}$$

From Eq. D.6, $\tau_{(z)}$ is related to the compression zone height at each side (z_1, z_2). Compression zone height can be calculated based on the bending moment as shown in Fig D.4. The total moment M at beam length location x can be divided into 2 parts: moment from plastic zone M_1 and moment from the elastic zone M_2. the detailed calculation is shown below:

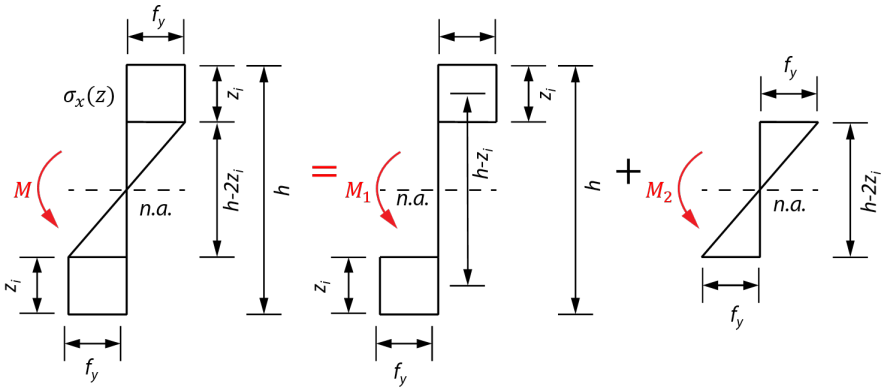

(a) M (b) M_1 (c) M_2

Figure D.4 – Normal stress for elastic-plastic stage(bilinear model)

$$
\begin{aligned}
M_1 &= f_y \cdot b z_i (h - z_i) \\
M_2 &= 1/6 \cdot b (h - 2z_i)^2 \cdot f_y \\
M_{Ed} &= M_1 + M_2 \\
&= f_y \cdot b [z_i (h - z_i) + 1/6 \cdot (h - 2z_i)^2] \\
&= 1/6 \cdot f_y \cdot b (h^2 + 2hz_i - 2z_i^2) \\
0 &= 2z_i^2 - 2hz_i - h^2 + \frac{6M_{Ed}}{f_y b}
\end{aligned}
$$

$\Longrightarrow$

$$
\begin{aligned}
z_i &= \frac{2h \pm \sqrt{4h^2 + 8(-\frac{6M_{Ed}}{f_y b} + h^2)}}{4} \\
z_i &= h/2 \pm \sqrt{\frac{3}{4}h^2 - 3\frac{M_{Ed}}{f_y b}} < h/2 \\
z_i &= h/2 - \sqrt{\frac{3}{4}h^2 - 3\frac{M_{Ed}}{f_y b}}
\end{aligned} \tag{D.7}
$$

Set: M_1=M because M_2=M+dM=M+Vd_x then:

$$
z_1 = h/2 - \sqrt{\frac{3}{4}h^2 - 3\frac{M}{f_y b}} \tag{D.8}
$$

$$
z_2 = h/2 - \sqrt{\frac{3}{4}h^2 - 3\frac{M + Vdx}{f_y b}} \tag{D.9}
$$

$$
z_1 - z_2 = \sqrt{\frac{3}{4}h^2 - 3\frac{M + Vdx}{f_y b}} - \sqrt{\frac{3}{4}h^2 - 3\frac{M}{f_y b}} \tag{D.10}
$$

Set $A = \frac{3}{4}h^2 - 3\frac{M}{f_y b}$ *and* $B = \frac{3V}{f_y b}$ then:

$$
h/2 - z_1 = \sqrt{A} \tag{D.11}
$$

$$
h/2 - z_2 = \sqrt{A - Bdx} \tag{D.12}
$$

$$
z_2 - z_1 = \sqrt{A} - \sqrt{A - Bdx} \tag{D.13}
$$

Taken Eq. (D.11, D.12, D.13) into Eq. D.6 we can get:

$$\tau(z) = f_y \cdot \frac{\sqrt{A}-\sqrt{A-Bdx}}{2\sqrt{A-Bdx}\cdot dx}\cdot[\sqrt{A}-\sqrt{A-Bdx}+\frac{A-Bdx-z^2}{\sqrt{A}}]$$

$$\tau(z) = f_y \cdot \frac{\sqrt{A}-\sqrt{A-Bdx}}{dx}\cdot\frac{[\sqrt{A}-\sqrt{A-Bdx}+\frac{A-Bdx-z^2}{\sqrt{A}}]}{2\sqrt{A-Bdx}}$$

$$\lim_{dx\to 0}\tau(z) = f_y \cdot \lim_{dx\to 0}\frac{\sqrt{A}-\sqrt{A-Bdx}}{dx}\cdot\lim_{dx\to 0}\frac{[\sqrt{A}-\sqrt{A-Bdx}+\frac{A-Bdx-z^2}{\sqrt{A}}]}{2\sqrt{A-Bdx}}$$

$$\lim_{dx\to 0}\tau(z) = f_y \cdot \lim_{dx\to 0}\frac{\sqrt{A}-\sqrt{A-Bdx}}{dx}\cdot\frac{A-z^2}{2A}$$

because $\lim_{x\to 0}\sqrt{A}$-$\sqrt{A-Bx}$=0, based on L'Hôpital's rule :

$$\lim_{x\to 0}\frac{\sqrt{A}-\sqrt{A-Bx}}{x} = \frac{(\sqrt{A}-\sqrt{A-Bx})'}{x'} = \frac{B}{2\sqrt{A-Bx}} = \frac{B}{2\sqrt{A}}$$

$$\lim_{dx\to 0}\tau(z) = f_y \cdot \frac{B}{2\sqrt{A}}\cdot\frac{A-z^2}{2A} = f_y \cdot \frac{B(A-z^2)}{4A\sqrt{A}} = \frac{2V}{\sqrt{3}b}\cdot\frac{\frac{3}{4}h^2-3\frac{M}{f_y b}-z^2}{(h^2-4\frac{M}{f_y b})^{3/2}}$$

Thus, when $M_{El,Rd}$<M_{Ed}<$M_{pl,Rd}$:

$$\tau(z) = \begin{cases} \frac{2V}{\sqrt{3}b}\cdot\frac{\frac{3}{4}h^2-3\frac{M}{f_y b}-z^2}{(h^2-4\frac{M}{f_y b})^{3/2}} & ;\mid z\mid \leq m \\ 0 & ; m<\mid z\mid \leq h/2 \end{cases} \tag{D.14}$$

The maximum shear stress is at z=0

$$\tau_{max} = \tau(z=0) = \frac{f_y}{4}\cdot\frac{B}{\sqrt{A}} = \frac{\sqrt{3}V}{2b\cdot\sqrt{h^2-4\frac{M}{f_y b}}} \tag{D.15}$$

D.2.1 With uniformly distributed loads

Different from as model 2, model 1 is loaded with a uniformly distributed load. In this way, bending moment and shear force change constantly along whole beam. For an infinite small beam slice dx, the action effects at each side can be calculated as follows :

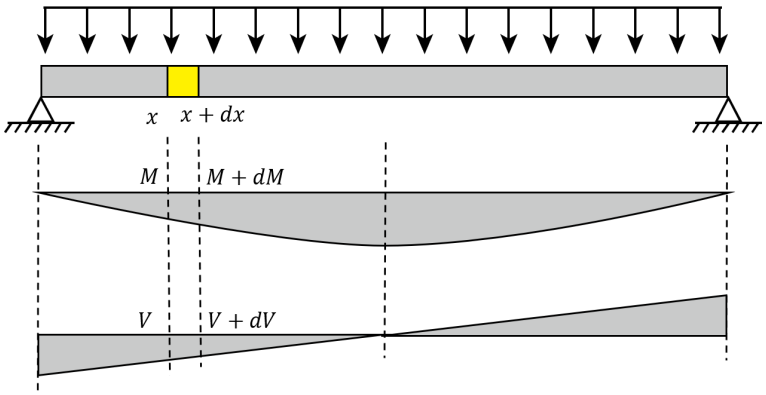

Figure D.5 – Action effects on model 1

on left side:

$$V_1 = V$$
$$M_1 = M$$

on right side:

$$V_2 = V + (q_d + g_d)dx$$
$$M_2 = M + Vdx + \frac{1}{2}(q_d + g_d)dx^2$$

For platic stage, taken into Eq.D.1

$$\begin{aligned}\tau(m)dx &= \int_{h/2}^{m} \frac{M_2 z}{I_y}dz - \int_{h/2}^{m} \frac{M_1 z}{I_y}dz \\ &= \int_{h/2}^{m} \frac{(Vdx + \frac{1}{2}(q_d + g_d)dx^2)z}{I_y}dz \\ \tau(m) &= \int_{h/2}^{m} \frac{(V + \frac{1}{2}(q_d + g_d)dx)z}{I_y} = \int_{h/2}^{m} \frac{Vz}{I_y}dz = \frac{VS_y(m)}{I_y b}\end{aligned}$$

Thus, for elastic stage the same formula can be used.

For elastic - plastic stage taken into Eq. (D.8,D.9)

Set $A = \frac{3}{4}h^2 - 3\frac{M}{f_y b}$ *and* $B = \frac{3V}{f_y b}$ and $C = \frac{3(q_d+g_d)}{2f_y b}$ then:

$$h/2 - z_1 = \sqrt{A}$$
$$h/2 - z_2 = \sqrt{A - Bdx - Cdx^2}$$
$$z_2 - z_1 = \sqrt{A} - \sqrt{A - Bdx - Cdx^2}$$

$$\tau(z) = f_y \cdot \frac{\sqrt{A} - \sqrt{A - Bdx - Cdx^2}}{2\sqrt{A - Bdx - Cdx^2} \cdot dx} \cdot [\sqrt{A} - \sqrt{A - Bdx - Cdx^2} + \frac{A - Bdx - Cdx^2 - z^2}{\sqrt{A}}]$$

following same calculation procedure for model 1, we can easily get:

$$\tau(z) = \begin{cases} \frac{2V}{\sqrt{3}b} \cdot \frac{\frac{3}{4}h^2 - 3\frac{M}{f_y b} - z^2}{(h^2 - 4\frac{M}{f_y b})^{3/2}} & ;\mid z \mid \leq m \\ 0 & ; m < \mid z \mid \leq h/2 \end{cases}$$

It is also reasonable that because $\frac{1}{2}(q_d + g_d)dx^2$ is infinitesimal of higher order of Vdx, thus it is negligible. For uniformly distributed loads, the same formula as concentrated loads can be used for both elastic and elastic-plastic stage.

D.3 Benchmarks of the results

D.3.1 Benchmarks on development of plastic zone

Plastic zone area can be calculated based on Eq. D.7 . Comparisons were made from the results of theoretical equation and ANSYS. (Fig D.6) The comparison shows very similar curves. For model 1, which is loaded with the concentrated load, differences can be noticed at x = 3m where the pointed load is applied because of stress concentration. For model 2 which is under distributed loads, plastic zone boundary follows a curved zone when applied loads is small. With the increasing moment, the curvature is decreasing. Finally, when the maximum bending resistance is reached, the plastic zone turns into a triangle at mid-span.

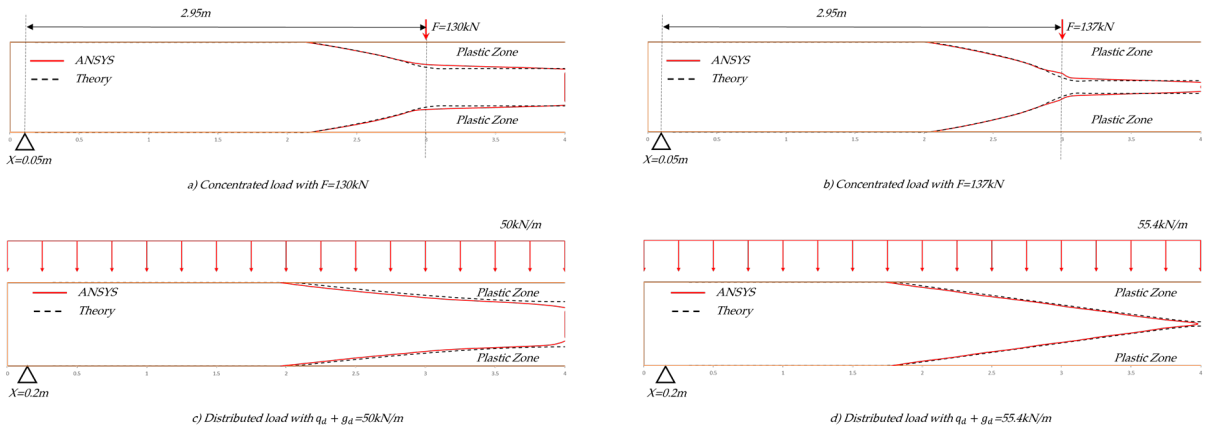

Figure D.6 – Comparison of plastic zone

D.3.2 Benchmarks on vertical shear stress

The results of shear stress at different cross sections (x= 1m, 2m, 3m, 3.48m, 4m for model 1, and M_{Ed} =267kNm, 334kNm, 363kNm, 389kNm) are compared in Fig D.7.For both models, plastic bending resistance is nearly reached.

Model 1 shows exactly the same results between theoretical curve and ANSYS curve, the maximum shear stress in the plastic zone (x= 2m, 3m, 3.48m) keeps constant. Except for the shear stress of cross-section x = 4m which always be zero, with increasing distance, shear stress zone height gradually shrinkage to a zone near neutral axis.

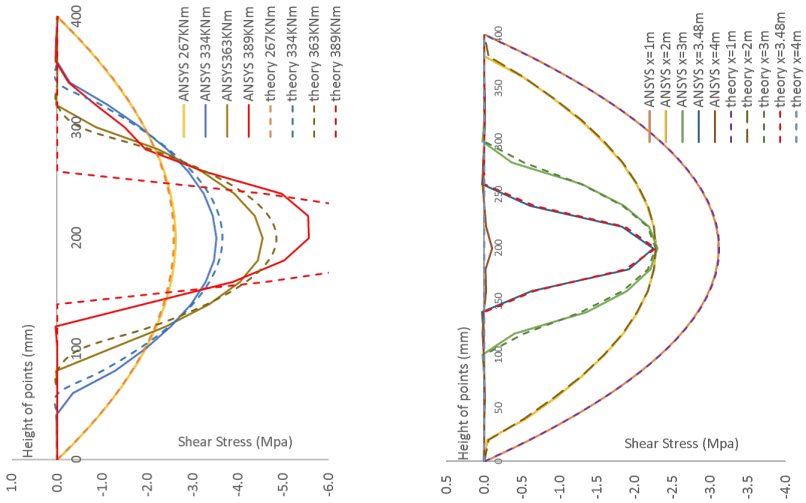

a) Model 2-137kN (Full load) *b) Model 1-55.4kN/m (Full load)*

Figure D.7 – Comparison of shear stress along beam height direction (model 1 & 2, full load)

For Model 2 differences between theory and ANSYS increase when the cross section is near the load plate, which resulting from the influence of stress concentration. Maximum shear stress increase with the bending moment. But for ANSYS the shear stress at cross-section with a moment of 398kNm get much smaller value due to the influence of load applied area. In plastic stage, both curves show shear stress equal to zero inside the plastic region.

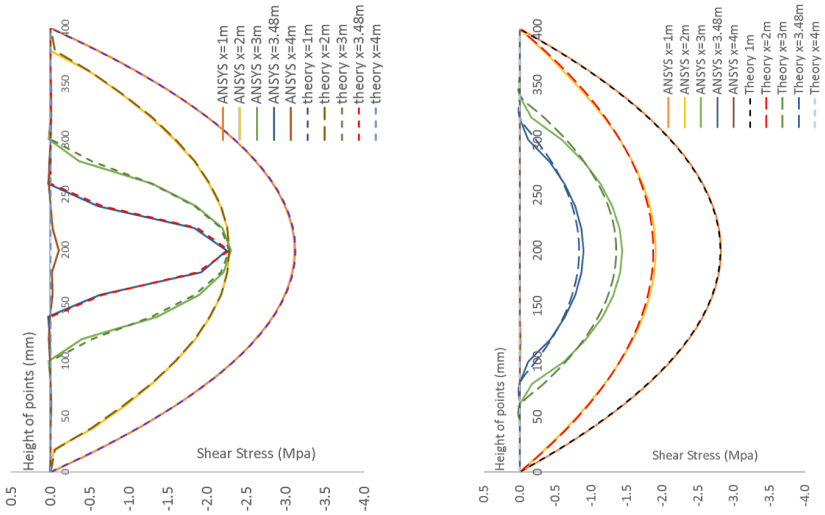

a) Model 1-55.4kN/m(Full load) *b) Model 1-50kN/m*

Figure D.8 – Comparison of shear stress along beam height direction (model 1 full load & not-full load)

Another comparison of model 1 under the full load and a not-full load is present in Fig D.8. It can be concluded that, when the full load is not reached, the maximum shear stress decreases together with its height, the shear stress inside the plastic zone (x=3m, x=3.5m, x=4m) is smaller than the shear stress inside elastic zone (x=1m, x=2m).

D.3.3 Benchmarks on longitudinal shear stress distribution of model 1

From ANSYS results, it can be concluded that at support regions and area near the concentrated loads, shear stress is greatly distributed. Thus, it is more reasonable to compare model 1, where a plastic zone is not influenced by the loads. The comparison of longitudinal stress at different beam heights (y= 0mm, 60mm, 120mm, 200mm) is shown in Fig D.9 for full load case and in Fig. D.10 for not-full load case.

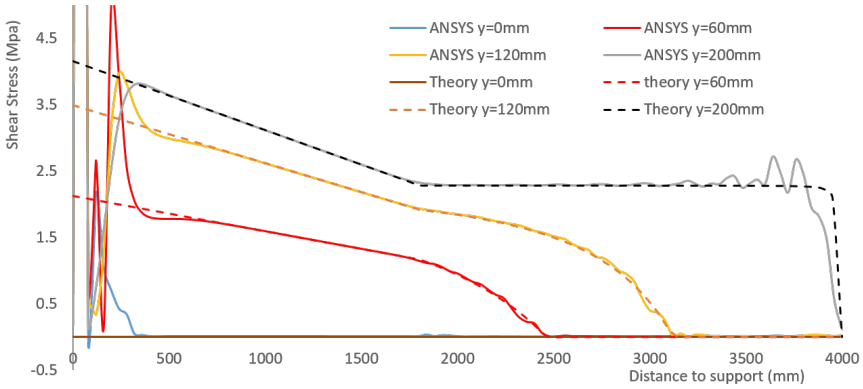

Figure D.9 – Longitudinal shear stress of model 1 (full load)

Except for the support region, all theoretical curves match very well with ANSYS. For curve y=200mm, the longitudinal shear stress distribution is near a tri-linear curve, which

reduced to zero at mid-span. ANSYS gives a strange wave near x=4000mm zone, which is perhaps resulting from not enough mesh size and symmetry condition near this location. For not-full load case, both curves change linearly in elastic region, and non-linearly in plastic section.

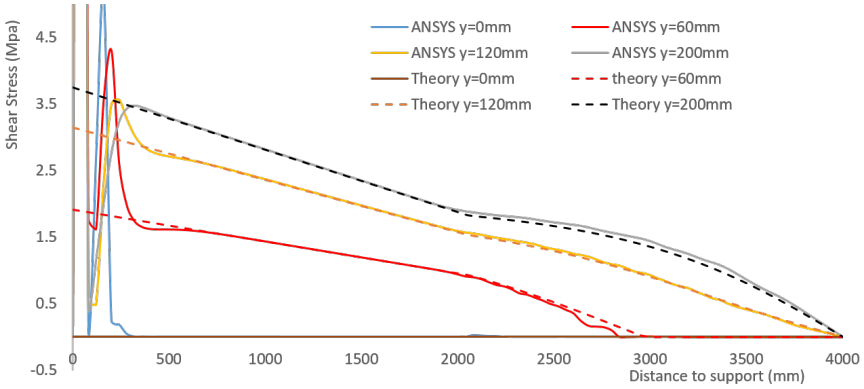

Figure D.10 – Longitudinal shear stress of model 1 (not full load)

D.4 Analytical results of longitudinal shear stress distribution

The benchmarks in the section 3.3.5 prove that the theoretical formula can give reliable results. Thus, it can be used to research on the development of distribution of longitudinal shear stress under different Loads. Fig D.11 illustrate changes of longitudinal shear stress with increasing loads. 4 cures are plotted in each sub figure represent the horizontal layers of y= 0mm, 60mm, 120mm, 200mm. The loads change from the elastic stage (a) to elastic-plastic stages (b to f).

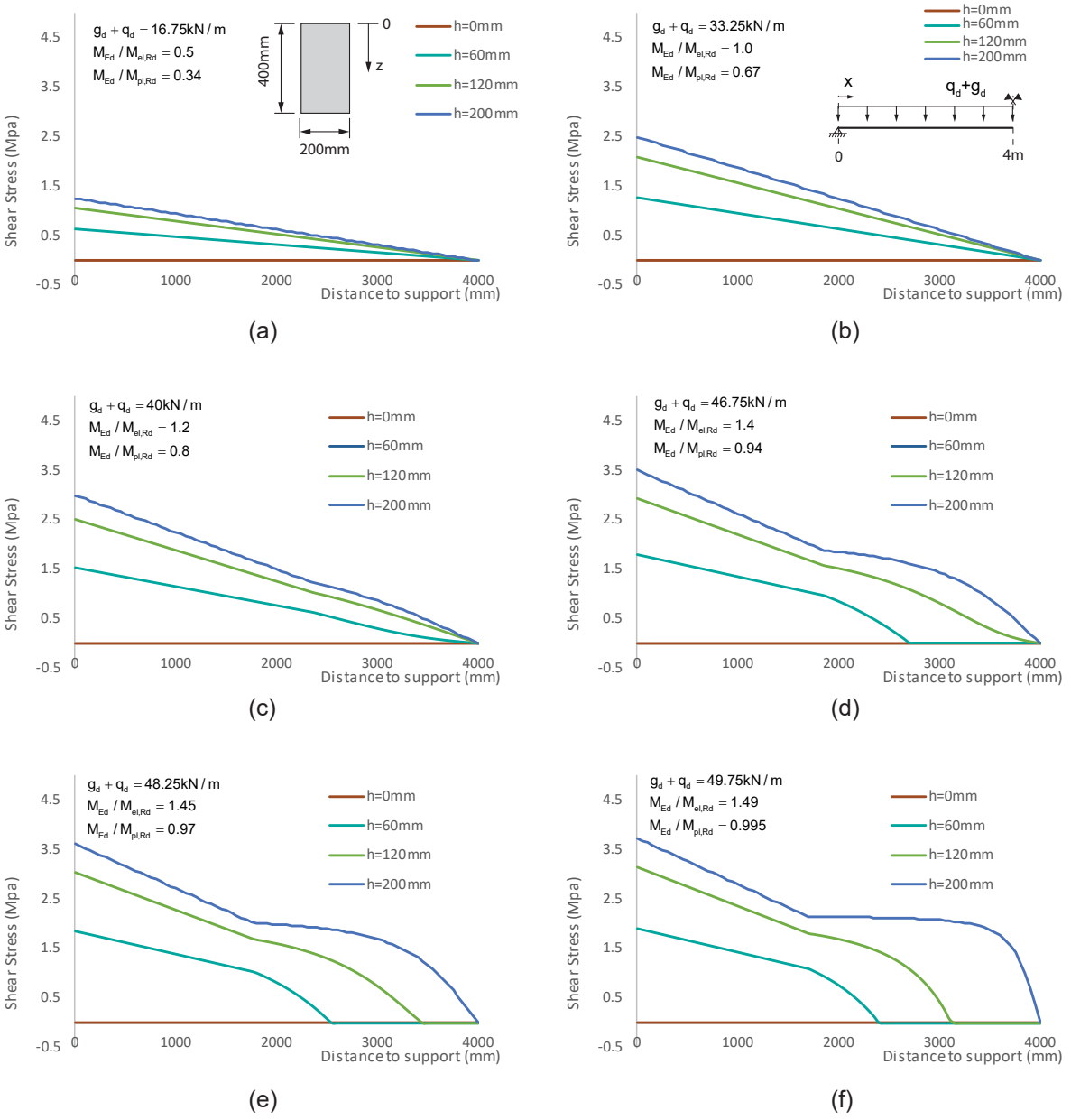

Figure D.11 – Longitudinal shear stress development with increasing loads

In elastic stage, longitudinal shear stress increases in portion to the shear force, which is also linear along beam axis direction. After entering the plastic stage, a hump appears near mid-span area and increases with the load. Except for the layer at neutral axis (y=200mm) and at surface (y=0mm), longitudinal shear stress reduces to zero before mid-span.

Appendix E

Simplified hand-calculation approach of bending moment resistance when steel section reach full plastic based on strain-limited design

In section 7.1.2.3 a proposal of engineering simplification of longitudinal shear distribution when steel section in full plastic, is provided. To use the simplified method, the bending moment resistance when steel section reach full plastic based on strain-limited design $M_{ap,Rd}$ is required. To calculate the $M_{a1,Rd}$, to obtain it strain-limited design can be used. With a numerical calculation software, it can be calculated by setting the strain-limit point as the steel top fiber with yielding strain. However it is also possible to obtain with help of a design chart as shown in Fig. E.1. With the chart, the concrete equivalent force location z_c for situation of $M_{a1,Rd}$ can be easily obtained, afterwards the $M_{a1,Rd}$ can be obtained by Eq.E.4.

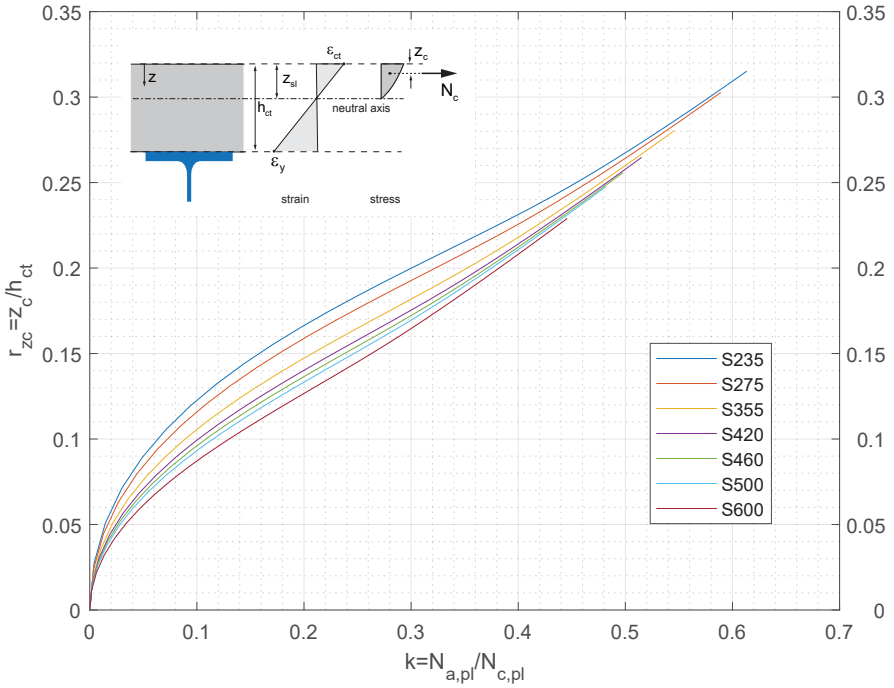

Figure E.1 – The r_{zc} diagram of composite beam with concrete classes no greater than C50/60

$$N_{a,pl} = A_a \cdot f_y \tag{E.1}$$

$$N_{ct,pl} = b_{eff} h_{ct} \cdot f_{cd} \tag{E.2}$$

$$k = \frac{N_{a,pl}}{N_{c,pl}} \tag{E.3}$$

$$M_{al,Rd} = N_{a,pl} \cdot (\frac{h_a}{2} + r_{zc} h_{ct}) \tag{E.4}$$

Develop of the design diagram in Fig. E.1 is based on strain limited design with parabolic-rectangle stress-strain model for concrete classes limited to C50/60. The calculation is explain as below. First the strain at top fiber and the position of neutral axis should be obtained according to the following analysis:

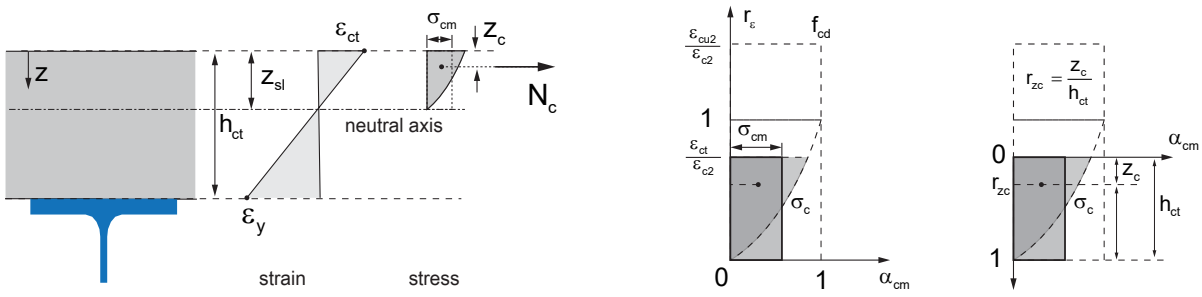

Figure E.2 – The development of r_{zc} diagram

$$N_c = b_{eff} z_{sl} \sigma_{cm} \tag{E.5}$$

σ_{cm} is the mean stress value of the concrete section, with the prabolic-rectangle stress-strain model:

$$\sigma_{cm}(\varepsilon_{ct}) = \frac{\int_o^{\varepsilon_{ct}} \sigma_c(\varepsilon_c) d\varepsilon_c}{\varepsilon_{ct}} \tag{E.6}$$

$$\sigma_c(\varepsilon_c) = \begin{cases} f_{cd} & \varepsilon_c > \varepsilon_{c2} \\ f_{cd}(1-(1-\frac{\varepsilon_c}{\varepsilon_{c2}})^n) & \varepsilon_c \leq \varepsilon_{c2} \end{cases} \tag{E.7}$$

$$\tag{E.8}$$

According to Eurocode 2, for concrete class smaller than C50/60, the $\varepsilon_{c2} = 0.002$ and $n = 2$. If we further set:

$$\sigma_{cm} = f_{cd} \alpha_{cm}(\varepsilon_{ct}) \quad and \quad r_\varepsilon = \frac{\varepsilon_{ct}}{\varepsilon_{c2}} \tag{E.9}$$

$$\tag{E.10}$$

We can get the following shape function related to the stress-strain relationship:

$$\alpha_{cm}(r_\varepsilon) = \begin{cases} r_\varepsilon - \frac{r_\varepsilon^2}{3} & r_\varepsilon < 1 \\ 1 - \frac{1}{3 r_\varepsilon} & r_\varepsilon \geq 1 \end{cases} \tag{E.11}$$

$$\tag{E.12}$$

Thus the forces in concrete can be expressed as follow, which by equilibrium should be also equal to the forces in the steel section.

$$N_{a,pl} = N_c = b_{eff} z_{sl} f_{cd} \alpha_{cm}(\varepsilon_{ct}) \tag{E.13}$$

As the neutral axis location is related to the strain value at top fiber of cross-section, it can be expressed as below, for simplification we can further set the ratio to h_{ct} as r_{zsl}:

$$z_{sl} = \frac{\varepsilon_{ct}}{\varepsilon_{ct} + \varepsilon_y} h_{ct} = r_{zsl} \cdot h_{ct} \tag{E.14}$$

$$N_{a,pl} = b_{eff} h_{ct} f_{cd} \cdot \alpha_{cm} r_{zsl} \tag{E.15}$$

$$\frac{N_{a,pl}}{b_{eff} h_{ct} f_{cd}} = \frac{N_{a,pl}}{N_{ct,pl}} = \alpha_{cm} r_{zsl} \tag{E.16}$$

Further we can set the values $N_{a,pl}/N_{c,pl}$ as parameter k and the ratio $\varepsilon_y/\varepsilon_{c2}$ as parameter a, the relationship between "k" and the "r_ε" can be obtained:

$$k = \frac{N_{a,pl}}{b_{eff} h_{ct} f_{cd}} \quad a = \frac{\varepsilon_y}{\varepsilon_{c2}} \tag{E.17}$$

$$r_{zsl} = \frac{\varepsilon_{ct}}{\varepsilon_{ct} + \varepsilon_y} = \frac{r_\varepsilon}{r_\varepsilon + a} \tag{E.18}$$

$$k(r_\varepsilon) = \frac{r_\varepsilon}{r_\varepsilon + a} \alpha_{cm}(r_\varepsilon) \tag{E.19}$$

The parameter "r_ε" represents the strain value, it can also be transfer to the relationship of location of neutral axis "r_{zsl}".

$$k(r_{zsl}) = \begin{cases} a\frac{r_{zsl}^2}{1-r_{zsl}} - \frac{a}{3}\left(\frac{r_{zsl}}{1-r_{zsl}}\right) & r_{zsl} < \frac{1}{a+1} \\ ar_{zsl} - \frac{1-r_{zsl}}{3a} & r_{zsl} \geq \frac{1}{a+1} \end{cases} \tag{E.20}$$

Now as the shape of the concrete stress diagram is changing constantly, thus the location z_c of the equivalent force N_c is also not fixed. Using similar way explained in section.xx, their relationship with ε_{ct} and r_ε, however can be obtained.

$$r_{c1} = \frac{z_{sl} - z_c}{z_c} \tag{E.21}$$

$$\frac{z_{sl} - z_c}{z_c} = \frac{\int_o^{\varepsilon_{ct}} \sigma_c(\varepsilon)\varepsilon_i d\varepsilon}{\varepsilon_{ct}\int_o^{\varepsilon_{ct}} \sigma_c(\varepsilon) d\varepsilon} \tag{E.22}$$

$$r_{c1} = \begin{cases} \frac{8r_\varepsilon^2 - 3r_\varepsilon^3}{12r_\varepsilon^2 - 4r_\varepsilon^3} & r_\varepsilon < 1 \\ \frac{5+6(r_\varepsilon^2-1)}{12r_\varepsilon - 4} & r_\varepsilon >= 1 \end{cases} \tag{E.23}$$

With the parameter r_{c1} calculated, the value of z_c is known:

$$z_c = (1 - r_{c1})z_{sl} = (1 - r_{c1})r_{zsl}h_{ct} \tag{E.24}$$

The relationship between z_c and the h_{ct} is expressed below, it is difficult to solve it explicitly, however as they are only related to the steel grades and concrete top fiber strain, the relationship can be plotted in a diagram as shown in Fig. E.1 for quick checking.

$$r_{zc} = \frac{z_c}{h_{ct}} = (1 - r_{c1})r_{zsl} \tag{E.25}$$